Electron Collision Processes in Atomic and Molecular Physics

Book · January 2014

Minaxi Vinodkumar
V. P. & R. P. T. P. Science College, Vallabh Vidyanagar 388 120, Gujar…

Electron Collision Processes in Atomic and Molecular Physics

Electron Collision Processes in Atomic and Molecular Physics

Editor
P. C. Minaxi Vinodkumar

Narosa Publishing House
New Delhi Chennai Mumbai Kolkata

Electron Collision Processes in Atomic and Molecular Physics

230 pgs.

Editor
P. C. Minaxi Vinodkumar
Associate Professor
V. P. & R. P. T. P. Science College
Vallabh Vidyanagar
Anand, Gujarat

NAROSA PUBLISHING HOUSE PVT. LTD.

22 Delhi Medical Association Road, Daryaganj, New Delhi 110 002
35-36 Greams Road, Thousand Lights, Chennai 600 006
306 Shiv Centre, Sector 17, Vashi, Navi Mumbai 400 703
2F-2G Shivam Chambers, 53 Syed Amir Ali Avenue, Kolkata 700 019

www.narosa.com

Printed from the camera-ready copy provided by the Editor.

ISBN 978-81-8487-343-6

Published by N.K. Mehra for Narosa Publishing House Pvt. Ltd.,
22 Delhi Medical Association Road, Daryaganj, New Delhi 110 002

Printed in India

PREFACE

It gives me great pleasure to present this monograph comprising articles of research work presented by eminent scientists at the ‘National Conference on Electron Collision Processes in Atomic and Molecular Physics (ECPAMP) organized by V. P. & R. P. T. P. Science College, Vallabh Vidyanagar, Gujarat to commemorate the centenary of Neil Bohr’s atomic model. It was an apt occasion for a scientific discourse on atomic and molecular phenomena and the conference witnessed host of expertise talks on the topics of current interest in the field of atomic and molecular processes.

At the National perspective, research work in the field of Atomic and Molecular Physics is in the ascending note with an overwhelming number of young physicists showing interest and joining the atomic and molecular fraternity. The broadness of the field is clearly evident from the variety of topics covered in this conference and the articles presented in this monograph. The insightful contributions of seasoned scientists are immensely appreciated and the motivation provided by them to the young participants is acknowledged with gratitude.

Calculations based on ab-initio methods and approximate theoretical methods for various scattering cross sections of different target molecules at wide energy range of the incident particles are presented in this book. While some of the articles focus upon the fundamental aspects of the molecular interactions with charge particles and radiation, others deal with variety of applications of the atomic and molecular collision data investigated. Many articles explored applications related to environmental science, semiconductor physics, plasma physics, astro-chemistry, radio-biology etc.

This book includes compilation of a total of fifty scientific articles of repute. The first two articles include the key note address delivered by Prof. P. C. Deshmukh, IIT Madras and an invited article on “Bohr’s Legacy” written by Prof Nigel Mason of the Open University, Milton Keynes, UK. Other articles presented in this monograph are broadly classified and divided in three chapters. Chapter one contains a total of twenty one articles on total cross sections of charge particle collisions with molecular targets: measurements and calculations. Chapter two includes compilation of seventeen articles related to theoretical estimations and experimental measurements on ionization cross sections of selected atoms and molecules. And chapter three contains ten articles related to applications of charge particle collision data and properties of selected atomic and molecular targets.

Looking at the variety of research topics and wealth of experimental as well as theoretical data reported through the articles presented in this book, I am confident that it will be best utilized and used as reference book by researchers and scientists working in this field of atomic and molecular physics and allied branches of applied fields.

It is my pleasure to acknowledge the help and full cooperation of Chairman CVM, Dr. C. L. Patel and other CVM personal, Principal Dr. Bhavesh Patel, Mr. Piyush Lashkari, my staff members and research students for their moral support and help. I acknowledge with reverence the financial aid provided by various funding agencies: DAE-BRNS, DST- New Delhi, UGC-Pune and QuantemolN- UK. I am grateful to Prof. K. N. Joshipura (SPU), Prof. P. C. Deshmukh (IIT Madras), Prof. E. Krishnakumar (TIFR Mumbai), Prof. Lokesh Tribedi (TIFR Mumbai), Dr. K. P. Subramanian (PRL, Ahmedabad), Prof. Vinodkumar (SPU), Dr. Bobby Antony (ISM Dhanbad) and Dr. Chetan Limbachiya (Kadi, Gujarat) for their valuable support and guidance in organizing this conference as well as to all authors for their timely submissions of contributions presented in this monograph.

P. C. Minaxi Vinodkumar

CONTENTS

Chapter 1: Total Cross Sections of Charge Particle Collisions with Molecular Targets: Measurements and Calculations

Chapter 2: Theoretical Estimations and Experimental Measurements on Ionization Cross Sections of Selected Atoms and Molecules

Chapter 3: Applications of Charge Particle Collision Data and Properties of Selected Atomic and Molecular Targets

INVARIANCE PRINCIPLES AND SPECTRA OF THE FIRST GROUP ATOMS

P.C. Deshmukh
Department of Physics
Indian Institute of Technology Madras
Chennai 600036
Email: pcd@physics.iitm.ac.in

I. CONSERVATION PRINCIPLES FROM THE PHYSICAL LAW

One can clearly demark physics before and after Einstein[1]. One of his outstanding contributions is the recognition of symmetry/invariance as an important principle in physics. Symmetry plays a pivotal role in nature. It has an intimate relationship with conservation principles, and with the 'Character of the Physical Law' [2]. At a fundamental level, physics deals largely with the discovery and understanding of the physical law(s) of nature. It thus becomes pertinent to ask just what is meant by *a/the (physical) law(s) of nature*. This quest aspires to explain the physical universe in terms of a minimum number of principles/laws. One could even perhaps hope that all physical phenomena are comprehensible in terms of just one law. We are perhaps far from this goal as yet, nonetheless, it is intriguing that most of the physical phenomena can be explained in terms of just a very few number of laws. Much of the excitement in physics is the recognition of this approach which seeks to know the *most* from the *least*.

One does not know yet if there is then just a single law of nature which really provides the 'theory of everything'. It is nevertheless important to inquire just what is meant by a law of nature. Following early insights provided by Albert Einstein and Emmily Noether, Eugene Wigner[3] provided deep insights on these fundamental questions and elucidated just what is meant by the laws of nature and what are their connections with symmetry and invariance principles. Inspired by Wigner's perceptivity [3], these ideas can possibly be summarized in three observations:

(i) The regularities in the phenomena which physical science endeavours to uncover are called the laws of nature.
(ii) The elements of the behaviour which are not specified by the laws of nature are called initial conditions.
(iii) The invariance principles themselves depend on the dividing line between initial conditions and laws of nature.

Two questions, apparently opposite to each other, can be asked with regard to the connections between invariance/conservation principles and the laws of nature: (a) Are the conservation principles consequences of the laws of nature? Or, (b) are the laws of nature the consequences of the symmetry principles that govern them? Following Feynman[2], we begin with the universal law of gravity as an illustration of the law of nature. We consider a mass m_1 at a point whose position vector is $\vec{R}_1$ in a state of gravitational interaction with another mass m_2 at a point whose position vector is $\vec{R}_2$. The equation of motion which describes the gravitational inverse square law for the 'relative motion' of the smaller mass relative to the larger mass, with its position vector given by $\vec{r} = \vec{R}_2 - \vec{R}_1$, is then given by:

$$\ddot{\vec{r}} + \kappa \frac{\vec{r}}{|\vec{r}|^3} = \vec{0} \quad , \tag{1}$$

where $\kappa = G(m_1 + m_2) \approx Gm_1$, for $m_1 \rangle\rangle\rangle m_2$, and has dimensions $[\kappa] = L^3T^{-2}$.

The scalar product of the equation of motion, Eq.1, with velocity vector $\vec{\mathrm{v}} = \dot{\vec{r}}$ gives

$$\mathrm{v} \lim_{\delta t \to 0} \frac{\delta \mathrm{v}}{\delta t} = -\frac{\kappa \lim\limits_{\delta t \to 0} \frac{\delta r}{\delta t}}{r^2} . \tag{2}$$

Integrating Eq.2 with respect to time yields the conservation of energy:

$$\frac{\mathrm{v}^2}{2} - \frac{\kappa}{r} = E , \tag{3}$$

E being the specific (*i.e. per unit mass*) energy, which has emerged as the constant of integration. Integration with respect to *time* as the mathematical operation that yields the conservation of energy is no accident; it comes from the fact that energy and time are canonically conjugate variables. Likewise, cross product of the equation of motion with the position vector $\vec{r}$, together with the recognition that the gravitational force is a *central field force,* immediately yields the conservation of ('specific', i.e. per unit mass) angular momentum $\vec{H} = \vec{r} \times \dot{\vec{r}} = \vec{r} \times \vec{\mathrm{v}}$. We see that it essentially stems from the *isotropy* of the interaction. Furthermore, cross product of the equation of motion with the specific angular momentum $\vec{H}$ yields, after some straight forward manipulation, the conservation of yet another vector, namely the Laplace-Runge-Lenz[4] (LRL) vector,

$$\vec{A} = \left(\vec{\mathrm{v}} \times \vec{H}\right) - \kappa \hat{e}_\rho . \tag{4a}$$

The LRL vector is sometimes alternatively (*but equivalently*) defined as

$$\vec{A} = \frac{\left(\vec{p} \times \vec{L}\right)}{\mu} - \kappa \hat{e}_\rho , \tag{4b}$$

wherein the *new* κ now has dimensions $\mathrm{ML^3T^{-2}}$.

The constancy of the LRL vector, directed always from the focus to the perigee of the ellipse, explains the fact that in the gravitational two-body problem whose closed orbits are described by an ellipse, the major axis of the ellipse is fixed; there is no rosette motion (i.e., there is no precession). The necessary and sufficient condition that the LRL[5] vector is fixed is the fact that the gravitational potential goes as $\frac{1}{r}$, and the force as $\frac{1}{r^2}$. Since the inverse square law of the force appears as a necessary condition, the symmetry related to the constancy of the LRL vector and associated fixation of the ellipse's major axis is often called as the 'dynamical' symmetry. It is almost startling that straight-forward mathematics such as integration, scalar and vector products, as described above reveal the intimacy between symmetry and conservation laws. One can only perhaps attribute this to the "unreasonable"[6] power of mathematics in explaining physical laws.

We note from the above discussion that the symmetry associated with respect to temporal evolution of an isolated system (whose Lagrangian has *no explicit dependence on time*) is associated with the conservation of energy, symmetry associated with the isotropy of the gravitational interaction is associated with the conservation of angular momentum, and the 'dynamical' symmetry of the $\frac{1}{r}$ gravitational interaction is connected with the constancy of the LRL vector and the associated fixation of the Kepler-ellipse in the two-body problem. We find that conservation principles are derivable, quite simply, from the physical law. In the next section we ask if the *reverse* process is possible.

II. PHYSICAL LAWS FROM THE CONSERVATION PRINCIPLES

We consider a system of N particles in a medium that is homogenous. An infinitesimal virtual [4] instantaneous displacement of the entire N-particle system through $\overrightarrow{\delta S}$ in this medium would result in a new configuration that would find itself in an environment that is completely indistinguishable from the previous one. No external force is applied in the virtual displacement. Denoting the force on the kth particle by the ith by $\overrightarrow{F}_{ik}$, we find, since internal forces do no work toward the virtual displacement, that

$$0 = \delta W = \left\{ \sum_{k=1}^{N} \overrightarrow{F}_k \right\} \bullet \overrightarrow{\delta s} = \left\{ \sum_{k=1}^{N} \sum_{i=1, i\neq k}^{N} \overrightarrow{F}_{ik} \right\} \bullet \overrightarrow{\delta s}, \tag{5}$$

$\overrightarrow{F}_k$ being the force on the k^{th} particle due to the *remaining* N -1 particles .

The necessary and sufficient condition that Eq.5 holds for an *arbitrary* displacement is that

$$\vec{0} = \left\{ \sum_{k=1}^{N} \overrightarrow{F}_k \right\} = \sum_{k=1}^{N} \frac{d\vec{p}_k}{dt} = \frac{d}{dt} \sum_{k=1}^{N} \vec{p}_k = \frac{d\vec{P}}{dt}. \tag{6}$$

We have used, to arrive at Eq.6 from Eq.5, the first two laws of Newton, but of course not the third. Rather, the third law *follows* from Eq.6 since application of Eq.5 to a two-body system results in

$$\frac{d\overrightarrow{p_2}}{dt} = -\frac{d\overrightarrow{p_1}}{dt}, \text{ i.e., } \overrightarrow{F}_{12} = -\overrightarrow{F}_{21}, \tag{7}$$

which of course is Newton's III law, that action and reaction are equal and opposite. We see here that the *physical law* has followed from an invariance/symmetry principle. Likewise, from the fact that the LRL vector is a constant *if and only if* the interaction is governed by the inverse square law, one could have *deduced* the $\frac{1}{r}$ *form* of the gravitational interaction.

We thus find that indeed it is possible to get a physical law *from* a symmetry/conservation principle, just as we saw in Section I that conservation principles *follow* from the physical law.

III. SYMMETRY OF THE ATOMIC HAMILTONIAN, AND SPECTRA OF THE I GROUP ATOMS

In Section I we saw that conservation principles are derivable from the physical law, and in Section II we saw that the physical law is obtainable from the underlying symmetry associated with the conservation principles. As to which way the relationship has its most natural flow is best explained by Wigner[7,8]: " It is now natural for us to derive the laws of nature and to test their validity by means of the laws of invariance, rather than to derive the laws of invariance from what we believe to be the laws of nature".

We now examine the importance of symmetry with regard to specific interest in atomic physics. The discrete symmetries, namely parity (P), charge conjugation (C) and time-reversal (T) symmetry constitute an important cornerstone of the standard model of physics. PCT symmetry has important implications in atomic physics [9, 10, 11, 12]. Also, important physical *processes* to *probe* the atom, namely electron-atom collisions and atomic photoionization, are related to each other by the time-reversal symmetry, discussed elsewhere [11].

In the present article, we focus on an interesting consequence of the so-called 'dynamical symmetry' of the Coulomb interaction, also described by the $\frac{1}{r}$ attraction between the electron and the proton in the Hydrogen atom. This symmetry, and/or its breakdown, has an important consequence on the spectra of the atoms belonging to the I Group of the periodic table.

The importance of studying the symmetry aspects of the hydrogen atom is best illustrated by the fact that amongst the atoms that belong to the I Group of the periodic table, all the alkali atoms, *except the Hydrogen atom*, have the famous D1, D2 lines. The splitting between the D1 and D2 lines is due to the relativistic spin-orbit interaction, but more importantly, the prime reason that they occur at all is that the energy of the (excited) 3p level is higher than that of the 3s level, as in the case of the sodium atom (Fig.1).

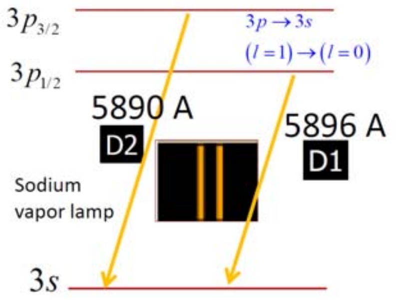

Fig. 1: There would be no D1,D2 lines in the sodium atom's spectrum if the energy of the 3p state were the same as that of the 3s state.

The absence of such lines only in the Hydrogen atom amongst all elements of the I group is due to the degeneracy of the Hydrogen atom’s eigen-states with different values of the orbital angular momentum, l, for a given value of the principal quantum number n. The Hydrogen atom’s eigenvalues are given by the famous Balmer-Rydberg-Bohr $\frac{1}{n^2}$ law, independent of l, whereas the eigenvalues of states of other atoms in the Group I depend not just on the principal quantum number as per the Balmer-Rydberg-Bohr law, but *also* on the orbital angular momentum quantum number. This $l-dependence$ enables the transitions that generate the D lines, and along with the relativistic spin-orbit splitting, we get the D1,D2 transitions. What connects this problem to the symmetries in Sections I and II is the fact that *degeneracy* and *symmetry* go together in quantum mechanics. The symmetry and invariance principle responsible for the peculiar degeneracy in the Hydrogen atom is that of the LRL vector describing the $\frac{1}{r}$ Coulomb potential in the electron-proton interaction. It seems not known if it is merely a coincidence that the form of the Coulomb interaction is similar to that of the gravitational interaction, both governed by the inverse square law. Regardless, the constancy of the LRL vector has important consequences for the quantum mechanics of the Hydrogen atom. However, unlike the Kepler orbit of ‘classical mechanics’, the quantum Hydrogen atom does not have any ‘orbit’. An orbit can be defined only if position and momentum are simultaneously measurable. We therefore do not talk about (Bohr-type) orbits, but *quantize* the LRL vector, following Pauli[13], now referred to as the Pauli-Lenz operator:

$$\vec{A} = \vec{A}_{QM} = \frac{1}{2\mu}\left[\vec{p}\times\vec{L} - \vec{L}\times\vec{p}\right] - \kappa\hat{r} \quad . \tag{8}$$

We note that quantization results in $\vec{A}$ of Eq.8 to be a vector *operator*. In contrast, the corresponding term in classical mechanics represented by Eq.4 is not an operator; it is only a vector. The Pauli-Lenz quantum operator commutes with the Hamiltonian for the Hydrogen atom.

It should be noted that the 1-dimensional radial Schrödinger equation for the Hydrogen atom does *not* explain the degeneracy of the Hydrogen atom, as can be seen directly from it:

$$\frac{1}{r^2}\frac{d}{dr}\left(r^2\frac{dR}{dr}\right) - \frac{l(l+1)}{r^2}R + \frac{2m}{\hbar^2}\left[E - V(r)\right]R = 0 \, . \tag{9}$$

It is well known that in a 1-dimensional problem, none of the energy values of the discrete spectrum is degenerate. Hence, it seems natural, from Eq.9, that the energies of all states with quantum numbers *n*, *l* corresponding to *different* values of *l* have *different* energies. Eq.9 does *not* therefore account for the degeneracy in the Hydrogen atom with regard to the different values of *l*. One can count this degeneracy easily. It is given by:

$$\sum_{l=0}^{n-1}(2l+1) = 2\sum_{l=0}^{n-1} l + \sum_{l=0}^{n-1} 1 = 2\frac{n(n-1)}{2} + n = n^2 - n + n = n^2 \, . \tag{10}$$

The $n^2 - fold$ degeneracy of the Hydrogen atom follows from the geometric (isotropic) symmetry of the Hamiltonian which provides for $(2l+1)-fold$ degeneracy for each allowed values of *l*, together with an *additional* symmetry responsible for the fact that all states with $l = 0,1,2,3,...,(n-1)$ of the Hydrogen atom are degenerate, but not so for other atoms of the I Group atoms. The radial Schrödinger equation does *not* account for the degeneracy in the Hydrogen atom. It is therefore often referred to as 'accidental' degeneracy.

To explain the $n^2 - fold$ degeneracy of the Hydrogen atom, we must examine the symmetry group of the Hydrogen atom, inclusive of the Pauli-Lenz operator of Eq.8. The three components of the Pauli-Lenz vector operator $\vec{A}$, along with the three components of the angular momentum operator $\vec{l}$ provide, a *closed* algebra even if only over the subspace of Hilbert space of eigenvectors belonging to a *particular* bound state energy eigenvalue E. This follows from the fact, as can be verified with some bit of patient algebra, that the following relations hold:

$$\left[L_i, L_j\right] = i\hbar\varepsilon_{ijk}L_k\ , \tag{11a}$$

$$\left[A_i, L_j\right] = i\hbar\varepsilon_{ijk}A_k\ , \tag{11b}$$

and
$$\left[A_i, A_j\right] = -2i\frac{\hbar}{\mu}H\varepsilon_{ijk}L_k\ . \tag{11c}$$

The appearance of the Hamiltonian operator on the right hand side of Eq.11c restricts the algebra of $\vec{L},\vec{A}$ to be closed only over the subspace of Hilbert space of eigenvectors belonging to a *particular* bound state energy eigenvalue E. The three components of the angular momentum operator $\vec{L}$, together with the three components of the Pauli-Lenz vector operator $\vec{A}$, constitute a set of six generators of the Lie Group of dimensions six, known as the SO(4) group, of Rank 2. Now, as per Racah's theorem, the number of Casimir[14] operators for the group is equal to the rank of the group. The two Casimir operators of the SO(4) group can be written as:

$$C_1 = I^2 + K^2 \tag{12a}$$

And
$$C_2 = I^2 - K^2, \tag{12b}$$

Where
$$\vec{I} = \frac{1}{2}\left(\vec{L}+\vec{A}'\right) \text{ and } \vec{K} = \frac{1}{2}\left(\vec{L}-\vec{A}'\right), \tag{12c}$$

with
$$\vec{A}' = \sqrt{\frac{-\mu}{2E}}\vec{A}. \tag{12d}$$

Both the Casimir operators commute with each of the six generator of the SO(4) group. The operators $\vec{I}$ and $\vec{K}$ satisfy the commutation algebra for quantum angular momentum vector operators as can be verified:

$$\left[I_x, I_y\right]_- = i\hbar I_z \text{ etc. and } \left[K_x, K_y\right]_- = i\hbar K_z \text{ etc.} \tag{13}$$

$\vec{I}$ and $\vec{K}$ are referred to as quantum '*pseudo*' angular momentum vector operators since they combine the polar vector $\vec{A}$ with the axial vector $\vec{L}$. The eigenvalues of

I^2 and K^2 are thus given respectively by $\hbar^2 i(i+1)$ and $\hbar^2 k(k+1)$ as is well-known from angular momentum algebra.

Now, $i = k$, since it can be seen that

$$C_2 = \vec{L} \bullet \vec{A}' = 0 \,. \tag{14a}$$

The eigenvalue of the operator C_1 is therefore:

$$2\hbar^2 k(k+1) = c_1 = 2\hbar^2 i(i+1) \,. \tag{14b}$$

Again, since $C_1 = I^2 + K^2$, we get

$$c_1 = \frac{1}{4}\left(\vec{L}^2 + \vec{L}\bullet\vec{A}' + \vec{A}'\bullet\vec{L} + \vec{A}'^2\right) + \frac{1}{4}\left(\vec{L}^2 - \vec{L}\bullet\vec{A}' - \vec{A}'\bullet\vec{L} + \vec{A}'^2\right), \tag{15a}$$

$$\text{i.e., } c_1 = \frac{1}{2}\left(\vec{L}^2 + \vec{A}'^2\right) = \frac{1}{2}\vec{L}^2 + \frac{1}{2}\vec{A}'^2 = \frac{1}{2}\vec{L}^2 + \frac{1}{2}\left(\frac{-\mu}{2E}\right)\vec{A}^2 \,. \tag{15b}$$

Now, using the fact that

$$\vec{A}\bullet\vec{A} = \frac{2}{\mu} H\left(\vec{L}^2 + \hbar^2\right) + \kappa^2 \,, \tag{16a}$$

we get:

$$c_1 = \frac{1}{2}\vec{L}^2 + \frac{1}{2}\left(\frac{-\mu}{2E}\right)\left\{\frac{2H}{\mu}\left(L^2 + \hbar^2\right) + \kappa^2\right\}, \tag{16b}$$

$$\text{i.e., } \qquad c_1 = -\frac{1}{2}\hbar^2 - \frac{1}{2}\left(\frac{\mu}{2E}\right)\kappa^2 = -\left(\frac{\mu}{4E}\right)\kappa^2 - \frac{1}{2}\hbar^2 \,. \tag{16c}$$

We have recognized in Eq.16 that $\frac{H}{E} = 1$, since over the domain of our exercise, which is the subspace of eigenvectors belonging to a given bound state energy eigenvalue *E*, the Hamiltonian *H* would always return essentially the same eigenvalue *E*.

From Eq.14 and 16, it follows that:

$$c_1 = 2\hbar^2 k(k+1) = 2\hbar^2 i(i+1) = -\left(\frac{\mu}{4E}\right)\kappa^2 - \frac{1}{2}\hbar^2 \,, \tag{17}$$

which gives the Balmer-Rydberg-Bohr expression:

$$E = -\frac{\mu\kappa^2}{2\hbar^2\left\{4i(i+1)+1\right\}} = -\frac{\mu\kappa^2}{2\hbar^2 n^2} \,, \tag{18a}$$

$$\text{with } n = (2i+1) \,, \tag{18b}$$

recognized immediately as the *principal quantum number*.

Now, *i*, being a (‘*pseudo*’) angular momentum quantum number as per Eq.13, has a degeneracy which is $(2i+1)-fold$. Likewise, *k* has a degeneracy which is

$(2k+1)-fold$. Since the principal quantum number n can get its integer value $n=2i+1=2k+1$, either from i or from k (with $i=k$), the quantum state with a given value of the principal quantum number n has a degeneracy given by $(2i+1)\times(2i+1)=n^2$, very much in accordance with Eq.10. The n^2-fold degeneracy which is peculiar only to the Hydrogen atom amongst all the atoms of the I Group elements, regarded earlier only as 'accidental degeneracy' in the Schrödinger formulation, has a proper explanation in its SO(4) symmetry. This symmetry does not hold for any of the other atoms of the I Group elements, since they have $Z>1$ protons and for them only in the asymptotic limit, $r\to\infty$, does the potential seen by the outer *n, l* electron goes as $-\frac{1}{r}$; but as $r\to 0$, the potential goes as $-\frac{Z}{r}$. The potential is no longer strictly described by the $-\frac{1}{r}$ law in the *entire* region of space, as required for the Pauli-Lenz operator to represent a constant of motion, as discussed earlier. The energy of all atoms with $Z>1$ is then expressed by a modified law, which goes as $E_n^{(Z>1)}\to E_{n,l}\to\frac{1}{(n-\mu_l)^2}$ whereas for the Hydrogen atom we have $E_n^{(Z=1)}\to\frac{1}{n^2}$, independent of *l*. μ_l is called as the 'quantum defect' and it depends on the orbital angular momentum quantum number. This important result is integrated comprehensively in the *quantum defect theory of the atomic spectra*[15]. Finally, and not surprisingly, the fact that $\vec{I}$ and $\vec{K}$ are *pseudo* angular momentum vector operators which combine a polar with an axial vector, is responsible for the fact that in the Hydrogen atom, states with opposite parity are degenerate.

IV. CONCLUSIONS

Symmetry plays a pivotal role in nature. From the conservation laws of energy, momentum and angular momentum that are determined by the invariance of the physical system/processes with respect to translations in time, and in homogeneous and isotropic space respectively, to the symmetry in Maxwell's equations with regard to the electric and magnetic fields, through the symmetry in nature revealed as the wave-particle duality, the subject of invariance in nature becomes only increasingly mindboggling. Other forms of symmetries such as the dynamical symmetry, discrete symmetries such as parity, time-reversal and charge conjugation, also impact physical processes in the universe. The reduction of the 3-dimensional Schrödinger equation to 1-dimensional radial equation explains why the energies of states with different l values have different energies in atoms such as sodium, but their degeneracy in the Hydrogen atom requires the recognition of the SO(4) symmetry of the Hamiltonian for the Hydrogen atom. This important difference between the symmetry of the Hydrogen atom and that of the other atoms of the I Group elements is responsible for the appearance of the D1, D2 lines in all I Group atoms except the Hydrogen atom. One must note that the present treatment is essentially non-relativistic, and appropriate modifications need to be made toward a fully relativistic [16] formulation. It must be added that the present approach not merely generates the eigenvalues of the Hydrogen atom and explains its degeneracy without using the Schrödinger equation, it also provides the radial wavefunctions[17] of the Hydrogen atom. That one obtains the eigenvalues and the eigenfunctions without even using the Schrödinger equation is not surprising, since we have of course used the essentials of quantum mechanics, which is to use the state vectors and the quantum operators instead of the classical representation of a system by a point in phase space.

V. ACKNOWLEDGMENTS

This article is based on the keynote address I was invited to deliver at the National Conference on Electron Collision Processes in Atomic and Molecular Physics, March 7-9, 2013. I am extremely grateful to the organizers for the opportunity to give the talk and write this article. We all enjoyed the hospitality and the vibrant academic atmosphere at the conference. The pedagogical treatment discussed above is based on discussions in several well-known common books on quantum mechanics, such as those by Schiff, Arno Bohm, Greiner, and Landau and Lifshitz.

References

[1] Capria, Marco Mamone (Ed.) ‘*Physics Before and After Einstein*’ (IOS Press, 2005)

[2] Feynman, R.P. ‘*The Character of the Physical Law*’ (‘Messenger Lectures’ at Cornell University in 1964, published by Modern Library, 1994) http://www.youtube.com/watch?v=j3mhkYbznBk [Link downloaded on 2013-08-15]

[3] Wigner, E.P. ‘*Events, laws of nature, and invariance principles*’ (‘Nobel Lecture’ delivered on December 12, 1963 http://www.nobelprize.org/nobel_prizes/physics/laureates/1963/wigner-lecture.pdf [Link downloaded on 2013-08-15]

[4] Goldstein, H., Poole, C.P.(Jr.) and Safko, J.L. ‘*Classical Mechanics (3rd Edition)*’ Addison-Wesley; 3 edition (June 25, 2001)

[5] Modules 1 and 4 at the link → http://nptel.iitm.ac.in/courses/115106068/; [Link downloaded on 2013-08-15]

[6] Wigner, E.P. ‘The unreasonable effectiveness of mathematics in the natural sciences’ Richard courant lecture in mathematical sciences delivered at New York University on May 11, 1959, Communications on Pure and Applied Mathematics, Vol. 13, pages 1–14, (1960).

[7] Brading, Katherine and Castellani, Elena, "Symmetry and Symmetry Breaking", *The Stanford Encyclopedia of Philosophy* (Spring 2013 Edition), Edward N. Zalta (ed.), http://plato.stanford.edu/archives/spr2013/entries/symmetry-breaking/ [Link downloaded on 2013-08-15]

[8] Wigner, E.P. ‘*Symmetries and Reflections*’, (Bloomington, Indiana: Indiana University Press, 1967).

[9] Marie-Anne Bouchiat and Claude Bouchiat ‘*Parity violation in atoms*’ Rep. Prog. Phys. **60** 1351 (1997)

[10] B. E. Sauer , J. A. Devlin, J. J. Hudson, D. M. Kara, I. J. Smallman, M. R. Tarbutt and E. A. Hinds ‘*Time reversal symmetry violation in the YbF molecule*’Hyperfine Interact 214:119–126 (2013)

[11] P. C. Deshmukh, Dilip Angom and Alak Banik ‘*Symmetry in Electron-Atom Collision and Photoionization Process*’, DST-SERC-School publication (Narosa, November 2011); collection of articles based on lecture course given at the DST-SERC School at the Birla Institute of Technology, Pilani, January 9-28, 2011.

[12] P. C. Deshmukh and J. Libby ‘*Symmetry Principles and Conservation Laws in Atomic and Subatomic Physics’* Resonance, **15**, 832 (2010) and Resonance, **15**, 926 (2010)

[13] Pauli, W. Z.Phys. **36** 336-363 (1926)

[14] Casimir, H.B.G. Proc. Roy. Soc. Amsterdam **34** 844 (1931)

[15] Fano, U. and Rau, A.R.P. ‘*Theory of Atomic Collisions and Spectra*’, Academic Press, (1986)

[16] Jing-Ling Chen, Dong-Ling Deng, and Ming-Guang Hu, ‘*SO(4) symmetry in the relativistic hydrogen atom*’, Phys. Rev. A 77, 034102 (2008)

[17] http://nptel.iitm.ac.in/courses/115106057/6 ; [Link downloaded on 2013-08-17]

BOHR’S LEGACY

N. J. Mason
Department of Physical Sciences, The Open University, Walton Hall,
Milton Keynes. MK7 6AA, United Kingdom

1. INTRODUCTION

In 2013 we are celebrating the centenary of the publication of the Bohr model, depicting the atom as a small, positively charged nucleus surrounded by electrons that travel in circular orbits around the nucleus - similar in structure to the solar system, but with attraction provided by electrostatic forces rather than gravity. The model's key success lay in explaining the Rydberg formula for the spectral emission lines of atomic hydrogen. While the Rydberg formula had been known experimentally, it did not gain a theoretical underpinning until the Bohr model was introduced. Not only did the Bohr model explain the reason for the structure of the Rydberg formula, it also provided a justification for its empirical results in terms of fundamental physical constants.

This simple, easy to visualize model has thus become the normalized picture of the structure of the atom widely used in education as well as standardized in the media. The Bohr model is therefore still commonly taught to introduce students to atomic structure before moving on to the more accurate, but more complex, valence shell atom which has stronger basis in the underlying quantum mechanics that subsequently was shown to explain atomic structure.

Looking at the postulates upon which the theory is based, the first postulate seems reasonable on its own, acknowledging the existence of the atomic nucleus, established by the scattering experiments of Ernest Rutherford in 1911, and assuming classical mechanics. However, the other three postulates introduce quantum-mechanical effects, making the theory an uncomfortable union of classical and quantum-mechanical ideas. The second and third postulates seem particularly ad hoc. The electron travels in a classical orbit, and yet its angular momentum is quantized, contrary to classical mechanics. The electron obeys Coulomb's law of classical electromagnetic theory, and yet it is assumed to not radiate, as it would classically. Thus these postulates result in good predictions for the hydrogen atom, but they lack a solid fundamental basis.

Despite these limitations the development of the Bohr model is correctly seen as a ground breaking change in science heralding the birth of quantum mechanics which directly led to many of the great scientific advances of the last century. This legacy will now be briefly reviewed.

2. SPECTROSCOPIC LEGACY

The most immediate legacy of the Bohr model lay in the development of spectroscopic investigations of atomic and later molecular systems. Indeed the ‘Rydberg formula’ $E_n = E_i - R / (n - \delta)^2$, where E_i is the ionisation energy (IE_1) n is the principal quantum number of the Rydberg orbital of energy E_n, R is the Rydberg constant (13.61 eV), and δ the quantum defect resulting from the penetration of the Rydberg orbital into the core is still commonly used in the analysis of VUV spectra of molecular systems to identify and distinguish between Rydberg and valence states.

Figure 1 shows a typical VUV spectra recorded on the Astrid Synchrotron in Denmark. The VUV spectra of 1,4-pentadiene, C_5H_8 above 6.0 eV consists of a few structures superimposed on a diffuse absorption feature extending to the lowest ionisation energy (IE). The proposed Rydberg structures, labelled in Figure 1, are presented in Table 1. Quantum defects in the range 0.9-1.0, ~0.5, and 0.02-0.16 are expected for ns, np, and nd transitions, respectively. Such data is invaluable for developing spectroscopic based analytical techniques such as REMPI or LIF, in the former such Rydberg states are used as the ‘ladder’states for photo-ionisation of the molecule such that it can detected and concentrations evaluated in for example industrial or environmental environments separately from its isomer, isoprene which would be indistinguishable in direct electron ionisation as used in traditional mass spectroscopy.

Figure 1: Vibrational progressions and Rydberg series assignment in the 8.0 – 11.0 eV absorption band of 1,4-pentadiene, C_5H_8

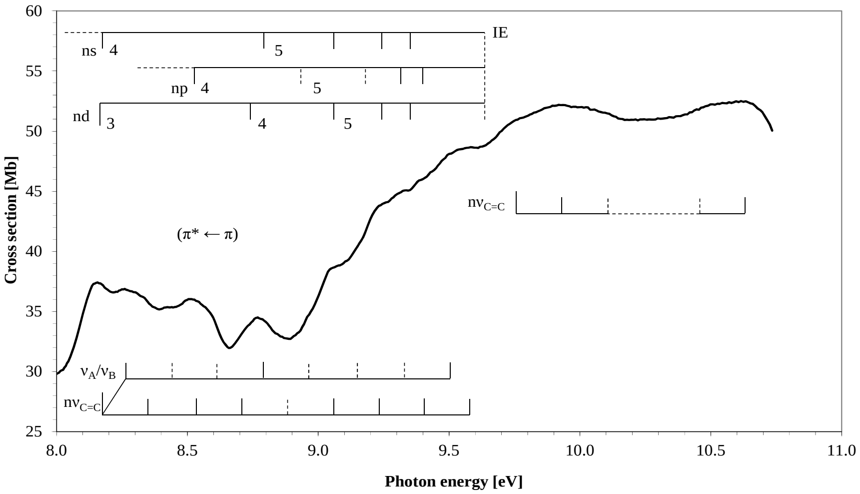

Table 1 – Energies (eV), quantum defects, and assignments of the ns, np and nd Rydberg series converging to the $\tilde{X}\,^2A$ ($9b^{-1}$) ionic electronic ground state of 1,4-pentadiene, C_5H_8

Vertical energy	Quantum defect (δ)	Assignment
IE_1=9.62eV$^{\alpha}$		
6.49(4) (s)	0.91	3s
8.157	0.95	4s
8.768	1.00	5s
9.043 (s)	1.14	6s
9.225 (s)	1.13	7s
9.336 (w)	1.07	8s
7.26(3) (s)	0.59	3p
8.509	0.50	4p
8.92(0) (w)	0.59	5p
9.16(4) (w)	0.54	6p
9.29(4) (s)	0.54	7p
9.37(8) (s)	0.50	8p
8.157	-0.05	3d
8.71(9) (s)	0.11	4d
9.04(3) (s)	0.14	5d
9.225	0.13	6s
9.336	0.08	7s

$^{\alpha}$ Vertical value. (s) Indicates a shoulder; (w) weak structure (the last decimal of the energy value is given in brackets for these less-resolved features).

3. COLLISION STUDIES

Within a year of Bohr's model being published it was also verified in the first electron- atom collision experiment, that of Frank and Hertz (F&H). By measuring the energy lost by an electron after collision with an atom F&H showed that kinetic energy from the electron was 'absorbed' by the atom in discrete amounts coincident with the excitation energy of specific excited states of the atom. Hence F&H not only validated the philosophy of the Bohr model but introduced the concept that by studying electron collisions it is possible to probe the spectroscopy of atoms and molecules. Today Electron Energy Loss Spectroscopy (EELS) is one of the most standard analytical technique. Figure 2 shows a representative example of an EELS spectra for electrons scattering from tetrahydrofuran (THF) revealing the vibrational excitation of the target by 10eV electron. Thus the F&H experiment which itself validated Bohr model opened a new field of science that of collision physics today the role of electron interactions with atoms and molecules is recognised as underpinning a wide range phenomena and is vital in many diverse industries.

***Figure 2; electron Energy loss spectrum of 10eV electrons scattered from tetrahydrofuran (THF) at an scattering angle of 110°. Vibrational excitation of the molecules is revealed*.**

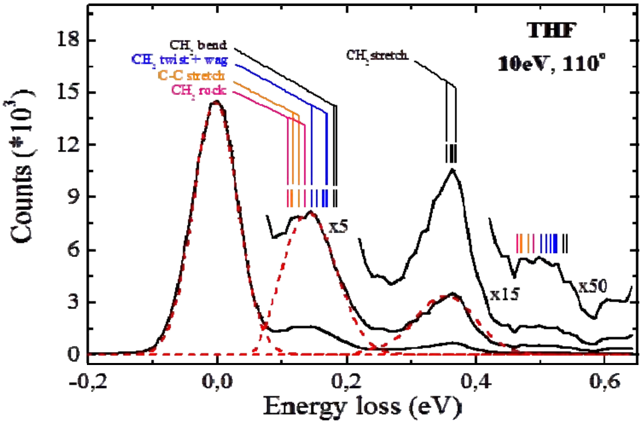

Electron induced reactions in both the gaseous and condensed phases initiate and drive many of the basic physical and chemical processes in science and technology with applications from industrial plasmas to radiation damage in living tissue. For example, in contrast to previous hypotheses, collisions of very low energy (sub-ionization) secondary electrons with the components of DNA molecules (or to the water around them) has been shown to be a crucial process in inducing radiation damage in the DNA of living systems. Understanding electron interactions with larger biomolecules is therefore providing new insights to radiation damage and thence the development of new, alternative radiotherapies. In the technological field electron induced reactions underpin most of the multibillion dollar modern semiconductor industry since it is those reactive fragments produced by electron impact of etchant gases that react directly with the silicon substrate. Studies on electron scattering from molecules capable of improving the etch rate of surfaces are leading to development of new (environmentally cleaner) plasma technologies. Electron induced processes are also of extraordinary importance for determination of structure and chemical reactivity of species adsorbed on surfaces. Indeed recently it has been demonstrated that, using STM based technology, discrete electron reactions may be performed at the individual molecular level thus introducing the prospect of designer synthesis on the nanoscale.

4. CONCLUSIONS

The publication of the Bohr model of the atom was a landmark in the development of modern science opening the door to the development of quantum mechanics and a host of experimental techniques. Although it was soon shown to be only an approximate solution and flawed in many ways its simplicity and ability to present an easily conceptualised picture of the atom ensures that it will continue to be taught and used for generations to come., It is therefore entirely fitting to celebrate the centenary of its publication and to reflect on the consequences of that seminal paper.

ELECTRON MOLECULE COLLISIONS USING QUANTEMOL

Will Brigg and Jonathan Tennyson
University College London

1. INTRODUCTION

Electron molecule collisions play an important role across many fields, ranging from the chemistry of the interstellar medium, to ionising radiation in the body and DNA damage. Where experiment cannot always provide cross sections - for a number of potential reasons - simulation can be the answer.

The Theory behind these simulations is based on the R-Matrix method; in which the calculation space is divided into two regions. An *Inner Region* - where the physics is complicated - and an *Outer Region* - where greatly simplified equations can be solved [1].

The collection of programs used to carry out these calculations is the UKRmol Suite [2]. The flexibility of the suite allows many different models to be utilised, each suited to different molecules, or for better calculating specific properties.

With this flexibility, also comes complexity. Quantemol Ltd aims to provide means of calculating these cross sections and properties to users who are not familiar with the codes. First, through simplifying the process by which a calculation is run - through the use of the Quantemol-N program; and second, by performing calculations in house for users and customers.

2. THEORY

The basics of the R-Matrix theory revolve around the division of space, and the calculation of complex interactions between all the target's electrons and the scattering electron, and then from the boundary between the inner and outer regions - where the target electronic density become zero - the propagation of the scattering electron wave function out to some larger distance, where asymptotic behaviour is found.

In the inner region, exchange and correlation effects are taken into account for all the electrons, the eigenfunctions of the total Hamiltonian as like so:

$$\Psi_k^{N+1}(x_1 \cdots x_{N+1}) = A\sum_{ij} a_{ijk}\Phi_i(x_1 \cdots x_N)u_{ij}\ (x_{n+1}) + \sum_i b_{ik}\chi_i(x_1 \cdots x_{N+1})$$

where A is the antisymmetry operator, $\Phi_i(x_1 \cdots x_N)$ are the target orbitals, and $u_{ij}\ (x_{n+1})$ the continuum orbitals where x_n are the spin coordinates of the n^{th} electron.

The continuum orbitals are generated by othogonalising a set of GTOs centered on the center of mass. GTOs are used to describe all the orbitals because it both simplifies the many integrations carried out in the procedure, and allows them to be calculated to a higher precision. The $\chi_i(x_1 \cdots x_{N+1})$ terms are known as the L^2 terms, they represent the short range correlation and polarisation effects. They are constructed from the target occupied, and virtual molecular orbitals.

By limiting the possible configurations, we obtain different models, which represent the target to varying degrees of accuracy. The simplest example of this is only including a single configuration - the ground state of the molecule. This is the static-exchange model. Expanding on this and including more configurations, we allow electronic excitation - the electrons may occupy all orbitals, each different excitation is a new configuration. On top of this, these can be augmented with more functions, which are not true eigenstates of the system - this is known as the *R-Matrix with Pseudo States* method (*RMPS*). The *pseudo states* are obtained by orthogonalising a set of orbitals created from an even tempered basis set centred on the centre of mass.

Using these wave functions, and their eigenvalues along with other information of the target, the *R-Matrix* is built. In the outer region, a single centre multipole expansion suffices, the R-Matrix is propagated out and matched to known asymptotic solutions. The size of the basis set used for the continuum determines the angular part of the partial wave expansion, which for most cases converges rapidly. If the molecule has a permanent dipole though, this is not the case, a Born correction is applied to account for missing higher partial waves [3].

Various matrices are created by the outer region modules of the code during the calculation - **K**, **T**, etc. - these can be easily extracted and used as inputs to other codes.

2.1 Quantemol-N

With the flexibility of the codes, comes complexity. This unfortunately can mean that it takes time to competently run the codes. Quantemol-N provides access to these codes, without the steep learning curve. The user simply needs to enter a few parameters using a graphical interface - the number of orbitals included in the model, the symmetry, basis set, etc. -and let the calculation run.

3. CONCLUSION

The R-Matrix method and the codes using them have many examples of their use, and many comparisons with experiment are available in the literature, with a list pertaining to many processes given in [2] (including, but not limited to elastic scattering, electron excitement, rotational excitement, dissociative attachment, dissociative recombination, impact dissociation and impact ionisation).

References

[1] Tennyson J., (2010), Phys. Rep. **491**, 2.
[2] Carr et al., (2012), Eur.Phys. J. D **66**, 58.
[3] Norcross et al., (1982), Phys. Rev. A **25**, 226.

COLLISION STUDIES OF NEGATIVE IONS WITH ATOMS USING CLASSICAL TRAJECTORY MONTE CARLO SIMULATION

David Joseph and Lalit Kumar Vatts
Optical Engineering Section, Department of Applied physics
Guru Jambheshwar University of Science and Technology,
Hisar- 125001, Haryana
E-mail: davdjp07@gmail.com

1. INTRODUCTION

The classical –trajectory Monte Carlo method has been widely used for ion-atom collisions. In this method classical equations of motion of a three (in some cases more) –body system are solved rigorously by numerical computations under randomly generated initial conditions that simulate quantum-mechanical distribution of initial states. Though CTMC is based on purely classical mechanics, it has been proven to be a powerful method that gives reliable cross sections for a variety of ionization and charge transfer processes. In our present problem the focus is on the charge exchange collisions of H^- with alkaline earth atoms (Ca, Mg) using Classical –Trajectory Monte Carlo Method [1-3].

CLASSICAL –TRAJECTORY MONTE CARLO METHOD

The method was chosen for a variety of reasons. It has the advantage of giving both the ionization and electron-capture cross sections consistently in the same calculation .Quantum theories are particularly difficult to apply in the region of collision velocities comparable to the orbital electron velocities of the target atom. However, all relevant quantum-mechanical theories based on the perturbation theory, finally, perturbation theories such as Born approximations are not really appropriate where strong interactions are involved such as in the case of a heavy multicharged ion colliding with a light, low –Z target. Nevertheless, the convergence of the perturbation series is an open question even at present.

2. THEORY

By averaging over many appropriately chosen three-dimensional trajectories, the Monte Carlo method has been successfully used to estimate the cross sections for chemical reactions. Pioneering work began with the study of the $H + H_2$ reaction by Hirschfelder et al. (1936). However, because the classical trajectories had to be calculated by hand, only one trajectory was undertaken in this early study. Since the advent of the computers, the classical trajectories method has become an extremely powerful technique for calculating cross section for chemical reactions and has been used quite successfully for calculating the charge exchange and ionization cross section.

We outline the approach used here in which the formulation is in terms of appropriate ***center-of –mass*** coordinates.

Hamilton's equations of motion for a three-body system are numerically solved for numerous trajectories. The impact parameter of projectile A colliding with target BC, and the orientation and momentum of C moving about B are randomly selected by Monte Carlo method.

A represents the H^+ or positive ion.

B represents the Ca^+ or Mg^+ target.

C represents the electron initially moving about Ca^+ or Mg^+.

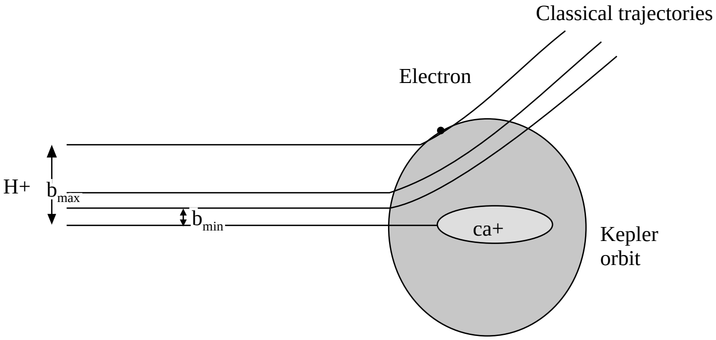

Collision of $H^{++} e^- + Ca^+$ with energy range 1 to 100 keV

This shows the electron capturing by proton in collision with Ca atom. The forces between the three bodies are taken to be coulombic. In the present work the interaction potential used to describe the interaction between target ionic core and the remaining electron (e−+ Ca+ and Mg+) is written as,

$$V(r) = -Z0/r + ((Z1 + Z2r)/r) \exp(-Z3r)$$

Where $Z0$, $Z1$, $Z2$, and $Z3$ are the parameters and r is the distance between the electron and the target core. The parameters given in Table 1, are chosen to give a correct asymptotic behavior of the potential at large and small values of r. Individual trajectories for the A+BC reaction are evaluated by placing A at large distance from BC and integrating the equations of motion until A is at large distance from B. If at the end of collision C is still in an orbit around B, then there was no reaction. However, if C is found bound to A, charge transfer occurred and is appropriately tabulated in the computer program. If C is found not bound either A or B, then ionization occurred during the collision.

THE FORMULATION OF THE METHOD

For the point masses m_a ,m_b and m_c with Cartesian coordinates C_j (j=1,2,3,……9) are generalized coordinate , where C_1 ,C_2 ,C_3 represent the Cartesian coordinates of particle C (electron) with respect to B(Ca^+). C_4 ,C_5 ,C_6 are the Cartesian coordinates of particle A(H^+) with respect to the center of mass of the pair, and C_7 ,C_8 ,C_9 are the Cartesian coordinates of the center of mass of the entire three-body System. Likewise, P_j (j=1,2,3……..9) represent the conjugate momenta that are coupled to the C_j coordinates.

Hamiltonian function H' for potential V (c_j) has the form: [4-6].

$$H' = \frac{1}{2m_A}\sum_{i=1}^{3} p_i^2 + \frac{1}{2m_B}\sum_{i=4}^{6} p_i^2 + \frac{1}{2m_C}\sum_{i=7}^{9} p_i^2 + v(q_1, q_2, \cdots q_n) \qquad (1)$$

P_i and q_i are the momenta and generalized coordinates $v(q_i)$ is the potential. Cartesian coordinates of the colliding partners after the collision have been used to determine the centre of mass scattering angle. The angular differential cross sections for the single electron capture were computed using the formula: [7,8].

$$d\sigma_{cap}/d\Omega \quad =2\pi\, b_{max}\Sigma_j\, b_j^{(i)}/\,(N\Delta\Omega)$$

and the standard deviation for the cross section is given by,

$$\Delta\sigma_{cap} = \sigma_{cap}((N - N_{cap})/\,(NN_{cap}))^{1/2}$$

N is the total number of trajectories calculated for an impact parameter less than *b*max. *Ncap* is the number of trajectories that satisfy the criteria for capture, $b_{(i)}^{j}$ is the impact parameter for which the criteria for capture is fulfilled and $\Delta\Omega$ is the emission solid angle interval of the captured electron.

The statistical error limit to a good approximation can be written as,

$$\Delta\sigma \approx \sigma/N^{1/2}{}_{cap}$$

4. RESULTS AND CONCLUSIONS

The CTMC simulation is being carried out for atomic collisions. The focus in the present study is on Negative ion – Atom collision processes. Differential cross section for single electron capture to all the states is calculated at different incident energies. Further studies are aimed at Laser Excited Targets.

References

[1] Pandey M. K., Dubey R. K., and Tripathi D. N., (2007), Eur. Phys. J. D **41**, 275.
[2] Perumal A. N. and Tripathi D. N., (2001), Phys. Rev. A **64**, 042709.
[3] Karpuls M., Porter R. N., and Sharma R. D., (1965), J. Chem. Phys **43**, 3259.
[4] Abrines R. and Percival I. C., (1966), Proc. Phys. Soc. **88**, 861.
[5] Abrines R. and Percival I. C., (1966), Proc. Phys. Soc. **88**, 873.
[6] Olson R. E. and Salop A., (1977), Phys. Rev. A. **16**, 531.
[7] Pascale J., Olson R. E., and Reinhold C. O., (1990), Phys. Rev. A **42**, 5305.
[8] Olson R. E. and Liu B., (1979), Phys. Rev. A **20**, 1366.

THEORETICAL TOTAL CROSS SECTIONS FOR METHANOL ON ELECTRON IMPACT

Minaxi Vinodkumar[1,*], Avani Barot[1], Chetan Limbachiya[2] and Nigel Mason[3]
[1]V. P. & R. P. T. P. Science College, V. V. Nagar - 388120, Gujarat, India
[2]P. S. Science College, Kadi - 382715, Gujarat, India
[3]Department of Physical Sciences, Open University, Milton Keynes, MK7 6AA, United Kingdom
Email: *minxivinod@yahoo.co.in

1. INTRODUCTION

Studies on electron impact with methanol have gained prominence in recent years since electron interactions with methanol are important in the understanding of energy and material balances in combustion plasmas and also in the chemistry of such species in terrestrial atmosphere. Moreover such collision data play pivotal role in modelling spark ignition in alcohol-fuelled internal combustion engines [1]. The interest in electron impact studies has also grown due to the discovery of presence of methanol in interstellar space and in the atmospheres of planets in the solar system supporting ionospheres. In addition, methanol is an intermediate size molecule that can serve as a benchmark for developing theoretical models of electron interaction with larger biomolecules [2].

In present work we report electron impact total cross sections (TCS) for methanol over an extensive range of impact energies circa from very low energy of 0.1 eV to high energy of 2000 eV. Inspecting the range of incident energy it is quite clear that a single theoretical formalism cannot be employed for the entire energy range hence we have partitioned the work in two prime energy regimes. Below 15 eV, we carried out *ab–initio* calculations with fixed nuclei approximation employing the UK molecular R–matrix method through Quantemol–N software [3] and above the threshold of the target we employ the well–established Spherical Complex Optical Potential (SCOP) formalism [4]. The two formalisms give consistent results at the transition energy (~11 eV) enabling us to provide the cross sections over such a wide range which will serve as an important data base.

2. THEORY

2.1. LOW ENERGY FORMALISM

We employed a double zeta plus polarization (DZP) basis set for the target wave function representation and Cs point group symmetry of the order four. The Quantemol–N modules GAUSPROP and DENPROP generate target properties and constructs the transition density matrix from the target eigenvectors obtained from configuration integration (CI) calculation.

R–matrix is the most widely used low energy electron collision method. It involves division of configuration space into two spatial regions namely the inner region and the outer region. The inner region accommodates the total wave function of the target plus scattering electrons. The short range potentials are dominant in this region e.g. static, exchange and correlation polarization potentials. In the outer region the only long range multipolar interactions between the scattering electron and the target are included. A single center approximation is assumed here enabling quick, simple and fast solutions in the outer region. The R-matrix radius is taken as $12a_o$.

For the inner region the total wave function for the system is expressed as,

$$\psi_k^{N+1} = A\sum_I \psi_I^N(x_1,\cdots,x_N)\sum_j \zeta_j(x_{N+1})a_{Ijk} + \sum_m \chi_m(x_1,\cdots,x_{N+1})b_{mk} \tag{1}$$

Where A is the anti-symmetrization operator, x_N is the spatial and spin coordinate of the n^{th} electron, ξ_j is a continuum orbital spin-coupled with the scattering electron and a_{Ijk} and b_{mk} are variational coefficients determined by the diagonalization of N+1 Hamiltonian in the calculation. The χ_m are multi-center quadratically integrable functions. The R-matrix provides the link between the inner region and the outer region.

2.2. HIGH ENERGY FORMALISM

We have used well-established SCOP formalism [5] which employs a partial wave analysis to solve the Schrödinger equation with various model potentials as its input.

$$V_{opt}(E_i,r)=V_{st}(r)+V_{ex}(r,E_i)+V_p(r,E_i)+iV_{abs}(r,E_i) \tag{2}$$

Here $V_{st}(r)$ is static potential, $V_{ex}(r,E_i)$ is exchange potential, $V_p(r,E_i)$ is polarisation potential and $V_{abs}(r,E_i)$ is an absorption potential. The basic input to calculate these potential is the spherically averaged molecular charge density which is determined using the constituent atomic charge densities using the Hartree Fock wave functions. The complex potential thus formulated is used to solve the Schrödinger equation numerically through partial wave analysis. This calculation will produce complex phase shifts for each partial wave which carries the signature of interaction of the incoming projectile with the target. At low impact energies only a few partial waves are significant, but as the incident energy increases more partial waves are needed for convergence. The phase shifts thus obtained are employed to find the relevant cross sections, total elastic (Q_{el}) and the total inelastic cross sections (Q_{inel}) the sum of which gives the total scattering cross section Q_T [6].

3. RESULT AND DISCUSSION

The results obtained from the two different methods *viz* the R–matrix method and the SCOP method, are consistent and there is a smooth transition at the overlap of the two formalisms. In Fig.1 we have shown TCS at low energy. CH_3OH being a polar molecule, Born correction is employed which leads to overestimation at low energies as is observed for Bouchiha et al. [2]. While agreement with Khakoo et al. [7] is seen at higher energies, good matching is observed with experiments [8-10] throughout the energy range.

Figure 1: Total Cross sections for e -CH_3OH scattering (low energy). Solid line: present Q-mol no Born results; Dash line: present Q-mol with the Born results; Short dash dot line: Bouchiha et al. [2] no Born; Short dash line: Bouchiha et al. [2] with the Born; Dotted line: Lee et al. [11]; dash dot line: Khakoo et al. [7]; Open Hexagons: Szmytkowski and Krzysztofowicz [8]; Solid Spheres: Sueoka et al. [9]; Open Squares: Schmieder [10]; and Astricks: Khakoo et al. [7].

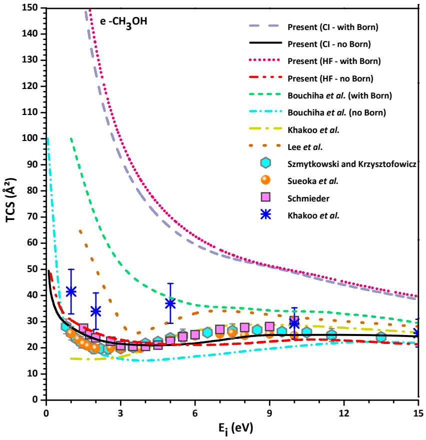

Figure 2: Total Cross sections for e -CH_3OH scattering. Solid line: present Q-mol results; Dash line: present SCOP results; Short dash dot line: Bouchiha et al. [2]; Short dash line: Lee et al. [6]; Dash dot line: Khakoo et al. [7]; Dash dot-dot line: Ming and Hua [12]; Open up Triangles: Sugohara et al. [13]; Open Diamonds: Silva et al. [14]; Ashtricks: Khakoo et al. [7]; Open Hexagons: Szmytkowski and Krzysztofowicz [8]; Solid Spheres: Sueoka et al. [9] and Open Squares: Schmieder [10].

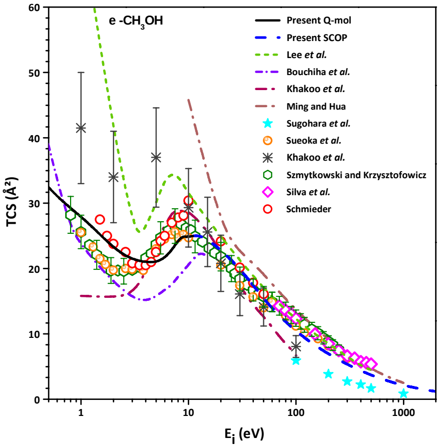

In Fig. 2 the consistency of data from R-matrix and SCOP at the transition energy (11 eV) is shown. The values of Ming and Hua [12] are very high compared to all the other data below 20 eV due to additivity as used by them. The results of Lee et al. [11] are in very good agreement with the present results beyond 20 eV. The computed values of Khakoo et al. [7] are slightly higher around threshold but beyond the threshold their values are in better agreement. The experimental results [6, 8-10] show good agreement with present data. The values of Sugohara et al. [13] are lower than the other data.

4. CONCLUSION

We have performed close coupling calculations (at static, exchange plus polarization level) employing the UK molecular R-matrix code below ionization threshold of the target while the SCOP formalism is used beyond it. The results using these two formalisms are consistent and show a smooth transition at the overlap energy (~11 eV) confirming the validity of our theories and hence enabling us to predict the total cross sections from low energy of 0.1 eV to high energy 2000 eV.

Our results are in good agreement with available data throughout the energy range. Therefore, we are confident that this methodology may be employed further to calculate total cross sections over a wide range of energy.

ACKNOWLEDGEMENT

MVK acknowledges DST, New Delhi for major research project (SR/S2/LOP/26-2008) and CGL thank UGC, New Delhi for major research project (F.No.40-429/2011 (SR)) for financial support under which part of this work is carried out. NJM recognizes support from the EU Framework programme for the development of the VAMDC e-infrastructure.

References

[1] Block B., Moser P., and W. Hentschel, (1997), *Opt. Eng.* **36,** 1183.

[2] Bouchiha D., Gorfinkiel J. D., Caron L. G., and L. Sanche, (2007), *Low-energy electron collisions with methanol.* J. Phys. B: At. Mol. Opt. Phys. **40,** 1259.

[3] Tennyson J., (2010), *Electron-molecule collision methods using R-Matrix method.* **491,** 29.

[4] Jain A. and Baluja K. L., (1992), *Total (elastic plus inelastic) cross sections for electron scattering from diatomic and polyatomic molecules at 10–5000 eV:* H_2, Li_2, *HF*, CH_4, N_2, *CO*, C_2H_2, *HCN*, O_2, *HCl*, H_2S, PH_3, SiH_4, *and* CO_2. Phys. Rev. A 45, 202.

[5] Vinodkumar M., Limbachiya C., Korot K., and Joshipura K. N., (2008), *Theoretical electron impact elastic, ionization and total crosssections for silicon hydrides,* SiH_x *(x = 1, 2, 3, 4) and disilane,* Si_2H_6 *from threshold to 5 keV*; Euro. Phys. J. D **48,** 333.

[6] Vinodkumar M., Joshipura K. N., Limbachiya C., and Antony B. K., (2006), *Electron impact total and ionization cross-sections for some hydrocarbon molecules and radicals.* Eur. Phys. J. D **37**, 67.

[7] Khakoo M. A., Blumer J., Keane K., Campbell C., Silva H., Lopes M. C. A., Winstead C., McKoy V., da Costa R. F., Ferreira L. G., Lima M. A. P., and

Bettega M. H. F., (2008), *Low-energy electron scattering from methanol and ethanol.* Phys. Rev. A **77,** 042705.

[8] Szmystkowski Cz. and Krzysztofowicz A. M., (1995), *Electron scattering from isoelectronic, N_e=18, CH_3X molecules (X = F, OH, NH_2 and CH_3).* J. Phys. B: At. Mol. Opt. Phys. **28,** 4291.

[9] Sueoka O., Katayama Y., and Mori S., (1985), At. Coll. Res. Jpn. Prog. **11,** 17.

[10] Schmieder F., (1930), *Z. Elektrochem. Angew.* Phys. Chem. **36**, 700.

[11] Lee M.-T., de Souza G. L. C., Machado L. E., Brescansin L. M., dos Santos A. S., Lucchese R. R., Sugohara R. T., Homem M. G. P., Sanches I. P., and Iga I., (2012), *Electron scattering from methanol and ethanol: A joint theoretical-experimental investigation.* J. Chem. Phys. **136,** 114311.

[12] Ming T. and Hua W., (2011), *Total cross sections for electron scattering from CH_3OH and CH_3CH_2OH molecules in the energy range from 10 to 1000 eV.* Nuclear Instruments and Methods in Physics Research B **269,** 1094.

[13] Sugohara R. T., Homem M. G. P., Sanches I. P., de Moura A. F., Lee M. -T., and Iga I., (2011), *Cross sections for electron scattering by methanol in the intermediate-energy range.* Phys. Rev. A **83,** 032708.

[14] Silva D. G. M., Tejo T., Muse J., Romero D., Khakoo M. A., and Lopes M. C. A., (2010), *Total electron scattering for methanol and ethanol at intermediate energies.* J. Phys. B: At. Mol. Opt. Phys. **43,** 015201 (2010).

ELECTRON IMPACT TOTAL CROSS SECTION FOR ETHANOL

Avani Barot[1] and Minaxi Vinodkumar[1]
[1]V. P. & R. P. T. P. Science College, Vallabh Vidyanagar - 388 120, Gujarat, India
E-mail: [1]minaxivinod@yahoo.co.in

1. INTRODUCTION

The discovery of small alcohols in the interstellar space and in the atmospheres of Planets in the solar system has motivated theoreticians as well as experimentalists to study the electron interaction with them. Further, in future concentration of the small alcohols in the atmosphere are expected to increase due to their use in renewable energy sources. Theoretically electron impact total cross sections (TCS) are reported by Khakoo et al. [1], Lee et al. [2] and Ming and Wang [3] and experimentally the data are reported by, Khakoo et al. [1], Lee et al. [2], Silva et al. [4] and Schmieder [5] Present work reports electron impact total cross section for ethanol over a wide range of impact energies from 1 eV to 2000 eV.

2. THEORY

The present calculations employ two distinct methodologies, namely the R–matrix [6] and the SCOP [7], which are appropriate in two distinct regimes of impact energies, one below the ionization threshold of the target and the other above it. The main task in the present scattering calculation lies in the solution of time independent Schrodinger equation. For this the inner region wave function is constructed using close coupling approximation. For the inner region the total wave function for the system is expressed as,

$$\psi_k^{N+1} = A\sum_I \psi_I^N\left(x_1,\cdots,x_N\right)\sum_j \zeta_j(x_{N+1})a_{Ijk} + \sum_m \chi_m(x_1,\cdots,x_{N+1})b_{mk} \qquad (1)$$

Where, A is the anti-symmetrization operator that takes care of exchange effect, x_N is the spatial and spin coordinate of the nth electron, ξ_j is a continuum orbital spin-coupled with the scattering electron and a_{Ijk} and b_{mk} are variational coefficients determined by the diagonalization of N+1 Hamiltonian in the calculation. The accuracy of the calculation depends solely on the accurate construction of this wave function given in equation (1). The complete molecular orbital representation in terms of occupied and virtual target molecular orbitals are constructed using the Hartree–Fock Self–Consistent Field method with Gaussian–type orbitals (GTOs) and the continuum orbitals of Faure et al. [8] and include up to g (l = 4) orbitals. For low partial waves $(l \leq 4)$ T matrices computed from the R–matrix calculations are employed to compute the cross sections. The R-matrix is propagated to an asymptotic region where the radial wave-functions describing the scattering electron can be matched to analytical expressions. Coupled single centre equations describing the scattering in the outer region are integrated to identify the K–matrix elements. The high energy calculations are done using Spherical Complex Optical Potential formalism. The details of this methodology are available in our earlier publications and hence not repeated here [9-12].

3. RESULT AND DISCUSSION

In the present work, we have performed a comprehensive computation of the total cross sections for electrons colliding with ethanol in the gas phase. The calculations were carried out using the fixed–nuclei static–exchange–polarization approximation at the equilibrium geometry of the ground-state of e -C_2H_5OH. The *ab-initio* calculations are computationally viable only up to around 20 eV, while the SCOP formalism could be employed successfully from threshold of the target to 2000 eV. The results obtained from the two different methods are consistent and there is a smooth transition at the overlap of the two formalisms. Thus, it is possible to provide the total cross section over a wide range of impact energies from meV to keV. The results are provided vide Figure 1.

Figure. 1: Total cross section for e –C_2H_5OH. Solid line: Present Q-mol results; Dash line: Present SCOP results; Dash-Dot-Dot line: Khakoo et al. (SEP) [1]; Short Dash-Dot line: Khakoo et al. (SE) [1]; Short Dash line: Lee et al. [2]; Dash-Dot line: Tan and Wang [3]; Ashtrick: Khakoo et al. [1]; Open Star: Lee et al. [2]; Solid Sphere: Silva et al. [4] and Open Square: Schmieder [5].

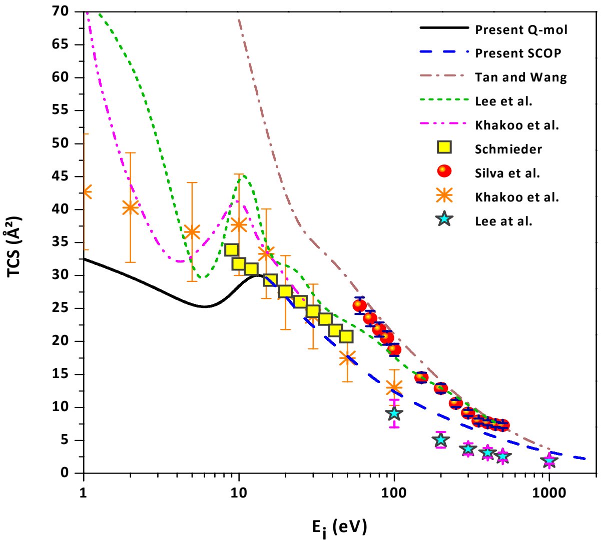

Figure 1 shows comparison of the present data for e -C_2H_5OH scattering with previously available data. Present data finds excellent agreement with experimental data of Khakoo et al. [1] above 10 eV, while below it they are high compared to present data. This may be attributed to the difficulty in measuring the differential cross section at low energy. The experimental data of Lee et al. [2] are lower compared to present data as expected as they represent total elastic cross section. The experimental data reported by Schmieder [5] finds very good accord with present data except a few data at low eV below 8 eV. The measurements of Silva et al. [4] are slightly higher compared to present data. Theoretical results of Tan and Wang [3] are highest compared to all data presented here as they have used revised additivity rule. Lee et al. [2] have employed complex optical potential and computed total cross sections. Their data are higher compared to present data throughout the energy range.

4. CONCLUSION

Present results are in general good agreement with available data above 10 eV while below it they are lower compared to all other data. A good transition is observed in the data computed through two different methodologies viz. R-matrix and SCOP. Therefore, we are confident that this methodology may be employed further to calculate total cross sections over a wide range of energy can be used to compute total cross sections for exotic targets where experiments are difficult. Such total cross section data is important in a variety of applications from aeronomy to plasma modeling. Accordingly such a methodology maybe built into the design of online database to provide ‘data users’ with the opportunity to request their own set of cross sections for use in their own research.

References

[1] Khakoo M. A., Blumer J., Keane K., Campbell C., Silva H., Lopes M. C. A., Winstead C., McKoy V., da Costa R. F., Ferreira L. G., Lima M. A. P., and Bettega M. H. F., (2008), *Low-energy electron scattering from methanol and ethanol.* Phys. Rev. A 77, 042705.

[2] Lee M.-T., de Souza G. L. C., Machado L. E., Brescansin L. M., dos Santos A. S., Lucchese R. R., Sugohara R. T., Homem M. G. P., Sanches I. P., and Iga I., (2012), *Electron scattering from methanol and ethanol: A joint theoretical-experimental investigation.* J. Chem. Phys. **136,** 114311.

[3] Ming T. and Hua W., (2011), *Total cross sections for electron scattering from CH_3OH and CH_3CH_2OH molecules in the energy range from 10 to 1000 eV.* Nuclear Instruments and Methods in Physics Research B **269,** 1094.

[4] Silva D. G. M., Tejo T., Muse J., Romero D., Khakoo M. A., and Lopes M. C. A., (2010), *Total electron scattering for methanol and ethanol at intermediate energies.* J. Phys. B: At. Mol. Opt. Phys. **43,** 015201 (2010).

[5] Schmieder F., (1930), *Z. Elektrochem. Angew.* Phys. Chem. **36**, 700.

[6] Tennyson J., (2010), *Electron-molecule collision methods using R-Matrix method.* **491,** 29.

[7] Jain A. and Baluja K. L., (1992), *Total (elastic plus inelastic) cross sections for electron scattering from diatomic and polyatomic molecules at 10–5000 eV: H_2,*

Li_2, HF, CH_4, N_2, CO, C_2H_2, HCN, O_2, HCl, H_2S, PH_3, SiH_4, and CO_2. Phys. Rev. A 45, 202.

[8] Faure A., Gorfinkiel J. D., Morgan L. A., and Tennyson J., (2002), GTOBAS: fitting continuum functions with Gaussian-type orbitals Comput. Phys. Commun.**144,** 224.

[9] Vinodkumar M., Limbachiya C., Barot A., and Mason N., (2013), *Comprehensive computation of electron impact rotationally elastic total cross sections for methanol over an extensive range of impact energy (0.1 to 2000 eV).* Phys. Rev. A **87,** 012702.

[10] Vinodkumar M., Limbachiya C., Barot A., and Mason N., (2012), *Theoretical total cross sections for e -SO_2 scattering over a wide energy range (0.1−2000 eV) revealing a 3.4-eV shape resonance.* **86,** 012706.

[11] Vinodkumar M., Barot A. and Antony B., (2012), *Electron impact total cross sections for acetylene over an extensive range of impact energies (1 eV–5000 eV),* J. Chem. Phys. **136**, 184308.

[12] Vinodkumar M. and Barot M., (2012), *Scattering of N_2O on electron impact over an extensive energy range (0.1 eV – 2000 eV).* J. Chem. Phys. **137**, 074311.

ELECTRON IMPACT TOTAL CROSS SECTION FOR F_2O OVER A WIDE RANGE OF IMPACT ENERGIES (0.1-2000 eV)

Dhanoj Gupta and Bobby Antony
Department of Applied Physics, Indian School of Mines, Dhanbad – 826004, Jharkhand, India

1. INTRODUCTION

Electron impact collision cross section database over a wide range of impact energies are required to model and underpin the interactions in various applied fields of plasma physics, semiconductor industry, atmospheric sciences, radiation damage and therapy. Total cross section data are useful for the study of electron transport properties in gases, as the sum of all possible collision defines a mean free path [1]. The present study focuses on scattering of F_2O molecule by electron impact. The only e-F_2O scattering calculation is done by Gupta and Baluja [2] using R-matrix method. Their calculation is confined up to 15 eV only. In the present study, the calculation is done over a wide energy range from 0.1 eV to 2 KeV.

2. THEORY

In the present study we have made use of two distinct formalisms to calculate the total cross section for a wide energy range from 0.1 eV to 2000 eV. For low energies the R-matrix method through Quantemol-N [3] software and from ionization threshold up to 2 KeV Spherical Complex Optical Potential SCOP [4] is employed. For a detailed discussion on the theories refer to our previous articles [3, 4]. However, it is imperative to discuss the target model used for low energy calculation, since its correct representation assures reliable cross section data.

2.1 Target model for low energy calculation

F_2O is a bent molecule with a bond length of 1.412 Å and F-O-F bond angle of 103.167^0 [5]. For the target wave function we have employed double zeta plus polarization (DZP) Gaussian basis set. It belongs to C_{2V} point group symmetry of order 4. The ground state electronic configuration for F_2O is $1b_2^2\ 1a_1^2\ 2a_1^2\ 3a_1^2\ 2b_2^2\ 4a_1^2\ 1b_1^2\ 5a_1^2\ 3b_2^2\ 1a_2^2\ 4b_2^2\ 6a_1^2\ 2b_1^2$. Out of 26 electrons 6 are frozen in $1a_1\ 2a_1\ 1b_2$ molecular orbitals while 20 electrons are kept in active space of $3a_1\ 4a_1\ 5a_1\ 6a_1\ 7a_1\ 1b_1\ 2b_1\ 2b_2\ 3b_2\ 4b_2\ 5b_2\ 1a_2$ orbitals. 16 target states were represented by 480 configuration state functions (CSFs). The number of channels included in the calculation was 100. The target properties generated using the above inputs are tabulated in table 1 along with available comparison.

Table 1: Target properties

Target properties	Present	Others
First excitation energy (eV)	4.13	4.21 [2]; 3.82 [6]
Ground state energy (Hartee)	-273.62	-273.52 [2]
Dipole moment (a.u)	0.11	0.224 [2]; 0.297 [5]
Rotational constant (cm^{-1})	1.94	1.96 [5]

Figure. 1. **Total cross section for e-F_2O scattering with available data.**

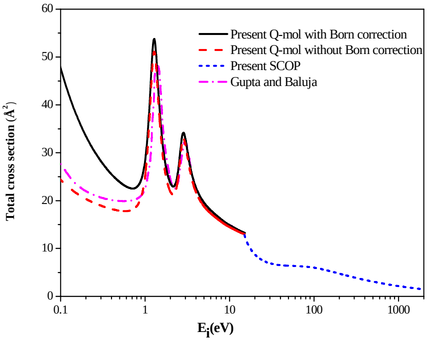

3. RESULT AND DISCUSSION

In Fig. 1 we have plotted the results of total cross section for e-F_2O scattering with cross section along y-axis in $Å^2$ and energy in eV along x-axis (in logarithmic scale) along with available comparison of Gupta and Baluja [2] at low energy. The shape resonance predicted by Gupta and Baluja [2] at 1.4 eV and 2.8 eV are very well reproduced by our calculation at 1.24 eV and 2.69 eV. The total cross section after ionization threshold is computed for the first time which gives a complementary result at the overlap of two formalism and has helped us to predict cross section for a vast energy range.

4. CONCLUSION

We have successfully employed R-matrix method through Quantemol-N software for low energy calculation upto 15 eV and the high energy calculation are done with SCOP formalism. The high energy calculation is a maiden attempt. The two methodologies matches fairly well at the transition point. The present study confirms the results of Gupta and Baluja [2] and also shows the swiftness and reliability of the Quantemol-N/SCOP with which it produces cross section and other results in real quick time. Hence, this particular hybrid methodology may be integrated to other systems where there is scarcity of data. We hope the present study will motivate the experimentalist and theoreticians to do more study on this particular target.

References

[1] Vieira P. L., Blanco F., Oller J. C., Munoz A., Perez J. M., Vinodkumar M., Garcia G. and Mason N. J., (2005), *Electron scattering cross section for* SF_6 *and* SF_5CF_3 *at intermediate and high energies (100-10000 eV)*. Phys. Rev. A **71**, 032720.

[2] Gupta M. and Baluja K. L., (2006), *Electron –*F_2O *collision study using the R –matrix method*. Phys. Rev. A **74**, 052713.

[3] Vinodkumar M., Barot A. and Antony B., (2012), *Electron impact total cross section for acetylene over an extensive range of impact energies (1 eV–5000 eV)*, J. Chem. Phys. **136**, 184308.

[4] Naghma R., Mahato B. N., Vinodkumar M. and Antony B. K., (2011), *Electron impact total ionization cross section for atoms with z = 49-54*. J. Phys. B: At. Mol. Opt. Phys. **44,** 105204.

[5] Website: http://cccbdb.nist.gov/.

[6] Valenta K. E., Vasudevan K. and Grein F., (1980), *Ab intio studies of the geometry, electronic spectrum, and vertical ionization potentials of oxygen difluoride (*F_2O*)*. J. Chem. Phys. **72**, 2148.

CALCULATED ELECTRON IMPACT TOTAL IONISATION CROSS SECTIONS FOR FURAN MOLECULES

Mohit Swadia[1,*], Chetan Limbachiya[1], Minaxi Vinodkumar[2],
K. N. Joshipura[3]
[1]P.S. Science & H. D. Patel Arts College, Kadi, Gujarat (India)
[2]V.P. & R.P.T.P. Science College, Vallabh Vidyanagar, Gujarat (India)
[3]Department of Physics, Sardar Patel University, V. V. Nagar, Gujarat (India)
Email: *mohit4physics@gmail.com

1. INTRODUCTION

Recent studies of radiation induced damage to DNA have demonstrated that single-strand and double-strand breaks in DNA by secondary low energy electrons (below 20 eV), play a dominant role for the understanding of the damage effects in living cells and tissues. This has stimulated strong interest concerning the scattering of electrons by biologically relevant molecules. Much ongoing effort has been undertaken by theoretical and experimental groups to provide a deeper insight into the mechanisms related to the radiation damage of DNA, which includes both direct processes (ionization, electronic, rotational, and vibrational excitations) as well as compound processes such as resonances (dissociation and dissociative electron attachment) [1]. In this paper we report the electron induced total ionisation cross sections for Furan. We have employed Spherical Complex Optical Potential (SCOP) formalism [2] to calculate total elastic cross sections Q_{el}, total inelastic cross sections Q_{inel} and have used Complex Scattering Potential – ionization contribution (CSP-ic) method [2] to extract ionization cross sections, Q_{ion}, from the calculated Q_{inel}. The calculated total cross sections are examined as functions of incident electron energy and are compared with the lone available measurements of Szmytkowski [3]. We also have calculated the Q_{ion} using the BEB method [4]. Overall good agreement is observed.

2. THEORY

The SCOP formalism provides Q_{el} and Q_{inel} such that,

$$Q_T(E_i) = Q_{el}(E_i) + Q_{inel}(E_i) \tag{1}$$

We have deduced the Q_{ion} from Q_{inel} using Complex Scattering Potential-ionization contribution (CSP-ic). We define the following energy dependent ratio of cross sections,

$$R(E_i) = \frac{Q_{ion}(E_i)}{Q_{inel}(E_i)} \qquad \text{such that } 0<R\lesssim 1 \qquad (2)$$

This dynamic ration is found to be,

$$R(E_i)\begin{cases} = 0 \; for \; E_i \leq I \\ = R_P \; at \; E_i = E_P \\ \cong 1 \; for \; E_i \gg E_P \end{cases} \qquad (3)$$

Here, R_p is the value of R at $E_i = E_p$ where E_p stands for the incident energy at which, the Q_{inel} attains its maximum value.

3. RESULT AND DISCUSSION

Present SCOP-CSP-ic results show overall good agreement with the measured data [3] except at the peak region. The present BEB results are in excellent agreement with the experimental results [3] throughout the energy range.

Figure 1: Total Ionisation Cross sections of e- Furan. Solid line-Present Q_{ion} (SCOP), dashed lines- Present Q_{ion}(BEB), Square- Q_{ion} by Szmytkowski et al. [3].

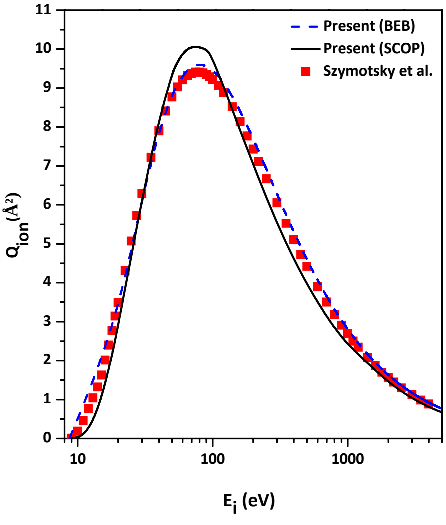

4. CONCLUSION

The study of furan and other 5 member ring structures such as Tetrahydrofuran may be taken up using SCOP – CSP-ic formalism.

ACKNOWLEDGEMENT

Chetan Limbachiya thanks UGC (F.No.40-429/2011 (SR)) and Minaxi Vinodkumar thanks DST (SR/S2/LOP-26/2008) for major research projects.

References

[1] Khakoo et al., (2010), *Low-energy elastic electron scattering from furan*; Phys. Rev. A **81**, 062716.

[2] Vinodkumar et al., (2013), *Electron impact total ionization cross sections for all the components of DNA and RNA molecule;* IJMS; DOI: 10.1016/j.ijms.2013.01.004.

[3] Szmytkowski et al., (2010), *Cross sections for electron scattering from furan molecules: Measurements and calculations;* Phys. Rev. A **82**, 032701.

[4] Kim Y. K. and Rudd M. E., (1994), *Binary-encounter-dipole model for electron-impact ionization*. Phys. Rev. A **50**, 3954.

TOTAL CROSS SECTIONS ON ELECTRON IMPACT FOR H_2 MOLECULE

K. M. Korot[a], A. Y. Barot[b], H. S. Bhutadia[c] and M. Vinodkumar[b]
[a]Government Engineering College, Modasa
[b]V. P. & R. P. T. P. Science College, Vallabh Vidyanagar
[c]Government Engineering College, Patan

1. INTRODUCTION

Molecular hydrogen, H_2, is the simplest molecule in nature. It is the most abundant molecule in universe, particularly in interstellar space. It is also the main constituent in the atmospheres of the outer planets. Plasmas containing H_2 are widely used in plasma technology for applications such as thin film deposition and material treatment. The H_2 plasma is a source of positive (H^+) and negative (H^-) ion beams. H_2 is known to be abundant in the edge region of fusion devices. The behaviour of H_2 in the edge plasma is crucial in the understanding of the boundary condition, and hence the plasma-wall interaction, in the fusion plasma [1].

H_2, has been studied widely overall impact energies considered here. Experimental results are reported by: Randell et al. (0.03–0.15 eV) [2], Ferch et al. (0.02–1.5 eV) [3], Subramanian and Kumar (0.21-9.14 eV) [4], Szmytkowski et al. (0.4–250 eV) [5], R. K. Jones (1–50 eV) [6], Deuring et al. (6–100 eV) [7], Hoffman et al. (20-500 eV) [8], while theoretical data are reported by Jain et al. (10-2000 eV) [9] and reccomonded data by Karwasz et al. (0.1-1000 eV) [10].

Presently we have made use of the R-matrix based Quantemol-N softwere and spherical complex optical potential (SCOP) to evaluate total cross-sections.

2. THEORY

The present calculations rest on two distinct methodologies which are well established in two regimes of impact energies, one below the ionization threshold of the target and other above it. Below ionization threshold of the target we employ *ab initio* calculations using R-matrix formalism [11] through Quantemol-N [12] software. Above this incident energy we have used the SCOP formalism [13] to compute the total cross section.

2.1. Low energy calculations

The accuracy of collision data depends on the accuracy with which we can represent the target wave function. Hence, it is imperative to have an appropriate target model.

For H_2, the present calculations were performed in the reduced symmetry D_2h sub-group and the target state was represented in the ground state by $1ag^2$. The Basis set is defined using EMSL (Environmental Molecular Sciences Laboratory) *Gaussian Basis Set Order Form* 2009 [14]. Full CI has been used for the calculation of this molecule with only 2 electrons. 12 target states were employed in the close-coupling expansion method for scattering calculations.

Using the Quantemol-N softwere the total cross sections are calculated for energy regime starting from 0.01 to 15 eV. The Quantemol-N software makes use of *ab initio* R-Matrix code. The *ab-initio* R-matrix method relies on the division of configuration space into two spatial regions namely inner region and the outer region. In the inner region calculation the wave function has been constructed using the close-coupling (CC) approximation which can be written as,

$$\psi_k^{N+1} = A\sum_I \psi_I^N\left(x_1,\cdots,x_N\right)\sum_j \zeta_j(x_{N+1})a_{Ijk} + \sum_m \chi_m(x_1,\cdots,x_{N+1})b_{mk} \tag{1}$$

where all the terms have their usual meaning and given in ref. [15,16]. The R-matrix has been used to obtain T-matrices which in turn give various total cross sections. The details of theory can be found in our previous publications [15,16].

2.2. High energy calculations

Since Quantemol-N makes use of R-Matrix code, it has the limitation that it can only calculate accurate cross sections below the ionization threshold of the molecule being considered. Beyond the ionization threshold of the target the scattering calculations are carried out using the well-established Spherical Complex Optical Potential (SCOP) formalism [17,18].

In the SCOP method, the spherical part of the complex optical potential is treated exactly in the partial wave analysis. The complex potential calculation for electron scattering provides total elastic cross sections, Q_{el} and its counterpart total inelastic cross sections, Q_{inel} such that the total scattering cross section (TCS) is given by,

$$Q_T\left(E_i\right) = Q_{el}\left(E_i\right) + Q_{inel}\left(E_i\right) \tag{2}$$

3. RESULTS

The theoretical approach adopted here can be divided into two parts, one using the Quantemol-N formalism up to ionization threshold of the target (~15 eV) and the other using the SCOP formalism beyond 15 eV. The present results for molecular hydrogen are shown in Figure 1 along with available experimental and theoretical comparisons. The present results are also tabulated in table 1 for ready reference.

Table 1: Total (complete) cross sections for H_2 in Å^2

E_i (eV)	Q_T	E_i (eV)	Q_T	E_i (eV)	Q_T
0.01	9.88	15	7.54	100	2.23
0.05	10.41	20	6.09	200	1.26
0.1	10.81	25	5.30	300	0.87
0.5	12.02	30	4.75	500	0.54
1	12.90	35	4.34	800	0.34
5	13.97	45	3.75	1000	0.27
10	10.08	50	3.53	2000	0.14

The present results are higher below 1 eV and are lower by ~10% at the peak position than other experimental investigations [2-8]. Above 5 eV present results are in very good accord with all the experimental data. The theoretical calculations of Jain [9] are lower than present results up to 50 eV & beyond 50 eV they are in very good agreement with the present results. The shape of the Jain [9] data curve is similar to the present results. The present results are also compared with the reccomonded data of Karwasz et al. [10] and at higher energies good agreement is observed.

Figure 1: Total (complete) cross sections for e –H_2 scattering. Solid line → Present Q_T using Qmol; Dashed line → Present Q_T using SCOP; Solid Circles → Randell et al. [2]; Diamonds → Ferch et al. [3]; Solid squres → Subramanian and Kumar [4]; Stars → Szmytkowski et al. [5]; Estrick → R. K. Jones [6]; Up Triangles → Deuring et al. [7]; Open Circles → Hoffman et al. [8]; Short dashed Dot → Jain [9]; Dashed Dot → Karwasz et al. [10].

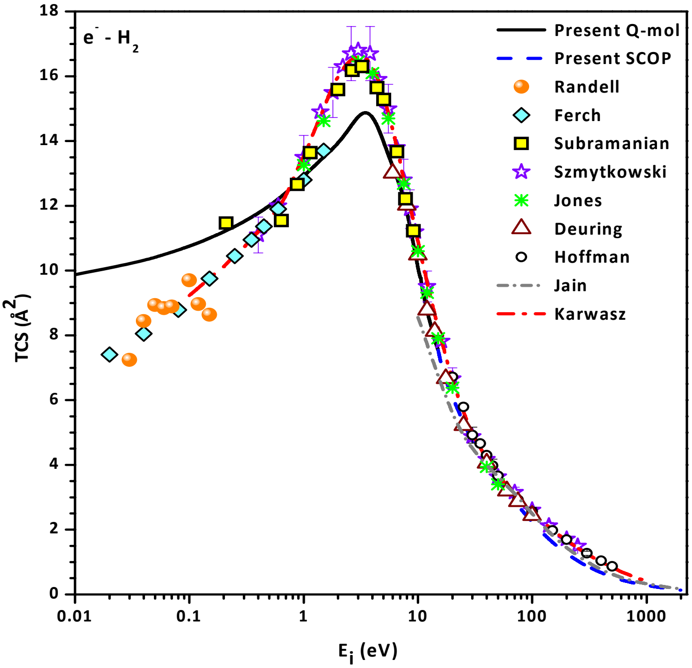

4. CONCLUSION

It is observed that in general there is good agreement between the present results and all the available data over the entire incident energy range. It should be noted that the results obtained using the two methods (Quantemol-N and SCOP) match remarkably well at the interface while maintaining the shape and slope of the curve. Moreover, whilst there are minor discrepancies at 15 eV where the two methods overlap, these are well within the experimental error bars and therefore the composite calculation is capable of providing a data set that is self-consistent and able to produce a reliable total scattering cross sections.

References

[1] Yoon J. S., Song M. Y., Han J. M., Hwang S. H., Chang W. S., Lee B. J., and Itikawa Y. (2008), *Cross Sections for Electron Collisions with Hydrogen Molecules*. J. Phys. Chem. Ref. Data **37,** 913.

[2] Randell J., Lunt S. L., Mrotzek G., Ziesel J. P., and Field D., (1994), *Low energy electron scattering in H_2, N_2 and O_2*; J. Phys. B: At. Mol. Opt. Phys **27** 2369.

[3] Ferch J., Raith W., and Schroder K., (1980), *Total cross section measurements for electron scattering from molecular hydrogen at very low energies*. J. Phys. B: At. Mol. Opt. Phys **13,** 1481.

[4] Subramanian K. P. and Kumar V., (1989), *Total electron scattering cross sections for molecular hydrogen at low electron energies*. J. Phys. B: At. Mol. Opt. Phys **22** 2387.

[5] Szmytkowski C., Maciag K., and Karwasz G. P., (1996), *Absolute electron-scattering total cross section measurements for noble gas atoms and diatomic molecules*; Phys. Scr. **54,** 271.

[6] Jones R. K., (1985), *Absolute total cross section for electron scattering from molecular hydrogen from 1 to 50 eV*. Phys. Rev. A **31,** 2898.

[7] Deuring A., Floeder K., Fromme D., Raith W., Schwab A., Sinapius G., Zitzewitz P. W., and Krug J., (1983), *Total cross section measurements for positron and electron scattering on molecular hydrogen between 8 and 400 eV*. J. Phys. B: At. Mol. Opt. Phys **16,** 1633.

[8] Hoffman K. R., Dababneh M. S., Hsieh Y. F., Kauppila W. E., Pol V., Smart J. H., and Stein T. S., (1982), *Total-cross-section measurements for positrons and electrons colliding with H_2, N_2 and CO_2*; Phys. Rev. A **25,** 1393.

[9] Jain A. and Baluja K. L., (1992), *Total (elastic plus absorption) cross sections for electron scattering fromdiatomic and polyatomic molecules at 10-5000 eV*. Phys. Rev. A **45** 202.

[10] Karwasz G. P., Brusa R. S., and Zecca A., (2003), *Photon and Electron Interactions with Atoms, Molecules and Ions*. **17,** Pt. C, Springer, New York. (Edited by Itikawa Y.).

[11] Tennyson J., Brown D. B., Munro J. M., Rozum I., Varambhia H. N., and Vinci N., (2007), *Quantemol-N: an expert system for performing electron molecule collision calculations using the R-matrix method*. J. Phys. Conf. series **86,** 012001.

[12] Varambhia H. N., Munro J. J., and Tennyson J., (2008), *R-matrix calculations of low-energy electron alkane collisions*. Int. J. Mass Spectrom. **271,** 1.

[13] Vinodkumar M., Limbachiya C., Korot K., and Joshipura K. N., (2008), *Theoretical electron impact elastic, ionization and total crosssections for silicon hydrides, SiH_x ($x = 1, 2, 3, 4$) and disilane, Si_2H_6 from threshold to 5 keV*; Euro. Phys. J. D **48,** 333.

[14] From: http://www.emsl.pnl.gov/forms/basisform.html.

[15] Vinodkumar M., Limbachiya C. G., Joshipura K. N. and Mason N. J., (2011), *Electron impact calculations of total elastic cross sections over a wide energy range – 0.01 eV to 2 keV for CH_4, SiH_4 and H_2O*, Euro. Phys. J. D **61,** 579.

[16] Vinodkumar M., Bhutadia H., Antony B., and Mason N., (2011), *Electron-impact rotationally elastic total cross sections for* H_2CO *and HCOOH over a wide range of incident energy (0.01–2000 eV)*; Phys. Rev. A **84,** 052701.

[17] Joshipura K. N., Vinodkumar M., Limbachiya C., and Antony B. K., (2004), *Calculated total cross sections of electron-impact ionization and excitations in tetrahedral* (XY_4) *and* SF_6 *molecules*. Phys. Rev. A **69,** 022705.

[18] Vinodkumar M., Limbachiya C., Korot K., Joshipura K. N., and Mason N., (2008), *Electron impact calculations of total and ionization cross-sections for Germanium Hydrides* (GeH_X; $X = 1–4$) *and Digermane*, Ge_2H_6; Int. J. Mass Spectrom. **273,** 145.

TOTAL SCATTERING CROSS SECTION OF S_2 BY ELECTRON IMPACT

Rahla Naghma and Bobby Antony
Department of Applied Physics, Indian School of Mines, Dhanbad, JH-826004

1. INTRODUCTION

Total cross section (TCS) data for e- molecule collision are needed in a variety of applications such as the study of planetary atmospheres and interstellar clouds, plasma physics, laser physics etc. Diatomic sulphur, S_2 is of astrophysical as well as of industrial interest. It is found in the atmosphere of Jupiter and its satellite Io. S_2 is also detected in the atmosphere of some comets and dense molecular clouds. In industry, S_2 molecules can be seen in reactive ion etching reactor using SF_6 plasmas [1, 2]. In this work we have calculated the TCS for e-S_2 collision for incident energy ranging from 0.1 eV to 2 keV.

2. THEORY

We have used two methodologies for TCS calculation for S_2 molecule by electron impact in the present energy range. For low incident energy we performed calculation using UK molecular R-matrix code [3] through Quantemol –N software [4] and for incident energy above the ionization threshold of the target molecule calculation is done by employing the spherical complex optical potential (SCOP) [5] formalism. These two methods are well described in the references. Here we give details of the target model used for the low energy calculations.

S_2 is a linear open shell molecule with bond length of 1.8892$Å^2$ [6]. We used double zeta plus polarization basis set to represent the target wave function. Our R matrix code utilizes Gaussian type orbital to represent the target electronic state as well as the scattering electrons. The natural symmetry of S_2 is $D_{\infty h}$ while due to the restriction of R-matrix code calculations were performed with D_{2h} symmetry. Out of 32 electrons of S2 20 electrons are frozen and the remaining 12 are kept in the active space. No. of target states employed in the close coupling expansion are 32and 60 configuration state functions are used for an accurate representation of these 32 target states. Number of channels included in the configuration is 100. The target properties like ground state energy, first excitation energy and rotational constant computed by us are compared with the previous works in Tab. 1 and we have an overall good agreement with the previous available results.

Table 1: Target properties

Target properties	Present	Previous
Ground state energy (Hartree)	795.006	-795.03737 [2] -795.14768 [7]
First excitation energy (eV)	0.57	0.60 [1] 0.603 [2] 0.55 [8]
Rotational constant (cm^{-1})	0.2955	0.2954 [6]

Figure 1: TCS of S_2 in Å^2 by electron impact.

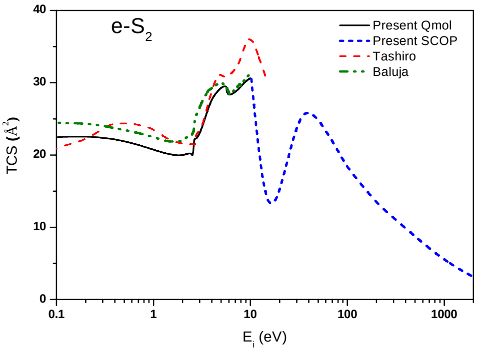

3. RESULT AND DISCUSSION

Fig. 1 represents the total cross section for e-S_2 scattering from 0.1 to 2000 eV and also shows comparison with [1] and [2]. It is clear from the graph that cross section calculated by the R-matrix code and SCOP formalism shows consistency at the transition point. The present TCS at energy up to 10 eV shows similar shape with the previous results [1, 2] and also in magnitude the low energy results are in reasonable agreement with available data [1, 2]. Around 2.6 eV we notice one peak in the cross section curve. This is due to resonance belongs to degenerate $^2B_{2u}$ and $^2B_{3u}$ ($^2\Pi_u$) symmetry and is in agreement with the resonance detected by [1, 2].

4. CONCLUSION

This work reports total electron scattering cross section for S_2 molecule by using two methodologies. At impact energies up to ionization threshold of the target the ab initio R matrix method is used through Quantemol –N software while at energies above the ionization threshold to 2 keV we have employed the SCOP formalism. The data computed by the two methods are consistent at the transition point around 10 eV. We predicted resonance around 2.6 eV which is in excellent agreement with the previous [1,2]. The present data is generally in reasonable agreement with the available data. The target properties like the ground state energy, first excitation energy and rotational constant computed by us are found to agree well with the previous available theoretical and experimental findings as given in Tab.1. This work will motivate the experimentalist to perform experiment and also theoretician to do computation on this molecule.

References

[1] Tashiro M., (2008), *Electron impact excitation of S_2 molecules*. Chem. Phys. Lett. **453,** 145.

[2] Rajvanshi J. S. and Baluja K. L.,(2011), *Electron-impact study of S_2 molecule using the R-Matrix method.* Phys. Rev. A **84,** 042711.

[3] Tennyson J., (2010), *Electron-molecule collision calculations using the R-matrix methods*. Phys. Rep. **491**, 29.

[4] Tennyson J., Brown D. B., Munro J. J., Rozum I., Varambhia H. N. and Vinci N., (2007), *Quantemol-N: an expert system for performing electron molecule collision calculations using the R-matrix method*. J. Phys.: Conf. Series **86**, 012001.

[5] Naghma R., Mahato B. N., Vinodkumar M. and Antony B. K., (2011*), Electron impact total ionization cross section for atoms with z = 49-54*. J. Phys. B: At. Mol. Opt. Phys. **44**, 105204.

[6] http://cccbdb.nist.gov/

[7] Tait A. D., Dixon M. and Banyard K. E., (1974), J. Phys. B **7,** 1908.

[8] Kiljunen T, Eloranta J, Kunttu H., (2000), *Electronic structure and short-range recombination dynamics of S_2 in solid argon [J]*. J. Chem. Phys. **112,** 7475.

ELECTRON IMPACT SCATTERING BY NO_2 MOLECULE

D. Gupta[1], R. Naghma[1], M. Vinodkumar[2] and B. K. Antony[1]
[1]Dept of Applied Physics, Indian School of Mines, Dhanbad, India
[2]V. P. & R. P. T. P. Science College, Gujarat, India

1. INTRODUCTION

Nitrogen dioxide is an atmospheric pollutant as it produces ground-level ozone, and hence acts as a source for the formation of smog. The highly toxic gaseous nitric acid and other organic nitrates can are easily formed in air. Nitrogen dioxide also contributes to increased respirable particle level in the atmosphere. However, the greatest concern is the indirect green house effect of NO_2 [1]. Such gases have high impact on chemical and physical processes in the atmosphere, even though they have negligible direct greenhouse effect. Hence, N_2O plays crucial role in the atmospheric chemistry where it belongs [2]. These atmospheric compounds are very reactive and are found to affect the climate 'indirectly' through its contribution to the total radiative forcing [3]. Even though great deal of work has been done on this molecule, there is a clear evidence of lack of enough data, especially below 100 eV. In this work we have used two methodologies at energy regimes. At low energies, the molecular R-Matrix code through Quantemol-N package [4] is used, while at intermediate and high energies spherical complex optical potential (SCOP) formalism [5,6] has been employed to obtain the cross section data.

2. THEORY/EXPERIMENT

Both theoretical methodologies are well described in details elsewhere [5,6]. Here we briefly depict the salient features only. NO_2 is a trigonal planar molecule with bond angle of 134.2 degrees. The central Nitrogen atom is bonded with one of the oxygen atom by double bond and with other oxygen atom by a single bond of identical bond length 2.25 au. We have used a double zeta plus polarization (DZP) Gaussian basis set to construct the target wave function for an accurate representation of each orbital, along with C_{2V} point group symmetry of the order 4. The ground state Hartree-Fock electronic configuration of NO_2 molecule is ${}^{1}b_2^{2}$, ${}^{1}a_1^{2}$, ${}^{2}a_1^{2}$, ${}^{3}a_1^{2}$, ${}^{2}b_2^{2}$, ${}^{4}a_1^{2}$, ${}^{5}a_1^{2}$, ${}^{3}b_2^{2}$, ${}^{1}b_1^{2}$, ${}^{4}b_2^{2}$, ${}^{1}a_2^{2}$, ${}^{6}a_1^{1}$. Six out of 23 electrons were frozen in ${}^{1}a_1$, ${}^{2}a_1$ and ${}^{1}b_2$ molecular orbitals while the remaining 17 electrons are kept free in active space. The target molecular orbital space is divided into core (inactive), valence (active), and virtual orbitals. These target molecular orbitals are supplemented with a set of continuum orbitals, centred on the centre of mass of the molecule. A total of 8 electronic excited target states are represented by 1391 configuration state functions (CSF's) for the ground state and the number of channels included in the calculation is 25. The R-matrix radius is taken as 10 a_0 while R-matrix calculation is propagated up to 100 a_0.

Table 1. Target properties obtained for the e-NO_2 molecule.

Properties of NO_2	**Present**	**Experimental**	**Theoretical**
Ground-state energy (au)	-204.15	-	-204.07 [7] -204.06 [8] -203.95 [10] -204.05 [11]
First excitation energy (eV)	3.01	3.02 [12]	3.08 [4]
Rotational constant (cm^{-1})	7.99	8.00 [13]	
Dipole moment (D)	0.50	0.316 [14]	0.33 [5] 0.45 [4] 0.45 [11]

The target properties obtained in the low energy calculation is given in Tab. 1. The ground state energy obtained is -204.15 Hartree which is in very good agreement with -204.07 Hartree given by Munjal et al. [7], -204.06 Hartree given by Curik et al. [8], -203.94 Hartree reported by Fink [9] and -204.05 Hartree given by Jackels and Davidson [10]. The first electronic excitation energy is 3.01 eV which is in agreement with the experimental value of 3.02 eV reported by Lievin et al. [19] and theoretical value of 3.08 eV predicted by Munjal et al. [7]. The present computed dipole moment is 0.5 D which is close to the theoretical values of 0.45 D predicted by Munjal et al. [7] and Jackels and Davidson [10] and slightly higher compared to 0.316 D reported by Leonardi et al. [14] and 0.33 D predicted by Curik et al. [11]. The present rotational constant of 7.99 cm-1 is in agreement with the experimental value 8.0 cm-1 reported in CCCBDB database [13]. The comparison of the calculated target properties for NO_2 with available theoretical and experimental results reflect the fact that the basis set and hence the wave functions used in our calculations are reasonable and of good quality to produce reliable cross section data.

2.1 Low energy

In the R-matrix method, the configuration space is divided into two spatial regions. The inner region is of radius 'a' about the centre of mass of the target called R-matrix radius, which is around 10 a.u. while the outer region is infinite. This choice depends on the stability of the results obtained in the calculations. In our methodology we assume a fixed-nuclei (FN) approximation neglecting any dynamics involving the nuclear motion (rotational and vibrational). The inner region is chosen such that it accommodates the wavefunction of the target molecule. Here the scattering electron is indistinguishable from the electrons. The interaction potentials i.e. static, exchange and correlation polarization potentials are dominant in this region. In the outer region, the scattering electron is far away from the target electron and there is no residual molecular charge density hence exchange and correlation are assumed to be negligible and the only long range multipolar interactions between the scattering electron and the target are included. A single center approximation is

assumed here and this suffices quick, simple and fast solutions in the outer region. For the present system the inner R-matrix radius is taken as 10 a_o while the outer region calculations are extended up to 100 a_o and found to give consistent results.
The wavefunction for the inner region using close coupling (CC) approximation [4] given by,

$$\psi_k^{N+1} = A\sum_I \psi_I^N\left(x_1,\cdots,x_N\right)\sum_j \zeta_j(x_{N+1})a_{Ijk} + \sum_m \chi_m(x_1,\cdots,x_{N+1})b_{mk} \qquad (1)$$

Where A is the anti-symmetrization operator and all other terms have their usual menaing as given in ref. [4]. With this wavefunction, a static exchange calculation has a single Hartree-Fock target state in the first sum. The second sum runs over the minimal number of configurations usually 3 or fewer, required to relax orthogonality constraints between the target molecular orbitals and the functions used to represent the configuration. Our fully close-coupled calculation uses the lowest number of target states, represented by a CI expansion in the first expansion and over a hundred configurations in the second. For the present problem we have used 8 lowest energetically excited target states. These configurations allow for both orthogonality relaxation and short-range polarization effects.
The complete molecular orbital representation in terms of occupied and virtual target molecular orbitals is constructed using the Hartree-Fock Self-Consistent. The coupled single centre equations describing the scattering in the outer region are integrated to identify the K-matrix elements. K-matrix is a symmetric matrix whose dimensions are the number of open channels. All the observables can be deduced from the K-matrix. K-matrices are used to obtain T-matrices using the definition

$$T = \frac{2iK}{1-iK} \qquad (2)$$

The T-matrices are in turn used to obtain the physically observable quantity like various total cross sections. The K-matrix is diagonalized to obtain the eigenphase sum, which is further used to obtain the position and the width of the resonances.

2.2 Intermediate to high energy

For intermediate to high energy (~15 eV to 2000 eV) scattering calculation we have used SCOP formalism. In this methodology the charge density, $\rho(r)$ of the target is modeled through the parameterized Hartree-Fock (H-F) wavefunctions given by Cox and Bonham [5]. A single centre approximation is assumed for NO_2 molecule, where the charge density of each atom is expanded from the centre of mass of the system. Such an expansion will be dependent on the bond length, bond angle and individual mass of atoms of the molecule. The final spherical charge density is renormalized to account for the total no of electrons in the system. The final potential will be dependent on the radial vector 'r' and incident energy of the projectile E_i given by,

$$V_{opt}(r,E_i) = V_R(r) + iV_I(r,E_i) \qquad (3)$$

Here the first term represents the real potential of the projectile-target system and second imaginary term depicts the absorption potential. The real potentials of the e -

NO_2 is made of static, exchange and polarization potentials. The imaginary absorption potential is given by [6],

$$V_{abs}(r,E_i) = -\rho(r)\sqrt{\frac{T_{loc}}{2}}\left(\frac{8\pi}{10k_F^3E_i}\right)\theta(p^2 - k_F^2 - 2\Delta)(A_1 + A_2 + A_3) \tag{5}$$

This complex potential is used to solve the Schrödinger equation through the method of partial waves. The phase shifts obtained help us to obtain the required cross section. At low incident energies only few partial waves are required, but as the incident energy increases more and more partial waves are required for convergence.

3. RESULT AND DISCUSSION

A comprehensive study of electron collision with nitrogen dioxide is reported here for the energy range from 0.5 to 2000 eV. The *ab-initio* calculations were used till around 15eV and SCOP formalism were employed from ionization threshold of the target.

Figure 1. TCS for e -NO_2 scattering. Solid line: Present Q-mol; Dash line: Present SCOP; Dot line: Munjal et al. [7]; Dash dot line: Curik et al. [8]; Dash dot dot line: Shi et al. [15]; Short dash line: Sun et al.[16]; line+square: Zecca et al. [17]; Stars: Szmytkowski et al. [19]

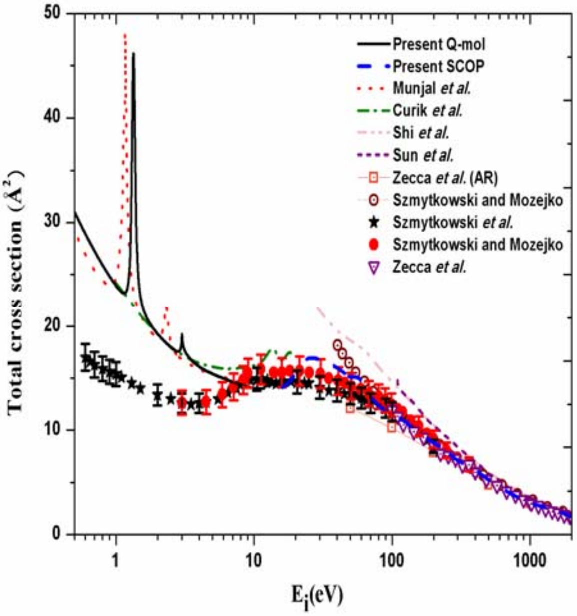

In figure 1. we have plotted the comparison of present total cross section with all previous theoretical and experimental data over the extensive range of impact energies from 0.5 eV to 2000 eV. The cross section data is found to have a smooth transition between the two formalisms (R-matrix and SCOP). Szmytkowski et al. [17] has reported two sets of data and is quite low for both cases compared to all theoretical data at energies below 5 eV. Also, it is interesting to see that no structures are present in their measurements. The peaks at 1.4 and 3 eV correspond to O^- DEA channel, which is confirmed by Rangwala et al. [18]. Beyond 6 eV present data are in good agreement with the results of Szmytkowski et al. [17]. For intermediate to high energy, the comparison is found to quite good with all the other data.

4. CONCLUSION

Despite NO_2 being very important atmospheric molecule, only few literatures were found on the low energy electron impact collision studies. Here we have presented here a comprehensive calculation of very low to high energy electron impact scattering data. The consistency of the calculation using these two formalisms at the transition energy allows us to predict data over such a wide energy range. The numerical method is based on fixed nuclei, single center, close coupling formalism at low energy and simple local and parameter free models potentials at intermediate to high energy. Our data seems to compare well with other results. Additionally, present data shows a strong peak at 1.33 eV with a value of 42.53 $Å^2$ which is very close to the peak at 1.17 eV (48.14 $Å^2$) reported by Munjal et al. [4]. The study by Rangwala et al. [18] have reported the position of O^- DEA channels at 1.4 eV, 3 eV and 8.3 eV respectively for e-NO_2 scattering, confirming this possibility which is comparable with present study.

References

[1] Fuglestvedt J. S., Isaksen I. S. A., and Wang W. C., (1996), *Estimates of indirect global warming potentials for CH_4, CO and NO_X. Climatic Change* **34,** 405.

[2] Abedi A., Cieman P., Coupier B., Gulejova B., Buchanan G. A., Marston G., Mason G., Scheier P., and Mark, T. D., (2004), *Dissociative electron impact ionization of N_2O_5.* Int. J. Mass Spectrom. **232,** 147.

[3] Wild O., Prather M. J., and Akimoto H., (2001), *Indirect long-term global radiative cooling from NO*x *emissions.* Geophys. Res. Letts. **28,** 1719.

[4] Tennyson J., Brown D. B., Munro J., Rozum I., Varambhia H. N., and Vinci N., (2007), *Quantemol-N: an expert system for performing electron molecule collision calculations using the R-matrix method.* J. Phys.: Conf. Series. **86**, 012001.

[5] Vinodkumar M., Bhutadia H., Antony B. K., and Mason N. J., (2011), *Electron-impact rotationally elastic total cross sections for H_2CO and HCOOH over a wide range of incident energy (0.01–2000 eV).* Phys. Rev. A **84**, 052701.

[6] Naghma R., Mahato B. N., Vinodkumar M., and Antony B. K., (2011), *Electron impact total ionization cross sections for atoms with $Z = 49–54$.* J. Phys. B: At. Mol. Opt. Phys. **44,** 105204.

[7] Munjal H., Baluja K. L., and Tennyson J., (2009), *Electron collisions with the NO_2 radical using the R-matrix method*. Phys. Rev. A **79**, 032712.

[8] Curik R., Gianturco F. A., Lucchese R. R., and Sanna N., (2001), *Low-energy electron scattering and resonant states of $NO_2(X\ ^2A_1)$.* J. Phys. B: At. Mol. Opt. Phys. **34,** 59.

[9] Fink W. H., (1971), *Calculations of the Ground and Excited State Energies of NO_2.* J. Chem. Phys. **54,** 2911.

[10] Jackels F. and Davidson E. R., (1976), *The two lowest energy $^2A'$ states of NO_2.* J. Chem. Phys. **64,** 2908.

[11] Lievin J., Delon A., and Jost R., (1998), *Absorption cross section of NO_2 by the reflection method from* ab initio *calculations involving the three low lying electronic states.* J. Chem. Phys. **108,** 8931.

[12] Website: http://cccbdb.nist.gov/

[13] Leonardi E., Petrongolo C., Hirsch G., and Buenker R. J., (1996), *Ab initio study of NO_2. V. Nonadiabatic vibronic states and levels of the* X $^2A_1$/Ã $^2B_2$ *conical intersection.* J. Chem. Phys. **105,** 9051.

[14] Cox H. L., and Bonham R. A., (1967), *Elastic Electron Scattering Amplitudes for Neutral Atoms Calculated Using the Partial Wave Method at 10, 40, 70, and 100 kV for* $Z = 1$ *to* $Z = 54$. J. Chem. Phys. **47,** 2599.

[15] Shi D., Sun J., Zhu Z., and Liu Y., (2005), *A modification potential method for electron scattering total cross section calculations on several molecules at 30–5000eV,* Chinese Phys. **14**, 120.

[16] Sun J., Shi D., Zun Z., and Liu Y., (2003), *Electron impact total (elastic + inelastic) cross sections with simple molecules consisting of N & O atoms at 100 - 1600 eV.* Chin. Opt. Lett. **1,** 624.

[17] Zecca A., Melissa R., Brusa R. S., and Karwasz G. P., (1999), *Additivity rule for electron-molecule cross section calculation: A geometrical approach;* Phys. Lett. A **257,** 75.

[18] Szmytkowski C., Maciag K.., and Krzysztofowich A. M., (1992), *NO_2 total absolute electron-scattering cross sections.* Chem. Phys. Lett. **190**, 141.

[19] Rangwala S. A., Krishnakumar E., and Kumar S. V. K., (2003), *Dissociative-electron-attachment cross sections: A comparative study of NO_2 and O_3.* Phys. Rev. A **68**, 052710.

ELECTRON IMPACT SCATTERING STUDIES OVER A WIDE RANGE OF ENERGY

Mayuri Barot[1*], Minaxi Vinodkumar[1] and Nigel Mason[2]
[1]V. P. & R. P. T. P. Science College, Vallabh Vidyanagar-388 120,
Gujarat, India
Email: *barot_mayuri@yahoo.com

1. INTRODUCTION

The total electron scattering cross section quantifies the strength of the electron molecule interaction at any particular energy and is an important parameter in many areas of applied science including atmospheric science, astrochemistry, plasma technology and radiation damage. Combining the results of a low energy R-matrix code through Quantemol-N software [1] with a high energy quantum mechanical methodology based on the spherical complex optical potential formalism [2] allows us to report the total cross sections over such a wide range. This work presents results of some selected molecular targets such as HCl, HBr, N_2, N_2O, CF_2, SiF_2, SO_2, C_2H_2 etc. as exemplars of the methodology.

Hydrochloric acid (HCl) finds application in almost all sectors of industry. Hydrogen bromide (HBr) is used both as a reagent and as a catalyst in a variety of organic reactions. Further hydrogen bromide in combination with hydrochloric acid and chlorine is used for plasma etching of polysilicon. Scattering of electrons with nitrogen gas is a favoured fundamental process in the atmosphere due to abundance of electrons produced as a result of photoionization of many upper atmospheric constituents by solar uv radiations. A systematic study of this phenomenon forms the basis for understanding gas discharge devices, plasma processing, laser kinetic modeling and the physics of planetary atmosphere. Investigation of electron collision with nitrous oxide (N_2O) has been the topic of interest recently due to its presence in various planetary environments and its role in the chemistry of these environments. Molecular radicals play an important role in of electron-driven processes, including radiation damage in tissue, gas discharges, low-temperature plasma etch environments, and deposition technologies. In particular radicals in fluorocarbons are expected to play significant role in the etching process and evolution of plasma. Additionally fluorocarbons, feedstock gases are frequently used as etching gases in many applications which finally lead to electron impact dissociation to the productions of CFx (x = 1 - 3) radicals that are responsible for several important chemical and physical processes in substrates. Similarly free radicals of SiF_2 serves as an important species in fluorine based plasmas used to etch and deposit silicon layers in the fabrication of microelectronic devices and solar cells. The reaction of acetylene (C_2H_2) with hydroxyl radicals is very significant in the combustion of other atmospheric and astrophysical processes. Electron interactions with SO_2 play an important role in magnetosphere plasma dynamics of the Jovian system, the plasma assisted treatment of bio-compatible materials and biomedical surfaces, in models of diffuse discharge switches and in understanding the underlying physics and chemistry of combustion process. Models which aim to represent technological plasmas accurately depend upon precise cross sectional data including absolute electron collision rates for all the possible electron interactions with the constituent neutral species and radicals.

2. THEORY

The aim of present work is to show that, by combining two well developed theoretical formalisms, it is possible to provide a self-consistent set of data for the total scattering cross section of electrons on polyatomic targets for a wide incident energy range, from 0.01 eV to 2000 eV. The crux idea behind the R-matrix formulation lies in dividing the complete configuration space into two regions called inner region having R-matrix radius ‘a’ which is usually 10 a.u. and the outer region extending to the radius of 100 a.u.. In the inner region calculation the wave function has been constructed using the close-coupling (CC) approximation which can be written as,

$$\psi_k^{N+1} = A\sum_I \psi_I^N\left(x_1,\cdots,x_N\right)\sum_j \zeta_j(x_{N+1})a_{Ijk} + \sum_m \chi_m(x_1,\cdots,x_{N+1})b_{mk} \tag{1}$$

Where all the terms have their usual meaning and given in ref. [3]. The R-matrix has been used to obtain T-matrices which in turn give various total cross sections.

High energy electron scattering is modelled using the well-established SCOP formalism [4] which employs partial wave analysis to solve the Schrödinger equation with various model potentials as its input. The interaction of incoming electron with the target molecule can be represented by a complex potential comprising of real and imaginary parts as,

$$V_{opt}(r,E_i) = V_R(r) + iV_I(r,E_i) \tag{2}$$

such that,

$$V_R(r,E_i) = V_{st}(r) + V_{ex}(r,E_i) + V_p(r,E_i) \tag{3}$$

Where, E_i is the incident energy. Equation (2) corresponds to various real potentials to account for the electron target interaction namely, static, exchange and the polarization potentials respectively. These potentials are obtained using the molecular charge density of the target, the ionization potential and the polarizability as inputs. The molecular charge density may be derived from the atomic charge density by expanding it from the center of mass of the system. Thus, the single-center molecular charge density is obtained by a linear combination of constituent atomic charge densities, renormalized to account for covalent molecular bonding. The atomic charge densities and static potentials (V_{st}) are formulated from the parameterized Hartree-Fock wave functions given by Cox and Bonham. The parameter free Hara’s ‘free electron gas exchange model’ is used for the exchange potential (V_{ex}). The polarization potential (V_p) constructed from the parameter free model of correlation-polarization potential given by Zhang et al. [5]. The target parameters like ionization potential (IP) and dipole polarizability (α_o) of the target used here are the best available from the literature. The well-known quasi-free model form of Staszeweska et al. [6] is employed for the absorption part (V_{abs}). All the related references are given in our earlier papers.

The complex potential thus formulated is used to solve the Schrödinger equation numerically through partial wave analysis.

3. RESULT AND DISCUSSION

The total cross sections are computed using Molecular R-matrix Code for low energy below ionization threshold of the target and above it by Spherical Complex Optical Potential. The numerical values are listed below.

Table 1: Total Cross Section (Å^2)

E_i (eV)	**Total Cross Sections (Å^2)**							
	HCl	**HBr**	**N_2**	**N_2O**	**CF_2**	**SiF_2**	**C_2H_2**	**SO_2**
0.1	588.73	397.28	10.83	63.28	30.43	783.57	25.23	1581.51
0.4	194.85	123.92	12.73	26.77	24.26	229.40	27.34	493.03
0.6	134.58	88.88	12.86	22.32	25.29	168.71	26.49	354.88
0.8	104.97	70.92	12.90	20.05	32.76	137.69	25.51	273.68
1.0	87.41	60.17	12.91	18.75	62.73	119.01	24.68	224.39
2.0	48.91	41.36	15.30	35.54	21.07	82.24	23.83	94.66
5.0	37.27	36.27	14.71	14.07	15.10	49.38	33.61	67.48
10	34.70	30.29	11.79	12.35	13.65	32.80	23.62	44.44
15	26.96	20.05	11.01	14.73	15.23	25.62	19.05	37.47
20	23.01	17.48	11.26	13.67	13.79	17.95	17.53	34.56
40	15.27	12.90	10.67	14.88	12.59	12.32	13.09	19.81
80	11.43	10.99	08.78	12.19	11.29	10.31	9.08	18.96
100	10.32	09.98	07.95	10.79	10.42	9.01	8.13	18.18
200	07.37	07.21	05.28	7.20	7.39	5.55	5.32	12.79
400	03.71	04.95	03.69	4.80	4.85	3.31	3.16	7.98
500	03.19	04.33	03.21	4.08	4.19	2.80	2.65	6.74
700	02.55	03.52	02.53	3.58	3.33	2.17	2.00	5.16
800	02.30	03.24	02.29	3.11	3.04	1.95	1.79	4.63
900	02.11	03.01	02.09	3.11	2.79	1.77	1.62	4.21
1000	01.96	02.82	01.92	2.72	2.58	1.63	1.49	3.86
1500	01.65	02.18	01.36	2.38	1.89	1.14	1.05	2.73
2000	01.16	01.83	01.06	2.08	1.51	0.88	0.81	2.11

4. CONCLUSION

In the present work our aim is to provide total cross sections for electron scattering over a wide range of impact energies between 0.1 eV and 2 keV. Since a single formalism cannot be employed over such a wide range, we have used the UK molecular R-matrix code using Quantemol-N at low impact energies to yield *ab-initio* results while at high energies we have employed the SCOP formalism. Since the results from two formalisms show smooth transition at the transition energy, we have confidence that the methodology we propose may be used to calculate such cross sections in other molecular systems where experiments are difficult (e.g. exotic systems and radicals). Such data sets are needed in a variety of applications from aeronomy to plasma modelling. Accordingly such a methodology maybe built into the design of online databases to provide a ‘data user’ with the opportunity to request their own set of cross sections for use in their own research. Such a prospect will be explored by the emerging Virtual Atomic and Molecular Data Centre (VAMDC) http://batz.lpma.jussieu.fr/www_VAMDC/.

ACKNOWLEDGEMENT

M.V.K. thanks Department of Science and Technology, New Delhi (SR/S2/LOP/26-2008) for financial support through Project Grant for Major Research project under which part of this work is done.

References

[1] Morgan L. A., Tennyson J., Gillan C. J., (1998), *The UK molecular R-matrix codes.* Comput .Phys.Commun **114**, 120.

[2] Jain A., (1988), *Theoretical study of the total (elastic + inelastic) cross sections for electron –H_2O (NH_3) scattering at 10-3000 eV.* J. Phys. B: **21**, 905.

[3] Limbachiya C., Vinodkumar M., Mason N. J., (2011), *Calculation of the electron impact rotationally elastic cross section for NH_3, H_2S and PH_3 over the energy range from 0.01 eV to 2 keV.* Phys. Rev. A, **83**, 042708.

[4] Vinodkumar M., Joshipura K. N., Limbachiya C., and Antony B. K., (2006), *Electron impact total and ionization cross-sections for some hydrocarbon molecules and radicals.* Eur. Phys. J. D **37**, 67.

[5] Zhang X., Sun J., and Liu Y., (1992), *A new approach to the correlation potential- low- energy electron elastic scattering by He – atoms.* J. Phys. B: At. Mol. Opt. Phys. **25,** 1893.

[6] Staszewska G., Schewenke D. W., Thirumalai D., and Truhlar D. G., (1983), *Quasifree-scattering model for the imaginary part of the optical potential for electron scattering*. Phys. Rev. A **28**, 2740.

SCREENING CORRECTED TOTAL CROSS SECTIONS FOR $PH(CH_3)_2$ AND PH_2CH_3 ON ELECTRON IMPACT

A. Chaudhari[1], H. Bhutadia[1], M. Vinodkumar[2]
and C. Limbachiya[3]
[1]Government Engineering College, Patan, Gujarat
[2]V. P. & R. P. T. P. Science College, V. V. Nagar, Gujarat
[3]P. S. Science College, Kadi, Gujarat

1. INTRODUCTION

Electron impact cross sections on molecules are of great interest due its possibilities in the investigation of various applied areas like plasma physics, semiconductor industry, micro-electronics, atmospheric sciences and pollution remediation. A well-organized database on electron impact collision cross sections is essential for the modelling of such interactions in these environments. Even though many researchers are involved in this area of research, collection of various cross sections by experimental measurements alone are not feasible in the time scale required by the industry. Hence, alternative theoretical methods like Spherical Complex Optical Potential (SCOP) [1] formalism can be handy.

Recently, trimethylphosphine, $P(CH_3)_3$ (TMP) was considered as a prospective candidate for this purpose. For an effective study on the use of this gas, it is imperative to understand the effect of TMP upon electron interaction. Derivatives of TMP ($PH(CH_3)_2$, PH_2CH_3) may also be considered as potential candidates for alternative P-doping source in the semiconductor industry.

The study of dynamics and cross sections of electron molecule collision forms the essential basis for understanding the characteristics of any target molecule. The relations between electron scattering cross sections and physico-chemical properties of target molecules have been investigated since the earliest systematic measurements of cross sections [2]. These correlations indicate the role of target properties in the scattering process, while the semi-empirical formulae describing these correlations will help to estimate total cross sections (TCS) of targets for which experimental investigation are difficult and theoretical data is sparse. The analytical formula so obtained using these parameters can also be used to generate the total cross section data at very high energies where the partial wave analysis becomes impractical [3,4,5].

Despite the importance of the study of electron impact scattering for these targets there are very less efforts done both on theoretical and experimental fronts which has motivated us to carry out this study. Electron impact total cross sections for these molecules have been very recently reported by Shi et al. [6] using additivity method and modified additivity method to take into account the geometrical screening effect for impact energies 30 to 5000 eV. They presented calculated total cross section by two modified additivity (MAR) methods. In the first case they have used the empirical fraction given by Jiang et al. [7] which they call 'original MAR' (oMAR) and for the second case they have estimated the empirical fraction considering the geometrical dimension of the molecule, which they call their 'present MAR' (pMAR). The pMAR seems to compare better with other data available. There are no measurements reported for total cross sections for $PH(CH_3)_2$ and PH_2CH_3 to best of our knowledge. In the absence of reliable data for these important molecules, present study finds importance in supplementing efforts by other researchers.

2. THEORETICAL METHEDOLOGY

Independent atom model (IAM) is the simplest method to find cross sections for molecules on electron impact and are found to be successful particularly at high energies. In this model the molecule is substituted by its constituent atoms and such a crude approximation results in overestimating cross sections particularly at energies below 100 eV. This overestimation can be understood due to two facts: (i) the closely packed molecule is not fully transparent to low energy electrons ($E_i \lesssim$ 100 eV) and (ii) the mutual overlapping by neighbouring atoms and partial screening by the outer atoms are ignored [5]. Hence, it is evident that the inclusion of "screening effect" will lead to a decrease in molecular scattering cross section than that predicted by IAM [8].

In the present work we have considered the targets $PH(CH_3)_2$ and PH_2CH_3. These molecules are similar in their geometrical structure. CH_3 is trigonal planar and the central carbon atom is partially shielded or 'shadowed' due to the overlapping of neighboring hydrogen atoms. Hence, the central atom is not exposed to the entire flux of incoming electrons. This "shadowing effect" may be treated geometrically in scattering problems and is usually referred as 'geometrical screening' [8,9]. In the present work we have used single centre approach - group additivity rule to calculate total cross sections for the targets selected.

The SCOP formalism has been very successful in predicting electron impact total cross sections for many molecular systems [9-11]. The detailed description of the theory may be obtained from our previous work [9-11]. Our aim is to calculate total cross section (Q_T) for present targets employing the SCOP model. The successful application of this method for calculating various electron impact cross sections for BF_3 and BCl_3 previously [9] has motivated us to perform these calculations.

3. RESULT

Figures 1 and 2 show the total cross sections for e-$PH(CH_3)_2$ and e-PH_2CH_3 scattering with available comparisons respectively. In both the curves the present results are qualitatively in good agreement with results of Shi et al [6]. At high energies, the curve merges indicating that screening is not important.

Figure 1: Total cross sections for $PH(CH_3)_2$ in $Å^2$. Solid line, Present Q_T; Dash, Present $Q_{T,SC}$ (With Screening Correction); Dash-dot, Shi et al. (oMAR) [6]; Dash-dot-dot, Shi et al. (pMAR) [6]; Line with circles, Present fit using Analytical formula[4].

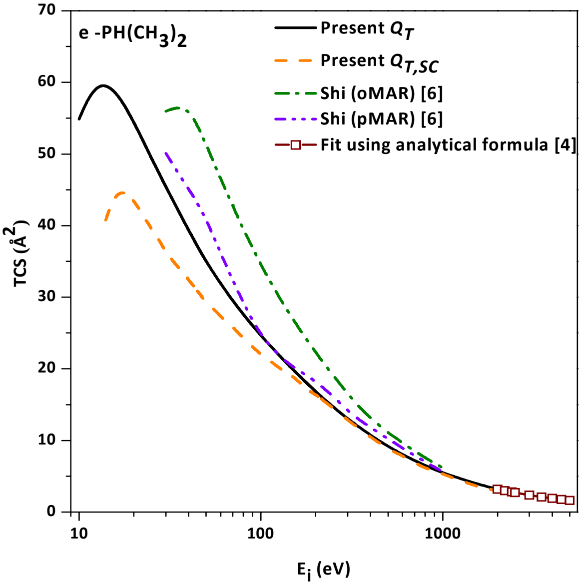

Figure 2: Total cross sections for PH_2CH_3 in $Å^2$. Solid line, Present Q_T; Dash, Present $Q_{T,SC}$ (With Screening Correction); Dash-dot, Shi et al. (oMAR) [6]; Dash-dot-dot, Shi et al. (pMAR) [6]; Line with circles, Present fit using analytical formula [4].

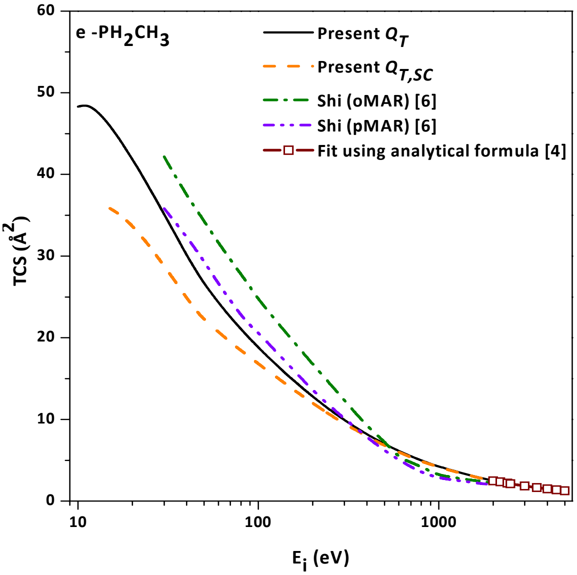

4. CONCLUSION

Screening effect is more pronounced at lower impact energy and gives better representation of the target and gives better cross sections.

References

[1] Jain A. and Baluja K. L., (1992), *Total (elastic plus inelastic) cross sections for electron scattering from diatomic and polyatomic molecules at 10–5000 eV: H_2, Li_2, HF, CH_4, N_2, CO, C_2H_2, HCN, O_2, HCl, H_2S, PH_3, SiH_4, and CO_2*. Phys. Rev. A **45**, 202.

[2] Brüche E., (1929), *Ergebnisse der exakten Naturwissenschaften*. **8,** 185.

[3] Bransden B. H. and Joachain C. J., (2003), *Physics of Atoms and Molecules, Pearson Education.*

[4] Vinodkumar M., Limbachiya C, Korot K. and Joshipura K. N., (2008), *Theoretical electron impact elastic, ionization and total cross sections for silicon hydrides, SiH_x (x = 1, 2, 3, 4) and disilane, Si_2H_6 from threshold to 5 keV;* Eur. Phy. J. D; **48;** 333.

[5] Szmystkowski Cz. and Krzysztofowicz A. M., (1995), *Electron scattering from isoelectronic, N_e=18, CH_3X molecules (X=F, OH, NH_2 and CH_3).* J. Phys. B: At. Mol. Opt. Phys., **28,** 4291.

[6] Shi D. H., Sun J. F., Zhu Z. L., and Liu Y. F., (2010), *Total cross sections of electron scattering by molecules NF_3, PF_3, $N(CH_3)_3$, $P(CH_3)_3$, $NH(CH_3)_2$, $PH(CH_3)_2$, NH_2CH_3 and PH_2CH_3 at 30–5000 eV.* Eur. Phys. J. D **57,** 179.

[7] Jiang Y. H., Sun J. F., and Wan L. D., (2000), *Additivity rule for the calculation of electron scattering from polyatomic molecules*. Phys. Rev. A **62,** 062712.

[8] Blanco F. and Garcia G., (2003), *Screening corrections for calculation of electron scattering from polyatomic molecules*. Phys. Lett. A **317,** 458.

[9] Vinodkumar M., Korot K., Limbachiya C., and Antony B., (2008), *Screening - corrected electron impact total and ionization cross sections for boron trifluoride (BF_3) and boron trichloride (BCl_3).* J. Phys. B: At. Mol. Opt. Phys. **41,** 245202.

[10] Vinodkumar M., Korot K., and Bhutadia H., (2010), *Calculations of total and ionization cross-sections on electron impact for alkali metals (Li, Na, K) from threshold to 2 keV;* Int. Journal of Mass Spectrometry. **294,** 54.

[11] Vinodkumar M., Bhutadia H., Antony B., and Mason N., (2011), *Calculation of electron-impact rotationally elastic total cross sections for NH_3, H_2S, and PH_3over the energy range from 0.01 eV to 2 keV.* Phys. Rev. A **83**, 042708.

ELECTRON SCATTERING BY H_2O AND NH_3

P. M. Patel[1], M. Y. Barot[1] and K. L. Baluja[2]
[1]Department of Physics, V. P. & R. P. T. P. Science College
Vallabh Vidyanagar - 388 120, India
[2]Department of Physics and Astrophysics, University of Delhi
Delhi - 10007, India

1. INTRODUCTION

It is common knowledge now that cross sections of various processes of electron scattering on molecules are required in many applications [1]. The spherical complex optical potential (SCOP) method appears to be reliable and practical technique of predicting σ_t values for a large variety of molecules [2].

In the SCOP method, the spherical part of the complex optical potential is treated exactly in a partial wave analysis to yield cross section parameters. The neglect of non-spherical terms in the full expansion of the optical potential is based on the fact that such an anisotropic contribution is very small in the intermediate and high energy regions. In the present work, we have calculated basically the electron impact total cross sections σ_t for H_2O & NH_3 molecules at incident energies almost from the threshold of electron excitation to 5KeV. We have also estimated the total ionization cross sections σ_i from total inelastic cross sections and compared with available experimental results. The present calculations are based on the complex optical potential approach and use variable phase approach method [3,4].

2. THEORY

The interaction of the electron-molecule system can be represented by a local complex optical potential [5].

$$V_{opt}(r) = V_R(r) + iV_{abs}(r) \tag{1}$$

Where, the real part is a sum of three parts,

$$V_R(r) = V_{st}(r) + V_{ex}(r) + V_{pol}(r) \tag{2}$$

The static potential $V_{st}(r)$ is calculated from the unperturbed target wave function Ψ_0 at the Hartree-Fock level. The term $V_{ex}(r)$ accounts for electron exchange interaction, while the $V_{pol}(r)$ represents approximately the short-range correlation and long range polarization effects. In this energy region, a local and real potential model for exchange and polarization is adequate. The $V_{abs}(r)$ is the absorption potential.

First we determine the target charge density $\rho(r)$ of a given molecule

$$\rho(r) = \int |\psi_0|^2 \, dr_1 \, dr_2 \cdots dr_z = 2\sum_a |\phi_a(r)|^2 \tag{3}$$

All four potential terms (V_{st}, V_{ex}, V_{pol}, and V_{abs}) are functions of $\rho(r)$.

$$V_{st}(r) = \int \rho(r_1) |r - r_1|^{-1} \, dr_1 - \sum_{i=1}^{M} Z_i \, |r - R_i|^{-1} \tag{4}$$

The V_{ex} is the Hara-free-electron-gas-exchange (HFEGE) model [6] and V_{pol} is calculated in the correlation-polarization (COP) approximation [7,8,9]. Thus, the accurate evaluation of ρ(r) is important in our SCOP model. We employed various single-centre expansion programs to determine the charge density and various potentials for linear and nonlinear molecules.

The imaginary part of the optical potential V_{abs} is the absorption potential, which represents approximately the combined effect of all the inelastic channels. Here we employed a semiempirical absorption potential as discussed by Truhlar and co-workers [10].

After generating the full optical potential of a given electron-molecule system, we treat it exactly in a partial-wave analysis by solving the set of first order coupled differential equations for the real and imaginary parts of the complex phase-shifts function under the variable phase approach (VPA) [11].

To obtain the total ionization cross section σ_i a semi-empirical approach [4] is applied to derive it from the calculated σ_{abs}. The total inelastic cross section σ_{inel} or σ_{abs} may be partitioned as,

$$\sigma_{abs}(E_i) = \sigma_i(E_i) + \sum \sigma_{exc}(E_i) \tag{10}$$

With σ_i the total cross section for all allowed ionization processes and $\sum \sigma_{exc}$ the sum over total excitation cross sections for all accessible electronic transitions. The second term arises mainly from low-lying dipole allowed transitions for which the cross section decreases rapidly at high energies. The quantity $\sum \sigma_{exc}$ becomes less important than σ_i at energies well above the ionization threshold [12].

We have obtained the electron-impact total cross sections σ_t and ionization cross sections σ_i for molecular targets H_2O & NH_3 at energies $E_i \geq 10$eV. And compared with available experimental data.

3. RESULT AND DISCUSSION

Figure 1 represent our theoretical σ_t and σ_i for e^- -H_2O scattering along with measured data. The present σ_t is agree with the experimental measurement above 100eV. Our calculated σ_t is overestimate about 5 to 10% near 20-50eV. The experimental σ_t [17] are in good agreement with present results. The calculated σ_i is overestimate about 10% near intermediate energies due to other inelastic channels are open near these energy range. In general, good agreement between our calculated σ_i and experiments for energies above 200eV, where the absorption effects are expected to be important.

FIG. 1 Total Cross Sections of H_2O

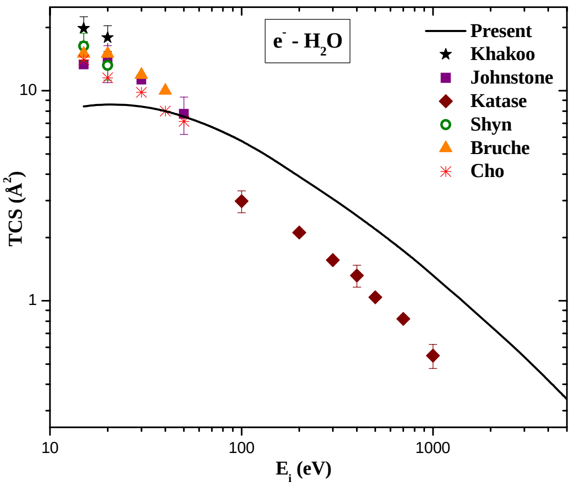

FIG. 2 Total Cross Sections of NH_3

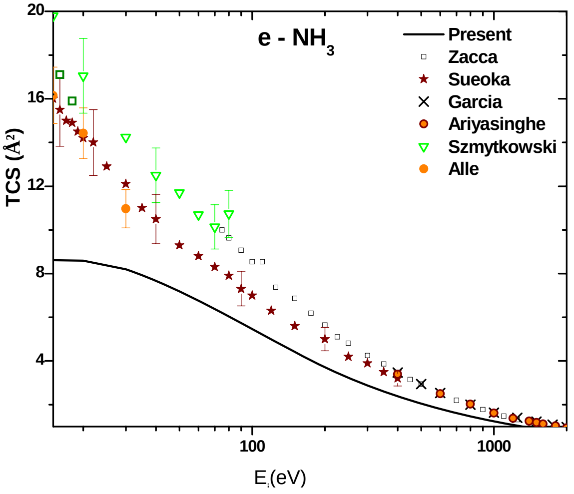

Figure 2 corresponds to e^- -NH_3 scattering. Our calculated σ_t is compared with available experimental measurement. We are also notice that σ_{int} values lie below the σ_t. We reproduce the shape of σ_t. This provides good estimation of our calculated σ_t. The present σ_i is compared with experimental measurements .Our calculated and experimental data agree in the entire energy range. The overestimation near 100eV about 5% due to other inelastic processes.

3. CONCLUSION

We have presented the total and total ionization cross sections of the intermediate and high energy electron impact. A complex optical potential is derived for each system from target wave functions and its spherical part is employed to yield total cross sections under the complex phase-shifts analysis. We have avoided any kind of fitting procedure in the present calculation. The present model mainly requires the target charge density, polarizability, ionization potential etc. of the molecule. At and above 100eV, our results for all the molecules studied here are in good agreement with available measurements. The method employed here is easy and practical and requires no prior information on the cross section parameter.

ACKNOWLEDGEMENT

One of the authors PMP is gratefully acknowledge the University Grant Commission, Western Regional Office, PUNE for the financial support in form of minor research project (No.47-648/08, WRO).

References

[1] Michelin S. E., Kroin T., and Lee, M. T. (1996), J. Phys. B: At. Mol. Opt. Phys. **29,** 2115.

[2] Jain A. and Baluja K. L., (1992), *Total (elastic plus inelastic) cross sections for electron scattering from diatomic and polyatomic molecules at 10–5000 eV:* H_2, Li_2, *HF*, CH_4, N_2, *CO*, C_2H_2, *HCN*, O_2, *HCl*, H_2S, PH_3, SiH_4, *and* CO_2. Phys. Rev. A **45,** 202.

[3] Pandya C. V., Patel P. M., and Baluja K. L., (2009), *FIZIKA A* **18,** 3 133.

[4] Patel P. M., Pandya C. V., and Baluja K. L., (2010), *FIZICA A* **19,** 1, 47.

[5] Joshipura K. N. and Patel P. M., (1996), J. Phys. B: At. Mol. Opt. Phys. **29,** 3925.

[6] Hara S., (1967), J. Phys. Soc. Jpn. **22,** 710.

[7] O’Connel J. K. and Lane N. F., (1983), Phys. Rev. A **27,** 1893.

[8] Padial, N. T. and Norcross D. W., (1984), Phys. Rev. A **29**, 1742.

[9] Gianturco F. A., Jain A., and Pantano L. C., (1987), J. Phys. B: At. Mol. Opt. Phys. **23,** 571.

[10] Staszewska G., Schwenka D. W., Thirumalai D., and Trhular D. G., (1983), Phys. Rev. A **28,** 2740.

[11] Calogero F., (1974), *Variable Phase Approach to Potential scattering (Academic, New York).*

[12] Zecca A., Karwasz G. P., Brusa R. S. and Szmytkowski Cz., (1992), Phys. Rev. A **45**, 2777.

TOTAL ELECTRON SCATTERING CROSS SECTIONS OF H_2O AND CH_4 MOLECULES USING A WEIGHTED ADDITIVITY METHOD

Hardik Desai[1*], Minaxi Vinodkumar[2] and P.C.Vinodkumar[1]

[1]Department of Physics, Saradar Patel University, Vallabh Vidyanagar, India
[2]V. P. & R. P. T. P. Science College, Vallabh Vidyanagar – 388 120 Gujarat, India
Email: [*]hardikdesai.phy@gmail.com

1. INTRODUCTION

Electron scattering with atoms and molecules is basically an electromagnetic interaction of the coulomb type and hence the scattering cross section must depend on the details of the charge content, its distribution within the target volume and the energy of the incident electrons. Though the exact quantum mechanical treatment become cumbersome, there exist many attempts to compute the scattering cross section of charge particle with simple targets to complex molecular targets such as the e-H_2O, e-CH_4, e-HF, e-NH_3 etc.[1-5]. In many cases the direct quantum mechanical methods work well for atomic targets rather than for the molecular targets. So it would be of interest to compute the scattering cross section of molecular targets using the atomic scattering cross sections of the constituting atoms of the molecule. Such attempts are generically known as additivity method [1, 2]. For more complex molecular targets even group additivity methods have been developed and are available in literature [3, 4].

However the direct addition of the respective atomic (or group) cross sections in many cases led to larger mismatch with the experimental data [5] and requires further improvements to the additivity approach. Hence, we propose here a weighted additivity method (WAM) to compute the total scattering cross sections where in two weight factors, one corresponding to the partial atomic charge and other corresponding to the partial spatial extension with reference to the molecule have been introduced to the simple additivity method. This method has been applied to few simple but important molecules like H_2O and CH_4 for illustration purpose.

2. METHODOLOGY

As per the weighted additivity method (WAM), the e - molecule scattering cross section ($Q_{e\text{-}M}$) is expressed in terms of the electron-atom cross sections ($Q_{e\text{-}Ai}$) of the different species of the atomic composition (A_i) of the molecule as :

$$Q_{e-M} = \sum_i S_i W_{Z_i} Q_{e-A_i} \tag{1}$$

Where W_{Z_i} and S_i are the two weight factors corresponding to the electron fraction of the atomic species (Z_i, A_i) with reference to the effective electrons of the molecule (Z_{eff}) and its average spatial distribution of the constituting atomic species with reference to the target molecular size respectively. These weight factors are explicitly expressed as

$$W_{Z_i} = \frac{Z_i - \delta}{Z_{eff}} \tag{2}$$

and

$$S_i = \frac{< r_i^2 >}{< r_M^2 >} \tag{3}$$

Where

$$Z_{eff} = \frac{\sum_{i \neq j} n_i Z_j}{\sum_i n_i} \tag{4}$$

n_i refers to the number of A_i species of atoms in the molecule and δ refers to the respective atomic electrons engaged with the molecular bonding. The choice, $\delta = 0$ means that the effect of atomic electrons engaged in the molecular bonding is not considered. Also $< r^2_i >$ and $< r^2_M >$ correspond to the average spatial extension of the i^{th} atomic species and the molecule respectively. In this case, the electron impact atomic scattering cross sections and the atomic and molecular sizes are required to estimate the total cross sections of e - Molecule scattering.

For the present study we have used the e - atom scattering data (e-H, e-O and e-C) for different electron energies computed by Minaxi Vinodkumar et.al, based on spherical complex optical formalism [5]. The average radius and bond length of the present molecules are obtained from NIST CCCBDB databank [6].

3. RESULT AND DISCUSSION

In this study, we report a weighted additivity method (WAM) to compute the electron-molecule collision cross section in terms of the representing electron-atom collision cross sections. As illustration to this method we present the total scattering cross section calculated for two very common but important molecules (i.e. e -H_2O & e - CH_4). The computed results on the total cross-sections are shown in the Fig. 1 and Fig. 2. for e-H_2O and e-CH_4 scattering respectively. Other theoretical and experimental data are also plotted for comparison. In the case of e-H_2O, the present results are in better comparison with the experimental data of C. Szmytkowski (Solid

Triangle) [7] and G. Garcia (Star) [8] than the theoretical results based on more rigorous calculations of [5].

Fig.1. The total scattering cross section (WAM - Line with solid 3D-circle) for H_2O molecule in comparison with other ***theoretically calculated data*** *: (SC -Line with Circle [5],A.Jain - Solid Pentagons [7] and K. N. Joshipura – Inverted Triangle [8])* ***Experimental data*** *of (C. Szmytkowski - Solid Triangle [9] and of G. Garcia-Star [10])*

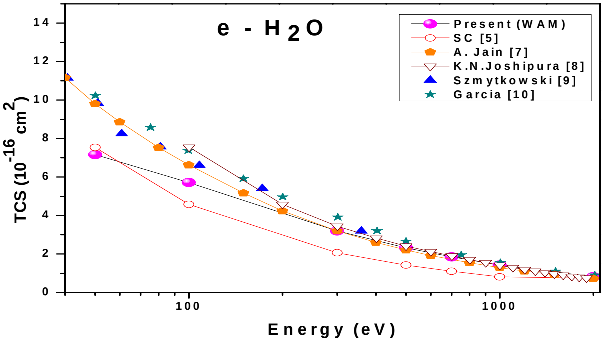

Fig. 2. The total scattering cross section (WAM - Line with solid 3D-circle) for CH_4 molecule in comparison with other ***theoretically calculated data*** *by M.Vinodkumar - Line with Circle [11],Jain & Baluja – Half shaded circle [12],* ***experimental data*** *of Sueoka O. and S. Mori - Pentagons [13] and of Kanik et al. -Solid Inverted Triangle [14]*

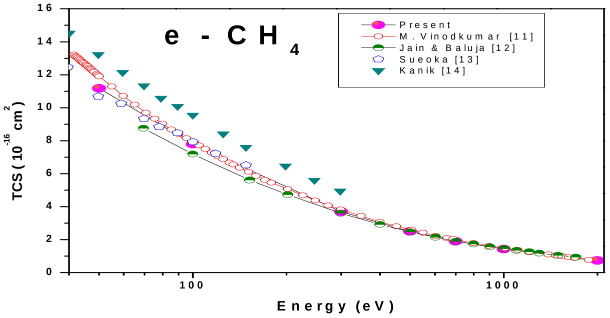

The present results for e $-CH_4$ are also in good agreement with the **theoretical studies** based on the Spherical Complex Optical Potential formalism (SCOP) by M.Vinodkumar [11] and Jain & Baluja [12]. Present results are also have a fine match with the experimental data of Sueoka [13]. While the Kanik et. al. [14] results are higher than all three theoretical estimates. At lower energies (below 80 eV), present results are in better agreement with the Sueoka [13] results as compared to [11]. Present results are found good with experimental results by Sueoka [13] as compared to result obtained by [12] for the whole available experimental energy range.

It is obvious to see that the present study based on weighted additivity method is in better agreement with the experimental data or as comparable with results based on other rigorous theoretical method [5, 11-12]. We look forward to apply this weighted additivity method for more molecular targets and would like to extend it for lower energy range.

References

[1] K.N.Joshipura, Minaxi Vinodkumar, Yogesh Thakar & C. G. Limbachiya, (1999), *Additivity approximations for molecules and radicals* Ind. J. Phys. B **73,** 245.

[2] Minaxi Vinodkumar, YogeshThakar, ChetanLimbachiya and K N Joshipura,(1998), *Additivity approach in electron molecule collision theory* Prajna Journal of Pure and Applied Physics **8,** 111.

[3] K.N. Joshipura, M. Vinodkumar, (1997), *Group additivity method*, Z. Phys. D **41**, 133

[4] B.K. Antony, K.N. Joshipura, N.J. Mason, (2005), *Group additivity method*, J. Phys. B: At. Mol. Opt. Phys. **38**,189.

[5] Dr. Minaxi Vinodkumar ,(1999), Collision process of electrons with atoms radicals and polyatomic molecules-A theoretical study'; Ph.D thesis.

[6] Editor: Russell D. Johnson III , NIST Computational Chemistry Comparison and Benchmark Database, NIST Standard Reference Database number 101 Release 15b, August 2011, http://cccbdb.nist.gov

[7] Ashok Jain, (1988), *Theoretical study of the total (elastic+inelastic) cross sections for electron -H_2O (NH_3) scattering at 10-3000 eV* J. Phys. B: At. Mol. Opt. Phys. **21**, 905

[8] K N JOSHIPURA, (1998), *Total cross sections for electron scattering from well-known and exotic molecules,* PRAMANA journal of Physics **50**, 555-561

[9] C. Szmytkowski, (1987), *Absolute Total Cross Sections for electron water vapour scattering,* Chem. Phys. Lett. **136**, 363

[10] G. Garcia private communicaton.

[11] M. Vinodkumar, K.N. Joshipura, C.G. Limbachiya, and B.K. Antony, (2006), *Electron impact total and ionization cross-sections for some hydrocarbon molecules and radicals,* Eur. Phys. J. D **37**, 67–74

[12] Jain, K.L. Baluja,(1992),*Total (elastic plus inelastic) cross sections for electron scattering from diatomic and polyatomic molecules, Phys. Rev. A* ***45****, 202*

[13] Sueoka, O., and S. Mori, (1986*), Total cross sections for low and intermediate energy positrons and electrons colliding with CH_4, C_2H_4 and C_2H_6 molecules* J.Phys B,**19**,4035.

[14] Kanik, I., S. Trajmar, and J. C. Nickel, (1992), *Total cross section measurements for electron scattering on CH_4 from 4 to 300 eV,* Chem. Phys. Lett., **193**, 281

COMPARATIVE STUDY OF ELECTRON AND POSITRON SCATTERING WITH CO_2 MOLECULES

H. N. Kothari[1], U. R. Patel[2, 3] and K. N. Joshipura[3]
[1]Universal College of Engineering and Technology, Gandhinagar - 382721
[2]Gandhinagar Institute of Technology, Gandhinagar - 382721
[3]Department of Physics, Sardar Patel University, V. V. Nagar - 388120

1. INTRODUCTION

Carbon dioxide is an important molecule in view of its occurrence in the atmospheres of Venus and Mars. In laboratory CO_2 is widely used in gaseous discharges or in low temperature plasma devices. In the present paper we have used the Spherical Complex Potential methodology, extended for ionization contribution [1-4] to calculate various total cross sections of CO_2 molecule by electron and positron impact from 15 to 2000 eV.

Positron is an important probe alternative to electron for investigating atoms molecules and solids. Our previous calculations on positron scattering with inert gases and diatomic molecules like N_2 and CO [4] have shown a good agreement with experimental results. We begin by noting that previous calculations of positron scattering with CO_2 molecules have disagreement with the respective experimental data. Therefore we are motivated to calculate total and ionization cross sections of present target with both projectiles, for a comparative study. Moreover, a mutual comparison of different total cross sections of e^+ - CO_2 also brings out interesting features especially at low energies.

2. THEORY

In our previous papers [1-4] we have successfully calculated ionization and total cross sections of several atomic/molecular targets using the methodology SCOP for electron impact. The ionization cross sections can be calculated using our well-known method *CSP*-ic (Complex scattering Potential- ionization contribution), discussed in [1-4]. In the present theoretical calculation, the target charge density, bond length and ionization potential are the basic input parameters which we have employed to calculate total (complete) cross sections Q_T, as a sum of total elastic and total inelastic cross sections. Also calculated are the ionization cross sections Q_{ion} of CO_2 molecules. Semi-empirical but reasonable arguments are invoked to extract the ionization cross sections from total inelastic cross section. We omit details here since these are given in [1-4].

3. RESULTS AND CONCLUSION

In fig.1. we have shown comparative plots of total cross sections (Q_T) of CO_2 molecule by e^- and e^+ impact from 15 to 2000 eV. Here our theoretical Q_T of electrons has a different shape as compared to the electron-data of Itikawa [5] at low energies. But at high energies it shows good agreement with measured e^- impact results of Garcia [6]. Our positron scattering Q_T have very good agreement in all energies with all measured results of Kwan et al.[7], Charlton et al. [8] and Hoffman et al. [9].

***Figure 1: e^+ CO_2 Red solid line present Q_T, black square Q_T by Kwan et al.* [7], *blue triangle Q_T by Charlton et al.* [8] *and purple square Q_T by Hoffman et al.* [9]. *e^{--} - CO_2 Black solid line the present Q_T, green solid line Q_T by Itikawa* [5] *and brown circle Q_T by Garcia et al.* [6].**

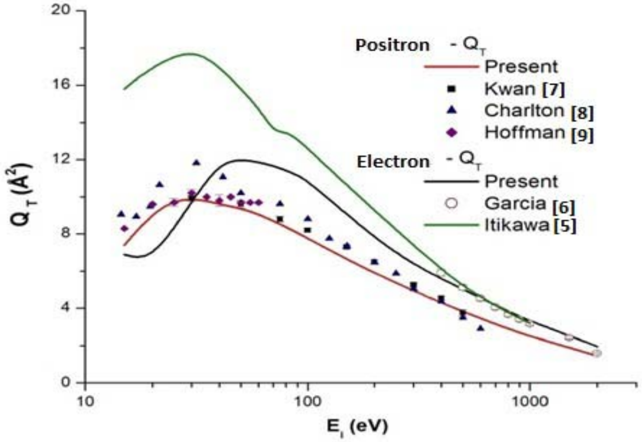

Our theoretical results of positrons can be interpreted in terms of the basic difference between electron and positron projectiles, particularly at low energies. We have analysed that our Q_T of e^- is around 1.5 times higher than that of e^+ at peak of ionization cross section (around at 70 eV). At high energies the present positron Q_T tend to merge with the Q_T of electrons as given by [5] and [6], as expected theoretically. However there are significant differences among the results of the two projectiles, as also among the different data-sets for the positron scattering. Therefore further studies, both theoretical and experimental, are required in this regard.

References

[1] Joshipura K. N., Vinodkumar M., Limbachiya C. G., Antony B. K., (2004), *Calculated total cross sections for electron impact ionization and excitations in tetrahedral (XY_4) and SF_6 molecules.* Phys. Rev. **A 69,** 022705.

[2] Kothari H. N., Pandya S. H., and Joshipura K. N., (2011), *Electron impact ionization of plasma important $SiCl_x$ (x=1-4) molecules: theoretical cross sections.* J. Phys. B: At. Mol. Phys. **44,** 125202.

[3] Kothari H. N. and Joshipura K. N., (2010), *Positron Scattering and Ionization of neon atoms – theoretical investigations.* Chin. Phys. **B 19,** 103402.

[4] Kothari H. N. and Joshipura K. N., (2011), *Total and ionization cross section of N_2 and CO by positron impact- Theoretical investigation.* Pramana – J Phys. **76,** 477.

[5] Itikawa Y., (2002), *Cross Sections for electron collisions with carbon dioxide.* J. Phys. Chem. Ref. Data **31,** 749.

[6] Garcia G. and Manero F., (1996), *Total cross sections for electron scattering by CO_2 molecules in the energy range 400–5000 eV* Phys. Rev. A **53,** 250.

[7] Kwan Ch. K., Hsieh Y. F., Kauppila W. E., Smith S. J., Stein T. S., Uddina M. N., and Dababneh M. S., (1983), *$e^{\pm}$-CO and $e^{\pm}$ -CO_2 total cross-section measurements.* Phys. Rev. A **27,** 1328.

[8] Charlton M., Griffith T. C., Heyland G. R., and Wright G. L., (1980), *Total scattering cross sections for intermediate-energy positrons in the molecular gases H_2, O_2, N_2, CO_2 and CH_4.* J. Phys. B **13,** L353.

[9] Hoffman K. R., Dababneh M. S., Hsieh Y. -F., Kauppila W. E., Pol V., Smart J. H., and Stein T. S., (1982), *Total-cross-section measurements for positrons and electrons colliding with H_2, N_2, and CO_2.* Phys. Rev. A **25**, 1393.

SCATTERING STUDIES OF Cl_2O BY ELECTRON IMPACT

Biplab Goswami and Bobby Antony
Department of Applied Physics, Indian School of Mines, Dhanbad 826004,
Jharkhand, India

1. INTRODUCTION

Electron interaction with molecular targets is considered to be an important field of research in plasma physics, radiation physics and space sciences. The highly reactive and unstable nature of Cl_2O molecules makes it difficult to perform experimental investigations on them. Cl_2O has substantial application in industry for hypochlorite formation [1]. In the present article the scattering dynamics of Cl_2O molecule has been studied using two distinct methodologies as discussed below.

2. THEORY

The present calculations are based on two methodologies. We have employ ab-initio R-matrix method through Quantemol-N [2] at low energies and spherical complex optical potential (SCOP) [2] formalism at high energies. In the inner region calculation the wave function has been constructed using the close-coupling (CC) approximation which can be written as

$$\psi_k^{N+1} = A\sum_I \psi_I^N\left(x_1,\cdots,x_N\right)\sum_j \zeta_j(x_{N+1})a_{Ijk} + \sum_m \chi_m(x_1,\cdots,x_{N+1})b_{mk} \qquad (1)$$

Where all the terms have their usual meaning and given in ref. [2]. The R-matrix has been used to obtain T-matrices which in turn give various total cross sections. The target parameters obtained are tabulated in table 1 and found to be in good agreement with previous results [1].

Table 1: Target properties of Cl_2O.

Target Properties of Cl_2O	**Present**	**Theory [1]**
Ground state energy(au)	-993.723	-
First excitation energy (eV)	3.154	3.17
Rotational constant (cm^{-1})	1.3993	1.4041
Dipole moment (D)	0.3819	0.3815

The SCOP method [2] is employed to estimate electron impact total inelastic, Q_{inel} and total elastic, Q_{el} cross sections using the complex potential,

$$V(r, E_i) = V_{st}(r) + V_{ex}(r, E_i) + V_{pol}(r, E_i) + iV_{abs} \tag{2}$$

By solving the Schrödinger equation using above potential, we get the scattering amplitude as,

$$f(k,\theta) = \frac{1}{2k}\sum_{l=0}^{\infty}(2l+1)\exp(i\delta_l)\sin\delta_l P_l(\cos\theta) \tag{3}$$

Employing this various total cross sections is computed.

3. RESULT AND DISCUSSION

There is a notable feature around 5.34 and 8.96 eV similar to that of Baluja et al [1]. The cross section is in good agreement with the only data available at low energy [1]. This hump contributes to the resonance in TCS curve. The total cross section calculated through SCOP at high energies gives good comparison at the transition energy of around 10 eV. No other comparison is available for this range.

Figure 1. Total cross section of e-Cl_2O scattering.

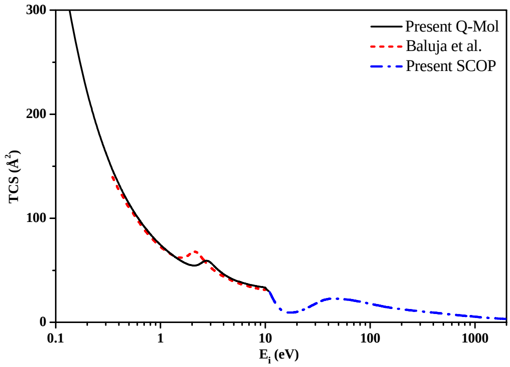

4. CONCLUSION

Calculations on e-Cl_2O become complex due to so many low lying energy states. In the present study we have performed meV to MeV e^- impact scattering by Cl_2O. The low energy cross section gives very good comparison with Baluja et al. [2] as expected. The cross section at high energies is a maiden attempt.

References

[1] Baluja K. L., Mason N. J., Morgan L. A. and Tennyson J., (2001), *Electron collisions with Cl_2O using the R-matrix method.* J. Phys. B: At. Mol. Opt. Phys. **34,** 2807.

[2] Vinodkumar M., Barot A., and Antony B., (2012), *Electron impact total cross section for acetylene over an extensive range of impact energies (1 eV–5000 eV).* J. Chem. Phys.**136,** 184308.

SCREENING CORRECTED TOTAL CROSS SECTIONS FOR $NH(CH_3)_2$ AND NH_2CH_3 ON ELECTRON IMPACT

H. S. Bhutadia[1], M. Y. Barot[2], K. M. Korot[3] and M. Vinodkumar[2]
[1]Government Engineering College, Patan, Gujarat
[2]V. P & R. P. T. P Science College, V. V. Nagar, Gujarat
[3]Government Engineering College, Modasa, Gujarat

1. INTRODUCTION

Electron driven processes on molecules are of great interest due its possibilities in the investigation of various applied areas like plasma physics, semiconductor industry, micro-electronics, atmospheric sciences and pollution remediation. A well-organized database on electron impact collision cross sections is essential for the modelling of such interactions in these environments. However, there is a serious void for cross section data on many important molecular systems. Even though many researchers are involved in this area of research, collection of various cross sections by experimental measurements alone are not feasible in the time scale required by the industry. Hence, alternative theoretical methods like Spherical Complex Optical Potential (SCOP) [1] formalism can be handy. Such methods albeit simpler, can effectively fill the gap since they produces cross section data quickly with reasonable accuracy.

Trimethylamine $N(CH_3)_3$ or TMA is a pollutant released to the environment from various exhaust like chemical industry, marine food manufacturers and also during cremation [2]. TMA is a highly volatile organic compound with a specific pungent property. It is dangerous to human beings and other living beings alike, as it has the property of tissue corrosion and tissue penetration. TMA is also considered to be an inhibitor of DNA, RNA and protein synthesis and is believed to have serious consequences on the development of fetus in animals [3]. Hence, removal of this highly toxic and malodorous organic waste is a top priority. For this purpose electron-driven techniques are being designed and conceptualized. However, for effective designing and construction of such devices where electron sources are employed, comprehensive data on electron scattering on these molecules are required [4]. Investigation on other derivatives of TMA ($NH(CH_3)_2$, NH_2CH_3) also finds importance due their production during electron irradiation of TMA in such environments.

The relations between electron scattering cross sections and physico-chemical properties of target molecules have been investigated since the earliest systematic measurements of cross sections [5]. These correlations indicate the role of target properties in the scattering process, while the semi-empirical formulae describing these correlations will help to estimate total cross sections (TCS) of targets for which experimental investigation are difficult and theoretical data is sparse. The analytical formula so obtained using these parameters can also be used to generate the total cross section data at very high energies where the partial wave analysis becomes impractical [6,7,8].

Electron impact total cross sections for these molecules have been very recently reported by Shi et al. [9] using additivity method and modified additivity method to take into account the geometrical screening effect for impact energies 30 to 5000 eV. They presented calculated total cross section by two modified additivity (MAR) methods. In the first case they have used the empirical fraction given by Jiang et al. [10] which they call 'original MAR' (oMAR) and for the second case they have estimated the empirical fraction considering the geometrical dimension of the molecule, which they call their 'present MAR' (pMAR). The pMAR seems to compare better with other data available. Experimental investigations are very sparse and are reported for both these target by Domaracka et al. [11].

2. THEORETICAL METHEDOLOGY

Independent atom model (IAM) is the simplest method to find cross sections for molecules on electron impact and are found to be successful particularly at high energies. In this model the molecule is substituted by its constituent atoms and such a crude approximation results in overestimating cross sections particularly at energies below 100 eV. This overestimation can be understood due to two facts: (i) the closely packed molecule is not fully transparent to low energy electrons ($E_i \lesssim$ 100 eV) and (ii) the mutual overlapping by neighbouring atoms and partial screening by the outer atoms are ignored [8]. Hence, it is evident that the inclusion of "screening effect" will lead to a decrease in molecular scattering cross section than that predicted by IAM [12].

In the present work we have considered the targets $NH(CH_3)_2$ and NH_2CH_3. We have made use of 'geometrical screening' [12,13] model with SCOP [13-15] to calculate the total cross sections for the present targets.

3. RESULT

Figures 1 and 2 show the total cross sections for e-NH(CH3)2 and e-NH2CH3 scattering with available comparisons respectively. Present results find very good accord with experimental results of Domaracka et al [11] and theoretical results of Shi et al [9]. Screening is more effective at low impact energies compared to high energies as seen from the curves

Figure 1: Total cross sections for $NH(CH_3)_2$ in $Å^2$. Solid line, Present Q_T; Dash, Present $Q_{T,SC}$(with screening correction); Dash-dot, Shi et al. (oMAR) [6]; Dash-dot-dot, Shi et al. (pMAR) [6]; Line with circles, Present fit using Analytical formula[4].

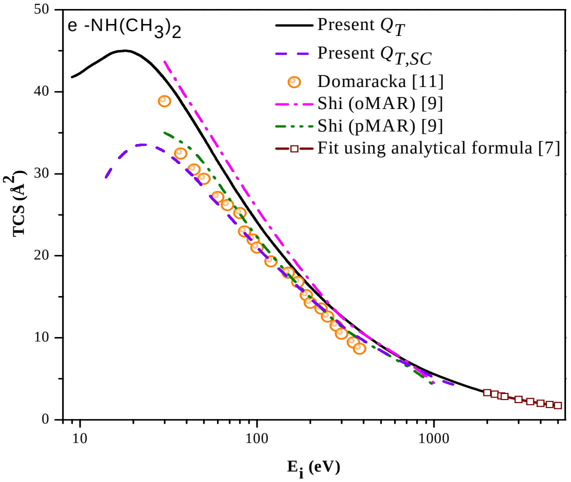

Figure 2: Total cross sections for NH_2CH_3 in Å^2. Solid line, Present Q_T; Dash, Present $Q_{T,SC}$(with screening correction); Dash-dot, Shi et al. (oMAR) [6]; Dash-dot-dot, Shi et al. (pMAR) [6]; Line with circles, Present fit using analytical formula [4].

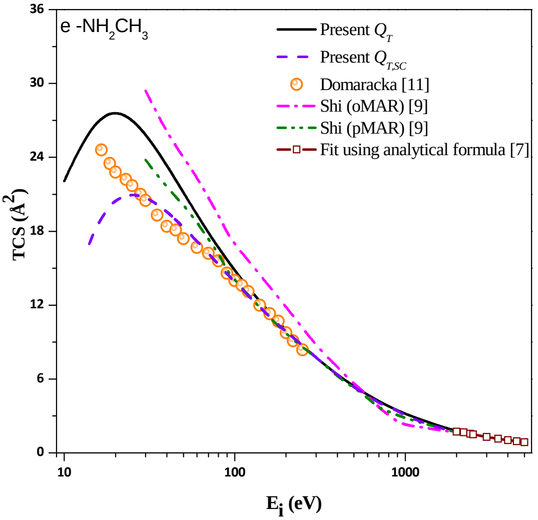

4. CONCLUSION

It was found that the calculation involving screening effect gives a better representation of the target system and produces better cross section data.

References

[1] Jain A. and Baluja K. L., (1992), *Total (elastic plus inelastic) cross sections for electron scattering from diatomic and polyatomic molecules at 10–5000 eV: H_2, Li_2, HF, CH_4, N_2, CO, C_2H_2, HCN, O_2, HCl, H_2S, PH_3, SiH_4, and CO_2.* Phys. Rev. A **45**, 202.

[2] Tanthapanichakoon W., Khongprasamkaln P., Charinpanitkul T., Tamon H., Sano N., and Okazaki M., (1999), Science Asia; **25,** 57.

[3] Guest I. and Varma D. R., (1992), *Teratogenic and macromolecular synthesis inhibitory effects of trimethylamine on mouse embruos in culture. J. Toxicol. Environ. Health.* **36,** 27.

[4] Szmytkowski Cz, Domaracka A., Możejko P., and Ptasińska-Denga E., (2007), *Collisions of electrons with trimethylamine $N(CH_3)_3$ molecules;* Phys. Rev. A; **75,** 052721.

[5] Brüche E., (1929), *Ergebnisse der exakten Naturwissenschaften*. **8,** 185.

[6] Bransden B. H. and Joachain C. J., (2003), *Physics of Atoms and Molecules, Pearson Education.*

[7] Vinodkumar M., Limbachiya C., Korot K., and Joshipura K. N, (2008), *Theoretical electron impact elastic, ionization and total cross sections for silicon hydrides, SiH_x ($x = 1, 2, 3, 4$) and disilane, Si_2H_6 from threshold to 5 keV.* Eur. Phys. J. D. **48,** 333.

[8] Szmystkowski Cz. and Krzysztofowicz A. M., (1995), *Electron scattering from isoelectronic, N_e=18, CH_3X molecules (X=F, OH, NH_2 and CH_3).* J. Phys. B: At. Mol. Opt. Phys. **28**, 4291.

[9] Shi D. H., Sun J. F., Zhu Z. L., and Liu Y. F., (2010), *Total cross sections of electron scattering by molecules NF_3, PF_3, $N(CH_3)_3$, $P(CH_3)_3$, $NH(CH_3)_2$, $PH(CH_3)_2$, NH_2CH_3 and PH_2CH_3 at 30–5000 eV.* Eur. Phys. J. D **57,**179.

[10] Jiang Y. H., Sun J. F., and Wan L. D., (2000), *Additivity rule for the calculation of electron scattering from polyatomic molecules*; Phys. Rev. A 62; 062712.

[11] Domaracka A., Możejko P., Ptasińska-Denga E., and Szmytkowski Cz., (2007), *Collisions of electrons with trimethylphosphine [$P(CH_3)_3$] molecules.* Phys. Rev. A 76, 042701.

[12] Blanco F. and Garcia G., (2003), *Screening corrections for calculation of electron scattering from polyatomic molecules*. Phys. Lett. A **317,** 458.

[13] Vinodkumar M., Korot K., Limbachiya C., and Antony B., (2008), *Screening-corrected electron impact total and ionization cross sections for borontrifluoride (BF_3) and boron trichloride (BCl_3);* J. Phys. B: At. Mol. Opt. Phys. **41,** 245202.

[14] Bhutadia H., Korot K., Antony B., and Vinodkumar M., (2010), *Screening Corrected electron impact total and ionization cross sections for $N(CH_3)_3$ and $P(CH_3)_3$. PRAJÑA - Journal of Pure and Applied Sciences* **18**, 140.

[15] Vinodkumar M., Bhutadia H., Antony B., and Mason N., (2011), *Calculation of electron-impact rotationally elastic total cross sections for NH_3, H_2S, and PH_3 over the energy range from 0.01 eV to 2 keV.* Phys. Rev. A **83**, 042708.

ELECTRON – SCATTERING WITH POLYATOMIC MOLECULES: SCREENING MODIFICATIONS IN GROUP ADDITIVITY RULE

P. Bhowmik*, R. Dawda and K. N. Joshipura
Department of Physics, Sardar Patel University
V. V. Nagar – 388 120, Gujarat
*Department of Agricultural Meteorology, Anand Agricultural
University, Anand – 388110, Gujarat

1. INTRODUCTION

Electron interactions with varieties of species and in variety of environments play a key role in understanding different atomic-molecular processes. In the present studies we have considered two large polyatomic molecules from different fields of application with different geometrical structure. Beginning with aerosol H_2SO_4 or sulfuric acid present in Earth's atmosphere, its concentration is increasing due to increase in amount of industrial pollution. Better understanding of various effects of atmospheric aerosols requires detailed information on how different sources and transformation processes modify the aerosol properties. On the other hand we have taken tetrahydrofuran (THF) which represents an analogue to the furan structure of the sugar in DNA backbone. Electron studies on this target helps in understanding the mechanism of DNA damage by ionizing radiation. There is need for more comprehensive theoretical investigations of electron scattering from such targets, with the models of radiation damage to estimate various cross sections for such bio-molecules. The paper presents ionization cross sections (Q_{ion}), total cross section (Q_T) of targets in the energy range from threshold to 2000 eV. Also attempted is probably the first calculation of electron H_2SO_4 scattering cross sections by complex spherical potential and group additivity rule. The properties of targets are listed in following table.

Table 1: Molecular properties of the present targets

Target	Ionization potential (eV)	Polarizability ($Å^3$)	Geometric correction factor Z
THF (C_4H_8O)	9.55	7.22	0.771
H_2SO_4	12.40	6.2	0.62

2. THEORY

We have used an improved Group Additivity Rule (GAR) to calculate Q_T and Q_{ion} for all large polyatomic molecules. In this method, the cross sections for different chemical functional groups in the molecule were calculated by the single centre approach and then contributions are added together to get the total cross section of the molecule. The number of scattering centres and their positions depend on the geometrical structure of the molecule. For example H_2SO_4 has three scattering centres two at OH group and one at SO_2. Cross sections for each group in the molecule are obtained theoretically by our CSP-ic method [1, 2]. Then the cross section contributions arising from these centers are added together to obtain the approximate total cross section as stated below,

$$Q(H_2SO_4) = Q(SO_2) + 2(OH) \tag{1}$$

Further, we have now modified this GAR in order to improve up on theoretical cross section obtained by group additivity. Let us consider the fact that polarizability of a molecule is a volume effect and has the unit and dimension of volume as Å^3. The cross sections has dimension of area as its unit is Å^2, so the geometrical area of a molecule AB can be represented by (polarizability)$^{2/3}$. Here A and B are different functional groups constituting the molecule. Therefore, a dimensionless parameter Z called geometrical correction factor is introduced The Z factor for H_2SO_4 is

$$Z = \frac{(\alpha_{H_2SO_4})^{\frac{2}{3}}}{(2*(\alpha_{OH})^{\frac{2}{3}}) + (\beta_{SO_2})^{\frac{2}{3}}} \tag{2}$$

Now the cross sections of H_2SO_4 molecule in the equation (1) can be modified to obtain cross sections with geometric corrections as follows.

$$Q(H_2SO_4) = Z[Q(SO_2) + 2(OH)] \tag{3}$$

3. RESULTS AND DISCUSSIONS

We have calculated Q_{ion} of H_2SO_4 by GAR, then compared it with the Q_{ion} which is taken as the sum of the experimental Q_{ion} of Tranovsky et al [3](for OH) and Orient et al [4] (for SO_2) and similarly that of Tarnovsky et al and Basner et al [5] (SO_2). It can be seen in Fig. 1 that Q_{ion} using GAR is larger than the sum of experimental Q_{ion}. This is due the fact that Group additivity does incorporate the bonding effects between OH and SO_2 group. We have also used the Modified GAR to incorporate correction factor Z. The corrected Q_{ion} obtained are compared again with Q_{ion} obtained by the summing Q_{ion} of the individual groups. It can be seen that the new reduced theoretical ionization cross sections are now comparable with Q_{ion} obtained from the experimental results at incident energies above 60 eV.

Fig 1 Q_T, Q_{ion} ***e-H_2SO_4 scattering by modified GAR.***

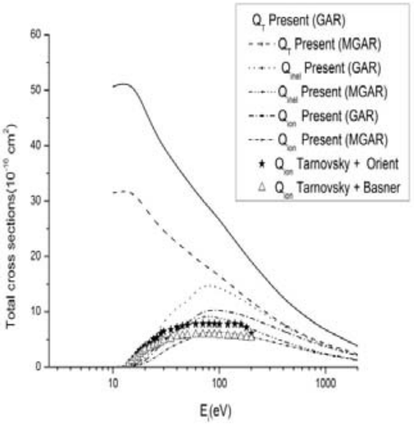

Fig 2 Q_T, Q_{ion} ***e-THF scattering by modified GAR.***

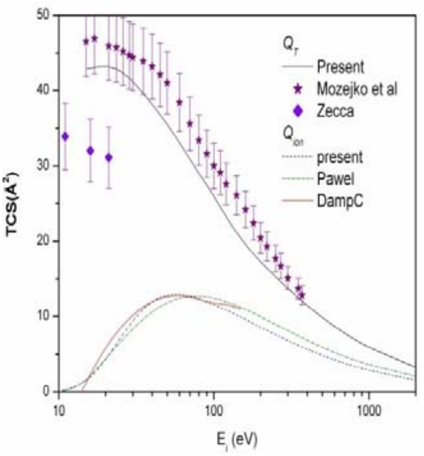

In fig 2 total cross sections and ionization cross sections of THF are displayed. At low and high energies, our Q_T are within the error bar of measurements reported by Pawel et al. [6] But at intermediate energies present result is slightly lower than the measurements. Moreover, measured cross section published by Zecca et al. [7] is much lower than Pawel et al. [8] and hence is lower than our result also. The Q_{ion} for THF as reported in fig 2 is in excellent matching with BEB result by Pawel *et al* and also with the measurements of Dampc et al. [9]. This shows that the modification introduced in this cyclic molecule is yielding good results and is showing a good match with the previous work reported for the target THF.

4. CONCLUSION

We have probably the first calculations of the theoretical cross sections for e- H_2SO_4 scattering. The model has reduced overestimation of cross sections at the present energy regime. Thus, modified GAR can be applied successfully on large polyatomic molecules to calculate various cross sections.

References

[1] Kothari H. N., Pandya S. H., and Joshipura K. N., (2011), *Electron impact ionization of plasma important $SiCl_x$ (x = 1-4) molecules: theoretical cross sections*. J. Phys. B: At. Mol. Opt. Phys. **44**, 25202.

[2] Pandya S. H., Shelat F. A., and Joshipura K. N., (2012), *Electron ionization of exotic molecular targets CN, C_2N_2, HCN, HNC and BF-Theoretical cross sections*; Int. J. Mass Spectrum; 323–324, 28.

[3] Tarnovsky V., Deutsch H., and Becker K., (1998), *Electron impact ionization of the Hydroxyl radical*. **109,** 932.

[4] Orienta O. J., and Srivastava S. K., (1984), Mass spectrometric determination of partial and electron impact ionization cross sections of SO_2 from threshold up to 200 eV. J. Chem. Phys.; **80**, 140.

[5] Basner R., Schmidt M., Deutsch H., Tarnovsky V., Levin A., and Becker K., (1995), *Electron impact ionization of the* SO_2 *molecule*. J. Chem. Phys. **103**, 211.

[6] Możejko P., Ptasinska, Domaracka A., and Szmytkowski Cz., (2006), *Absolute total cross sections measurement for electron collisions with tetrahydrofuran*. Phys. Rev. A **74,** 012708.

[7] Zecca A., Perazzolli C., and Brunger M., (2005), Positron and electron scattering from tetrahydrofuran; J. Phys. B: At. Mol. Opt. Phys **38,** 2079.

[8] Możejko P., and Sanche L., (2005), *Cross sections for electron-scattering from selected components of DNA and RNA.* Rad. Phys. Chem.**73**, 77.

[9] Dampc M., Linert I., Milosavljevic A. R., and Zubek M., **(**2007), *Differential cross sections for low energy elastic electron scattering from tetrahydrofuran in the angular range* 20^o - 180^o. Chem. Phys. Lett. **443,** 17.

HEAVY ION IMPACT ON URACIL: ABSOLUTE TOTAL CROSS SECTIONS MEASUREMENTS

A. N. Agnihotri[1], S. Kasthurirangan[2] and L. C. Tribedi[1]
[1]Department of Nuclear and Atomic Physics, TIFR, Mumbai
[2]Institute of Chemical Technology, Matunga, Mumbai

1. INTRODUCTION

Heavy ion impact studies on small atoms as well as large molecules and clusters have been of great interest for several decades. The studies address wide spectrum of interests ranging from fundamental interaction processes to the applications in several fields e.g., radiation damage modeling and astrophysics. While several studies are available on the dynamics of the interactions involving large molecules in collisions with highly charged heavy ions [1, 2], absolute cross section measurements have been scarce and limited to proton impact [3]. Uracil, being a base molecule of the Ribonucleic acid, is of great interest and the absolute TCSs can be a crucial input for modeling the radiation damage caused by the GeV energy ions used in Hadron therapy. The GeV energy ions, while going through the body, lose energy in a special manner and the energy loss peaks in a certain energy range called the Bragg peak [4].

2. EXPERIMENT

We have measured absolute total ionization cross sections of uracil in collisions with keV-MeV energy (Bragg peak range) highly charged C, O and F-ions for charge states (q) ranging from 4 to 9 [5,6]. A Wiley-McLaren type of recoil-ion mass spectrometer setup was used. The uracil was heated in an oven to produce an effusive jet of the molecules. The molecules were heated very slowly (~8 hours). A quartz crystal thickness monitor was mounted on the top of the jet to measure the flow rate of the molecules *in situ*, throughout the experiments. The keV and MeV energy ions were produced in an ECR ion source based ion accelerator [7] and Pelletron accelerator in TIFR, respectively. The ion beam, after collimation, was crossed with the effusive jet of molecules in a vacuum chamber. The ions and electrons, produced as a result of interaction were extracted in opposite directions and were detected by the channeltron detectors. The co-incidence between the ion and electron signals gives the time-of-flight spectrum (TOF) of the ions and fragments produced in collisions. Adding the yields of the parent ions and of the fragments, gives the total ionization yield. The absolute normalization [5] of the data was done by measuring the absolute electron emission cross sections of uracil in collisions with 42 MeV C^{6+} -ions in a separate experiment [8].

3. RESULTS AND DISCUSSIONS

Figure 1: Total ionization cross sections of uracil in collisions with (a) O^{6+}, (b) C^{6+}-ions [5,6].

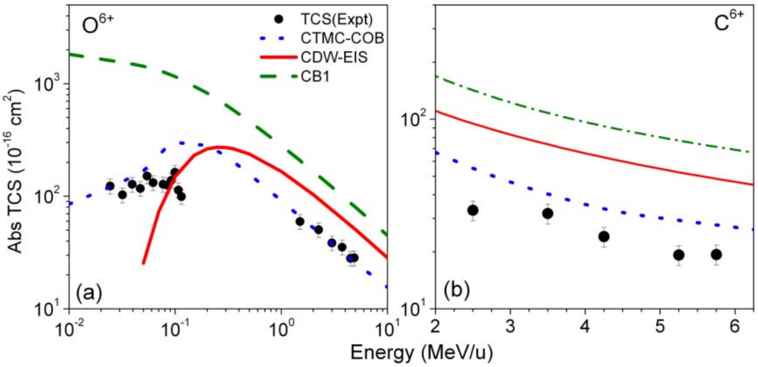

Fig. 1 shows the total cross sections plotted with projectile energy. In Fig 1(a), while going from low to high energies, the TCS increases, saturates and falls sharply indicating a peak in the middle energy range. This behavior is well known as the ionization cross sections peak in the intermediate velocity (v) range. The experimental data was compared with state-of-the-art CTMC-COB, CDW-EIS and CB1 models [5]. In general, the models overestimate the experiments by a factor of 2-3. However, in the high energy range the sharp fall is well reproduced. In low energy range the models, due to their perturbative nature, do not reproduce the experimental data.

Figure 2: Projectile-q and Z_P dependence of TCS. C-ions are shown by squares and O-ions by circles [5].

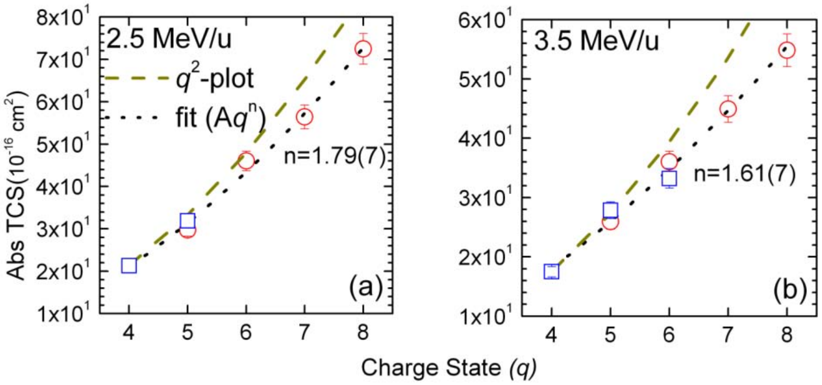

We have studied the charge state dependence of the TCS at several projectile energies [5,6]. The experiments show that the q-dependence of TCS (Figure 2) deviates from q^2 –dependence which is well known in case of ion-atom/small molecule collisions. The data was fitted with the function Aq^n. The average value of n was found to be ~1.5 [5,6]. The projectile nuclear charge (Z_P) - dependence of the TCS was studied using C and O-ions keeping the perturbation strength constant. In figure 2, the squares and the circles show the C and O-ions respectively. The cross sections were found to be independent of Z_P [5]. The details will be presented.

4. CONCLUSIONS

Absolute total ionization cross sections of uracil in collisions with highly charged C, O and F-ions are measured in a wide energy (keV-MeV) range. The TCS were measured with varying projectile charge states. The charge state dependence of TCS was found to be $q^{\sim 1.5}$ which is a deviation from the case of atoms and small molecules. The TCS were found to be independent from projectile Z.

References

[1] deVries J., Hoekstra R., Morgenstern R., and SchlathÖlter T., (2003), *Charge Driven Fragmentation of Nucleobases,* Phys. Rev. Lett. **91**, 5, 053401.

[2] Tabet J., Eden S., Feil S., Abdoul-Carime H., Farizon B., Farizon M., Ouaskit S., and Märk T. D., (2010), *20–150-keV proton-impact-induced ionization of uracil: Fragmentation ratios and branching ratios for electron capture and direct ionization*, Phys. Rev. A **81**, 012711.

[3] Iriki Y., Kikuchi Y., Imai M., and Itoh A., (2011), *Absolute doubly differential cross sections for ionization of adenine by 1.0-MeV protons,* Phys. Rev. A **84**, 032704.

[4] Montenegro E. C., Shah M. B., Luna H., Scully S. W. J., de Barros A. L. F., Wyer J. A., and Lecointre J., (2007), *Water Fragmentation and Energy Loss by Carbon Ions at the Distal Region of the Bragg Peak,* Phys. Rev. Lett. **99**, 213201.

[5] Agnihotri A. N., Kasthurirangan S., Nandi S., Kumar A., Galassi M. E., Rivarola R. D., Foj´on O., Champion C., Hanssen J., Lekadir H., Weck P. F., and Tribedi L. C., (2012), *Ionization of uracil in collisions with highly charged carbon and oxygen ions of energy 100 keV to 78 MeV,* Phys. Rev. A **85**, 032711.

[6] Agnihotri A. N. *et. al.*, (2012), *Absolute total ionization cross sections of uracil($C_4H_4N_2O_2$) in collisions with MeV energy highly charged carbon, oxygen and fluorine ions* , J. Phys. B (Submitted)

[7] Agnihotri A. N., Kelkar A. H., Kasthurirangan S., Thulasiram K. V., Desai C. A., Fernandez W. A. and Tribedi L. C., (2011), *An ECR ion source-based low-energy ion accelerator: development and performance* Phys. Scr. **T144** 014038.

[8] Agnihotri A. N. *et al.*, (2012), *Double differential distribution of electron emission in ionization of uracil in collisions with 3.5 MeV/u bare C-ions,* Phys. Rev. A (Submitted).

FAST-ION AND ELECTRON INDUCED ELECTRON EMISSION FROM ATOMS, WATER AND BIO-MOLECULES

Lokesh C. Tribedi
DNAP, Tata Institute of Fundamental Research, Colaba
Mumbai, India

1. INTRODUCTION

The experimental and theoretical investigations on ion-atom and electron-atom collisions have been extended to the large molecules and clusters in recent years [1-18]. We have investigated the electron double differential cross sections in ionization of simple atoms to large molecules induced by fast ions and electrons. A typical electron DDCS spectrum arising from the ionization of a target atom or molecule comprises of a peak at nearly zero energy. Such "target"-centered peak is known as soft-electron peak. The binary encounter electron emission is seen as a broad peak which can be explained by a classical model. The electron capture in continuum cusp (ECC) is a projectile centered process and is represented as a cusp in the electron spectrum observed in zero degree emission. In case of ion-atom ionization the electron emission is influenced by the two-center Coulomb interaction, giving a large asymmetry in forward-backward emission. When the projectile is a fast electron beam, then, of course, one gets a much more symmetric angular distribution owing to a negligible two center effect. In a major breakthrough, a series of experiments have been carried out in the last decade to explore the role of a diatomic molecule as a double slit. As a result of the coherence-driven Young type electron interference, an oscillatory structure has been observed in the electron DDCS spectrum. Such experiments are now extended for different collision systems, involving electrons, photons and fast ions as projectiles. In turn, the wealth of data of different types has helped the theoretical models to grow regarding the choice of molecular wavefunctions as well as the interaction potential. In case of ionization of clusters and large molecules including fullerenes and DNA/RNA base molecules, one has to invoke the collective excitation, many-body or size effects in order to understand the electron emission spectrum and their angular distributions. These studies address a wide spectrum of interests ranging from fundamental interaction processes to the applications in several fields e.g., radiation damage modeling for very high energy ion-beams passing through human body for radiation therapy, astrophysics, plasma physics etc. While several studies are available on the dynamics of the interactions involving large molecules in collisions with highly charged heavy ions, absolute cross section measurements have been scarce and limited mainly to proton impact. Uracil, being a base molecule of the ribonucleic acid (RNA), is of great interest and the absolute total ionization cross section can be a crucial input for modeling the radiation damage caused by the GeV energy ions used in Hadron therapy. The GeV energy ions, while going through the body, lose energy in a specific manner and the energy loss peaks in a certain energy range called the Bragg peak. The Bragg peak falls in the energy range of ~100s of keV to a few MeV. The dependence of the DDCS and the TCS on the projectile atomic number, charge state, energy, sign of charge (electron and positive ions), target atomic numbers (H, He, Ne) and type of molecules (H_2, N_2, O_2, H_2O, uracil, coronene) are investigated over the years. In this article we give a brief overview of our recent studies focusing mostly on the experiments with $O_2$and H_2O as target molecule.

2. EXPERIMENT

The fast highly charged ions are obtained from two different accelerators. i) The low energy ions (30 keV to a few MeV) ions can be obtained from the newly built ECR source based ion accelerator. A 14.5 GHz 500W electron cyclotron resonance plasma chamber is placed on a 400 kV deck which produces the ions of different charge states. An Einzel lens followed by a double focussing 90^0 bending magnet, producing a maximum field of 3000G, on the deck is used to select desired charge state. The ions accelerated across the several accelerating columns are then made to pass through a switching magnet. Three beamlines are built at 0^0, $+50^0$ and -50^0 out of five existing ports on the switching magnet. Each beamlines are equipped with various beam-optical components, such as, the electrostatic quadrupole triplet for focussing the ion-beams, a series of x-y deflectors, and diagnosis boxes containing Faraday cups and beam-profile monitors. A set of 4-jaw slits are also used to collimate the ion beams. So far, H, He, C, O, N, Ne and Xe beams are used mostly. Fully stripped C, O, N, Ne, He-like Ar and Xe^{29+}ions are used for experiments or to test the intensity optimization of the ion-beams. ii) The high energy ions (i.e. about 20-120 MeV) ions are obtained from the 14 MV tandem Pelletron accelerator at TIFR. A post accelerator carbon-foil-stripper assembly is used to produce higher charge state ions after passing through the analyzing magnet. The charge state selected ions are then made to pass through a couple of 4-jaw slits kept about a meter away from each other in order to collimate the beams. iii) In electron-collision experiments we use the fast electron beams of energy up to 10 keV which are obtained from a commercially available electron beam gun which is equipped with Einzel lens and x-y deflectors. Additional beamline components, such as, lens and deflector and a series of collimators comprise the e-beam line which delivers the beams to the target chamber. In some experiments which uses time-of-flight recoil-ion techniques one needs a pulsed electron beam which has also been developed.

In a typical experiment, the scattering chamber is flooded with the target gas at a low pressure, i.e., typically between 0.15 mT to 0.3 mT, as measured with the help of a capacitance manometer (in this case MKS Baratron). In case of the low energy electron detection experiment, we use a hemispherical electrostatic energy analyzer. In order to detect the low energy (~eV) electrons it is important to reduce the earth's magnetic field and two layers of thin (0.3-0.5 mm) μ-metal sheets are shown to be enough for this purpose i.e. to reduce the field in order to reduce it to less than 10 mG near the interaction region. A channel electron multiplier (CEM) placed just outside the exit slit of the analyzer is used to detect the energy analyzed electrons. Further details can be found in Nandi et al [12]. For each angle, the electron double differential cross section (DDCS) were determined from the measured electron counts at different energies for a prefixed amount of incident projectile charge collected on a Faraday cup. In case of experiment with water molecules the vapour produced at room temperature is used in a static gas condition. The difficulties arise due a relatively large background arising from the condensation and special precaution had to be taken in order to reduce the background contribution. For experiments with biomolecules and fullerenes, one has to use a vapor source i.e. an oven heated to a suitable temperature. Several experiments are in progress, such as, with uracil, adenine and fullerenes. The collimated ion beam was crossed with an effusive jet of molecules. In the time of flight based experiments the ions and electrons, produced in collisions, interaction were extracted in opposite directions and were detected by the channel electron multiplier detectors. The recoil-ions and electrons detected in coincidence, thus, give the time-of-flight spectrum (TOF) of the ions and fragments produced in collisions. In this report we discuss some of our recent experimental results using electron spectroscopy.

3. RESULTS AND DISCUSSIONS

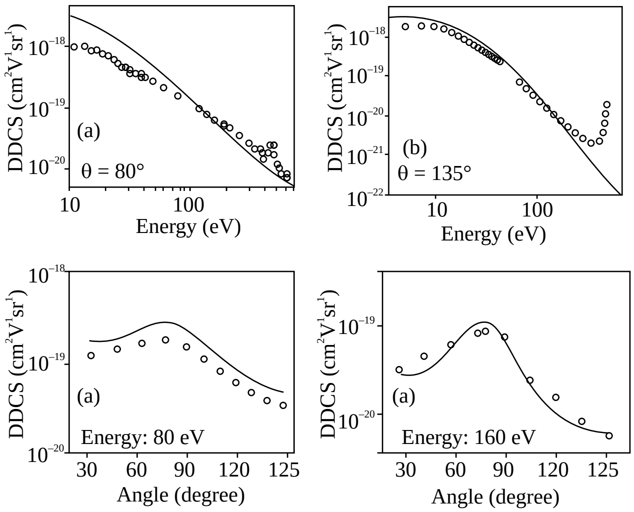

Figure 1 DDCS vs electron energy for angles 60^0 (a) and 135^0 (b) in case of 3.5 MeV/u C^{6+}+O_2 collisions. The angular distribution of DDCS at a fixed energy 80 eV (a) and 160 eV (b). (From Nandi et al [12])

In Figure 1(a-b) we show some representative results on the electron DDCS measurements on the di-atomic molecule O_2 in collisions with a fast bare carbon ions of energy 3.5 MeV/u. The main motivation was to investigate the Young type electron interference for multi-electronic homo-nuclear di-atomic molecular systems which are much less investigated. A few recent investigations with the N_2 and O_2 showed the second order oscillations in absence of any first order oscillatory structures. Tachino et al [17], however, predicted theoretically the absence of any oscillatory structure due to the possible nearly complete cancellation of the oscillations while adding the contributions from different orbitals. For each molecular orbital (MO), the initial bound wavefunction was written as a linear combination of slater-type orbitals (STOs) centred on each nucleus of the diatomic molecule. More details of the calculations will be found elsewhere. In the DDCS spectrum for both the angles apart from the continuum part the line spectrum arising from KLL Auger process is clearly seen. The CDW-EIS calculations seem to cross over the experimental distribution for 60^0. The overall agreement is better for 135^0. The Auger process, which represents inner-shell ionization, is not considered in the model. The angular distribution (Fig 1(c-d)) is very well reproduced for relatively higher energy electrons, such as, for 160 eV. But at lower energy (e.g. 80eV) the theory overestimates the data throughout the angular range, although the shape of the distribution is well reproduced.

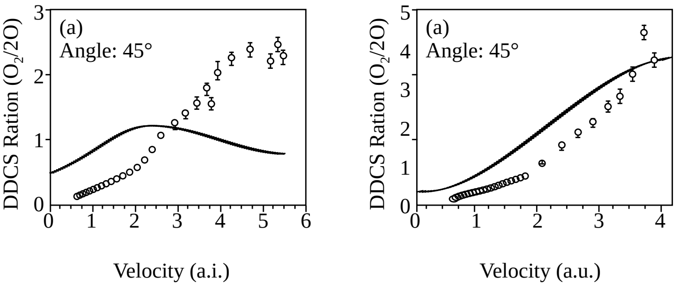

Figure 2 DDCS ratio (O2/2O) for 3.5MeV/u C6++O2: Comparison with CDW-EIS calculations
(From Nandi et. al. [12])

Now, in order to derive any oscillation in the electron spectrum one has to take the ratio of the DDCS for O_2 to that for atomic O. In this way the incoherent part of the DDCS are cancelled and the remaining part is the coherent part arising from the interference. In this way the oscillations in the electron spectrum was revealed in case of H_2. The DDCS ratios (O2/2O) are plotted in Fig 2(a-b) for two different angles. It is obvious that the ratios do not show any kind of oscillation. This is in apparent conflict of the observations for H_2-ionization. The monotonic increase of this quantity has been qualitatively reproduced by the model calculation. The details show similar behaviour for other angles too. The nonappearance of the oscillation has been understood in terms of cancellation of the contributions from different orbitals which are phase shifted from each other and produces no or slight oscillation while summed over to compare with the experimental data. Another way to observe such oscillation is to derive the forward-backward angular asymmetry which is sensitive to the oscillations in the DDCS spectrum. Figure 3 shows the asymmetry parameter as a function of electron velocity (k) in a.u. where is defined as [DDCS(150)-DDCS(30)/(DDCS(30)+DDCS(150)]. It is obvious that α(k) monotonically increasing function, showing no oscillation which is good agreement with the model calculation (not shown).

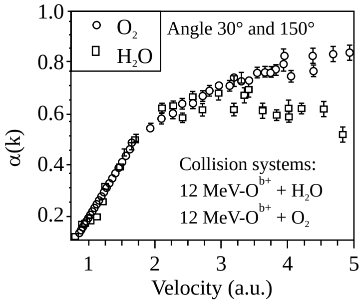

Figure 3 Comparison between O_2 and H_2O, for the forward-backward angular asymmetry parameter.

Similar data on e-DDCS i.e. results on its energy and angular distribution are obtained for water molecules. Since water is a major constituent of human body, experimental data on heavy ion induced electron emission provides important clue for the radiation damage caused during hadron therapy usually being used in high energy heavy ion accelerators. The different theoretical models are used to calculate such cross sections in order to use them for the radiation damage modelling. However, a stringent test to these models requires the accurate measurement of the electron DDCS. Fig 4(a-b) shows the emitted electron energy dependence of the DDCS for two different emission angles (60^0 and 105^0). In both cases the DDCS falls by about three orders of magnitude while going from 1 eV to 300 eV. This is different for O_2 (see Fig. 1(a)) for which the fall is by 2 orders for forward angle.

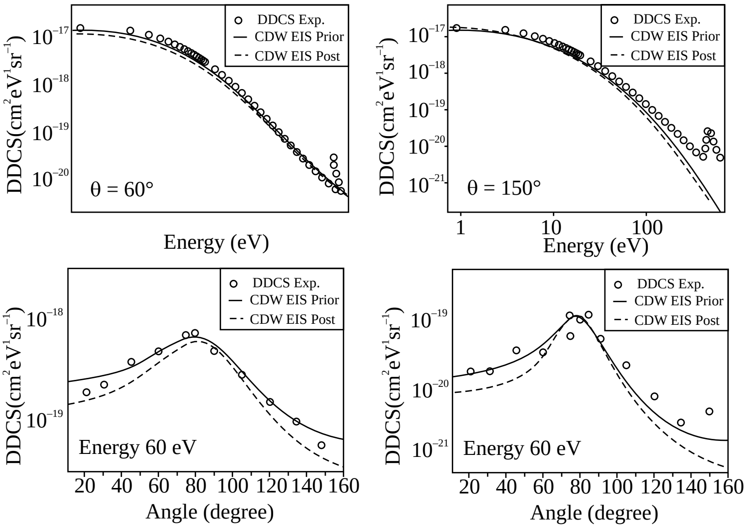

Figure 4 DDCS vs electron energy for angles 60^0 (a) and 105^0 (b) in case of 3.5 MeV/u C^{6+}+H_2O collisions. The angular distribution of DDCS at a fixed energy 60 eV (c) and 200 eV (d) (see Nandi et al. [16]).

However, for backward angles the fall is approximately similar for oxygen and water. The CDW-EIS calculation with prior form reproduces the distributions very well (solid line). The post form of the model is shown as dashed line which shows a slightly more deviation. The difference between the post-prior models is well reflected in the angular distribution plots, as shown in Fig. 4(c,d). It is obvious that the prior form (solid line) gives a much better agreement than the post-model, especially, for the forward and backward angles. Both the models come closer to the data around 90^0. The asymmetry parameter for the O_2 and H_2O molecule show almost similar behaviour (Fig. 4) for lower energy electrons. However at higher energy this parameter seems to fall unlike that in case of O_2 or even other atomic targets.

4. CONCLUSIONS

Heavy ion induced ionization and fragmentation studies with simple atoms and molecules are extended to clusters and large molecules including DNA/RNA base molecules, and PAH molecules. Low energy highly charged ions from an ECR based ion-accelerator have been used to complement the experiments conducted using the fast ion beams from high energy Pelletron accelerator and fast electron-beam obtained from an e-gun based setup. In particular, the combined influence of the two centre effect on electron DDCS spectrum and the coherence-driven Young type interference induced oscillation have been investigated for diatomic molecules. The DDCS ratios and asymmetry parameter do not show any appreciable oscillation for the O_2 target unlike that for H_2. In addition, the detailed investigation of the DDCS and total cross sections for water molecule under heavy ion impact has been initiated. The asymmetry parameter show a fall after initial increasing behaviour which is untypical of fast ion-atom collisions. On the other hand for large molecule, such as uracil, the asymmetry parameter is unusually large at low energies implying a large enhancement in the forward emission which is again dramatically different than that for O_2 molecules or for other simple atoms.

Acknowledgements: This work would not have been possible without the active participation of my colleagues. Particularly I would like to thank S. Nandi, A. N. Agnihotri, S. Kasthurirangan, and D. Misra for a very active and vibrant collaboration who are the authors of several joint publications related to the topics discussed here. I would also thank the Pelletron accelerator facility and the ECR-team for smooth running of the facilities.

References

[1] U. Kadhane et al. Phys. Rev. Lett. **90**, 093401 (2003)
[2] U. Kadhane et al. Phys. Rev. A (Rapid comm.) **75**, 041201 (R) (2007)
[3] A. H. Kelkar et al. J. Phys. B **40**, 2481 (2007)
[4] A.H. Kelkar et al.Nucl. Instrm. Meth. B **256** 114 (2007)
[5] A.H. Kelkaret al Phys. Rev. A**82**, 043201(2010)
[6] L.C. Tribedi and A.H. Kelkar, INJP 1749-1760 (2011)
[7] A.N. Agnihotri et al. Phys. Rev. A, **85**, 032711 (2012)
[8] L.C. Tribedi et al. Eur. Phys. J. D **66**: 303 (2012)
[9] S. Kasthurirangan et al. Rev. Sc. Instr. **83**, 073111(2012)

[10] D. Misra et al. J. Phys. B **45**, 225201 (2012)
[11] S. Nandi et al. Phys. Rev. A **85**, 062705 (2012)
[12] S. Nandi et al. J. Phys. B **45**, 215207 (2012)
[13] S. Nandi et al.Phys. Scr (2013) (in press)
[14] S. Kasthurirangan et al.Phys. Scr. (2013) (in press)
[15] A.N. Agnihotri et al. J.Phys.B (2013) (in Press)
[16] S. Nandi et al. Phys. Rev. A **87**, 052710 (2013)
[17] C. A. Tachino et al. J. Phys. B **45**,025201 (2011).
[18] D. Ohsawa et al. Phys.Rev. A **72**, 062710 (2005).
[19] A. N. Agnihotri et al. Phys. Scr. T **144**, 014038 (2011).

COLLISION OF NAPHTHALENE WITH ENERGETIC PROTONS

Preeti Manjari Mishra[1], Jyoti Rajput [2], C. P. Safvan [3], Sarita Vig[4] and Umesh Kadhane[1]

[1]Department of Physics, Indian Institute of Space Science & Technology, Trivandrum, India
[2]Deaprtment of Physics & Astrophysics, Delhi University, New Delhi, India
[3]Inter-University Accelerator Centre, Aruna Asaf Ali Marg, New Delhi, India
[4]Department of Earth & Space Science, Indian Institute of Space Science & Technology, Trivandrum, India

1. INTRODUCTION

The study of structural & dynamical properties of Polycyclic Aromatic Hydrocarbon is a research area of considerable interest in environmental & biological science as well as space physics because of its wide applications in electronic devices based on crystalline thin films, role in interstellar physics & chemistry [*Tielens 2008*] and mutagenic & carcinogenic nature [*Micelotta 2009*]. They constitute 10-30% of interstellar carbon [*Tielens 2008*] & formed as a byproduct due to incomplete combustion of fuel[*Portella et al 2005*]. Hydrogenated PAH [*Pathak et al 2008*], PAH cation [*Tielens 2008*] have been proposed as possible carrier for the diffuse interstellar bands. We try to study the stability & different dissociation/fragmentation/ionization mechanism of PAHs in the harsh environment of ISM, after interacting with proton from cosmic rays by doing ion atom collision experiment for naphthalene, a member of PAH family.

2. EXPERIMENTAL DETAILS

The experiment has been carried out in the Low Energy Ion Beam Facility, IUAC, New Delhi using an electron cyclotron resonance ion source. The proton projectile beam of energy 50 KeV to 240 KeV was made to collide with Naphthalene target effusing from a needle placed perpendicular to the projectile beam path. The ionic species produced were detected by a position sensitive micro channel plate detector after extraction by a linear two field time of flight mass spectrometer. Multi coincidence measurements were done in both ionization & electron capture mode by a multihit data acquisition system. The detail layout of the experimental set up is described elsewhere [*De et al 2006*].

2.1 Data Analysis

The intact as well as fragmented ions were detected under two modes: electron capture by projectile & electron emission by ionisation. The integrated areas were taken from the mass spectra by taking care of ion, projectile, electron detection efficiency & in some cases the least square fitting has been done to find out the H, 2H loss contribution from the parent ion.

3. RESULT AND DISCUSSION

3.1 Experimental Results

The two different experimental modes clearly isolate the physical processes on the basis of mass spectrum obtained. Fragmentation was found to depend weakly on projectile energy in both the cases, H^+ and double ionisation was found to depend strongly on the projectile energy and particularly so for electron capture mode. Single ionisation followed by double ionisation was found to be the dominant in the mass spectrum for both ionisation & capture mode. The singly & doubly charged intact molecular ion relative cross section in case of pure ionisation was found to be 5.5 times then the capture cross section. The classical over the barrier model [*Bárány et al 1985*] was used to estimate the capture cross section for singly charged Naphthalene which was found to be 86 x 10^{-16} cm ^{2} which is much larger than the molecular dimension. The single & doubly charged parent ion peak are associated with loss of H& 2H where 2H loss was found to be more significant process as compare to H loss in case of double ionisation. Relative fraction of H and 2H loss with respect to single ionisation is observed to be constant in the studied projectile energy range for electron emission as well as electron capture mode describing a statistical distribution of energy in the molecule, from these limiting values of rates of dissociation were found out.

Figure 1:Single electron capture mode.

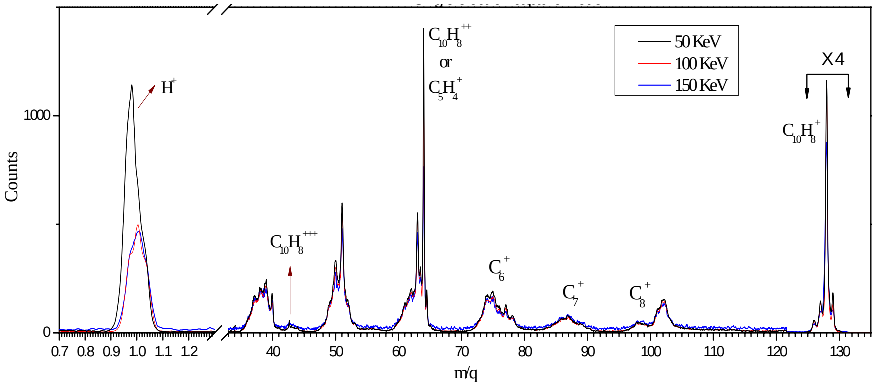

Mass spectrum for proton beam projectile showing the singly ionised Naphthalene along with H & 2H & C_2H_2 loss peak.

3.2 Theoretical Modelling

Two different theoretical technique were used for estimating electronic energy loss by an ion when it interacts with the target electrons by calculating i) stopping cross section [*Postma et al 2010*] ii) Average energy loss and straggling [*Kabachnik et al 1997, Lindhard et al 1964*] which are used to compare the threshold of relative ionization & H, 2H, C_2H_2 loss cross-sections obtained from present experiment. Monte carlo simulation was done to model the random trajectories of the projectile ions of different velocity & energy deposited by these trajectories were calculated by using statistical energy deposition model & electron density over the entire molecular volume obtained from optimized neutral naphthalene at B3LYP/6-311G with the help of GAUSSIAN 09. More investigation is on and details will be presented.

4. CONCLUSION

The photo excited or collisionally excited PAHs undergoes de-excitation either by emitting IR radiation or fragmentation by H-loss mechanism which is the weakest bond & most favorable channel to break since accumulating higher charges is unlikely for small sized PAHs. Therefore coupling of various collisional interactions to H-loss process is of great significance in understanding the survival and role of PAHs in ISM. In this present study we have explored the energy dissipation mechanism related to H, 2H loss & hence the catalytic activity & stability of PAHs under proton impact of different energy.

References

[1] A. Bárány, G. Astner, H. Cederquist, H. Danared, S. Huldt, P. Hvelplund, A. Johnson, H. Knudsen, L. Liljeby, and K.-G.Rensfelt (1985); *Absolute cross sections for multi-electron processes inlow energy* Ar^{q+}*-Ar collisions : Comparision with theory;* Nuclear Instruments & Methods in Physics Research section B , **9**;397.

[2] De S., Ghose P. N., Roy A., Safvan C. P.(2006); *A setup for probing ion-molecule cllision dynamics;* Nuclear Instruments and Methods in Physics Research Section B : Beam Interactions with Materials and Atoms; **243**; 435-441

[3] Lindhard J.,Winther A., K. Dan. Vidensk. Selsk (1964); *Matematisk-Fysiske Meddelelser* , **34**;4

[4] Kabachnik N. M., Kondratyev V. N., Roller-Lutz Z. & Lutz H. O. (1997); *Multiple ionization of atoms and molecules in collisions with fast ions: Ion-atom collisions*; Physical Review A; **56**;2848

[5] Micelotta E. R. (2009), *PAH processing in space,* Doctoral dissertation, Leiden Observatory, Faculty of Science, Leiden University.

[6] Pathak A. and Sarre P. J. (2008), *Protonated PAHs as carriers of diffuse interstellar bands;* Monthly Notices of the Royal Astronomical Society, **391**, L10-L14.

[7] Portella G., Poater J., Bofill J. M., Alemany P. and Sola M. (2005)*; Local Aromaticity of [n]acenes, [n]phenacenes, and [n]helicenes (n=1-9)",* The Journal of Organic Chemistry, **70**, 2509-2521.

[8] Postma J., Bari S., Hoekstra R., Tielens A. G. G. M. and Schlath lter T. (2010), *Ionization & fragmentation of Anthracene upon interaction with KeV protons & α particles ;* The Astrophysical Journal, **708**, 435-444.

[9] Tielens A. G. G. M (2008) ; *Interstellar Polycyclic Aromatic Hydrocarbon molecules;* Annual Review of Astronomy & Astrophysics, **46**, 289-337.

DIFFERENTIAL LOW ENERGY ELECTRON SCATTERING FROM WATER

M. A. Khakoo[1], K. Ralphs[1], L. R. Hargreaves[1], C. Winstead[2] and V. McKoy[2]
[1]Physics Department, California State University, Fullerton, CA 92834, USA
[2]A. A. Noyes Laboratory of Chemical Physics, California Institute of Technology, Pasadena, CA 91125, USA

1. INTRODUCTION

Recent work in our experimental group at Cal State Fullerton with theoretical collaboration from the group of Drs. Vincent B. McKoy and Carl Winstead at Caltech, USA has focused on (i) rechecking and improving our earlier elastic scattering differential cross-sections (DCS) for H_2O [1] and using these results to determine inelastic electron scattering DCSs from this molecule. Incident energies of interest are from 0.75eV to 100eV for elastic scattering and near-threshold energy of 9eV to 20eV for inelastic scattering, with scattering angles ranging from 5^o to 130^o. A summary of this work is presented here.

2. EXPERIMENT/THEORY

The experiment has been described in previous articles e.g. [1]. It comprises a well-tested, high resolution electron spectrometer with double hemispherical dispersers in both the electron gun and in the analyzer. The gun is capable of delivering a well-collimated electron beam of current ranging from 5nA to 30nA with an energy resolution of 25meV to 70meV. The analyzer is able to detect scattered electrons with scattering angles (θ) up to 130^o. The vacuum chamber housing the spectrometer is efficiently pumped by a 10" diffusion pump. The gas target is delivered by an aperture source (obviating the need to use gas kinetic cross-sections) [2] and the gas target can be moved to accurately and expediently determine background scattering rates [3]. Elastic DCSs were determined in the standard way using the relative flow method [1]. However, for this new set of data, we extended the old set to lower energies and covered the scattering angle region of 60^o to 120^o in finer steps using re-measured flow-rates. The elastic DCSs were taken at incident energies (E_0) of 0.75eV, 1eV, 1.5eV, 2eV, 3eV, 4eV, 5eV, 6eV, 8eV, 10eV, 15eV, 20eV, 30eV, 50eV and 100eV. Electron energy loss spectra of excitation of H_2O were analyzed using a sophisticated non-linear spectrum-unfolding program in the Mathematica™ environment, where multi-Gaussian shapes for electronic states could be used. These shapes were kept constant and only their relative heights were changed during the regression fitting. The profile of the allowed $\tilde{A}^1B_1$ state was determined from the photoabsorption spectrum of Mota et al. [4]. This procedure assumes the validity of the Franck-Condon approximation, which may be violated to a small extent by Rydberg-valence interactions in the molecule. Here we only present excitation to the lowest $\tilde{a}^3B_1$ and $\tilde{A}^1B_1$ states recently published in [5]. A typical fit to the energy loss spectrum for these states is given in figure 1.

The calculations for elastic scattering and excitation of the $^{1,3}B_1$ states were performed using the Schwinger Multi-Channel method (SMC) [5-8]. A detailed description of the SMC method may be found in the indicated references, so here we give only the details of the present calculations on H_2O. All calculations were carried out in the fixed-nuclei approximation at the ground-state equilibrium geometry. To describe both the ground and excited states of the target and the electron scattering system, we used the same basis set as in earlier work [1] on elastic scattering by H_2O, namely, the aug-cc-pVDZ basis set [6] with f -type Gaussians omitted and with a supplement of distributed s Gaussians. The ground state of H_2O was described at the Hartree–Fock level, and the $\tilde{a}^3B_1$ and $\tilde{A}^1B_1$ states were described in the improved virtual orbital (IVO) approximation [6], which gives 7.98 and 8.72 eV, respectively, for their vertical excitation thresholds, and 0.044 for the $\tilde{A}^1B_1$ state excitation oscillator strength. Note that our current computer codes require that the same IVO be used to describe both the singlet and the triplet excited states, and we used the triplet IVO in the present work. As previously observed by Gil et al [9], the triplet-coupled and singlet-coupled 4a1 orbitals are very similar, so little error should result from using the triplet orbital for both channels. Two different channel-coupling schemes were used in the work reported here: a three-channel scheme including only the elastic and $^{1,3}B_1$ channels, and a five-channel scheme that also included the neighboring ($1b_1 \rightarrow 2b_2$) $^{1,3}A_2$ states (which were also described in the IVO approximation, using the triplet-coupled $2b_2$ IVO). Because the present results omit both other open excitation channels and all closed channels, they do not account for polarization of the target by the projectile electron. We applied a version [10] of the standard Born-dipole correction procedure [10, 11] to combine a first-Born description of long-range scattering with the SMC description of the short-range interaction.

3. RESULT AND DISCUSSION

For elastic scattering, we show results at pertinent energies for brevity. We compare our results with the complex-Kohn calculation [12] and the experimental results of Shyn and Cho [13] and Cho et al. [14] as well as the Born-dipole approximation [1]. At E_0=2eV we observe excellent agreement of the present experiment with the Born-dipole and the complex-Kohn calculations of Rescigno and Lengsfield [12]. Our SMC DCSs show good agreement overall but are lower between 30° and 60°. The DCSs of [13], which are the lowest E_0 DCSs to compare with, are lower than ours at small θ. At the higher E_0 values of 6eV and 10eV, we compare with the DCSs of Cho *et al.*, which were considered the most accurate and recent values before ours. Agreement with our SMC and the complex-Kohn is very good overall, with some relative shape differences around 20° to 30°. We show good agreements between experiments at small θ, but our DCSs are much higher at θ=90° than those of Cho et al. [13]. We have seen this same trend in our earlier measurements [1], so this not new.

FIGURE 1. ***Electron energy loss spectra at E_0 = 15 eV and θ = 50°. Error bars are 1 standard deviation statistical uncertainties. The fitting of the $^3B_1$ + $^1B_1$ states (red line) and the contributions of individual components are indicated.***

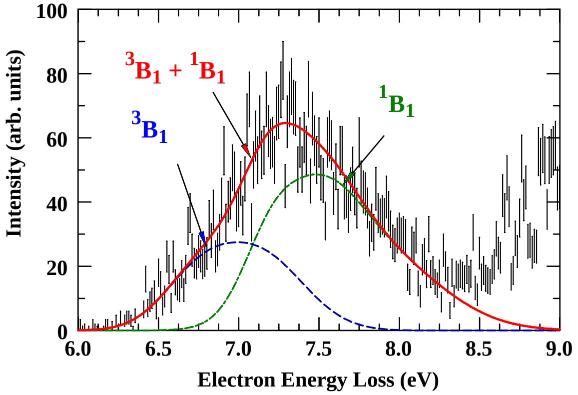

FIGURE 2. ***DCSs for elastic scattering for H_2O at E_0 = 2eV, 6eV and 10eV. For discussion see text.***

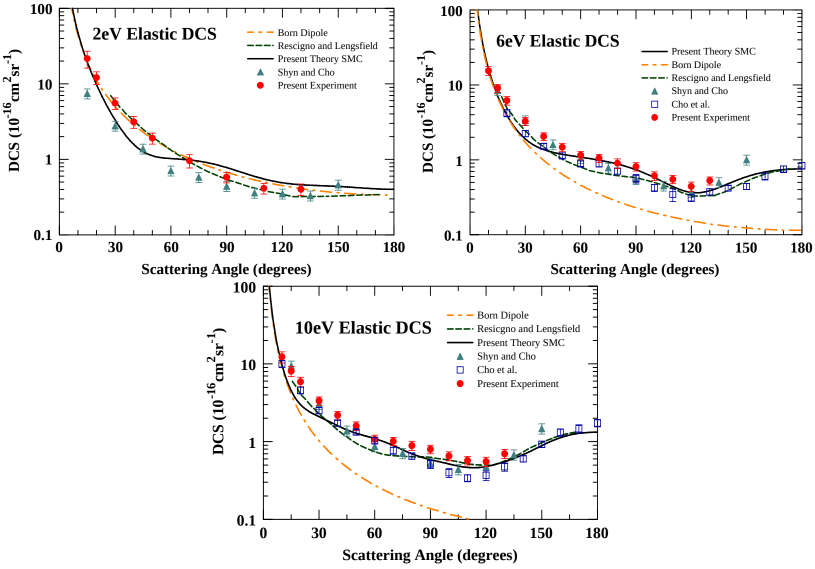

For the inelastic DCSs we also compare with the complex-Kohn calculations [9] and the measurements of Thorn [16]. We note that for the $^1B_1$ state there is excellent agreement between our 3-state and 5-state SMC results. We also note that agreement between the measurements for the relative excitation of the $^1B_1$ state (dipole-allowed) is very good. The DCSs of Thorn are lower than ours, which are in very good quantitative agreement with both theories.

FIGURE 3. DCSs for inelastic excitation of the $^3B_1$ and $^1B_1$ states of H_2O at our highest E_0 values of 15eV and 20eV.

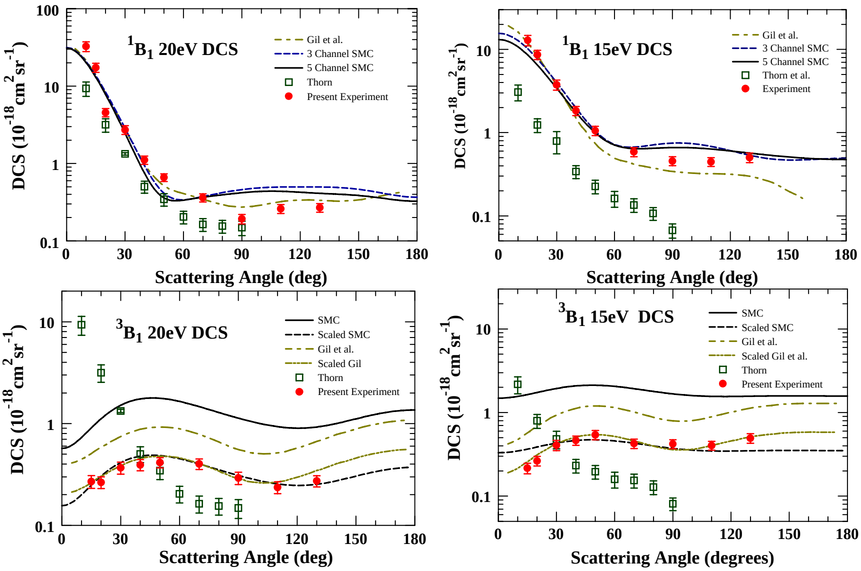

The fact that both theories are in very good agreement is encouraging, since other than Thorn [15] this is a first joint theoretical-experimental effort to determine accurate DCSs for excitation of this important ubiquitous polyatomic molecule. For the $^3B_1$ excitation quantitative differences between our SMC theory (5-state), Gil *et al.*'s results [9] and our measurements is found. Our measurements tend to be much lower than either calculation. When we scale both theoretical values we observe excellent shape agreement with our experiment. Surprisingly the DCSs of Thorn [15] show more of a dipole type excitation, which is unexpected for a singlet-triplet transition. This might be due to their Franck-Condon profile for the triplet state, which could include some of the singlet state (which is dominant).

4. CONCLUSIONS

We have reported DCSs for elastic and inelastic scattering from H_2O. Presently, we are determining the DCSs for excitation of the higher states and will present this in a long paper in the near future.

ACKNOWLEDGEMENTS

This work was sponsored by the US National Science Foundation under Grants PHY 0653452 (MAK) and PHY 0653396 (VM and CW). The work of VM and CW was supported by the Chemical Sciences, Geosciences and Biosciences Division, Office of Basic Energy Sciences, Office of Science, US Department of Energy, and made use of the Jet Propulsion Laboratory's Supercomputing and Visualization Facility.

References

1. M. A. Khakoo *et al*. Phys. Rev. A, **78**, 052710 (2010).
2. M. A. Khakoo *et al*. J. Phys. B, **40**, 3601 (2007).
3. M. Hughes *et al*. Meas. Sci. Technol., **14**, 841 (2003).
4. R. Mota *et al*. Chem. Phys. Lett. **416** 152 (2005).
5. L. R. Hargreaves *et al*. J. Phys. B, **45**, 201001 (2012).
6. K. Takatsuka and V. McKoy Phys. Rev. **24**, 2473 (1981).
7. C. Winstead and V. McKoy Adv. At. Mol. Opt. Phys. **36**, 183 (1996).
8. C. Winstead and V. McKoy Comput. Phys. Commun. **128**, 386 (2000).
9. T. J. Gil *et al*. Phys. Rev. A **49** 2642 (1994).
10. M. A. Khakoo *et al.* 2008 *Phys. Rev.* A **77**, 042705 (2008)
11. T. N. Rescigno and Schneider Phys. Rev. A **45**, 2894 (1992) and references therein.
12. T. N. Rescigno and B. H. Lengsfield Z. Phys. D **24**, 117 (1992).
13. T. W. Shyn and S. Y. Cho Phys. Rev. A **36**, 5138 (1987).
14. H. Cho *et al*. . J. Phys. B, **37**, 625 (2004).
15. P. A. Thorn PhD Thesis Flinders University, http://theses.flinders.edu.au/public/adt-SFU20080714.112505/index.html.

ABSOLUTE PARTIAL ELECTRON IONIZATION CROSS SECTION MEASUREMENTS

E. Krishnakumar
Tata Institute of Fundamental Research, Homi Bhabha Road, Colaba,
Mumbai - 400005

1. INTRODUCTION

Dissociative ionization (DI) and dissociative electron attachment (DEA) play a major role in electron induced chemistry. In order to understand the dynamics of these processes and for modelling the electron induced chemistry, it is necessary to have the absolute cross sections for these processes. Here we address various techniques that have been employed for this purpose and the various pitfalls that have been overlooked very often in using them or in assessing the reliability of the data obtained using them.

2. DISSOCIATIVE IONIZATION

The distinctive feature in DI as compared to simple ionization is that the ions are generally produced with relatively large kinetic energy. This has important consequences on the measurement of the corresponding absolute partial cross sections. Historically the electron ionization cross sections have been measured using the total ion tube [1, 2]. In this, the ions produced in a gas cell of finite length when a magnetically collimated beam of electrons pass through it are collected by an ion collector plate along the length of the gas cell. A uniform electric field across the electron beam direction, applied all along the length of the gas cell ensures the collection of all the ions at the collector plate. As the name suggests, this apparatus measures the total ionization cross sections, since there is no way of separating the ions of different mass to charge ratio (m/q) in it. However, by applying a small reverse field and allowing ions of initial kinetic energy large enough to overcome this reverse field, Rapp and colleagues provided lower limits for the DI cross sections for homo-nuclear diatomic molecules like H_2, N_2 and O_2 [3]. Like the case of DI, the DEA also produces ions of relatively large kinetic energy. In this case the difficulties are larger since the electron energy regime is very low and the ions being negative, the problem of segregating them from the secondary electrons exist.

3. MEASUREMENT OF PARTIAL CROSS SECTIONS

In order to measure the partial ionization cross sections, the apparatus should satisfy two conditions. The first one is that there should be a provision for separating the ions of differing m/q. The second one is the provision for absolute cross section measurement for each ion of a given mass to charge ratio. In order to measure absolute cross sections, one needs to know the target density, electron current the exact volume overlap of the electron beam with the target and the exact number of ions of a given m/q produced in the interaction region. Various techniques, both direct and indirect have been developed over the years for determining the absolute cross sections.

For separating the ions as per their m/q, one needs to employ a mass spectrometer. Even assuming that the target density, the electron beam current and the volume overlap of the target and the electron beam are well determined, the use of a mass spectrometer limits the accuracy in the determination of the number of ions of a given m/q. The extraction of the ions form the interaction region, their transfer into a mass spectrometer, the transmission efficiency of the mass spectrometer for these ions and the efficiency with which these ions are finally detected – all these are crucial parameters affecting the measurement of the absolute cross sections. The accuracy of the measurements depends on all these crucial factors and in the following sections various techniques are reviewed.

3.1. CROSSED BEAM METHODS:

In order to extract and mass analyse the ions, they have to be put through a mass spectrometer. Extended source of ions like that in a gas cell is difficult to be extracted entirely. The ideal source should be a point source of ions. This could be accomplished by the use of an effusive beam at room temperature or a fast neutral beam. In the effusive beam method, the Relative Flow Technique has been used to put the cross sections on absolute scale using the cross section for a known molecule as the standard [4]. In this experiment, the electron beam and the molecular beam are made to intersect at right angle and the ions are extracted along third orthogonal direction into a mass spectrometer. The velocity distribution of ions produced in DI are practically the same in the laboratory frame and the centre of mass frame of the target molecule, since its initial velocity is very small at room temperature and can be neglected. Hence, under isotropic angular distributions, these ions would be travelling in all direction from the source. In order to extract all these ions in a given direction one needs fairly high electric field. Even after that the trajectories of the ions would be diverging. They could be further focussed into the entrance aperture of a mass spectrometer using an electrostatic lens assembly. Fig. 1 shows such a typical arrangement. It may be noted that for ions of kinetic energy 5 eV, fairly high extraction field has to be applied. Even if a strong guiding magnetic field is used for the electron beam, this sort of field applied perpendicular to the electron beam direction would deviate it or even destroy it. The only way such field could be applied is by pulsing the electron beam and the extraction field. It may be noted that several DI and DEA experiments have been reported with CW electron beam and very low extraction field, making them suspect even for the relative cross section measurements.

Fig. 1: Simulation of ion trajectories for a point source of ions of initial kinetic energies ranging from 0 to 5 eV and ejected at right angles to the extraction direction in an extraction field of 100 V/cm and a set of focussing lenses. Each electrode in the lens is 20 mm long and 20 mm in radius. It can be seen that ions of different energy gets focussed at different points on the axis.

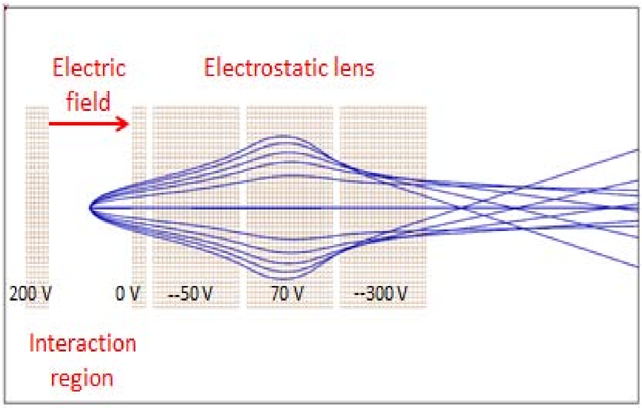

Even assuming that a pulsed electron beam and pulsed extraction field has been employed and the ions are focussed into a mass spectrometer, it does not ensure transport of all the ions to the detector. Whether it is a magnetic mass spectrometer, a quadrupole mass spectrometer (QMS) or a time of flight mass spectrometer (TOFMS), their transmission and mass resolution are strongly coupled to the entrance angle of the particles at the input aperture. For a QMS, which has been commonly used in these experiments, this limitation is more severe as it can transmit ions entering only in a narrow cone. Thus the use of high extraction field and an electrostatic lens to focus the ions along with a quadruple mass spectrometer does not ensure transfer of all the ions into the detector. Moreover, the QMS does not have uniform transmission for ions differing in m/q. This makes even the relative intensities of ions of various m/q at a given electron energy very difficult to determine. To conclude, for partial ionization cross section measurements, whether it is DI or dissociative electron attachment, the QMS is an inaccurate tool.

Magnetic spectrometers have not been used much for partial cross section measurements. However, TOFMS in various forms have been used. The standard and well known one is that of the Wiley McLaren geometry [5]. Here again, the entrance angle problem exists as the ion entering the field free flight tube beyond certain angle to the flight tube axis would get lost. This entrance angle problem was solved by having a segmented TOFMS, in which the segments are used as an electrostatic lens which focusses the ions to the detector. This geometry coupled to the pulsed electron beam and pulsed ion extraction technique was found to be a very reliable technique for measuring absolute partial ionization cross sections [6] and attachment cross sections [7] in conjunction with the relative flow technique. The first ever accurate cross sections for DI of H_2, D_2, N_2 and O_2 were measured using this technique [6, 8, 9]. For the case of DEA, this has been the most reliable technique so far [10 -14], except for the recent experiment using a velocity map imaging spectrometer [15]. This segmented flight tube technique has been improvised further by using a large area detector and longer flight tube to improve the mass resolution in order to measure the partial cross sections for organic molecules [16].

3.2. FAST NEUTRAL BEAM METHOD

This method was developed in the 1980s by Robert Freund and his colleagues at the Bell Labs and was later shifted to the group of Kurt Becker at New York University [17]. In this technique a fast neutral beam is collided with the electron beam. Due to the initial velocity of the neutral beam, the ions formed by electron impact continue to travel in the same direction as the neutral beam, but with a spread in velocities in the case of DI. The ions are focussed into a hemispherical electrostatic analyser for separation of the ions based on their kinetic energy and from the unionized neutral beam. Since in DI, the fragment ion has a smaller mass, its kinetic energy in the lab frame would be smaller than the kinetic energy of the parent ion, but with a spread in the kinetic energy corresponding to that released in the dissociation process. The cross sections could be measured on the absolute scale by direct measurement of the target density, the electron beam current and the volume overlap of the two beams. This apparatus was found to be reliable for measuring the partial cross section for the formation of parent ions [18]. However, the kinetic energy released in DI made it difficult to collect all the fragment ions and hence to make reliable measurements for these channels [19]. Apart from this, one of the limitations of this technique has been in the possibility that a fraction of the neutral molecules may be in electronically or vibrationally excited states since the fast neutral beam is produced by charge exchange collisions. Moreover, almost all the cross sections have been limited up to the electron energy of 200 eV. The biggest advantage of this technique has been that it could be used for measuring ionization cross sections of various atoms and radicals that do not exist in a gaseous state.

3.3. GAS CELL WITH TOFMS AND PSD:

The most reliable and direct method for measurement of absolute partial ionization cross sections seems to be the use of a gas cell with TOFMS and a position sensitive detector (PSD) [20]. This experiment is a modification of the total ion tube with a gas cell in which the number density of the molecules can directly be measured. A pulsed electron beam of given energy traverses this cell producing ions, before being measured in a Faraday cup. The ions are then pushed onto a PSD by a pulsed electric field. The arrival time of the ions at the detector helps in separating the various m/q ions. The position sensitive detector allows the exact estimation of the path length over which the electron beam interacted with the molecules in the gas cell. From the target pressure, the accumulated electron charge in the Faraday cup, the path length and the number of ions detected, the partial cross sections are obtained. Starting with diatomics, this technique has been used to measure the absolute partial ionization cross sections of a large number of molecules [21-25]. So far, this appears to be the most reliable technique for measuring DI cross sections.

3.4. FOURIER TRANSFORM MASS SPECTROMETRY

An indirect method of measuring the absolute cross sections has been developed by Alan Gascadden using a Fourier transform ion mass spectrometer [26]. In this, the ions produced by electron impact are trapped using a combination of magnetic and electric fields and the image currents corresponding to ions of each m/q are measured. By normalizing the image current with that due to an ion whose cross section for production from the precursor atom (e.g. Ar) is known, the cross sections are put on an absolute scale. In this set up also, extreme care has to be taken in trapping the ions which are produced with considerable kinetic energy in the DI process. The cross sections for N^+ and O^+ from NO_2, for example, are considerably different from that measured using the more reliable technique of Lindsay et al.[26]

3.5. VELOCITY MAP IMAGING (VMI) SPECTROMETRY

While the technique of using a position sensitive detector along with a gas cell and time of flight technique has remained the most accurate technique for measurement of partial ionization cross sections, it still may have some limitations, if the cross sections are too small and the ultra violet radiation and energetic neutral particles are considerably larger as compared to the ion signal. This technique still has not been demonstrated satisfactorily for partial cross sections for dissociative electron attachment (DEA), in which the negative ions are produced. One of the major issue to be tackled in detecting negative ions would be their separation from the continuous background of scattered electrons. So far the segmented TOF technique has been the most reliable one for the measurement of DEA cross sections. An improvement of this technique has been the use of a velocity map imaging (VMI) spectrometer for measuring the DEA cross sections for H_2 and D_2. The DEA cross sections for these molecules are extremely small and it had been suspected that previous measurements using total ion tube were affected by UV light and/or energetic neutrals. The only way to separate out these backgrounds was by using a time of flight technique. At the same time, one had to ensure that all the energetic H- or D- ions are collected, without being affected by the scattered secondary electrons. This was accomplished by imaging the entire Newton sphere of the ions using a VMI spectrometer free of any other background signal [15]. It is possible to use this technique routinely for cross section measurements for DEA or even for the case of DI.

4. CONCLUSION

Measurement of electron impact partial ionization cross sections of molecules remained a challenging problem due to the kinetic energy of the fragment ions arising from DI process. The first satisfactory technique was the pulsed electron and pulsed ion extraction coupled to a segmented time of flight spectrometer. This technique has remained as one of the reliable techniques till now. Partial cross section measurements using the commonly used QMS may not be reliable where the kinetic energy of the ions are larger than thermal. In the absence of any other reliable techniques, the fast neutral beam method remains the best one available for the case of those targets like various atoms and radicals that do not exist in a free state. The modified gas cell method employing the time of flight technique along with a position sensitive detector is currently the most reliable technique for partial ionization cross section measurements. The recent use of the velocity imaging technique along with the relative flow technique is promising for both DEA measurements and DI measurements.

References

[1] Rapp D. and Englander-Golden P., (1965), *Total Cross Sections for Ionization and Attachment in Gases by Electron Impact. I. Positive Ionization.* J. Chem. Phys. **43**, 1464.

[2] Schram B. L., De Heer F. J., Van der Wiel M. J., and Kistemaker J., (1965), *Ionization cross sections for electrons (0.6-20 keV) in noble and diatomic gases.* Physica **31**, 94.

[3] Rapp D., Englander-Golden P., and Briglia D. D., (1965), *Cross Sections for Dissociative Ionization of Molecules by Electron Impact.* J. Chem. Phys. **42**, 4081.

[4] Kishnakumar E. and Srivastava S. K., (1988), *Ionisation cross sections of rare-gas atoms by electron impact.* J. Phys. B **21**, 1055.

[5] Wiley W. C. and McLaren I. H., (1955), *Time-of-Flight Mass Spectrometer with Improved Resolution.* Rev. Sci. Instrum. **26**, 1150.

[6] Krishnakumar E. and Srivastava S. K., (1994), *Electron correlation effects in the dissociative ionization of* H_2. J. Phys. B **27**, L251.

[7] Krishnakumar E. and Nagesha K., (1992), *Dissociative attachment of electrons to* CS_2. J. Phys. B. **25,** 1645.

[8] Krishnakumar E. and Srivastava S. K., (1990), *Cross sections for the production of* N_2^+, $N^+ + N_2^{2+}$ *and* N^{2+} *by electron impact on* N_2, J. Phys. B **23**, 1893.

[9] Krishnakumar E. and Srivastava S. K., (1992), *Electron impact ionisation of* O_2, Int. J. Mass Spectrom. **113**, 1.

[10] Krishnakumar E. and Nagesha K., (1995), *Dissociative attachment studies by negative ion TOF spectrometry.* Rapid Com. Mass Spectrom. **9,** 336.

[11] Nandi D., Rangwala S. A., Kumar S. V. K., and Krishnakumar E., (2001), *Absolute cross-sections for dissociative attachment to* NF_3. Int. J. Mass Spectrom. **205**, 111.

[12] Prabhudesai V. S., Nandi D., Kelkar A. H., Parajuli R., and Krishnakumar E., (2005), *Dissociative electron attachment to formic acid.* Chem. Phys Letters, **405**, 172.

[13] Rawat P., Prabhudesai V. S., Aravind G., Rahman M. A., and Krishnakumar E., (2007), *Absolute cross sections for dissociative electron attachment to* H_2O *and* D_2O. J. Phys. B: At. Mol. Opt. Phys. **40**, 4625.

[14] Rawat P., Prabhudesai V. S., Rahman M. A., Bhargava Ram N., and Krishnakumar E., (2008), *Absolute cross sections for dissociative electron attachment to* NH_3 *and* CH_4. Int. J. of Mass Spectrom. **277**, 96.

[15] Krishnakumar E., Denifl S., Cadez I., Markelj S., and Mason N. J., (2011), *Dissociative electron attachment cross sections for* H_2 *and* D_2. Phys. Rev. Lett. **106**, 243201.

[16] Rahman M. A., Gangopadhyay S., Limbachiya C., Joshipura K. N., and Krishnakumar E., (2012), *Electron ionization of* NF_3, Int. J. Mass Spectrom. **319**, 48.

[17] Baiocchi F. A., Wetzel R. C., and Freund R. S., (1984), *Electron-Impact Ionization and Dissociative Ionization of the* CD_3 *and* CD_2 *Free Radicals.* Phys. Rev. Lett. **53**, 771.

[18] Freund R. S., Wetzel R. C., Shul R. J., and Hayes T. R., (1990), *Cross-section measurements for electron-impact ionization of atoms.* Phys. Rev. A **41**, 3575.

[19] Tarnovsky V., Kurunczi P., Rogozhnikov D., and Becker K., (1993), *Absolute cross sections for the dissociative electronimpact ionization of the* CF_x *(x = l-3) free radicals.* Int. J. Mass Spectrom. **121**, 181.

[20] Straub H. C., Renault P., Lindsay B. G., Smith K. A., and Stebbings R. F., (1995), *Absolute partial and total cross sections for electron-impact ionization of argon from threshold to 1000 eV.* Phys. Rev. A **52**, 1115.

[21] Straub H. C., Renault P., Lindsay B. G., Smith K. A., and Stebbings R. F., (1996), *Absolute partial cross sections for electron-impact ionization of* H_2, N_2, *and* O_2 *from threshold to 1000 eV.* Phys. Rev. A **54**, 2146.

[22] Straub H. C., Lindsay B. G., Smith K. A., and Stebbings R. F., (1998), *Absolute partial cross sections for electron-impact ionization of* H_2O *and* D_2O *from threshold to 1000 eV.* J. Chem. Phys. **108**, 109.

[23] Lindsay B. G., Rejoub R., and Stebbings R. F., (2003), *Absolute cross sections for electron-impact ionization of* N_2O, H_2S,*and* CS_2 *from threshold to 1000 eV.* J. Chem. Phys. **118**, 5894.

[24] Rejoub R., Morton C. D., Lindsay B. G., and Stebbings R. F., (2003), *Electron-impact ionization of the simple alcohols.* J. Chem. Phys. **118**, 1756.

[25] Lindsay B. G., McDonald K. F.,, Yu W. S., Stebbings R. F., and Yousif F. B., (2004), *Electron-impact ionization of* CCl_4 *and* CCl_2F_2, J. Chem. Phys. **121**, 1350.

[26] Jiao C. Q., DeJoseph Jr. C. A., and Garscadden, A., (2002), *Absolute cross sections for electron impact ionization of* NO_2. J. Chem. Phys. **117**, 161.

AUTOIONISATION RESONANCES IN MERCURY ATOM

Sindhu Kalyadan[1], Hari R. Varma[1] and P. C. Deshmukh[1, 2]
[1]School of Basic Sciences, Indian Institute of Technology Mandi,
Mandi 175001
[2]Department of Physics, Indian Institute of Technology Madras,
Chennai 600036

1. INTRODUCTION

Atomic mercury (Z=80) is an ideal system to study electron-electron correlations and relativistic effects. The region of autoionization is very important as it provides information about the coupling between the ionization and excitation channels. In the energy region of autoionization resonances, photoionization channels from $5d_{5/2}$ subshell are degenerate with the photoexcitation channels from the inner $5d_{3/2}$ subshell. These degenerate channels interfere and as a result resonance structures appear in the photoionization parameters of the $5d_{5/2}$ subshell. Experimental studies in this energy region have been reported by Zubek *et al.* [1] and theoretical studies by Baig [2]. In the present work, the autoionization resonance spectrum of atomic Hg in the energy region 15-17 eV has been studied using a combination of the relativistic random phase approximation (RRPA) and the relativistic multichannel quantum defect theory (RMQDT) [3, 4].

2. THEORY

The RRPA is used to obtain the quantum defect parameters for a few energy points in the immediate vicinity of the $5d_{3/2}$ threshold. The quantum defect parameters [4] were obtained using the experimental thresholds reported by M Zubek *et* al. [3]. The quantum defect parameters are only very weakly sensitive to energy, and the MQDT method rests on this important physical property. The use of RRPA addresses the inclusion of major many-body electron-correlation effects which play a pivotal role in the ionization spectrum of Hg. The energy insensitive MQDT parameters are used to study the autoionization resonances using the technique described in Ref.[4].

3. RESULTS AND DISCUSSION

Photoionization cross section from $5d_{5/2}$ subshell of Hg, plotted against the effective quantum number n^*, which is the difference between the principal quantum number (n) and the quantum defect (μ), is shown in Fig 1. As expected, the resonance structures are periodic with respect to n*. The quantum defect departs from zero since the atomic potential is not hydrogenic over the entire configuration space and the SO(4) symmetry of the hydrogen atom breaks down in a many-electron atom [5]. The quantum defects obtained in the present work using RMQDT+RRPA method are compared with the μ values reported in literature using the Hartree-Slater approximation [6] and also with those extracted from the work of Baig [2]. These results are presented in Table 1. A reasonably good agreement is found between these values.

The individual excitation channels are identified by doing the calculation at three different levels of truncation.

(i) $5d_{3/2} \longrightarrow f_{5/2}, p_{3/2}, p_{1/2}$

$5d_{5/2} \longrightarrow f_{7/2}, f_{5/2}, p_{3/2}$

(ii) $5d_{3/2} \longrightarrow f_{5/2}, p_{3/2}$

$5d_{5/2} \longrightarrow f_{7/2}, f_{5/2}, p_{3/2}$

(iii) $5d_{3/2} \longrightarrow f_{5/2}$

$5d_{5/2} \longrightarrow f_{7/2}, f_{5/2}, p_{3/2}$

Table1.Quantum defects μ_p and μ_f for atomic Mercury.

	RRPA+RMQT Present work	MQDT Baig [2]	HS Manson [5]
μ_p	4.23	4.20	4.01
μ_f	1.00	1.01	1.02

In Fig 2, we show the photoionization cross section against the photon energy. Notice that resonance structures are converging to the $5d_{3/2}$ threshold. The resonance structures also appear in the angular distribution parameter, β, and are shown in Fig 3. We have compared our RMQDT results with the available experimental [1] and theoretical results [2]. The results are found to be in reasonable agreement w.r.t. positions of the $5d_{3/2}$ excitation channels.

Figure1: Autoionization resonances in Hg, cross section as a function of effective quantum number coupling three ionization channels from $d_{5/2}$ and three excitation channels from $d_{3/2}$

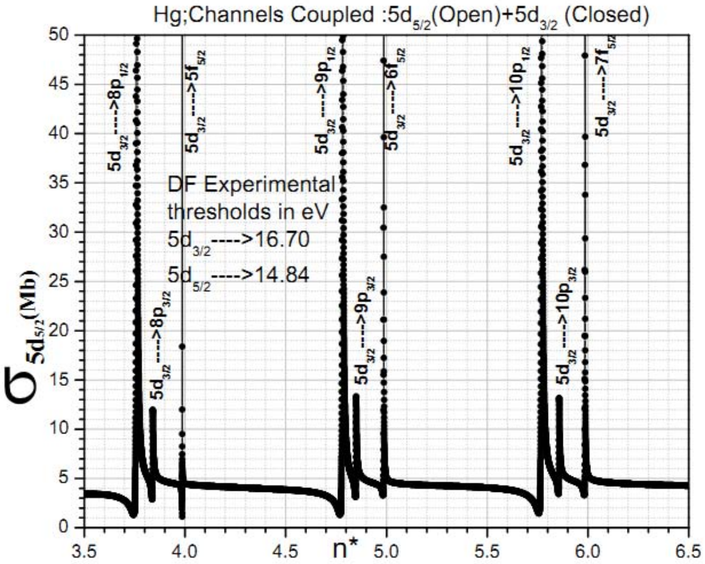

Figure 2: Autoionization resonances in Hg $5d_{5/2}$ cross section, coupling three ionization channels from $d_{5/2}$ and three excitation channels from $d_{3/2}$

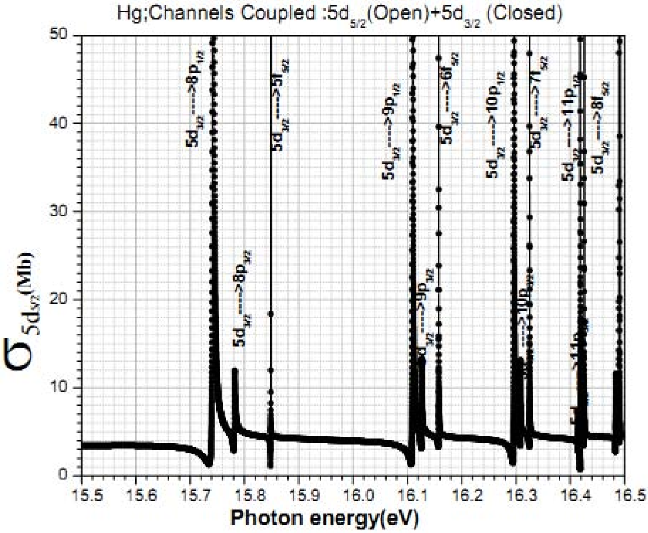

Figure 3: Autoionization resonances in Hg $5d_{5/2}$ angular distribution parameter, coupling three ionization channels from $d_{5/2}$ and three excitation channels from $d_{3/2}$

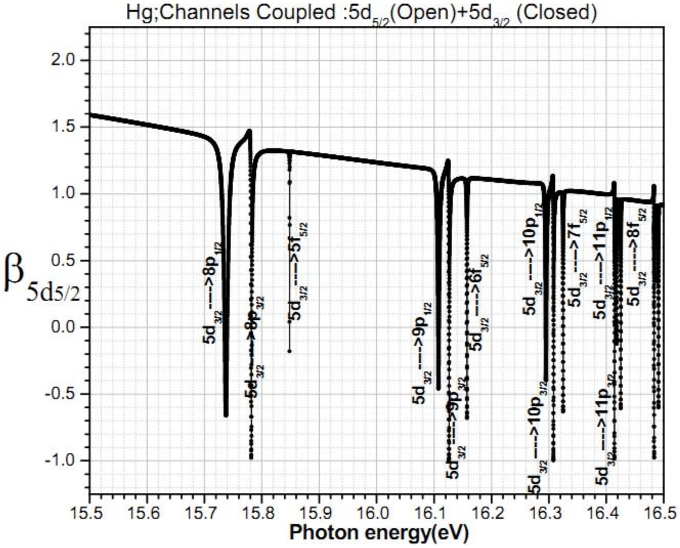

4. CONCLUSIONS

Autoionization resonance structures in Hg below $5d_{3/2}$ threshold have been investigated using a combination of RRPA and RMQDT and the individual resonances are identified. The results obtained are in reasonable agreement with the other experimental and theoretical data available.

Acknowledgements: The authors are grateful to the grant (SR/S2/LOP-0038/2010-I) from the Department of Science and Technology, Government of India.

References

[1] M Zubek *et a*l, (2005*) Measurements of angular distribution for photoionization of mercury into the $5d^9\ ^2D_{5/2}$ ionic state over the energy range from 15 eV to 17 eV* J. Phys. B **38**, 1657-1665.

[2] M.A Baig (2008) *High résolution measurement and MQDT analysis of the $5d^9$ $6s^2$ np, nf (J=1) autoionizing resonance of mercury* Eur. Phys.J.D **46**, 437-442.

[3] Johnson and Lin, (1979) *Multichannel relativistic random-phase approximation for the photoionization of atoms* Phys. Rev. A **20,** 964.

[4] Lee and Johnson, (1980) *Scattering and spectroscopy: Relativistic multichannel quantum-defect theory* Phys. Rev. A **22**, 979.

[5] P. C. Deshmukh and J. Libby

(a) Symmetry Principles and Conservation Laws in Atomic and Subatomic Physics -1 Resonance, 15, 832 (2010)

(b) Symmetry Principles and Conservation Laws in Atomic and Subatomic Physics -2 Resonance, 15, 926 (2010)

[6] S. T. Manson. (1969) *Dependence of the Phase Shift on Energy and Atomic Number for Electron Scattering by Atomic Fields*. Physical Review **182**, 97-103.

STUDY OF SINGLE IONIZATION OF ALKALI EARTH ATOMS

D. V. Singh[1], Raj Kumar Chauhan[2], Rajendra Kumar[1] and Jaswant Shishodia[3]
[1]Department of Physics, Gurukul Kangri Vishwavidyalaya
Haridwar, India-249404
[2]Department of Physics, Accurate Institute of Management and Technology, Greater Noida, India- 2013062
[3]Department of Physics, Banasthali University
Banasthali-India-304022

Abstract. We have calculated the triple differential cross section (TDCS) for alkali earth atoms i.e. beryllium, magnesium and calcium at excess energy 28.5eV, 38.5 eV, 48.5 eV and 58.5 eV. The calculation has been done using distorted-wave Born approximation (DWBA) in coplanar constant θ_{ab} = 180^o geometry. Post collision interaction (PCI) is incorporated through effective charge model. The results are compared with each other for alkali earth atoms at different excess energies.

Keywords Ionization, differential cross section, scattering angle PACS: **34.80Dp Atomic excitation and ionization by electron impact.**

1. INTRODUCTION

The Single ionization process is one of fundamental process of atomic and collision physics. Most of the study has been focused on heavier atom rather than lighter atoms like hydrogen and helium. Recently, Manchester group have reported the TDCS for alkali atoms in coplanar doubly symmetric geometry [1, 2]. The experimental data was compared with various theoretical approaches like DWBA, CCC (close coupling calculation) etc [2, 3]. They found that DWBA is successful approximation for low to high energy regime. But CCC is for very low energy. But there is one contradiction that both the theories do not comply with the explanation of the experimental results.

In this paper we have reported the TDCS of various alkali earth atoms i.e. beryllium, magnesium and calcium at excess energy 28.5eV, 38.5 eV, 48.5 eV and 58.5 eV. These atoms have two valance electrons in outermost orbital. TDCS is mainly calculated in coplanar constant geometry θ_{ab} = 180^o. TDCS for the ionization process for incident electron with energy E_i (momentum $\mathbf{k_i}$) can be defined in terms of direct (f) and exchange (g) amplitudes as follows.

$$\frac{d^3\sigma}{dE_b d\Omega_a d\Omega_b} = (2\pi)^4 \frac{k_a k_b}{k_i} 2\left(\frac{1}{4}\left|f+g\right|^2 + \frac{3}{4}\left|f-g\right|^2\right) \tag{1}$$

Where, in the DWBA

$$f = < \chi_a^{(-)}(\mathbf{r_0})\chi_b^{(-)}(\mathbf{r_1})\varphi_f(\mathbf{r_2})\left|\frac{1}{r_{01}}\right|\psi_i(\mathbf{r_1},\mathbf{r_2})\chi_i^{(+)}(\mathbf{r_0}) > \tag{2}$$

And
$$g = < \chi_b^{(-)}(\mathbf{r_0})\chi_a^{(-)}(\mathbf{r_1})\varphi_f(\mathbf{r_2})\left|\frac{1}{r_{01}}\right|\psi_i(\mathbf{r_1},\mathbf{r_2})\chi_i^{(+)}(\mathbf{r_0}) > \tag{3}$$

The shake-off and capture amplitudes have been ignored. Here $\chi_a^{(-)}$ and $\chi_b^{(-)}$ are normalized final state distorted waves of the two outgoing electrons having momenta $\mathbf{k_a}$ and $\mathbf{k_b}$ respectively. These are eigenfunctions of the distorting potentials U_a and U_b. The distorted wave for the incident electron, $\chi_i^{(+)}$ is normalized eigenfunction of the initial state distorting potential U_i, $\Psi_i(\mathbf{r_1},\mathbf{r_2}) \equiv \phi_i(\mathbf{r_1})\phi_i(\mathbf{r_2})$ Hartree-Fock wave function of the valence electrons of atoms and ϕ_f is similarly wave function of the valence electron of the residual ions in the ground state [4]. Here $\mathbf{r_0}$, $\mathbf{r_1}$ and $\mathbf{r_2}$ are respectively the position vectors of the projectile electron and the valence electrons of the target with respect to the target nucleus.

The energies are related by the conservation relation.

$$E_i = I + E_a + E_b \tag{4}$$

where I) is ionization potential of the target. The local exchange potential U_{exch} [5] given by

$$U_{exchi} = \frac{1}{2}\left\{(E - V) - \left[(E - V)^2 + 8\pi\rho_0\right]^{0.5}\right\} \tag{5}$$

where $E = E_i$, $V(r) = U_{atom}(r)$ and $\rho_0 = \frac{1}{2}\sum_j \left|\phi_j\right|^2$. The summation is over all atomic electrons.

The final state electron-electron interaction is incorporated following Jones et al [6] through the use of effective charges Z_a and Z_b which, for equal energy sharing are given by Eq. (6).

$$Z = Z_a = Z_b = \frac{1}{1 - Sin\frac{\theta_{ab}}{2}} \tag{6}$$

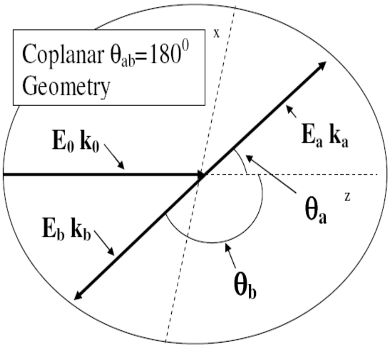

Post collision interaction (PCI) is included through effective charge mode for following coplanar constant $\theta_{ab} = 180^o$ geometry.

2. RESULTS AND DISCUSSION

We have calculated TDCS for the Be, Mg and Ca in coplanar $\theta_{ab} = 180^o$ geometry where energy of scattered and ejected electrons are equal and the ejection and the scattering, angle with the beam direction are same. All the results related to the geometry are discussed.

First we consider the results of coplanar $\theta_{ab} = 180^o$ geometry for the three atoms one by one which are shown in Figure 1 for Be, Figure 2 for Mg and Figure 3 for Ca. For beryllium there is a maximum near $\theta_a = 45^o$ at energy $E_a = 14.25$eV and TDCS becomes zero at $\theta_a = 90^o$. This angular variation is very much different from helium which has similar outer shell structure [i. e. two electrons in its valence 1s orbital]. For helium there is recoil peak at $\theta_a = 90^o$ and there is a minimum in TDCS near $\theta_a = 55^o$. We also find that the TDCS maxima get slightly shifted to higher scattering angle from $\theta_a = 45^o$ as the energy increases from $E_a=E_b=14.25$eV to 29.25eV.

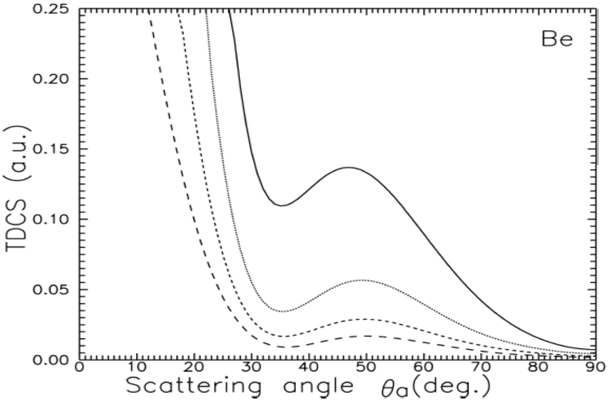

FIGURE1. Triple differential cross sections (in a.u.) for the ionization of Be in coplanar $\theta_{ab} = 180^o$ kinematics at excess energy: E_{ex} = ——— 28.5eV, …………… 38.5 eV, ------------ 48.5 eV and – – – – – 58.5 eV

In Figure 2 for magnesium slightly different behavior as compared to beryllium is found for E_a = 14.25eV. We observe that now TDCS at $\theta_a = 90^o$ is quite finite and becoming zero as the energy Ea increases. This structure is very similar to the obtained by Pan and Straces [7] through their calculation near the threshold energies at E_a = 1eV or 2eV excess energy.

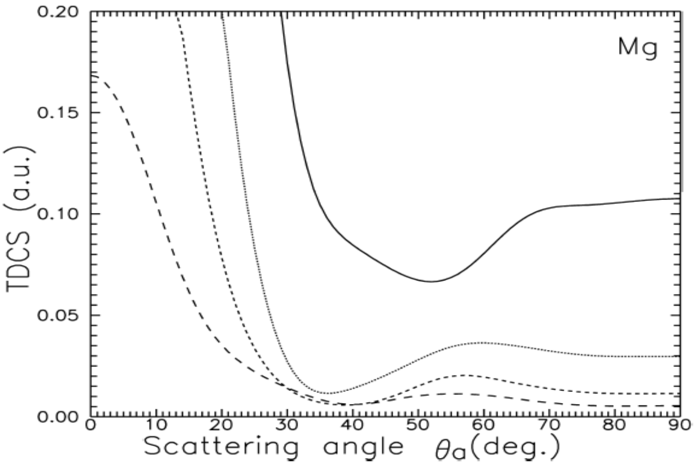

FIGURE2. Triple differential cross sections (in a.u.) for the ionization of Mg in coplanar $\theta_{ab}= 180^o$ kinematics at same excess energy as in Figure 1.

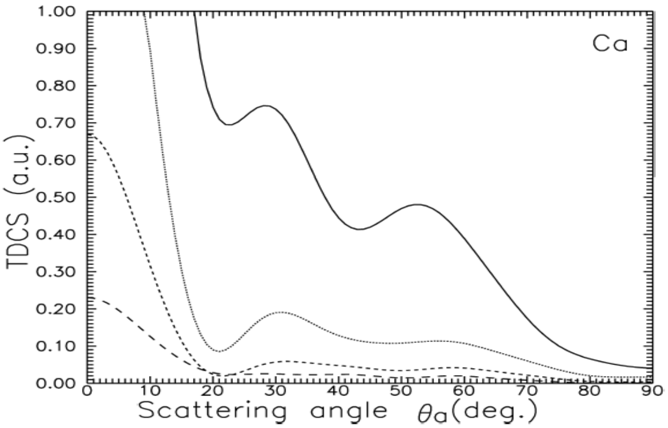

FIGURE3. Triple differential cross sections (in a.u.) for the ionization of Ca in coplanar $\theta_{ab}= 180^o$ kinematics at same excess energy as in Figure 1.

In figure 3 for the calcium atom the behavior of TDCS is further different from Be and Mg. We see double peak structure. First peak position in is at $\theta_a= 30^o$ and second is near $\theta_a = 55^o$ and there are three minima at $\theta_a= 20^o$, 45^o and finally at 90^o. Like the magnesium and beryllium atoms, the double peak structure disappears also for calcium atom as the excess energy increases from 14.25eV up to 29.25eV. We observe that as the electronic configurations vary from Be to Ca the behavior of TDCS shows different feature. Unfortunately there are no experiments to compare our theoretical calculation.

References

1. A. J. Murray, Phys. Rev. A **72**, 062711 (2005).
2. A. J. Murray and D. Cvejanovic, J. Phys. B **36**, 4875(2003).
3. R. K. Chauhan, M. K. Srivastava, and R. Srivastava, Phys. Rev. A **71**, 032708 (2005).
4. E. Clementi and C. Roetti, At. Data Nucl. Data Tables **14**, 177 (1974).
5. J. B. Furness and J. E. McCarthy, J. Phys. B **6**, 2280 (1973).
6. S. Jones, D. H. Madison, and M. K. Srivastava, J. Phys. B **25**, 1899 (1992).
7. C. Pan and A. F. Starace, Phys. Rev. A **47**, 2389 (1993).

ELECTRON IMPACT TOTAL IONIZATION CROSS SECTION OF Fe AND Cu ATOMS

D. N. Bhavsar[2], M. N. Shah[2], M. Y. Barot[1*], B. H. Pithadiya[1] and K. B. Suthar[1]

[1]V. P. & R.P.T.P Science College, Vallabh Vidyanagar-388 120
Gujarat, India

[2]Department of Physics, Sardar Patel University, Vallabh Vidyanagar-388 120, Gujarat, India

*Email: barot_mayuri@yahoo.com

1. INTRODUCTION

Study on electron impact scattering and ionization of atoms and molecules is of fundamental interest, since they play vital role in determining the chemistry of any environment during and after a collision process. The application of total ionization cross section (Q_{ion}) data by electron impact to various fields like atmospheric sciences, astrophysical and technological plasmas, radiation physics, mass spectroscopy and semiconductor industry [1] has already been realized. However, the concept of compilation of all the required data in a single database is still a distant reality. One of the reasons for this is the scarcity of cross section data for many targets like heavy atoms and exotic molecules and radicals. Also, the reliability of the available data has been a major concern. Under these circumstances our attention was directed towards the study of total and ionization cross sections of the atoms Fe, and Cu by electron impact. We are quite confident from our earlier work [2-4] that present results are reliable and found to be within the experimental errors (around 10%).

Iron is a metal in the first transition series. It is the most common element forming the planet Earth's outer and inner core. It is the fourth most common element in the Earth's crust. Iron plays an important role in biology, forming complexes with molecular oxygen in haemoglobin and myoglobin; these two compounds are common oxygen transport proteins in vertebrates. Iron is also the metal used at the active site of many important redox enzymes dealing with cellular respiration and oxidation and reduction in plants and animals. Copper is a ductile metal with very high thermal and electrical conductivity. The biological role for copper commenced with the appearance of oxygen in earth's atmosphere.

THEORY

Here, we have calculated total ionization cross section for Iron (Fe), and Copper (Cu) by employing the semi-empirical Complex Scattering Potential-ionization Contribution approach (CSP-ic) which is tested successfully earlier in predicting the total ionization cross section of a large variety of atomic and molecular targets. At incident energies (E_i) of the present interest, the inelastic channels in electron atom scattering consist of discrete excitations and ionizations, and this enables us to express the total inelastic cross-section as,

$$Q_{inel}(E_i) = \sum Q_{exc}(E_i) + Q_{ion}(E_i) \qquad (1)$$

In equation (1), the first term is the sum of the total excitation cross-sections for all the accessible electronic transitions. These transitions are dominated by low-lying dipole allowed states, for which the thresholds lie below the ionization energy. The second term stands for all the allowed ionization processes in the targets by electron impact. The detailed methodology is given in our earlier papers [2, 3] and hence not repeated here.

2. RESULT AND DISCUSSION

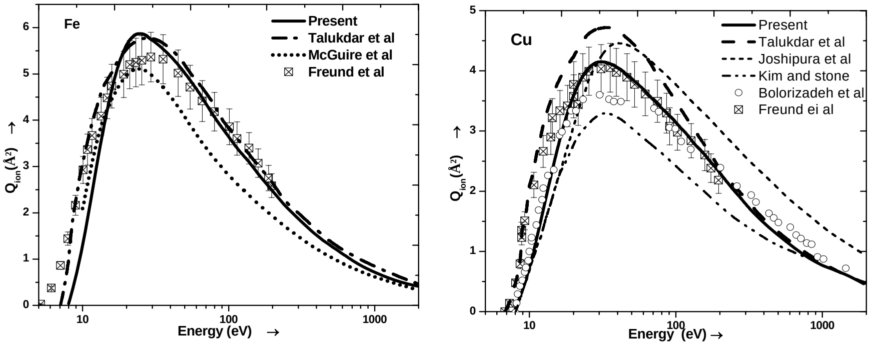

Fig -1 (b)

Fig - 1(c)

Figure 1 (a) Total ionization cross section of Fe; (b) Total ionization cross section of Cu; Solid line: Present Results, Dashed Line: Talukdar et al [4], Dash dot: Bartlett et al [5], Dash dot dot: Kim and Stone[6], short dashed line: Joshipura et al [7], Short dot: McGuire et al[8], Circle: Bolorizadeh et al[9], Square with cross: Freund et al [10].

Figure 1(a) shows comparison of total ionization cross section for e – Fe scattering with available comparisons. There is only one measurement done by Freund et al [10] while theoretical data is provided by Talukdar et al [4] and McGuire et al [8]. Present data is in excellent agreement with measurements of Freund et al [10] and Talukdat et al [4] beyond 30 eV below which there is little deviation with present data. Theoretical data of McGuire et al [8] are in very good agreement with present data below 10 eV above which they are lower compared to all data.

Figure 1 (b) shows the comparison of total ionization cross sections of e – Cu scattering with available comparisons. The experimental data is provided by two groups [9,10]. Theoretical data is provided by Joshipura et al [7], Kim and Stone [6] and Talukdar et al [4]. Present results are in good agreement with both the measurements. Theoretical data of Kim and Stone [6] is lower compared to all data presented here. Present data is in good agreement with data of Joshipura et al [7] till 20 eV beyond which they are higher compared to all data presented here. Theoretical data of Talukdar et al [4] is higher compared to present data till 100 eV, beyond which they are in excellent agreement with present data.

3. CONCLUSION

Present paper reports comprehensive study of electron impact total ionization cross sections for Fe and Cu atoms. Present results are in good agreement with other available experiments [9, 10] as well as theory [4-8] throughout the energy range and the methodology employed for this calculation is consistent, simple and fast. That's why we have confidence that the method which we employed is further works for other atoms as well as molecules for which experiments are difficult.

4. ACKNOWLEDGEMENT

D. N. Bhavsar is very much thankful to DST for providing the financial support through INSPIRE fellowship scheme as a full time Ph. D. student under which this work is done.

References

1. Boudaiffa B., Cloutier P., Hunting D., Huels M. A. and Sanche L. (2000) Science 287, 1658.
2. K N Joshipura, V Minaxi and U M Patel, (2001), J. Phys. B, At. Mol. Opt. Phys., **34**, 509.
3. K N Joshipura and C G Limbachiya, Int. J. Mass Spectrom. 216, 239 (2002)
4. Talukdar et al,(2008), *Empirical model for electron impact ionization cross sections of neutral atoms,* Eur. Phys. J. D,**46**, 281.
5. Bartlett, P. L., Stelbovics, A.T. (2002), *Calculation of electron-impact total-ionization cross sections,* Phys. Rev. A, **66**, 012707 .
6. Kim Y. K. and Stone, P.M.,(2007), *Ionization of silicon, germanium, tin and lead by electron impact*, J. Phys. B: At. Mol. Opt. Phys.**40**,1597
7. Joshipura K N, Vaishnav B G, Limbachiya C. G., (2006) *Ionization and excitation of some atomic targets and metal oxides by electron impact* , Pramana, **66**, 403.
8. McGuire E. J, (1977), *Electron impact ionization cross section in the born approximation,* Phys. Rev. A, **16**, 62
9. Bolorizadeh, M. A., Patton, C. J., Shah, M. B., and Gilbody, H. B., (1994) J. Phys. B: At. Mol. Opt. Phys. **27**, 175
10. Freund, R. S., Wetzel, R. C., Shul, R. J., and Hayes, T. R., (1990), Phys. Rev. A, **41**, 3575.

ASSOCIATION OF ATOMS AND FORMATION OF EXOTIC MOLECULAR IONS BY ELECTRON IMPACT ON MOLECULES

Bhas Bapat and Rajesh Kushawaha
Physical Research Laboratory, Ahmedabad 380009

1. INTRODUCTION

One of the channels of inelastic collisions between electrons and molecules is that of dissociative ionisation (DI). DI can be considered as a two-step process. The first step is electronic excitation leading to ionisation and formation of a molecular ion in an excited electronic state. The second step is the decay of the excited and unstable state, leading to the formation of molecular fragments (ionic or neutral). DI involves nuclear degrees of freedom, or rearrangement of bonds, i.e. changes in the geometry of the molecular ion. How drastic can the changes in the geometry be? Suppose one has a linear molecule ABC which undergoes dissociative ionisation via the formation of ABC^{2+}. Some "obvious" fragments that can result are A^+, B^+, C^+, AB^+, BC^+ and their neutral or doubly charged counterparts. But, is it possible for AC^+, or AC^{2+} or AC to be formed? If they are, what are the mechanisms that lead to association between atoms that are well-separated in the molecule? Is association limited to two atoms?

We have performed experiments with several organic molecules which show that association between two, or three atoms that are otherwise well-separated, can occur during the DI process. A consistent feature of DI of several classes of organic molecules is the formation of H_2^+ and H_3^+ by association between separated H atoms [1-4]. Our focus is on understanding the changes leading to association between atoms brought about by electron impact on molecules. As example, we have chosen the molecule dimethyl sulphoxide, in which several associative channels, some leading to the formation of very unusual molecular ions/radicals, are open.

2. EXPERIMENT

An effusive beam of molecules under study is made to intersect a beam of high energy (1.3 keV) electrons under single collision conditions. Ions formed in the crossed-beam reaction are analysed by an ion momentum spectrometer, the details of which can be found elsewhere [5], and is only briefly described here. The reaction occurs in a small volume, which is located in a region of uniform electric field. This field accelerates ions and electrons formed in the collision in two opposite directions towards two detectors. The electrons are detected by a microchannel plate close to the interaction region. Ions are first accelerated and then move through a field free drift region to a position sensitive detector consisting of a large diameter microchannel plate and a delay-line anode. Electron-ion coincidence is employed to determine the ion time-of-flight (TOF), while the delay-line anode enables determination of the ion arrival position (*x*,*y*). From the (*x*,*y*,TOF) information, one can retrieve the initial momentum vector of each ion striking the detector. For each electron trigger, up to four ions can be detected and their momentum vectors fully determined, thus facilitating a four-fold ion-ion coincidence. Such correlated ion momentum information can be exploited to investigation of the fragmentation dynamics highly charged molecular ions formed in the reaction. From the correlated momentum data, various kinematic parameters and or multi-fold differential cross-sections of chosen dissociation channels can be obtained.

3. RESULTS

As with most organic molecules, the first indication of an associative channel is in the appearance of peaks in the TOF spectrum corresponding to masses 2 and 3, readily identified as H_2^+ and H_3^+. Two other peaks that are indicative of association channels are at mass 19 and 31, corresponding to OH_3^+ and OCH_3^+. A distinctive feature of the mass peaks of associative ions is that the shape seems to be a superposition of two or more distributions. Such combination of distribution points to two possibilities: contribution of multitude of molecular ion excited states to dissociation, and different types of dissociation, i.e. single-step or multi-step, ultra-fast or delayed, Coulomb explosion or non-Coulomb explosion, etc. Moreover, a given ionic fragment can arise from different precursors, or different states of the same precursor. Since our detection method permits separation of channels leading to the formation of one, two or three ions, we can separate the contribution to each of these peaks from singly, doubly, and higher charged precursors and can further look into the kinematics of the fragmentation.

3.1. KINETIC ENERGY OF H_n^+ IONS

The kinetic energy of H_2^+ and H_3^+ ions arising from doubly and singly charged precursors are shown in Fig. 1. In the case of dissociation of singly ionised precursors, it is clear from the distribution that there are multiple components in the KE distribution. Coulomb explosion is not possible for singly ionised precursors, so the mechanism for their formation must be a slower process, involving shallow potential energy surfaces, which results in low kinetic energy ions and also involving some steeper potential energy curves, resulting in ion fragments with higher kinetic energies.

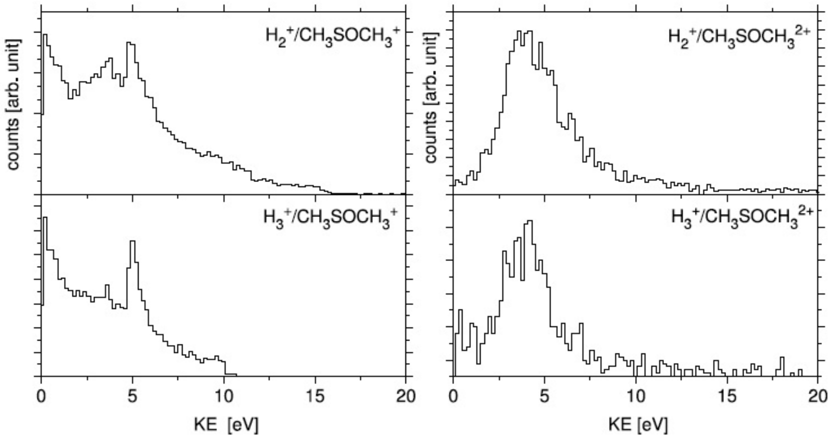

Figure 1: Kinetic energy distribution of H_2^+ and H_3^+ ions from singly- and doubly-charged DMSO.

3.2. DI-CATION FRAGMENTATION SEQUENCE

Dissociation of singly-charged precursors results in the formation of only one charged fragment, which is detected in the experiment, but there may be one or more neutral fragment, which is undetected. This makes it impossible to discern the fragmentation sequence. In contrast, for the dissociation of di-cations, we are able to determine the complete kinematics of two fragments, and this gives crucial inputs for determining whether the fragmentation is one-step or multi-step. Since the momenta of two of the three fragments are completely determined, we can derive the momentum of the third (neutral) fragment by applying the principle of momentum conservation, thereby obtaining the three momentum vectors unambiguously in many fragmentation channels.

Three channels involving association of two or more atoms in the break-up of a di-cation are observed, and all of these have a neutral S as one fragment.

$$CH_3SOCH_3^{2+} \rightarrow CH_3^+ + OCH_3^+ + S \qquad (1)$$

$$CH_3SOCH_3^{2+} \rightarrow H_3^+ + COCH_3^+ + S \qquad (2)$$

$$CH_3SOCH_3^{2+} \rightarrow OH_3^+ + CCH_3^+ + S \qquad (3)$$

All these reactions are intriguing – somehow the central S atom has slipped out of the skeleton! The second and third channels are the most puzzling: In the channel (2), not only has the S atom slipped out, the three H atoms and the distant O atoms have associated! Channel (3) involves association of the three H atoms and migration of one C and the O atom to the CH_3 group! Although we have clearly identified these channels, they are too weak to permit a meaningful kinematic analysis. Channel (1) which is found to have the highest probability among the three is no less puzzling and we perform a kinematic analysis. Association has occurred between O and CH_3, which necessarily means that the O atom has migrated during the reaction and this migration has taken place prior to the breakup of the C–S bond. To corroborate this conjecture, we exploit the kinematics determined from the experiment.

To visualise the break-up, we employ a three-body momentum map, or a histogram of events as a function of reduced momentum coordinates. The unit vector of the momentum of one of the fragments (CH_3^+, in the present case), is taken as the reference direction. The components of momenta of other fragments parallel and perpendicular to the reference vector are then plotted as a colour coded histogram in the momentum plane. Two different colour codes are used to show the momentum distributions of the two fragments. The reference vector is shown as a blue arrow, and the distribution of the magnitude of the reference momentum is shown as a 1-D histogram (also in blue).

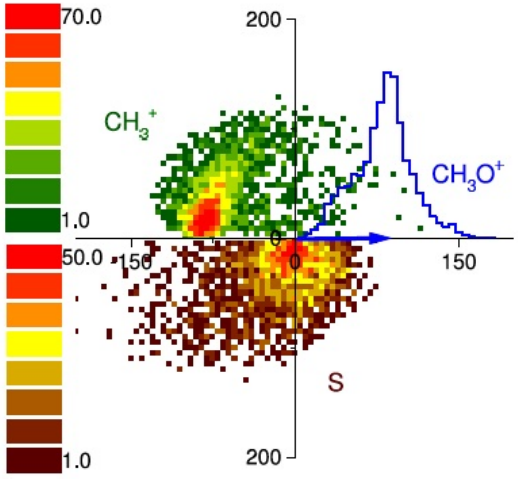

Figure 2: Momentum map for three-body break-up of $CH_3SOCH_3^{2+}$ as described by Eqn. 1.

The distribution of the momentum of CH_3^+ is broad and spreads out towards the perpendicular axis. In other words, its momentum is not anti-correlated to the momentum of OCH_3^+. This implies that in the break-up, the third body (neutral S) has shared some momentum. The sharing implies, that the break-up of $CH_3SOCH_3^{2+}$ into three bodies is simultaneous. However, more investigation is needed to understand the bond rearrangement leading to this fragmentation channel. Probing the ejected electrons is one way to get a better insight into the mechanisms.

4. CONCLUSION

We have observed several dissociation channels under electron impact on organic molecules. Association between otherwise separated atoms within the molecule takes place accompanied by large scale rearrangement of bonds, leading to the formation of unusual molecular ions or radicals. We have made an attempt to understand the fragmentation sequence leading to some of these unusual molecular ions from the kinematics of the fragments obtained experimentally.

References

[1] Sharma V. and Bapat B., (2006), *Determination of active sites for H atom rearrangement in dissociative ionization of ethanol.* J. Chem. Phys. **125,** 044305.

[2] Kushawaha R. K. and Bapat B., (2008), *Fragmentation dynamics of the methanol dication* Chem. Phys. Lett. **463,** 42.

[3] De S., Rajput J., Roy A., Ghosh P. N., and Safvan C. P., (2006), *Formation of* H_3^+ *due to Intramolecular Bond Rearrangement in Doubly Charged Methanol* Phys. Rev. Lett. **97,** 213201.

[4] Kushawaha R. K. and Bapat B., (2011), *Similarities in Kinetic Energy Distributions of Associative Fragments during Dissociative Ionization of Organic Molecules.* J. Korean Phys. Soc. **59,** 2905.

[5] Sharma V. and Bapat B., (2006), *An apparatus for studying momentum-resolved electron-impact dissociative and non-dissociative ionisation.* Eur. Phys. J. D **37,** 223.

ELECTRON IMPACT IONIZATION CROSS SECTIONS OF FULLERENE (C_{60})

Neelam Tiwari[1], Manoj Kumar Singh[2] and Surekha Tomar[3]
[1]Department of Physics, G. G. College, Kondagaon, C.G., India
[2]Department of Physics, BHU, Varanasi, U.P., India
[3]Department of Physics, R.B.S. College, Agra, U.P., India

1. INTRODUCTION

Atomic clusters concern astrophysicists, atomic and molecular physicists, chemists, molecular biologists, solid-state physicists, nuclear physicists, plasma physicists, technologists. The famous fullerene (C_{60}) provides a beautiful example of covalent bonding in clusters. In that case, the cluster exhibits a well-defined structure with electrons localized along the various links between the atoms.

2. THEORY

For fullerene (C_{60}) the total ionization cross sections have been measured by various groups [1, 2] and theoretically by Deutsch et al. [3] have calculated the cross section in the energy range threshold to 1000 eV. In Khare model [4] the present total ionization cross- section is,

$$\sigma_T = \sigma_{PBB} + \sigma_{PMB} + \sigma_i \tag{1}$$

$$\sigma_{PBB} = \frac{AN_i I_i}{(E' + hI_j)} \int_{I_j}^{E'} \frac{1}{\omega^3} \ln\left[\frac{\omega}{Q_-}\right] d\omega \tag{2}$$

$$\sigma_{PBB} = \frac{AN_i I_i}{(E' + hI_j)} \times \left[\left(1 - \frac{2}{t+1} + \frac{t-1}{2t^2}\right) + \left(\frac{5-t^2}{2(t+1)^2} - \frac{1}{t(t+1)}\right) - \left(\frac{(t+1)}{t^2}\ln\left(\frac{t+1}{2}\right)\right)\right] \tag{3}$$

$$\sigma_t = \frac{AN_i I_i}{(E' + hI_j)} \{\ln(1-\beta^2) + \beta^2\} \tag{4}$$

Where t = E'/ I_j, m is the rest mass of the electron, Q_- is the recoil energy, b_{nl} is the bethe parameter and β = v/c.

3. RESULT AND DISCUSSION

In the present calculation, only contributions to the ionization cross section arising from the two outermost carbon subshells, the 2s and 2p-orbitals, is consider. Mulliken population analysis of C_{60} includes only contributions from 240 out of the 360 C_{60} electrons in 120 of the 180 C_{60} orbitals [5].

Figure 1: Electron impact ionization cross sections for fullerene (C_{60}). ■, the present work; ●, by Deutsch [4]; ▲, by Matt [3]

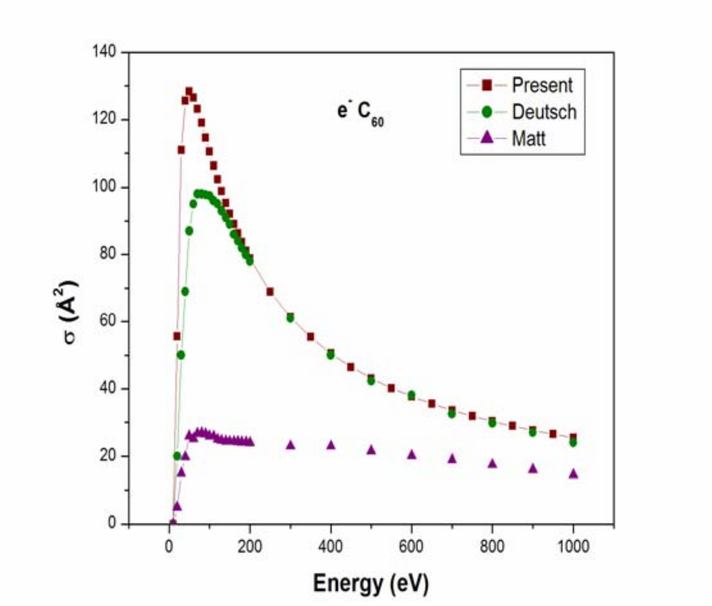

The present ionization cross sections for fullerene (C_{60}) are compared with the experimental and theoretical data. The outermost C_{60} orbitals contribute highly to the total ionization cross section. Deutsch et al. [3] have stated that almost entire energy range, their own [2] experimental results show discrepancy with their own calculated total cross-section estimations.

The present result is in satisfactory agreement with Deutsch [4] while both theoretical data is not in good agreement with experimental data [3].

4. CONCLUSION

The present approach can be extended to study the electron impact ionization of other clusters. Present method has been successfully tested for a number of molecular and atomic targets [6-8].

References

[1] Vostrikov A., Dubov D. Y. and Agarkov A. A., (1995), *Direct and delayed ionization of C_{60} clusters by electron impact.* Tech. Phys. Lett. **21,** 715.

[2] Matt S., Dunser B., Lezius M., Deutsch H., Becker K., Stamatovic A., Scheier P. and Märk T. D., (1996), *Absolute partial and total cross section functions for the electron impact ionization of* C_{60} *and* C_{70}. J. Chem. Phys. **105,** 1880.

[3] Deutsch H., Becker K., Pittner J., Bonacic - Koutecky V., Matt S. and Märk T. D., (1996), *Semi classical calculations of the cross section for electron-impact ionization of* C_{60}, J. Phys. B: At. Mol. Opt. Phys. **29,** 5175.

[4] Khare S. P., Sharma M. K. and Tomar S., (1999), *Electron impact ionization of methane.* J. Phys. B: At. Mol. Opt. Phys. **32,** 3147.
Mulliken R. S., (1949), *Quelques aspects de la theorie des orbitals moleculaires.* J. Chim. Phys. **46,** 675.

[5] Tiwari N., Kumar Y. and Tomar S., (2010), *Electron impact ionization crosssections of* C_2H_2 *and CH molecules at low and high energy range,* J. At. Mol. Sci. **1,** 301.

[6] Kumar Y., Tiwari N., Kumar M. and Tomar S., (2010), *Total ionization cross-sections of atmospheric molecules due to electron impact.* Ind. J. Pure App. Phys. **48,** 621.

[7] Tiwari N. and Tomar S., (2011), *K-shell ionization cross sections of light atoms due to electron impact.* J. At. Mol. Sci. **2,** 109.

IONIZATION OF ATOMIC MOLECULAR SYSTEMS BY ELECTRON IMPACT – THEORETICAL AND APPLICATION HIGHLIGHTS

K. N. Joshipura[1] and Siddharth H. Pandya[2]
Department of Physics, Sardar Patel University,
Vallabh Vidyanagar – 388 120 (Gujarat)
[+]Bahauddin Science College, Junagadh - 362 001 (Gujarat)
Email: knjoshipura@yahoo.com

Abstract

Ionization of atomic and molecular systems by electron impact is a very important process from pure as well as applied points of view. The Complex Scattering Potential - ionization contribution (CSP-ic) method explores this process as a fractional contribution in the overall inelastic scattering of electrons at above-threshold energies. Basic aspects of the method are outlined here along with applications in brief.

Key words: electron impact ionization, complex potential, cross sections, mean free paths

1. INTRODUCTION

In 2013 the world celebrated 100 years of the Bohr atom model, which paved the way to knowledge on atomic structure. The research field of electron impact ionization of atoms and molecules, which has grown along with this knowledge, is about equally old and still growing. *Ionization by moving electrified particles* - was the title of a historic and perhaps the first ever paper on electron impact ionization of atoms, written in 1912 by Sir J. J. Thomson. Soon after the Bohr atom model, the famous experiment on inelastic scattering of electrons by Hg atoms was performed in 1914 by Frank and Hertz, demonstrating the quantization of atomic energy levels. The research field became important in studying the passage of charged particles like electrons through gases, in nuclear radiation detectors. There is a fundamental scientific interest in electron atom/molecule ionization [1-3]. It plays a significant role in gaseous electronics, gas discharges, lighting devices, dielectric applications, semiconductor industries as also in mass spectrometry, ion gauges, Plasma Physics and Chemistry, Lasers and so on. Basically ionization induced by electrons results into energy loss of the incident projectile, while a variety of ionic (and neutral) species is produced from the target, and that is quite relevant in the environments of planets, their satellites, comets and other astrophysical objects. In the ionospheres of the Earth and other planets, photoelectrons of sufficient energy can produce ions plus neutral species and thus give rise to different chemistries [1, 2]. It is found that in the Martian ionosphere the production of ions in the E layer is mostly due to photoelectrons, which are produced by primary photo-ionization in the F layer. Progress in the atomic molecular ionization induced by electrons was reviewed about three decades back by Maerk [1]. Electron impact ionization of atoms/molecules poses a difficult quantum mechanical problem. A semi-empirical approach in this direction was developed in late '70s in the form of Khare-Jain formula [4]. In the last two decades, two theoretical methods viz., Binary Encounter Bethe (BEB) method of Kim et al [5, 6] and the Deutch Maerk (DM) formula [7] have been extensively employed in calculating cross sections (CS) of electron ionization.

Now, ionization occurs as a part of all admissible inelastic processes in a target induced by incident electrons (of energy E_i), in the background of elastic collisions. Therefore, we can evaluate total ionization cross section $Q_{ion}(E_i)$ as a fraction of total inelastic cross section $Q_{inel}(E_i)$, obtained in the spherical complex (optical) potential formalism. Thus our scattering dynamics starts with total interaction potential $V(r,E_i)=V_R(r,E_i) + iV_I(r,E_i)$, with r as the radial coordinate of the external electron. The real component V_R includes the static, exchange and correlation-polarization potentials, while the imaginary component V_I, i. e. absorption potential V_{abs} represents cumulatively the effect of all inelastic scattering, under flux and energy conservation [8]. The total (complete) CS is given by, $Q_T(E_i) = Q_{el}(E_i) + Q_{inel}(E_i)$.

2. THEORETICAL HIGHLIGHTS

At incident energies from first-ionization threshold (~ 10-15 eV) to 2000 eV, the cross sections Q_{el} and Q_{inel} are calculated by solving the Schroedinger equation with the appropriate spherical complex potential. Our calculated Q_{inel} represents inelastic scattering of electrons by the target, leading to various admissible transitions to discrete states as well as continuum. Therefore

$$Q_{inel} = \sum_{f} Q_{exc}(i \rightarrow f) + \sum Q_{ion} \qquad (1)$$

Where, the first term denotes the sum of all (electronic) *excitation* cross sections upon electron bombardment on the target (inital state *i*), corresponding to final states *f*. The second term in equation (1) indicates the sum-total of single, double, direct and dissociative ionization as the case may be. From here onwards we write it simply as Q_{ion}. Now, we ask a crucial question. Having calculated the Q_{inel}, how do we obtain the more important quantity Q_{ion}? Theoretical attempts to answer this question have led to the *Complex scattering potential - ionization contribution* (CSP-ic) method, vide [9,11]. With this method it has become possible in a semi-empirical way to go a step ahead and determine the two terms separately in eqn. (1). To achieve this aim, we introduce an energy-dependent ratio, R $(E_i) = Q_{ion}(E_i)/ Q_{inel}(E_i)$ such that, $0 \leq R \lesssim 1$, in view of eqn. (1).

In order to get a feel for this ratio function, consider first a standard target viz., Hydrogen atom, for which the first excitation threshold is 10.2 eV, while its ionization energy is 13.6 eV. In this case the (dipole allowed) 1s --> 2p excitation (followed by emission) is so strong that it competes with ionization even at high energies, resulting into R (E_i) ~ 0.5. In general the contribution (fraction) of Q_{ion} in Q_{inel} at the peak position E_p of the Q_{inel} is found to be ~ 70 %, for many (but not necessarily all) targets. It is thus possible to impose three conditions on the ratio function R corresponding to three energies, as follows.

$$R = 0, \quad \text{at and below threshold } E_i \le I \qquad (2\text{ - }a)$$
$$R = R_P, \text{ at intermediate energy, } E_i = E_p \qquad (2\text{ - }b)$$
$$R \approx 1, \quad \text{at high energy } E_i \gg E_p \qquad (2\text{ - }c)$$

Further details of representing R as a continuous function of energy, and deducing the ionization CS are discussed in [2, 9 - 11]. In eqn. (2) the input at an intermediate energy is semi-empirically chosen as 0.7, which attracts criticism. Therefore we look for general trends in the peak magnitude of total ionization CS, denoted by σ_{max}, as a function of well known and basic atomic/molecular properties viz., molecular polarizability α_0 and first ionization energy I. The σ_{max} exhibits a good linear dependence on the quantity $\sqrt{(\alpha_0/I)}$, and can be fitted to a relation

$$\sigma_{max} = A_1 \sqrt{(\alpha_0/I)} + A_2 \qquad (3)$$

The peak position 'ε_i' i. e. the incident energy at which the ionization CS reaches the maximum, also shows a general dependence on the threshold I of the target. Therefore an independent estimate of the σ_{max} and the corresponding energy ε_i can be made. This leads to a target specific estimate of the ratio R at an intermediate energy, which can be employed as input in eqn. (2-b).

3. RESULTS, DISCUSSION AND CONCLUSIONS

The CSP-*ic* method has been successfully applied to over a hundred common and exotic atomic-molecular targets in the last few years [9 - 13]. Presently an independent but target-specific determination of the ratio R is suggested, vide eqn. (2). We omit here the detailed results and comparisons with other data, which are discussed elsewhere in this Conference Proceedings.

Let us briefly dwell upon the applications of microscopic i. e. quantum mechanical cross sections to ionization processes in macro-systems or bulk media, like a gas medium. Suppose that a particular atomic or molecular species being ionized by the incident electrons, is embedded in a bulk system with N number of targets per cc. We can define 'macroscopic' ionization CS Σ_{ion} through the equation $\Sigma_{ion} = N.\ Q_{ion}$. The quantity Σ_{ion} is not a cross section as such, since it is measured in $(\text{length})^{-1}$. An important macro-parameter called the ionization mean free path (MFP) Λ_{ion} is then defined as follows.

$$\Lambda_{ion} = 1/\,\Sigma_{ion}$$

Figure 1 shows the typical ionization MFP for three of the most well known planetary/satellite environments. The lowest curve in this figure shows the MFP for the H_2 - dominated atmosphere of planet Jupiter. The blue curve corresponds to the N_2 - rich atmosphere of Titan, the satellite of Saturn, while the top-most curve represents CO_2 - rich Martian atmosphere. Appropriate number densities and altitudes are chosen to highlight typical values here. In each case, the dip in the MFP corresponds to the peak of the corresponding ionization CS. The energy of the MFP dip is also interpreted accordingly. The MFP can also be defined for other processes like elastic scattering, excitations etc. These quantities are useful inputs for modeling planetary/satellite atmospheres, for which observations are carried out by different space missions.

Thus in this short paper we point out a *micro - to - macro* approach for extending the applications of electron scattering studies to bulk media. Macro-quantities like MFP, collision frequency, ion production rates etc are useful inputs [2] to the modeling of the atmospheres / ionospheres of planets, comets and other astrophysical systems. For example, our calculated Q_{ion} on common atoms and molecules have been employed in modeling the effect of solar x-ray flare events in the Martian ionoshpere.

The *micro - to - macro* approach has been employed by us even for the condensed-matter systems, and ionization MFP have been calculated for electrons passing through (metallic) Si, SiO, SiO_2, Al_2O_3, Cu, CuO and various ices as well.

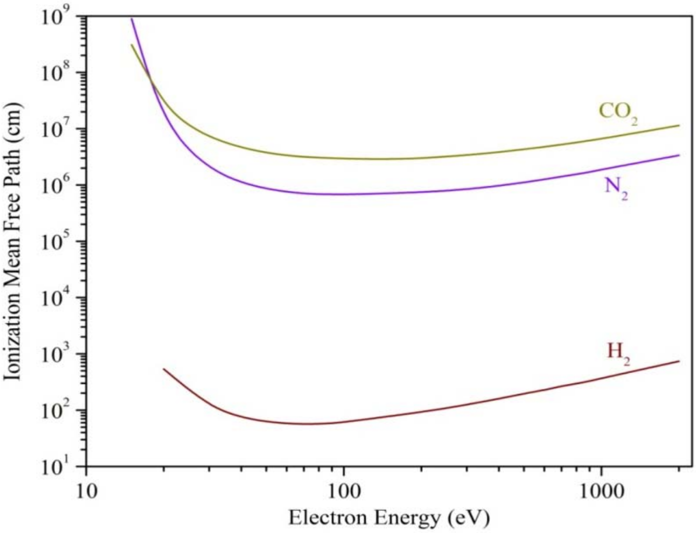

Figure 1 Ionization MFP of electrons with H_2 (on Jupiter), N_2 (on Titan) and CO_2 (on Mars), as functions of incident energies

References

[1]. T. D. Maerk in *'Electron - molecule interactions and their applications'* Ed. L. G. Christophorou, Academic Press New York (1984) p. 251

[2]. S. H. Pandya *et al*, Advances in Geo-sciences, Vol. **25**: *Planetary Science*, Ed. Anil Bhardwaj (World Scientific Publishing Company, Singapore) (2010) p. 225

[3]. G. P. Karwasz and A. Zecca in ‘O*ne century of experiments on Electron molecule scattering’*, Rivista Del Nuovo Cemento **24/1** (2001) 01

[4]. S. P. Khare and D. K. Jain, L. Phys. **B 9** (1976) 1429
[5]. Y. K. Kim et al, J. Chem. Phys. **106** (1997) 1026
[6]. NIST website, *www. physics.nist.gov/PhysRefData/Ionization/Xsection*
[7]. H. Deutsch et al, Int. J. Mass Spectrom. 197 (2000) 37–69
[8]. B. Bransden & C. J. Joachain, in *'Physics of atoms and molecules'*, Pearson Education (2004) p. 110
[9]. K. N. Joshipura et al, Phys. Rev. A 69 (2004) 022705
[10]. S. H. Pandya *et al*, Int. J. Mass Spectrom., **323–324**, (2012) 28
[11]. K. N. Joshipura et al, J. Phys. **B 43**, (2010) 13520
[12]. Minaxi Vinodkumar et al, J. Chem. Phys. **136** (2012) 184308
[13]. K. N. Joshipura et al, Pramana J Phys, **66** (2006) 403

ELECTRON SCATTERING STUDIES WITH ATOMIC BERRILIUM AND BeH, BeH$_2$ MOLECULES

F. M. Joshi[1] and K. N. Joshipura[2]
[1]G. H. Patel College of Engineering and Technology, V. V. Nagar - 388120, Gujarat, India
[2]Department of Physics, Sardar Patel University, V. V. Nagar - 388120, Gujarat, India

1. INTRODUCTION

Collision processes involving Beryllium are important since Be has been chosen for first-wall plasma facing components in ITER as mentioned by Pindzola et al. [1]. The increasing use of light elements such as helium, lithium, and beryllium as constituents of plasma facing components and as diagnostic tools in fusion plasma devices challenges plasma modelers to provide accurate simulations of the complex physical processes inherent in fusion plasmas [2]. Beryllium has been proposed as a first wall component for the plasma-facing material in the planned ITER experiment [3]. There have been only a few experimental efforts devoted to obtain cross sections of beryllium atom. On the theoretical side, studies of the elastic electron beryllium scattering cross sections have been made by Fursa and Bray [4,5].

Due to the lack of experimental data for this collision system, researchers in plasma modelling have to currently rely entirely on theoretical predictions as the input to their computational codes [6]. Beryllium hydride (BeH$_2$) is of interest to basic science researchers because of its relatively small number of electrons [7]. While BeH being an intermediate radical product in e -BeH$_2$ interaction, is also of interest. Along with BeH, Solid beryllium hydride is most commonly produced through a complicated controlled pyrolysis of beryllium-containing ethers [8], although it has also been condensed on cryogenic surfaces using laser ablated beryllium atoms in a hydrogen atmosphere [9]. Apart from this, BeH$_2$ is known to be a good storage of hydrogen due to its low mass and high hydrogen content. For all these reasons, there has recently been a renewal of interest in beryllium hydride in the scientific community [10-14].

In view of the above significance we theoretically determined electron impact cross sections for Be-atom, BeH and BeH$_2$. So far there is no experimental or theoretical data for electron impact cross section on these targets.

We have employed the SCOP and CSP-*ic* method for obtaining various TCS for these targets at incident energy ranging from ionization threshold to 2000 eV.

2. THEORY

In our publications [15-18] on electron–molecule scattering, theoretical efforts have been directed toward extracting the ionization contribution from the total inelastic cross section Q_{inel} derived from a complex scattering potential. Presently we have employed the well established Complex Scattering Potential ionization con-tribution (CSP-*ic*) formalism developed in the recent years [20–24] to obtain Q_{ion} along with other total cross sections for these tar-gets at energies E_i from I_E to 2 keV.
The ionozation potential of Be, BeH and BeH_2 are 9.32 eV, 8.28 eV and 10.82 eV.

3. RESULTS AND DISCUSSION

Turning to present theoretical results, we have shown all total cross sections for electron impact on atomic beryllium. The cross sections for electron impact on BeH and BeH_2 are shown as a function of incident energy. Detailed results will be presented and discussed in the conference.

Figure 1: Electron scattering total cross sections of Be- atom

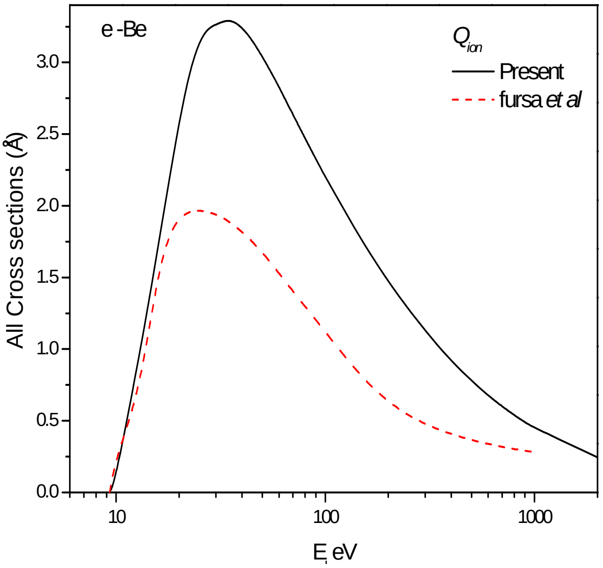

4. CONCLUSION

Our methodology of *SCOP* and *CSP-ic* has given reasonably good agreement for many atoms and molecules in past studies. Presently in case of Be atom the present theoretical results differ from experimental data because of a possibility of mixture of metastable atoms in neutral beam.

References

[1] Abdurahman A., Shukla A., and Dolg M., (2000), *Ab initio treatment of electron correlations in polymers: Lithium hydride chain and beryllium hydride polymer*. J. Chem. Phys. **112,** 4801.

[2] Bartschat K., Burke P. G., and Scott M. P., (1997), ***R**-matrix with pseudo-states calculation for electron collisions with neutral beryllium*. J. Phys. B: At. Mol. Opt. Phys. **30,** 5915.

[3] Bernath P. F., Shayesteh A., Tereszchuk K., and Colin R., (2002), *The Vibration Rotation Emission Spectrum of Free BeH_2*. Science **297**, 1323.

[4] Bolt H., Barabash V., Federici G., Linke J., Loarte A., Roth J., and Sato K., (2002), *Plasma facing and high heat flux materials – needs for ITER and beyond;* J. Nucl. Mater. **307,** 43.

[5] Colgan J., Loch S. D., Pindzola M. S., Ballance C. P., and Griffin D. C., (2003), *Electron-impact ionization of all ionization stages of beryllium.* Physical Review A; **68,** 032712.

[6] Doerner R. P., Baldwin M. J., Buchenauer D., De Temmerman G., and Nishijima D., (2009), *The role of beryllium deuteride in plasma-beryllium interactions.* Journal of Nuclear Materials. **390–391;** 681.

[7] Fursa D. V. and Bray I., (1997), *Convergent close-coupling calculations of electron - beryllium scattering*. J. Phys. B: At. Mol. Opt. Phys. **30**, L273.

[8] Fursa D. V. and Bray I., (1997), *Convergent close-coupling calculations of electron - beryllium scattering*. J. Phys. B: At. Mol. Opt. Phys. **30**, L273.

[9] Grochala W. and Edwards P. P., (2004), *Thermal Decomposition of the Non Interstitial Hydrides for the Storage and Production of Hydrogen.* Chem. Rev. **104**, 1283.

[10] Joshipura K. N., Kothari H. N., Shelat F. A., Bhowmik P., and Mason N. J., (2010), *Electron scattering with metastable $H^*_2(c^3\Pi_u)$ molecules: ionization and other total cross sections*; J. Phys. B: At. Mol. Opt. Phys. **43,** 135207.

[11] Joshipura K. N., Vaishnav B. G., and Gangopadhyay S. S., (2007), *Electron impact ionization cross-sections of plasma relevant and astrophysical silicon compounds: SiH_4, Si_2H_6, $Si(CH_3)_4$,SiO, SiO_2, SiN and SiS.* Int. J. of Mass Spectrum. **261**, 146.

[12] Joshipura K. N., Gangopadhyay S. S., Kothari H. N., and Shelat F. A., (2009), *Total electron scattering and ionization of N, N_2 and metastable excited $N^*_2(A^3\Sigma^+_u)$: Theoretical cross sections.* Phys. Lett. A **373,** 2876.

[13] Pandya S. H., Shelat F. A., Joshipura K. N., and Vaishnav B. G., (2012), *Electron ionization of exotic molecular targets CN, C_2N_2, HCN, HNC and BF - Theoretical cross sections.* Int. J. Mass Spectrum. **323-324**, 28.

[14] Pindzola M. S., Balance C. P., Robicheaux F., and Colgan J., (2010), *Electron impact double ionization of beryllium.* J. Phys. B: At. Mol. Opt. Phys. **43**, 105204.

[15] Sampath S., Lantzky K. M., Benmore C. J., Neuefeind J., Siewenie J. E., Egelstaff P. A., and Yarger J. L., (2003), *Structural quantum isotope effects in amorphous beryllium hydride.* J. Chem. Phys. **119,** 12499.

[16] Wang X. F. and Andrews L., (2005), *One-Dimensional BeH_2 Polymers: Infrared Spectra and Theoretical Calculations.* Inorg. Chem. **44**, 610.

ELECTRON INTERACTIONS WITH CuO IN GAS AND SOLID PHASES – THEORETICAL CROSS SECTIONS

U. R. Patel[1,2], K. N. Joshipura[2] and B. G. Vaishnav[3]
[1]Department of Physics, Sardar Patel University,
Vallabh Vidyanagar-388120
[2]Gandhinagar Institute of Technology, Gandhinagar-382721
[3]Physical Research Laboratory, Navrangpura, Ahmedabad-380009

1. INTRODUCTION

In recent decades, significant research has been done on the theoretical calculations of ionization cross sections, as a result of the collisions of electrons with different atomic and molecular targets. Different methods have been developed to calculate reliably the total ionization cross sections of mostly well-known and some exotic atomic and molecular targets. Many of the targets have also been investigated experimentally. Most of the metal oxides in which we are interested here are in solid phase and it is difficult to perform experiments and get data for such targets. In the present work we have studied the molecules which are very important but not studied theoretically or experimentally till date. This paper will report the electron impact ionization cross sections for gaseous and solid phase of CuO. To the best of our knowledge nobody has reported ionization cross sections for these targets and hence present work is significant. The chemical bonding between copper and oxygen atoms is interesting both as a prototype system to understand the basic chemical bonding properties between transition metals and oxygen and due to importance of copper in bio-inorganic chemistry for dioxygen metabolism as mentioned in [1]. CuO is also important in plasma and astrophysical applications.

2. THEORY

The method of calculating electron impact ionization as developed by us in the last few years has been described in our publications [2, 3]. We have presently calculated electron ionization cross sections of CuO (gas) by employing *CSP-ic* (complex scattering potential- *ionization contribution*) methodology. We have bifurcated total inelastic cross sections Q_{inel} into two main channels viz. ionization and electronic excitation as follows.

$$Q_{inel} = \sum_n Q_{ion} + \sum Q_{exc}$$

As discussed in our recent papers [3,4], a reasonable argument can be invoked to determine the ratio of total ionization cross section to total inelastic cross section, at given incident energy. The same method can be used for calculating electron ionization cross sections for CuO (solid) by considering its band gap along with the ionization energy. Also the basic input of our method i.e. charge density can be calculated in a different way as given in [5].

3. RESULT AND CONCLUSION

In fig.1. we have shown ionization cross section of CuO (gas). As far as our knowledge goes there are probably no data on CuO in solid or even gas phase and therefore the only comparison is either mutual or to a nearby situation. Additivity rule provides a rough guideline in such cases. So by simple addition of ionization cross sections of present Cu and O, we have made rough comparison. Due to the difference of ionization energy of CuO and Cu and O a good accord is not expected.

Figure 1: e^--CuO (gas) Red solid line the present Q_{ion}, black solid line present Cu + O

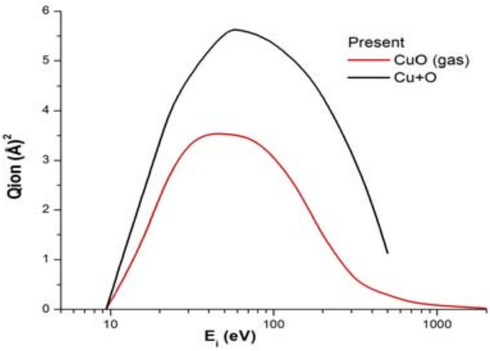

References

(1) Hongbin Wu., Desai S. R., and Lai-Sheng Wang., (1997), *Chemical bonding between Cu and Oxygen - Copper oxides vs O_2 complexes: A study of CuO_x (x=1-6) species by anion photoelectron spectroscopy*. J. Phys. Chem. A **101,** 2103-2111.

(2) Joshipura K. N., Gangopadhyay S. S., Kothari H. N., and Shelat F. A., (2009), *Total electron scattering and ionization of N, N_2 and metastable excited N_2^*: Theoretical cross sections.* Phys. Lett. A **373,** 2876.

(3) Kothari H. N., Pandya S. H., and Joshipura K. N., (2011), *Electron important ionization of plasma important $SiCl_x$ (x=1-4) molecules: theoretical cross sections.* J. Phys. B: At. Mol. Opt. Phys. **44,** 125202.

(4) Pandya S. H., Shelat F. A., Joshipura K. N., and Vaishnav B. G., (2012), *Electron ionization of exotic molecular targets CN, C_2N_2, HCN, HNC and BF- Theoretical Cross sections.* Int. J. Mass. Spectrom. **323-324**, 28.

(5) Salvat F., Mayol R., Molins E., and Parellada, (1985), *A simple model for electron scattering: elastic cross sections* J. Phys. D. Appl. Phys. **18,** 1401.

PARTIAL IONIZATION CROSS SECTIONS OF CO_2 AND N_2O MOLECULES UNDER THE IMPACT OF 10-25 keV ELECTRONS

P. Bhatt[*], and R. Shanker
Atomic Physics Laboratory, Department of Physics, Banaras Hindu University, Varanasi-221005, India
Email: *pbpragya@gmail.com

1. INTRODUCTION

The total- and partial ionization cross sections (PICSs) of atoms and molecules under impact of energetic particles have been the subject of numerous studies in the past [1-3]. However, these ionization cross section values for atmospheric molecules are limited and are of practical importance in various fields, such as, in fusion-edge plasma diagnostics; gas discharge; planetary-, stellar-, and cometary atmospheres; radiation chemistry; and mass spectrometry. In electron-impact dissociative ionization of a molecule, the molecule undergoes different stages of ionization, i.e., single, double, and higher. It is interesting to know how much each ionization stage of the parent molecule contributes to a specific ion product. This information is obtained with the help of 'precursor specific' PICSs.

The technique of multiple ion coincidence coupled with position encoding is used to obtain the PICSs and precursor specific PICSs for keV electron interactions with atmospheric molecules (N_2O and CO_2).

2. EXPERIMENT AND DATA ANALYSIS

The details of experimental setup and data analysis can be found in our previous publications [4-7]. Briefly, keV electrons extracted from an electron gun collide with a dilute gas beam emanating from a hypodermic needle. The collision products (positive ions and electrons) are extracted by application of a homogeneous electric field; electrons are detected by a channeltron and ions by a time- and position sensitive multi-hit detector. The electron signal serves as the timing reference for ion arrivals to a dual micro channel plate (MCP) of $\phi = 40$ mm. The ion detector has the facility of detecting up to four concomitant ion hits; only the time-of-flight (TOF) information of the ions is used in the present analysis, the position information of ions coupled with their TOFs is used for the case where the center of mass (COM) momentum of the system is needed to correct for background events [5-7]. The data is stored event by event in a list mode file which is used to analyze the data offline. Events involving the arrival of one, two, and three ions at the detector following a start pulse of ejected electron from the same event are termed as ‘singles’, ‘doubles’ and ‘triples’ respectively.

The background subtracted TOF spectra for all the ions generated for 10- and 12 keV electron impact on N_2O and CO_2, respectively are shown in Fig. 1. The integrated area for different ion peaks observed in the TOF spectrum divided by the peak-area of the parent molecular ion is used to calculate the relative PICSs. The relative ionic fractions represent probability of formation of an ion with respect to the total number of ions.

Figure 1: TOF spectra of all the ions produced for N_2O and CO_2 under 10- and 12 keV electron impact, respectively.

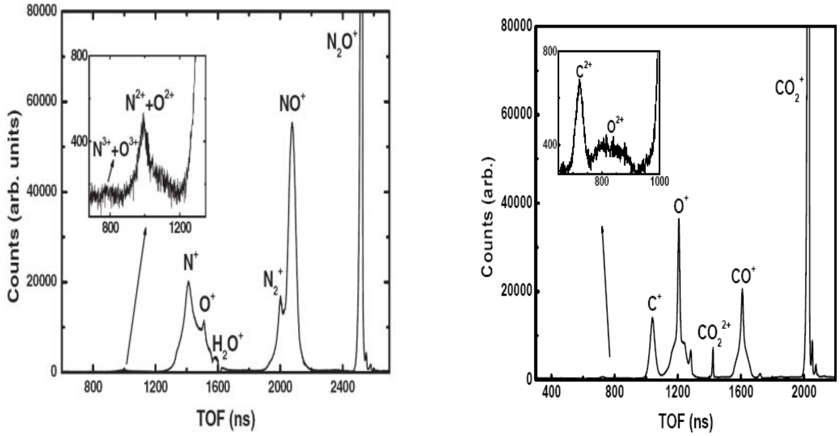

For obtaining the precursor specific PICSs of fragment ions, the counts observed in singles spectrum with a total charge of one are treated as events arising only from singly ionized parent molecule; similarly the counts observed in single to triple ion coincidences with a total charge of two and three are treated as events arising only from doubly and triply ionized parent molecule, respectively. These counts are corrected for the background events as described in [5-7]. The cross section values are put on a relative scale by dividing them with the cross section for formation of the singly charged parent molecule.

3. RESULT AND DISCUSSION

The relative PICSs values for CO_2 and N_2O under keV electron impact are obtained and presented in Tab. 1 and Tab. 2 respectively; the values of RIFs are also given in the tables. In both cases, the singly ionized parent molecule is the most abundant species; however, a doubly ionized metastable parent molecule is also observed for CO_2. Error in relative PICSs is lowest (<1%) for parent ion and reaches up to 14% for doubly charged fragment ions.

Table 1: PICSs for the ions produced in collisions of 12 keV electrons with CO_2 expressed relative to the cross section for formation of CO_2^+; last column gives the RIFs for these ions.

Ion Species	Relative PICSs (x10^{-2})	RIFs (%)
CO_2^+	100.0	65.72
CO^+	14.0	9.23
O^+	25.6	16.80
C^+	10.0	6.53
CO_2^{2+}	1.2	0.80
O^{2+}	0.9	0.57
C^{2+}	0.6	0.36

Table 2: (a) PICSs for the ions produced in collisions of 10-25 keV electrons with N_2O expressed relative to the cross section for formation of N_2O^+ (b) RIFs for these ions at 10 keV electron impact.

(a)

E_0 (keV)	Relative PICSs (x10^{-2})				
	NO^+	N_2^+	O^+	N^+	N^{2+}+O^{2+}
10	57.4	17.9	12.6	31.0	1.8
12	57.1	20.0	15.0	30.3	1.5
16	57.0	19.0	14.0	30.1	1.3
20	56.9	18.9	14.4	29.6	1.3
22	56.5	19.1	14.5	30.3	1.1
25	55.3	18.6	14.4	29.6	1.2

(b)

Ion Species	RIFs (%)
N_2O^+	45.3
NO^+	26.0
N_2^+	8.1
O^+	5.7
N^+	14.1
N^{2+}:O^{2+}	0.8

The precursor specific PICSs for CO_2 and N_2O are presented in Tab. 3 and Tab. 4, respectively for 12 keV electron impact. From our data, we estimate the contributions to the total ion yield of fragment ions from single, double, triple and quadruple ionization of CO_2 molecule at the considered impact energy of electrons to be 75.3%, 22.4%, 2.1% and 0.2%, respectively. Similarly for N_2O, the contributions from single, double, and triple ionization to the fragment ion yield is 81.8%, 17.8%, and 0.4%, respectively.

Table 3: Precursor-specific PICSs, σ_n, ($\times 10^{-2}$ cm^2) for fragment ions formed in collisions of 12 keV electrons with CO_2, the suffix n denotes the ionization state of CO_2 after the removal of n number of electrons.

Ion Species	σ_1	σ_2	σ_3	σ_4
CO^+	11.36	2.68	-	-
O^+	19.52	5.50	0.50	0.04
C^+	7.46	2.05	0.40	0.02
O^{2+}	-	0.75	0.09	0.02
C^{2+}	-	0.44	0.09	0.02

Table 4: Same as Table 3 but for N_2O.

Ion Species	σ_1	σ_2	σ_3
NO^+	51.0	6.1	0.02
N_2^+	15.5	2.1	-
O^+	8.5	3.6	0.15
N^+	22.4	8.0	0.31
N^{2+}:O^{2+}	-	1.4	0.02

4. CONCLUSIONS

We have used the multiple ion coincidence technique equipped with position sensitive detector to study single and multiple ionization of CO_2 and N2O under impact of keV electrons. The PICSs for the ions produced in these collision events are obtained. The precursor specific PICSs values imply the significance of multiple-ionization at the present energy of impact; the contribution of multiple-ionization towards the total fragment ion yield is found to be about 24% and 18% in case of CO_2 and N_2O, respectively.

Acknowledgements

The work was supported by the Department of Science and Technoloy, New Delhi.

References

[1]. Schram B. L., Boerboom A. J. H., and Kistemaker J., (1966), Physica **32**, 185.

[2]. Ma C., Bruce M. R., and Bonham R. A., (1991), Phys. Rev. A **44**, 2921.

[3]. Lindsay B. G. *et al.*, (2004), J. Chem. Phys. **121**, 1350.

[4]. Singh R., Bhatt P., Yadav N., and Shanker R., (2011), Meas. Sci. Technol. **22**, 055901.

[5]. Bhatt P., Singh R., Yadav N., and Shanker R., (2011), Phys. Rev. A **84**, 042701.

[6]. Bhatt P., Singh R., Yadav N., and Shanker R., (2012), Phys. Rev. A **85**, 034702.

[7]. Bhatt P., Singh R., Yadav N., and Shanker R., (2012), Phys. Rev. A **86**, 052708.

ELECTRON IMPACT IONIZATION OF FLUOROMETHANES

S. V. K. Kumar
Tata Institute of Fundamental Research, Homi Bhabha Road
Colaba, Mumbai 400 005

1. INTRODUCTION

Of the many man made gases, halo carbons are used in the industry as etchants and in daily life as refrigerants. Of these Hydro Fluoro Carbons (HFCs) are considered to be relatively environmentally friendly. CH_3F, CH_2F_2, CHF_3 and CF_4 are classified as fluoromethanes. The electron impact scattering and ionization cross section data of these molecules are important to model the plasmas as well as the atmospheric chemistry [1, 2]. Both experimental and theoretical cross sections have been reported for these molecules [3-8]. While the molecular cations CH_3F^+, $CH_2F_2^+$ and CHF_3^+ are stable CF_4^+ is not observable. None of the molecular anions of these four fluoromethanes have been reported. However, both fragment cations and anions have been reported along with the cross sections for their formation. As these molecules are a source of fluorine atoms the cross section for the formation of fragment ions is of importance. Electron impact total and partial ionization cross sections have been measured for these fluoromethanes by many groups. The most recent reports are from the Spanish group [3-5]. As an example the cross section for the formation of CF_2^+ ion from CH_2F_2, CHF_3 and CF_4 reported by the Spanish group of F. Castaño and co-workers along with that of our measurements from CF_4 is shown in Fig 1 below to highlight perceived difference.

It is clear from Fig 1 that there are undulations in the cross section curve plotted as a function of electron energy. However, for measurements are carried out in larger electron energy steps what appears to be a small undulation in the cross section for the formation of CF_2^+ from CF_4, turns out to be a clear peak riding on a rising background when experiments are done in finer energy steps. Such structures are mostly due to resonances.

Ionization cross sections have been calculated for many molecules using the Jain and Khare semi empirical model [9], Binary-Encounter-Bethe (BEB) method [10], SCOP and CSP-ic methods developed by Joshipura and Vinodkumar [11]. These methods are able to compute the ionization cross sections, but they do not address the observed structures. By performing experiments in smaller electron collision energy steps the finer details in the partial ionization cross sections are revealed, which can then be utilized to obtain complete structural information of the molecule.

It is also necessary that theoretical methods include additional factors to the above mentioned methods to reproduce the full experimental curves. It is the purpose of this presentation, using electron impact ionization of CF_4 as an example, to highlight the need to repeat cross section measurements in a detailed manner as well as to improve the theoretical methods to obtain a complete understanding of the electron impact ionization process over a wide energy range.

Figure 1: Experimental cross section for the formation of CF_2^+ from CH_2F_2, CHF_3 and CF_4. Our measured values are shown in the right lowest panel. The other three panels depict the cross sections report by Torres et al.[3-5]

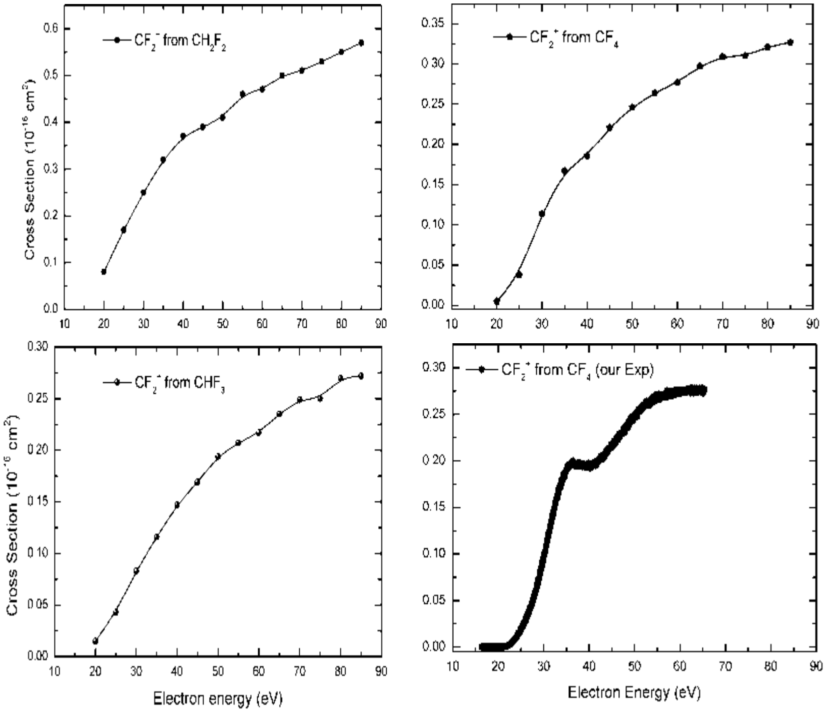

2. EXPERIMENT

We have measured the electron impact partial ionization cross sections of CF_4 using a crossed molecular beam setup with a recently designed Time of Flight Mass Spectrometer (ToFMS). The new design of the linear ToFMS gives nearly field-free interaction region without compromising on the mass resolution. The design addresses problems that would arise in a conventional Wiley-McLaren type of ToFMS i.e. field leakages into the charged particle-molecule interaction region from various components of the mass spectrometer, including that through the high transparency mesh used to obtain evenly distributed electric fields, and complete collection and transportation of the ions produced in the interaction region to the detector, which is essential for high sensitivity and cross section measurements. This ToFMS works over a wide range of masses from H^+ to a few hundred Daltons and would be the most suitable for low energy charged particle-molecule interaction studies. Schematic view of the experimental setup is shown in Fig 2.

Figure 2. The electron impact ionization cross section measuring setup. 1- Electron gun, 2- Electron beam, 3- Pusher (+250 V), 4- Faraday Cup, 5- Puller, 6- Spacer (Insulator), 7- Flight tube (-860 V), 8- Channel electron multiplier, 9- Channel electron multipliershielding box (Earth Potential). Dimensions of the Time – of – Flight Mass Spectrometer - Z-1 = 10 mm., Z-2 = 2 mm., Z-3 = 8 mm., Z-4 =160 mm., Z-5 =7 mm.

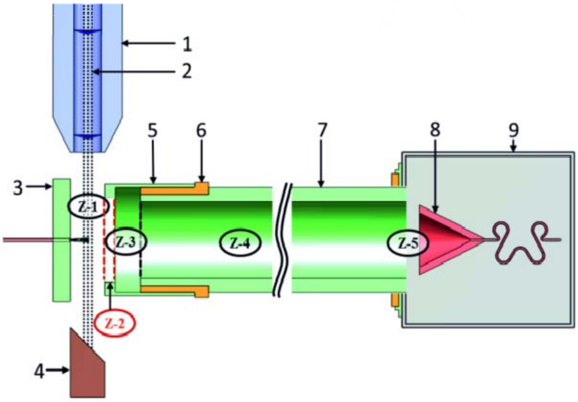

The experiments were carried out in crossed beam geometry and under single collision conditions. The electrons are produced by a Pierce type electron gun and guided into the interaction region and further into the Faraday cup, by a low-magnetic field ~50G produced by a pair of Helmholtz coils (which are ultra-high-vacuum compatible). The electrons interact with an effusive beam of CF_4 (Alfa gas with certified 99.995% purity used without any further purification). The uninteracted electrons reach the Faraday cup placed on the other side of the interaction region. The above setup is housed in a vacuum chamber, which is operated at a base pressure of 1×10^{-7} Torr. The cross sections measured are put on an absolute scale using the relative pressure technique [12] with the cross section values for argon [13] used as the standard reference. Experiments have been carried out at energy intervals of 0.1eV over the range 10 to 65eV.

3. RESULT AND DISCUSSION

The cross section measurements indicate (see Fig 1) that structures are present in the cross section function. Structures are observed for both atoms (e.g. Xe) and even small molecules (e.g. CS_2) [10]. However, not much attention has been paid to address the science behind the structures probably due the importance of the cross section numbers which is more relevant for modelling. One of the reasons for the observation of such structures is due to the excitation of one of the core electrons to one of the lowest unoccupied empty orbitals and the incoming electron getting trapped in the potential barrier. If this resonance is energetically in the ionization continuum of the neutral it could decay via ionization / dissociative ionization, other than resonant scattering. The current Binary-Encounter-Bethe (BEB) and, SCOP and CSP-ic computation methodologies largely concentrate on obtaining the best compatible cross section numbers and the overall shape of the curve. To bring out the complete picture of the ionization process it is necessary that resonance interaction terms are also included in future theories that calculate ionization cross sections.

For the resonance observed in the CF_2^+ channel for ionization from CF_4 we put forth four resonance states as possibilities: the valence core electron $2t_2$ being promoted to the LUMO $5a_1$ orbital with incoming electron attaching to the same orbital resulting in a $^2T_2$ resonance, which lies in the continuum of CF_4^+, which then very likely dissociates to $CF_2^+ + 2F$. The other possible resonance states could be due the promotion of the valence core electron $4a_1$ to the $5t_2$ orbital and the incoming electron also filling either the $5t_2$ orbital or the $5a_1$ orbital resulting in A_1 or T_2 resonance states respectively.

4. CONCLUSION

It has been shown that the cross section data on electron impact ionization of fluoromethanes available in the literature are spaced far apart and hence misses the structures that would be relevant to obtain a complete understanding of the ionization process. Theoretical methods need to incorporate terms that will reflect the observed resonances in the partial ionization cross sections.

References

1. Christophorou L. G., Olthoff J. K., (1999), *Electron Interactions With Plasma Processing Gases: An Update for CF_4, CHF_3, C_2F_6, and C_3F_8*. Journal of Physical and Chemical Reference Data. **28**, 967.
2. Mason N. J., (2009), *The status of the database for plasma processing*. Journal of Physics D: Applied Physics. **42**, 194003.
3. Torres I., Martínez R., Sánchez Rayo M. N. and Castaño F., (2000), *Electron impact dissociative ionization of the CH_2F_2 molecule: cross sections, appearance potentials, nascent kinetic energy distributions and dissociation pathways*. Journal of Physics B: Atomic, Molecular and Optical Physics. **33**, 16.
4. Torres I., Martínez R. and Castaño F., (2002), *Electron-impact dissociative ionization of fluoromethanes CHF_3 and CF_4*. Journal of Physics B: Atomic, Molecular and Optical Physics. **35**, 2423.
5. Torres I., Martínez R. and Castaño F., (2002), *Electron-impact dissociative ionization of the CH_3F molecule*. Journal of Physics B: Atomic, Molecular and Optical Physics. **35**, 11.
6. Torres I., Martínez R., Sánchez Rayo M. N. and Castaño F., (2001), *Evaluation of the computational methods for electron-impact total ionization cross sections: Fluoromethanes as benchmarks*. The Journal of Chemical Physics. **115**, 4041.
7. Sieglaff D. R., Rejoub R., Lindsay B. G. and Stebbings R. F., (2001), *Absolute partial cross sections for electron-impact ionization of CF_4 from threshold to 1000 eV*. Journal of Physics B: Atomic, Molecular and Optical Physics. **34**, 799.
8. Fiegele T., Hanel G., Torres I., Lezius M., Märk T. D., (2000) *Threshold electron impact ionization of carbon tetrafluoride, trifluoromethane, methane and propane*. Journal of Physics B: Atomic, Molecular and Optical Physics. **33**, 4263.

9. Jain D. K. and Khare S. P., (1976) *Ionizing collisions of electrons with CO_2, CO, H_2O, CH_4 and NH_3*. Journal of Physics B: Atomic and Molecular Physics. **9**, 1429.
10. Kim Y. K., Hwang W., Weinberger N. M., Ali M. A. and Rudd M. E. (1997) *Electron-impact ionization cross sections of atmospheric molecules*. The Journal of Chemical Physics. **106**, 1026.
11. Joshipura K. N., Vinodkumar M., Limbachiya C. G., and Antony B. K., (2004), *Calculated total cross sections of electron-impact ionization and excitations in tetrahedral (XY_4) and SF_6 molecules*. Physical Review A. **69**, 022705.
12. Krishnakumar E., Kumar S. V. K., Rangwala S. A., and Mitra S. K., (1997), *Dissociative-attachment cross sections for excited and ground electronic states of SO_2.* Physical Review A. **56**, 1945.
13. Straub H. C., Renault P., Lindsay B. G., Smith K. A., Stebbings R. F., *Absolute partial and total cross sections for electron-impact ionization of argon from threshold to 1000 eV*. (1995) Physical Review A. **52**, 1115.

THEORETICAL STUDY OF TOTAL IONIZATION CROSS SECTIONS FOR DNA/ RNA MOLECULE ON ELECTRON IMPACT

Mayuri Barot, Avani Barot, Chetan Limbachiya[1]
and Minaxi Vinodkumar
V. P. & R. P. T. P. Science College, V. V. Nagar-388120, Gujarat
[1]P. S. Science College, Kadi, Gujarat

1. INTRODUCTION

Biomolecules, in particular DNA/RNA components are very sensitive to high energy radiation damage which can occur due to primary, secondary or reactive processes [3]. In irradiated cells, the single and multiple ionization produces large number of secondary electrons that carry large fraction of the energy of the impinging radiation. The study of total ionization cross sections play an important role in investigating the lesion causing effects of electrons on DNA/RNA molecular components. In present work, we report the total ionization cross sections for all components of the DNA and RNA molecules viz. adenine, guanine, thymine, cytosine, uracil and backbone units (sugar phosphate) from threshold of the target to 2 keV. For computing total inelastic cross sections, we employed well established Spherical Complex Optical Potential (SCOP) [15-16] formalism and extracted total ionization cross sections using the Complex Scattering Potential – ionization contribution (CSP-ic) method [17-20].

2. THEORY

The absorption potential takes care of loss of flux into all allowed inelastic channels. For this we have used model potential of Staszewska et al. [24] which is non-empirical, quasifree, Pauli-blocking and dynamic in nature. The full form of model potential is represented by,

$$V_{abs}(r,E_i) = -\rho(r)\sqrt{\frac{T_{loc}}{2}} \times \left(\frac{8\pi}{10k_F^3 E_i}\right) \times \theta(p^2 - k_F^2 - 2\Delta)\cdot(A_1 + A_2 + A_3) \tag{1}$$

And

$$T_{loc} = E_i - (V_{st} + V_{ex}) \tag{2}$$

After generating the full complex optical potential for a given electron molecule system, we solve the Schrödinger equation numerically with Numerov method using partial wave analysis. Using these partial waves the complex phase shifts are obtained which are key ingredients to find the relevant cross sections. The phase shifts contains all the information regarding the scattering event. Using these complex phase shifts we evaluate total inelastic cross sections. The two vital components of total inelastic cross sections are given by,

$$Q_{inel}\left(E_i\right) = \sum Q_{exc}\left(E_i\right) + Q_{ion}\left(E_i\right) \tag{3}$$

Total ionization cross section may be estimated from total inelastic cross section by defining an energy dependent ratio $R(E_i)$ given by,

$$R\left(E_i\right) = \frac{Q_{ion}\left(E_i\right)}{Q_{inel}\left(E_i\right)} \tag{4}$$

such that, $0 < R \leq 1$.

As total ionization cross section is a continuous function of energy, we can express this ratio also as a continuous function of energy for $E_i > I$, used in earlier studies as [4-7].

$$R\left(E_i\right) = 1 - f\left(U\right) = 1 - C_1\left(\frac{C_2}{U+a} + \frac{\ln\left(U\right)}{U}\right) \tag{5}$$

here, U is the dimensionless variable defined by, $U = \dfrac{E_i}{I}$.

The dimensionless parameters C_1, C_2 and ‘a’ involved in the above equation are deduced by imposing the three conditions on the ratio as discussed below.

$$R(E_i)\begin{cases} = 0 \ \ for\ E_i \leq I \\ = R_p \ \ for\ E_i = E_p \\ \cong 1 \ \ for\ E_i >> E_p \end{cases} \tag{6}$$

where E_p is the peak of inelastic cross section.

The first condition is an exact condition wherein it states that no ionization process is possible below the ionization threshold of the target. According to the last condition, ionization contribution is almost equal to inelastic contribution at very high (~ 10 E_p) energies. R_P is the value of R at $E_i = E_p$, and it was observed that at the peak of inelastic cross section the contribution for ionization is about 70 to 80%. Here we have taken R_p as 0.7 for all the targets studied here.

3. RESULT AND DISCUSSION

Present work reports total ionization cross sections computed using CSP-ic method.

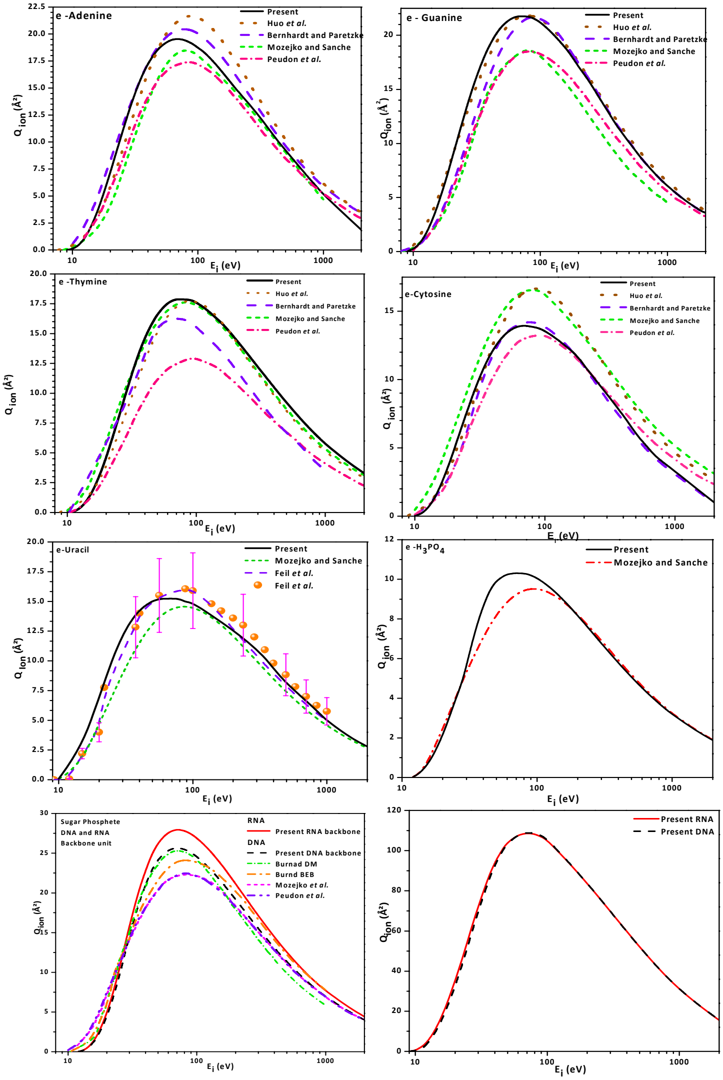

Figure: 1. (Color online) Total ionization cross sections for DNA/RNA Molecules.

Figs. 1(a), 1(b), 1(c) and 1(d): Electron impact total ionization cross sections for Adenine, Guanine, Thymine and Cytosine. Solid line: Present results; Dotted line: Huo et al. [12], Dash line: Bernhardt and Paretzke [11]; Short Dash line: Mozejko and Sanche [8]; Dash Dot line: Peudon et al. [13]. Fig. 1(e): Electron impact total cross sections for Uracil. Solid line: Present results; Short Dash line: Mozejko and Sanche [8]; Dash line: Feil et al. [6] and Sold Sphers: Feil et al. [6]. Fig. 1(f): Electron impact total cross section for H_3PO_4. Solid line: Present results. Dash Dot line: Mozejko and Sanche [8]. Fig. 1(g): Electron impact total ionization cross sections for sugar phosphate backbone for DNA and RNA Backbone unit. Solid line: Present RNA Backbone unit and Dash line: Present DNA Backbone unit; Short Dash-Dot line: Burnad (DM); Dash-Dot line: Burnd BEB; Short Dash line: Mozejko et al. [9] and Dash-Dot-Dot line: Peudon et al. [13] and Fig. 1(h): Total ionization cross sections for DNA (Short Dash line) and RNA (Dash-Dot line) molecules.

Fig. 1(a) shows comparison of present total ionization cross section for e –Adenine scattering with available theoretical results. No experimental ionization data are available for comparison to the best of our knowledge. Huo et al. [12], Mozejko and Sanche [8] and Peudon et al. [13] have employed BEB formalism. There are variations in their results as BEB is parameter dependent formalism. The present results are found to be in general agreement with all other data and are in best accord with the results of Bernhardt and Partezke [11], who employed DM formalism. The results of Huo et al. [12] are in very good agreement with present results up to 70 eV, but at the peak they are higher compared to all data presented here and beyond 200 eV again they are in good accord with the present results. The results of Mozejko and Sanche [8] are lower compared to all results presented here up to the peak and beyond it they are in very good agreement with the present results. The results of Peudon et al. [11] are lower compared to all the results.

Fig. 1(b) shows the comparison of present total ionization cross sections for e –Guanine scattering with the available comparisons. Results of Huo et al. [12] are in very good agreement with present results throughout the energy range, the results of Bernhardt and Paretzke [11] are lower compared to present results up to the peak but beyond it they are in excellent agreement with the present results. The results of Mozejko and Sanche [8] and Peudon et al. [13] are similar up to the peak and are lower by 14% at the peak compared to the present results. Again in this case the difference in the results obtained using BEB formalism [12, 13] is 14% near the peak.

A comparison of present total ionization cross sections for e –Thymine scatterings are shown along with other theoretical estimates in Fig.1(c). The BEB data of Mozejko and Sanche [8] and Huo et al. [12] are in excellent agreement with the present data throughout the impact energy range. The BEB results of Peudon et al. [13] are the lowest compared to all the results at the peak and the variations among the BEB results of [8,12,13] are about 28%. The DM results of Bernhardt and Paretzke [11] are in agreement with the present results up to 50 eV beyond which they suddenly drop and are lower compared to the present results.

Fig. 1(d) shows comparison of present total ionization cross sections for e –Cytosine scattering with the available results. The results of Bernhardt and Paretzke [11] obtained using DM formalism are in very good accord with present results throughout the impact energy range. The results of Peudon et al. [13] are in good agreement with present data throughout the energy range except near the peak where they are lower compared to present results. The results of Huo et al. [12] obtained using BEB formalism are in good agreement with the present results up to 30 eV, above which they are higher compared to present results. The results of Mozejko and Sanche [8] are higher compared to the present results throughout the energy range. The results obtained using BEB formalism [8,11,13] differs by 20% near the peak.

In order to report the results of all the components of RNA molecule, we show in Fig. 1(e) our recent results of total ionization cross section for e –Uracil scattering [14] with available results. This is the only component of RNA molecule for which an experimental work is reported by Feil et al. [6] and our results are in good accord with this measurements and with their theoretical data [6,8] throughout the energy range. However, the present results are lower than the results of Mozejko and Sanche [8] up to 100 eV then after they match well.

The comparison of present total ionization cross sections for e –H_3PO_4 scattering is shown in Fig. 1(f) along with the lone theoretical results of Mozejko and Sanche [8]. The present results of total ionization cross sections finds excellent agreement with the results of Mozejko and Sanche [8] for complete energy range except between 30 to 100 eV where present results are slightly higher. There is no other theoretical or experimental data for ionization cross sections of phosphoric acid to the best of our knowledge.

Fig. 1(g) represents the comparison of present total ionization cross sections for sugar phosphate backbone for DNA and RNA molecule. The total ionization cross section for sugar phosphate backbone of RNA molecule is presented for the first time. The total ionization cross section for sugar phosphate backbone for DNA molecule is calculated by Bernhardt and Paretzke [11], Mozejko et al. [9] and Peudon et al. [13]. These authors [9,11,13] have used BEB formalism while Bernhardt and Paretzke [11] used both BEB and DM formalism for computation of total ionization cross section. Present data is in excellent agreement with the DM data of Bernhardt and Paretzke [11] throughout the impact energy range. Present data is also in good accord with the BEB data of Mozejko et al. [9], Peudon et al. and Bernhardt and Paretzke [11] for the complete energy range except a slight variation near the peak region. The present peak energy coincides with all the data presented here. The structural difference between RNA and DNA backbone is that RNA backbone has additional O atom compared to DNA. Hence it is expected that total ionization cross section for RNA backbone should be higher compared to DNA backbone which is reflected in the curve.

Fig. 1(h) represents total ionization cross sections for the composite DNA and RNA structure. The composite DNA structure includes Adenine, Guanine, Cytosine, Thymine, Phosphoric acid and sugar phosphate backbone. The composite RNA structure includes Adenine, Guanine, Cytosine, Uracil, Phosphoric acid and sugar phosphate backbone. No comparison either theoretical or experimental is available to the best of our knowledge. It is seen that when electron interactions are considered with the DNA or RNA the position of their peak and the magnitude of ionization are nearly same. By this we infer that as far as electron driven processes such as lesions caused by secondary electrons generated through irradiation are concerned, both DNA and RNA structures will be affected identically.

CONCLUSION

Present work reports comprehensive study of electron impact total ionization cross sections for all the components of DNA and RNA molecules along with sugar phosphate backbone unit. The overall shape and strength of ionization cross section is nicely matched with the previous data for all the targets studied here. The study reflects three facts; the ionization cross section increases with increase in geometrical size of the target, the peak of ionization cross section is largely governed by the ionization threshold of the target and for electron driven effects, the DNA and RNA systems are identically affected. Present study has given us the confidence in our calculation and hence we are convinced that present method can reproduce reliable cross section data for complex targets with adequate accuracy and speed. Also, we hope that our effort will encourage experimentalists to perform measurements of these important targets.

References

1. L. Sanche, "*Radical and Radical Ion Reactivity in Nucleic Acid Chemistry*" (Greenberg, M. ed.), John Wiley & Sons, Inc., (2009) pp. 239 – 293.
2. A. Jain, Phys. Rev. A 34 (1986) 3707.
3. A. Jain and K. L. Baluja, Phys. Rev. A 45 (1992) 202.
4. M. Vinodkumar, K. Korot, and H. Bhutadia, Int. J. Mass Spectrom. 294 (2010) 54.
5. K. N. Joshipura, M. Vinodkumar, C. G. Limbachiya, and B. Antony, Phys. Rev. A 69 (2004) 022705.
6. M. Vinodkumar, K. N. Joshipura, C. Limbachiya, and N. J. Mason, Phys. Rev. A 76 (2006) 022721.
7. M. Vinodkumar, C. G. Limbachiya, K. Korot, and K. N. Joshipura, Euro. Phys. J. D 48 (2008) 333
8. P. Mozejko and L. Sanche, Radiation Physics and Chemistry, 73 (2005) 77.
9. P. Mozejko, A. Domaracka, E. Ptasinska-Denga, and C. Szmytkowski, Chemical Physics Letters, 429 (2006) 378.
10. G. Staszewska, D. W. Schwenke, D. Thirumalai, D. G. Truhlar, Phys. Rev. A 28 (1983) 2740.
11. Ph. Bernhardt and H. G. Paretzke, Int. J. Mass Spectrom. 223–224 (2003) 599.
12. W. M. Huo, C. E. Dateo, and G. D. Fletcher, NASA Technical Report; NAS-06-009 (2006).
13. A. Peudon, S. Edel, and M. Terrissol, Radiation Protection Dosimetry doi:10.1093/rpd/ncl452 (2006).
14. S. Feil, K. Gluch, S. Matt- Leubner, P. Scheier, J. Limtrakul, M. Probst, H. Deutsch, K. Becker, A. Stamatovic and T. D. Mark, J. Phys. B: At. Mol. Phys. 37 (2004) 3013

IONIZATION OF MOLECULES BY ELECTRON COLLISION

Neeraj Kumar, Rajbeer Singh and Satyendra Pal
Department of Physics, M.M.H. College, Ghaziabad-201001 (UP)

1. INTRODUCTION

Ionization of molecules is an important process in a wide range of environments and applications. Data relating to such processes form an important input into the understanding and modelling of such varied situations as the physics and chemistry of planetary atmospheres, electrical discharges, radiation damage in biological materials and plasma waste disposal techniques [1].

Recently, we have introduced a revisited Jain-Khare semi-empirical formulation for the calculation of ionization cross sections for C_{60} and SiF_4 molecules in the energy range from ionization threshold to 1000 eV which yielded results in satisfactory agreement with available experimental and theoretical data [2-3]. Subsequently, we have extended and generalized the same formulation for the evaluation of ionization cross sections corresponding to molecular clusters as a testimony of CO_2 viz. $(CO_2)_{240}$ and $(CO_2)_{1700}$ where the experimental and/or the theoretical data is available for comparison of the present results. The necessity to rely on this approach for the calculation of ionization cross sections for clusters/ fullerenes arises that it provides results in reasonably good agreement with experimentally measured cross sections, within experimental error bars, for several molecules of variety [4-5].

2. THEORY

The present calculations are carried out using the modified semi-empirical formalism developed by Khare and co-workers (see the discussion in Refs. 2-5). In brief, the ionization cross sections corresponding to the formation of the *i*th type of ion in the ionization of a molecule by the incident electron of energy *E* is given by

$$Q_i(E) = \frac{4\pi a_0^2 R}{E}\left[\frac{E}{(E-l_i)\left(1+\frac{l_i}{E}\right)}\left(M_i^2(E)-\frac{R}{E}S_i(E)\right)\ln\left[1+C_i(E-l_i)\right]\right.$$
$$\left.+\frac{R\,(E-l_i)}{E}S_i\int_0^{(E-l_i)}\frac{1}{(\varepsilon^3+\varepsilon^3)}\left(\varepsilon-\frac{\varepsilon^2}{(E-\varepsilon)}+\frac{\varepsilon^3}{(E-\varepsilon)^2}\right)d\varepsilon\right]$$

The symbols used in this equation have their usual meanings [3]. The theoretical description for calculations is also elucidated in our recent publications.

3. RESULT AND DISCUSSION

Fig. 1 shows the comparison of our total ionization cross section profiles for C_{60} fullerene with the experimental [6-9] and the theoretical data [10]. Our results underestimate the total cross sections measured by Foltin et al. [7] but lie within the experimental uncertainties. Note that the DM formalism calculations [11] and additive calculations [10] for total ionization cross sections (not shown) are much higher than our calculations and other data-sets [7,9]. Conceptually, the DM calculation relies on the additive rule, which builds the total ionization cross section by adding up contributions from the different C_{60} orbitals. This approach might not be applicable to a case-like structure such as C_{60}. It could be argued, for instance, that for the incoming projectile only about half of the 60 carbon atoms that constitute the C_{60} case are contributing to the cross sectional area as seen by the projectile (see for instance Ref. 7 for detailed discussion).

Figure 1: Total ionization cross section profiles (in the units of 10^{-16} cm^2) for the electron impact ionization on C_{60} (designated with solid lines) in comparison with the experimental data designated by: X– Foltin et al. [7], ◊- Tarnovski et al. [8] and O- Itoh et al. [9] and the theoretical data designated by: Δ- Deutsch et al. [10].

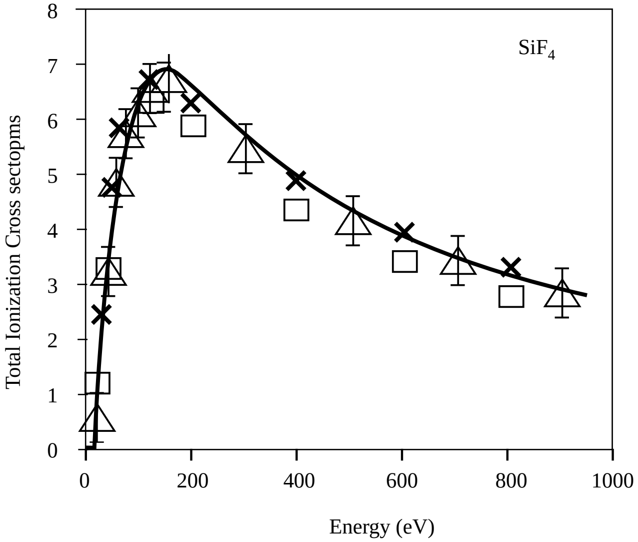

Figure 2 shows a good agreement of the total ionization cross section for SiF_4 molecule with the only available experimental data of Basner et al [12] and the theoretical cross section data sets of Kim et al [13] and Joshipura et al [14] in the complete energy range covered in the calculations.

Fig. 3 shows the comparison of our total ionization cross section profile for $(CO_2)_{240}$ and $(CO_2)_{1700}$ clusters with experimental [15] and theoretical data [16]. It is interesting to note that the cross sections corresponding to the clusters are in good agreement with the only experimental data [15] and the theoretical calculations [16].

At peak, our results for $(CO_2)_{240}$ and $(CO_2)_{1700}$ are about 20% and 10%, respectively higher than the experimental data (the data is accomplished with uncertainty of 25%) [15]. On the other hand, the theoretical data based on the additive rule show the similar trend as the experimental data. In their theoretical calculations, Deutsch et al. employed the experimental cross sections measured by Rapp et al. [17].

Figure 2: Total ionization cross sections (in the units of 10^{-16} cm^2) for electron impact ionization of SiF_4 (designated by solid line) in comparison with the available experimental data designated by, △- Basner et al [12] with error bars and theoretical data sets by □ – Kim et al [13] and ×– Joshipura et al [14].

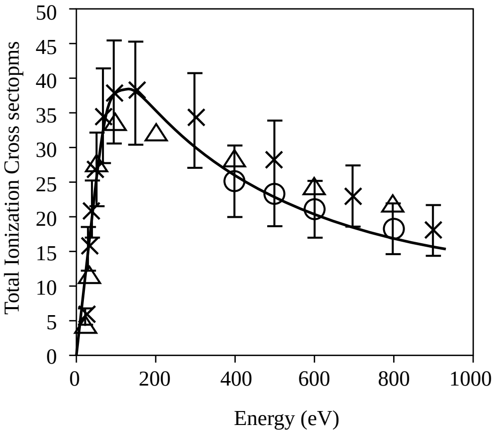

Figure 3: Total ionization cross section profiles corresponding the $(CO_2)_{240}$ and $(CO_2)_{1700}$ clusters by electron impact ionization (designated with solid lines) in comparison with the experimental data designated by: ▲ – Vostrikov et al. [15] and the theoretical data designated by: ♦- Deutsch et al. [16].

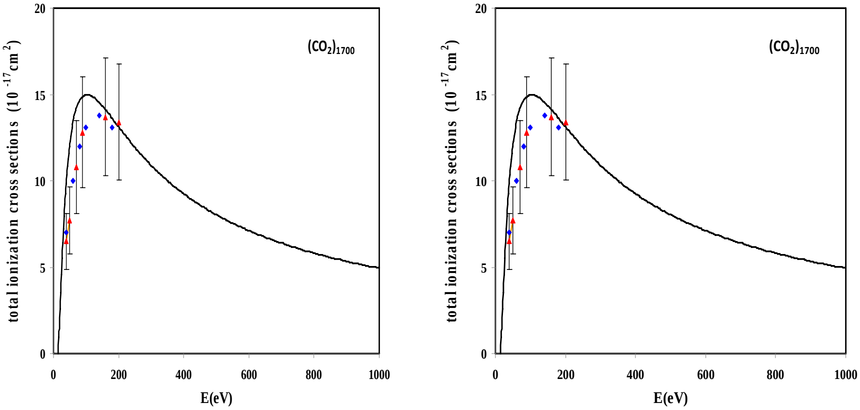

4. CONCLUSION

The accuracy of present results provides a justification of the use of the present formalism for the calculation of cross sections for these molecules/clusters, especially, in the low energy regime. The basis of these accuracies of results provides the framework to develop predictive capabilities that allow us to evaluate the ionization cross sections for other molecules/clusters where the experimental and theoretical data are scarcely available.

Acknowledgements

R. Singh is thankful to the Department of Science and Technology, Government of India for financial support with Grant No. PS/008/2011(SERC).

References

[1] Basner R., Becker K., Deutsch H. and Schmidt M., (2000), Inokuti M. and Becker K. (Eds.); *Adv At Mol Opt Phys: Fundamentals of Plasma Chemistry* **43,** 147; Academic Press, New York.

[2] Kumar N. and Pal S., (2009), *Evaluation of direct ionization cross sections for* C_{60} *by electron interaction* J. Phys. (Conf. Ser.) **163** 012029.

[3] Kumar N., Kumar R. and Pal S., (2012), *Electron Impact Ionization Cross Sections and Rate Coefficients for Molecules,* Adv. App. Math. Comp. Phy., World Education Publishers, Delhi, 160.

[4] Pal S., (2008), *Differential and partial ionization cross sections for electron impact ionization of plasma processing molecules:* CF_4 *and* PF_5, Phys. Scr. **77,** 055304.

[5] Pal S., Kumar N. and Anshu, (2009), *Electron-Collision-Induced Dissociative Ionization Cross Sections for Silane,* Adv. Phys. Chem. **2009** 309292.

[6] Matt S., Dünser B., Lezius M., Deutsch H., Becker K., Stamatovic A., Scheier P. and Märk T. D., (1996), *Absolute partial and total cross-section functions for the electron impact ionization of* C_{60} *and* C_{70}, J. Chem. Phys. **105,** 1880.

[7] Foltin V., Foltin M., Matt S., Scheier P., Becker K., Deutsch H. and Märk T. D., (1998), *Electron impact ionization of* C_{60} *revisited: corrected absolute cross section functions,* Chem. Phys. Lett. **289,** 181 and references therein.

[8] Tarnovski V., Kurunczi P., Matt S., Märk T. D., Deutsch H. and Becker K., (1998) *Absolute cross section for the formation of* C_{60}^+ *ions produced by electron impact on* C_{60}, J. Phys. B **31,** 3043.

[9] Itoh A., Tsuchida H., Miyabe K., Majima T., Imanishi N., (1999), *Ionization cross sections of* C_{60} *by fast electron impact,* J. Phys. B **32,** 277.

[10] Deutsch H., Scheier P., Becker K. and Märk T. D., (2003), *A semi-empirical concept for the calculation of electron-impact ionization cross-sections of neutral and ionized fullerenes,* Int. J. Mass Spectrom. **223-224** 1.

[11] Deutsch H., Becker K., Pittner J., Bonacic- Koutecky V., Matt S. and Märk T. D. (1996), *Semiclassical calculations of the cross section for electron-impact ionization of* C_{60}, J. Phys. B **29,** 5175.

[12] Basner R., Schmidt M., Denisov E., Becker K. and Deutsch H., (2001), *Absolute total and partial cross sections for the electron impact ionization of tetrafluorosilane* (SiF_4) J. Chem. Phys. **114,** 1170.

[13] Kim Y. -K. and Irikura K. K., (2000), *Proc. 2nd Int. Conf. on Atom. Molec. Data and Their Applications,* ed. by K.A. Berrington and K.L. Bell, **543,** 220, AIP Conf. Proc. (AIP, New York, NY).

[14] Joshipura K. N., Vinodkumar M., Antony B. K. and Mason N. J., (2003), *Theoretical total ionization cross-sections of* CH_x, CF_x, SiH_x, SiF_x ($x = 1\text{-}4$) *and* CCl_4 *targets by electron impact,* Eur. Phys. J. D **23,** 81.

[15] Vostrikov A. A., Dubov D. Y. and Predtechensky M. R., (1986), *Electron clusters interaction*, Preprint No. **150–86** 49 Inst. Thermophys. Sib. Br. of USSR Academy, Novosibirsk (in Russian).

[16] Deutsch H., Becker K. and Märk T. D., (1995), *A semi-empirical method to calculate cross-sections for the electron-impact ionization of clusters* Int. J. Mass Spectrom. Ion. Processes **144** L9.

[17] Rapp D. and Englander-Golden P., (1965), *Total Cross Sections for Ionization and Attachment in Gases by Electron Impact. I. Positive Ionization*, J. Chem. Phys., **43** 1464.

IONIZATION CROSS SECTIONS AND RATE COEFFICIENTS FOR α-TETRA HYDRO FURFURYL ALCOHOL

Neeraj Kumar, Rajbeer Singh and Satyendra Pal
Department of Physics, M. M. H. College, Ghaziabad-201001 (UP)

1. INTRODUCTION

α-tetrahydrofurfuryl alcohol (THFA; $C_5H_{10}O_2$) is an aromatic compound having the molecular structure similar to that of 2-deoxy-D-ribose (deoxyribose) [1]. This molecule has attracted enormous interest in the field of research because its electron charge cloud possesses a quite significant spatial extent (dipole polarizability, α = 70.18 au [2]) and has a relatively strong permanent dipole moment (μ ~2D [3]).

In the present work, we have extended and generalized the modified Jain-Khare semi-empirical formalism for the evaluation of the total ionization cross sections corresponding to the formation of the cations in the electron impact ionization of molecules [4] to the electron impact ionization of α-tetrahydrofurfuryl alcohol (THFA; $C_5H_{10}O_2$).

2. THEORY

The present calculations are carried out using the modified semi-empirical formalism developed by Khare and co-workers [4]. In brief, the ionization cross sections corresponding to the formation of the i^{th} type of ion in the ionization of a molecule by the incident electron of energy E is given by,

$$Q_i(E)=\frac{4\pi a_0^2 R}{E}\left[\frac{E}{(E-I_i)\left(1+\frac{I_i}{E}\right)}\left(M_i^2(E)-\frac{R}{E}S_i(E)\right)\ln[1+C_i(E-I_i)]+\frac{R(E-I_i)}{E}S_i\int_0^{(E-I_i)}\frac{1}{(\varepsilon^3+\varepsilon^3)}\left(\varepsilon-\frac{\varepsilon^2}{(E-\varepsilon)}+\frac{\varepsilon^3}{(E-\varepsilon)^2}\right)d\varepsilon\right]$$

where the various variables used have their usual meanings. An attempt has also been made to evaluate the *ionization rate coefficients* for the considered molecules as a function of temperature using Boltzmann Energy Distributions

$$R(E)=\frac{1}{k_B T}\left(\frac{8}{\pi\mu k_B T}\right)^{\frac{1}{2}}\int_{I_i}^{E} E Q_i(E) e^{\left(-\frac{8}{k_B T}\right)} dE$$

Where k_B, T and μ are the Botlzmann constant, absolute temperature and mass of the electron, respectively [5].

3. RESULT AND DISCUSSION

Fig. 1 shows the comparison of our total ionization cross section profiles for α-tetra hydro furfuryl alcohol ($C_5H_{10}O_2$) with the theoretical data derived by Mozejko et. al using the Binary-Encounter-Bethe (BEB) model [6]. Our results for total cross section reveal a good agreement with the theoretical data [6].

Figure 1. Total ionization cross section (in units of 10^{-16} cm^2) for α-tetra hydro furfuryl alcohol ($C_5H_{10}O_2$) in comparison with the theoretical data designated by : (▲-)Mozejko et al [6].

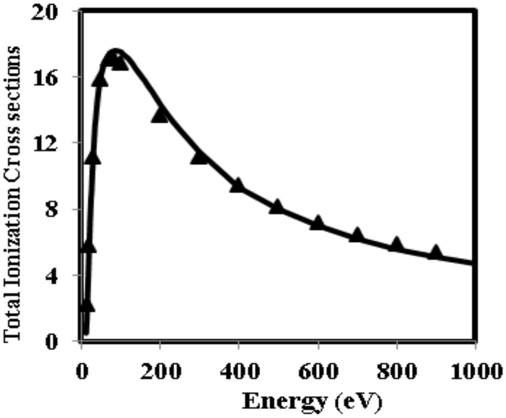

Figure 2. Ionization rate coefficients (in units of cm^3/sec) as a function of electron temperature/energy for α-tetra hydro furfuryl alcohol ($C_5H_{10}O_2$).

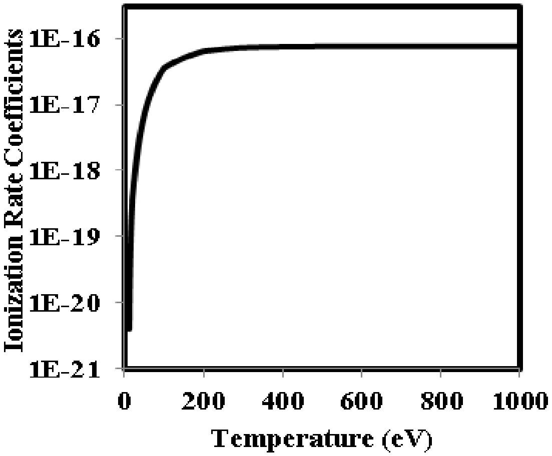

The ionization rate coefficients as a function of electron temperature shown in Fig. 2, have been evaluated using the calculated cross sections and Maxwell-Boltzmann distribution of the electrons energy.

References

[1] Milosavljevic A. R., Blanco F., Sevi´c D., Garcia G., and Marinkovic B. P., (2006), *Elastic scattering of electrons from tetrahydrofurfuryl alcohol,* Eur. Phy. J. D **40** 107.

[2] Szmytkowski Cz. and Ptasinska-Denga E., (2011), *Total electron-scattering cross section measurements for tetrahydropyran, $(CH_2)_5O$, molecules.* J. Phys. B: At. Mol. Opt. Phys. **44,** 015203.

[3] Mozejko P., Domaracka A., Ptasinska-Denga E., and Szmytkowski Cz., (2006), *Total cross-section measurements for electron collisions with α-tetrahydrofurfuryl alcohol ($C_5H_{10}O_2$).* Chem. Phys. Lett. **429,** 378.

[4] Kumar N. and Pal S., (2009), *Evaluation of direct ionization cross sections for C_{60} by electron interaction.* J. Phys. (Conf. Ser.) **163,** 012029.

[5] Steinfeld J. I., Francisco J. S., and Hase W. L., (1989), *Chemical Kinetics and Dynamics,* Chap. **6**, Prentic Hall Inc, New Jersey.

[6] Mozejko P. and Sanche L., (2005), *Cross sections for electron scattering from selected components of DNA and RNA.* Rad. Phys. Chem. **73,** 77.

[7] *Milosavljevic A. R., Blanco F., Sevi´c D., Garcia G., and Marinkovic B. P., (2006), Elastic scattering of electrons from tetrahydrofurfuryl alcohol, Eur. Phy. J. D 40 107.*

[8] *Szmytkowski Cz. and Ptasinska-Denga E., (2011), Total electron-scattering cross section measurements for tetrahydropyran, (CH2)5O, molecules. J. Phys. B: At. Mol. Opt. Phys. 44, 015203.*

[9] *Mozejko P., Domaracka A., Ptasinska-Denga E., and Szmytkowski Cz., (2006),* Total cross-section measurements for electron collisions with α-tetrahydrofurfuryl alcohol (C5H10O2). *Chem. Phys. Lett. 429, 378.*

[10] *Kumar N. and Pal S., (2009), Evaluation of direct ionization cross sections for C60 by electron interaction. J. Phys. (Conf. Ser.) 163, 012029.*

[11] *Steinfeld J. I., Francisco J. S., and Hase W. L., (1989), Chemical Kinetics and Dynamics, Chap. 6, Prentic Hall Inc, New Jersey.*

[12] *Mozejko P. and Sanche L., (2005), Cross sections for electron scattering from selected components of DNA and RNA. Rad. Phys. Chem. 73, 77.*

LOW ENERGY PHOTOIONIZATION OF XE 5S SUBSHELL

Aarthi Ganesan[1], Sudha Deshmukh[1], Gagan B. Pradhan[2], V. Radojevic[3], S.T. Manson[4] and P.C. Deshmukh[5]
[1]Department of Physics, CPGS, Jain University, Bangalore, India
[2]Department of Chemistry, University of Neveda, Las Vegas, US
[3]Department of Physics, Institute of Physics, Pregrevica, Beograd-Zemun, Serbia
[4]Department of Physics and Astronomy, Georgia State University, Atlanta, USA
[5]Department of Physics, IIT Madras, India

Abstract

We report the photoionization cross section and angular distribution of Xe 5s photoelectrons using Relativistic Random Phase Approximation *with* Relaxation. Relaxation effects have been found to move the Cooper minimum in the 5s to continuum *p* channels closer to the threshold.

1. INTRODUCTION

Study of the photoionization process is important to understand many body electron correlation effects in a quantum system. The process involves probing an atomic target such that photoelectrons are ejected into the continuum leaving the system ionized. An examination of the Cooper minima provides important insights in correlation and relativistic effects. At certain photon energies, the photoionization matrix element goes through a zero causing the cross section also to go through a zero, which however is often only a small non-zero minimum when the zeros in different channels do not occur at the same energy. The minimum in the cross-section is commonly known as the Cooper minimum [1]; its energy-dependence is strongly influenced by interchannel coupling and relativistic effects [2]. The presence of the Cooper minima in the region above 5s threshold using Relativistic Random Phase approximation [4] for Xe has been reported earlier [3, 4, 5]. In Ref.5, it was concluded that the discrepancy between the predictions of the RRPA and experiment were not due to the truncation of the RRPA, but due to the exclusion of non-RPA correlations. In the present study, the modified version of the relativistic random phase approximation which includes relaxation effects [6] is used to examine if the non-RPA correlations taken into account by relaxation effects overcomes the discrepancy between theory and experiment.

2. THEORY

The relativistic random phase approximation [3] and RRPA-*with*- relaxation [6] is extensively discussed in literature. The RRPA-R transition matrix element in the dipole approximation is given by [6]:

$$\left\langle \Phi_n \middle| \widehat{D} \middle| \Phi_0 \right\rangle = \gamma \left\langle \varphi_\varepsilon^{'} \middle| D \middle| \varphi_i \right\rangle \tag{1}$$

Where Φ_0 is the initial state configuration wave function constructed from the unrelaxed self-consistent orbitals, Φ_n is the excited-state wave function for the channel n constructed from the relaxed orbitals for *(N-1)* core electrons and one excited (*continuum* or *virtually excited*) orbital $\varphi_\varepsilon^{'}$ calculated in the field of the *(N-1)* electrons. The orbital φ_i is the *un*relaxed orbital of the corresponding hole, and $\widehat{D} = \sum_{k=1}^{N} D(k)$ and D are respectively the *many-particle* and the *single-particle* dipole operators. The factor γ comes from the overlap of the *(N-1)* electron core states, obtained from the ground-state configuration by setting the hole for a given channel, and is constructed from the unrelaxed and the relaxed orbitals. The overlap γ is always less than unity.

In the RRPA-R method, one obtains the continuum photoelectron orbitals in the potential of the *relaxed* ion. Two sets of orbitals are thus required for the wave function calculation; one with the single ground state configuration, and another with the relaxed state configuration. The effect of the overlap integral γ tends to *decrease* the photoionization cross section in certain cases, since $\gamma < 1$. However, the removal of electron increases the effective charge of the nucleus, which in turn tends to *increase* the value of the cross section. The combined relaxation effect [6] is then the result of these two competing effects caused by $\gamma < 1$ and the increase in the effective nuclear charge. The ionization energies used in the relativistic random phase approximation with relaxation are obtained as the *difference* in the total relativistic self-consistent energies of the neutral atom and the ion. For this purpose we have used the multiconfiguration Dirac-Fock [7] computer code of Grant *et al.*

In the present study, the following 20 dipole channels are coupled the *truncated* RRPA-R:

$4s_{1/2} \rightarrow p_{1/2}, p_{3/2}$

$4p_{1/2} \rightarrow d_{3/2}, s_{1/2}$

$4p_{3/2} \rightarrow d_{5/2}, d_{3/2}, s_{1/2}$

$4d_{5/2} \rightarrow p_{3/2}, f_{5/2}, f_{7/2}$

$4d_{3/2} \rightarrow p_{3/2}, p_{1/2}, f_{5/2}$

$5s_{1/2} \rightarrow p_{1/2}, p_{3/2}$

$5p_{1/2} \rightarrow d_{3/2}, s_{1/2}$

$5p_{3/2} \rightarrow d_{5/2}, d_{3/2}, s_{1/2}$

Calculations of the photoionization parameters using the RRPA (without relaxation) have already been reported in the literature [3, 4]. These were repeated in the present work for immediate comparison.

3. RESULT AND DISCUSSION

The discrepancy between theory and experiment with regard to the Xe 5s photoionization has been known for a long time [5] in which it was concluded that it is not due to truncation [3, 4] of the RRPA but possibly due to non – (R) RPA correlations. Photoionization with excitation and two-electron transitions are approximately accounted for by including overlap integrals between the initial and final orbitals [8]. The present work examines the application of the RRPA-*with-relaxation* to study Xe 5s photoionization.

Table 1 shows the Dirac Fock thresholds used for RRPA calculations. Also presented in this table are the ΔSCF thresholds used in the RRPA-R calculations, and also presented are the experimental thresholds. The photoionization cross section of Xe 5s is shown in Fig 1. In general, results of calculations of the matrix element in the length and velocity forms are identical in the RRPA, but they are somewhat different in the *truncated* RRPA. Both length and velocity forms are shown in the RRPA figures for the cross section (Fig.1) and the photoelectron angular distribution (Fig. 2). Due to the presence of the overlap integral in Eq.1, gauge invariance is lost in the RRPA-*with-relaxation* and results in the length-form differ from those in the velocity-form. Thus the geometric mean of the two forms is shown for the cross sections.

Table 1: Photoionization threshold in eV for subshells of atomic xenon included in the present calculations.

	DF	ΔE_{SCF}	Expt
4s	229.37	223.02	213.32
$4p_{1/2}$	175.57	169.43	163.9
$4p_{3/2}$	162.79	156.91	145.51
$4d_{3/2}$	73.77	68.47	69.5
$4d_{5/2}$	71.66	66.45	67.6
5s	27.48	26.47	23.4
$5p_{1/2}$	13.40	12.56	13.4
$5p_{3/2}$	11.97	11.23	12.1

As seen in Fig. 1, the Cooper minimum in the RRPA-R above the 5s threshold shifts toward the threshold in comparison with its position in RRPA. The photoelectron angular distribution curve shown in Fig 2 shows a corresponding shift toward the threshold.

The overall agreement with the experiment is distinctly better in the case of the RRPA-R photoionization cross sections, particularly just above the Cooper minimum, than the RRPA. This suggests that RRPA-R takes proper account of at least some of the non-(R)RPA correlations [8,9,10]. Nevertheless, both RRPA and RRPA-R results for the photoelectron angular distribution asymmetry parameters (Fig. 2) drop to much lower values than are found experimentally.

Figure 1: Photoionization cross section of Xe5s: Expt: solid circles [9], open circles [10], Theory: dash line RRPA 13ch (4d, 5s, 5p), Solid line RRPA-R 20ch (4s, 4p, 4d, 5s, 5p) present work.

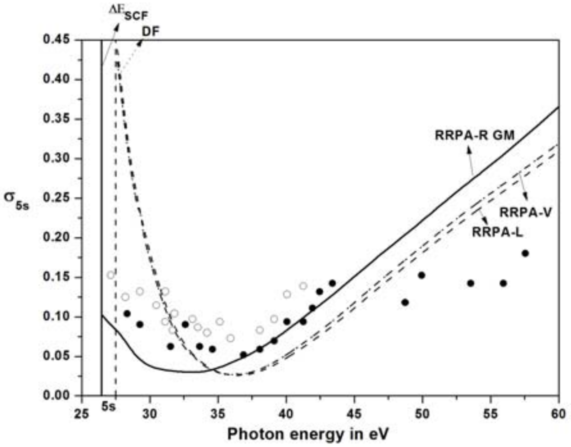

Figure 2: Angular Distribution of Xe5s photoelectrons: Expt: solid circles [9], Theory: dash line RRPA 13ch (4d, 5s, 5p), Solid line RRPA-R 20ch (4s, 4p, 4d, 5s, 5p) present work.

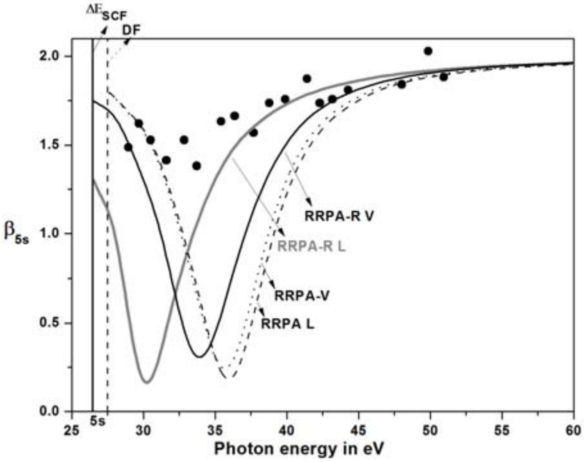

4. CONCLUSIONS

The inclusion of relaxation effects in the RRPA-*with Relaxation* method in addition to the effects of relativistic interactions and correlations shows a somewhat better agreement with experiment that the RRPA-*without-relaxation* in the interpretation of the photoionization of Xe5s. The residual disagreement of angular distributions is nevertheless an indication of other non – RPA correlations which must be important.

References

1. Cooper J.W. (1962) Photoionization from outer atomic subshells. A model study, Physical Review A **47,** 1841-1851.
2. Kutzner. M, Radojevic V. (1994) Effects of relaxation and interchannel coupling in inner-shell photoionization of atomic ytterbium, Physical Review A **49**, 2574-2579.
3. Johnson. W.R and Cheng K.T, (1978) Relativistic Effects on Low-Energy 5s to εp Photoionization for Xenon, Physical Review Letters, **40**, 1167-1170.
4. Johnson. W. R and Lin. C. D. (1979) Multichannel relativistic random phase approximation for the photoionization of atoms, Physical Review A **20**, 964-977.
5. Deshmukh P.C and Manson S.T (1985) Application of the relativistic random phase approximation to Xe 5s photoionization, Physical Review A, **32**, 3109
6. Radojevic V, Kutzner .M, Kelly H. P, (1989) Photoionization of the barium 4d subshell including relativistic and relaxation effects, Physical Review A **40,** 727-734.
7. Grant, I. P., B. J. McKenzie, P. H. Norrington, D. F. Meyers, and N. C. Pyper (1980) An atomic multiconfigurational Dirac-Fock package, Computer Physics Communications, **21**, 207-231.
8. Kutzner M., Radojevic V and Kelly H.P., (1989), Extended photoionization calculations for xenon, Physical Review A, **40**, 5052-5057.
9. Anders Fahlman, Carlson A. Thomas, Krause O. Manfred, (1983), Angular distribution of Xe-5s to continuum p Photoelectrons: Disagreement between experiment and Theory, Physical Review Letters, **50,** 1114-1117.
10. Gustafsson. T, (1977), Photoionization cross sections of the 5s electrons in Xe measured with synchrotron radiation, Chemical Physics letters, **51**, 383-385.

TIME DELAY IN PHOTOIONIZATION OF ATOMIC Sr

Ankur Mandal[1], Soumyajit Saha[1], P.C.Deshmukh[1]
and S. T. Manson[2]
[1]Department of Physics, IIT Madras, Chennai, India
[2]Department of Physics and Astronomy, Georgia State University, Atlanta, USA

ABSTRACT *In the present work, photoionization from atomic Strontium is studied using the RRPA and Wigner-Eisenbud time delay formalism used to determine the time delay in the* $5s_{1/2} \rightarrow \varepsilon p_{1/2}$ and $5s_{1/2} \rightarrow \varepsilon p_{3/2}$ *photoionization channels near the Cooper minima.*

1. INTRODUCTION

When a photon is absorbed by an atom, it is commonly believed that photoionization takes place instantly, i.e. there is no time delay between the instant at which the photon is absorbed and the instant at which the photoelectron is ejected. Recent experimental and theoretical studies [1, 2] have however shown that there is a tiny time delay between these two processes. Using attosecond streaking technique, Schultz et al. [1] measured a time delay in photoionization to be ~21 attosecond for photoelectrons ejected from the 2p orbitals of neon compared to photoelectrons ejection from the 2s orbitals. Klunder et al. [2] used interferometric measurement technique to measure the difference in time delay for photoelectron ejection from the 3p and the 3s orbitals of the Ar atom. Broadly speaking, time delay in photoionization is of the order of about 10 to 100 attosecond or so. Its accurate determination is of great importance for calibration of the atomic clock as well as in the understanding of many electron dynamics.

Kheifets and Ivanov [3] used the Hartree-Fock approximation to calculate the time delay measured by Schultz [1] in Ne atom. They obtained a group delay difference of 6.2 as between 2s and 2p subshells of Ne atom. Including the RPA correlations the difference was enhanced by 2.2 as. Even with the inclusion of electron correlations using the RPA, only about half of the ‘measured’ time-delay could be accounted for in Ref.3, which suggested that part of the measurement is caused by the streaking measurement technique was responsible for the discrepancy between theory and experiment. Moore et al. [4] and Dahlström et al. [5] accounted for both the XUV and IR fields and calculated this time delay 10.2 ± 1.3 as and 12 as respectively. All these calculated values are far however from the experiment. Further theoretical and experimental investigations are thus necessary.

2. METHODOLOGY

We have used the Wigner-Eisenbud formalism [6, 7] to determine photoelectron time delay. In this formalism, the time delay can be defined in terms of the phase shift that is accumulated by the emitted photoelectron wave function. Specifically, the time delay is obtainable as the *energy derivative of the phase shift*:

$$\Delta t = \hbar\left(\frac{d\eta}{dE}\right), \tag{1}$$

where η is the scattering phase shift and E is the photon energy.

Time delay is affected by the relativistic effects and also by the many-electron correlations that are present in the atomic system since photoionization is not strictly a single-electron process. To include many body correlations, we have used the Relativistic Random Phase Approximation (RRPA) [8]. The RRPA includes initial state correlations through time-backward Feynman-Goldstone ring diagrams and also final state correlations via time-forward Feynman-Goldstone ring diagrams (i.e., interchannel coupling). The many-body correlations are built in the RRPA on the Dirac-Hartree-Fock [9] atomic wave functions. The RRPA method and its applications are well documented in literature [10, 11]. In the present work, we have focused on the time-delay in $5s_{1/2} \to \varepsilon p_{1/2}$ and $5s_{1/2} \to \varepsilon p_{3/2}$ photoionization channels of atomic strontium. This being a preliminary study, we have included only these two channels in the *truncated* RRPA scheme.

3. RESULTS AND DISCUSSION

In Fig.1 we report the absolute value (labeled as ‘M’ in the figure) of the complex reduced matrix element for the dipole transition obtained using the RRPA for the two photoionization channels $5s_{1/2} \to \varepsilon p_{1/2}$ and $5s_{1/2} \to \varepsilon p_{3/2}$ in the energy region from the 5s threshold (4.94 eV) to photon energy of ~20eV. This figure shows that the Cooper minima in the $5s_{1/2} \to \varepsilon p_{1/2}$ and $5s_{1/2} \to \varepsilon p_{3/2}$ channels are respectively at about 10.7 eV and 13 eV. From the complex matrix element, the phase shifts η were calculated for the two channels and shown in Fig 2 in the region of the Cooper minima [12]. The matrix elements are also shown in this figure to relate the variations in the phase shifts as a function of energy to the positions of the Cooper minima.

Figure 1: Amplitude of the Transition Matrix elements

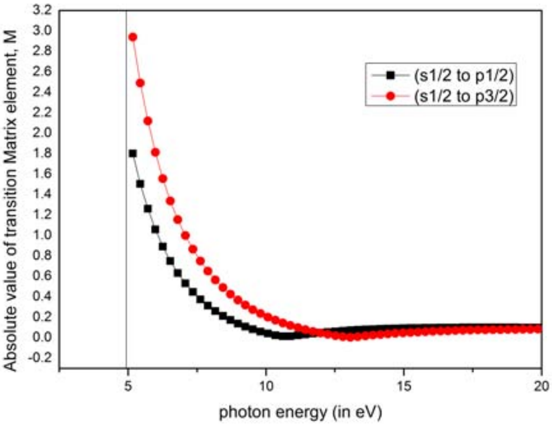

Figure 2: Phase shifts and amplitudes of the complex matrix elements near the Cooper minima

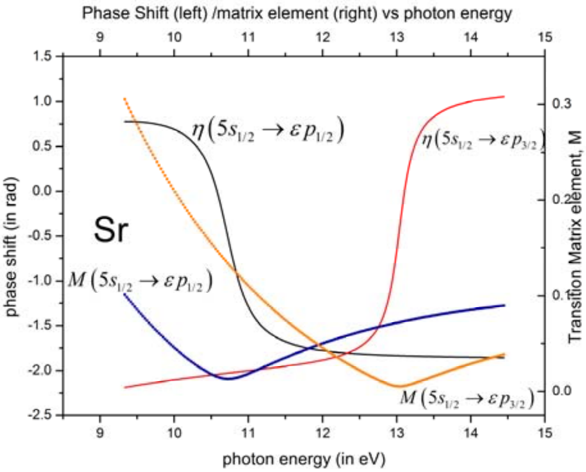

The Eisenbud- Wigner time delay for photoelectron ejection in the $5s_{1/2} \to \varepsilon p_{1/2}$ and $5s_{1/2} \to \varepsilon p_{3/2}$ channels were calculated from the derivatives of the η vs. energy curve, using Eq.1. The difference between the two time delays, δt (i.e. $t_{5s_{1/2}\to\varepsilon p_{1/2}} - t_{5s_{1/2}\to\varepsilon p_{3/2}}$), is calculated and shown in the Fig 3.

The present results show that the difference δt (i.e. $t_{5s_{1/2}\to\varepsilon p_{1/2}} t_{5s_{1/2}\to\varepsilon p_{3/2}}$) is practically zero in the energy region studied, except at the Cooper minimum in each of the two channels. At each of the two Cooper minima, $t_{5s_{1/2}\to\varepsilon p_{1/2}} < t_{5s_{1/2}\to\varepsilon p_{3/2}}$, making the difference δt negative. The difference in the time-delay is of the order of 10^{-15} seconds in the vicinity of the Cooper minima.

Here we have calculated the phase shifts and time delay for different transition channels at the vicinity of Cooper minima. The graphs show that the rapid variation of phase shift causes the variation in time delay in this region.

Figure 3: $\delta t = t_{5s_{1/2}\rightarrow\varepsilon p_{1/2}} - t_{5s_{1/2}\rightarrow\varepsilon p_{3/2}}$ ***vs. photon energy***

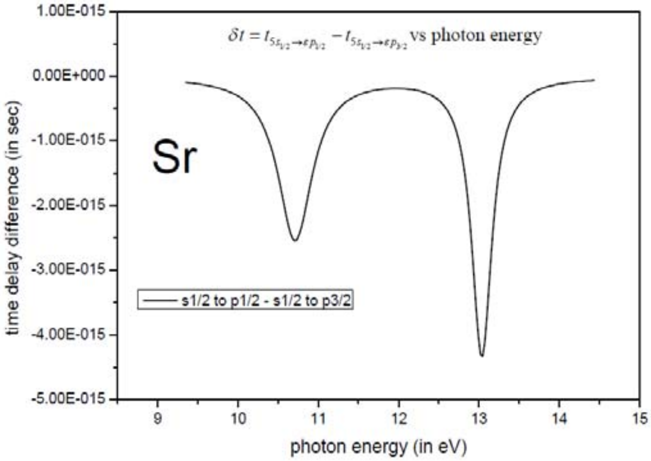

4. CONCLUSIONS

Much remains to be studied and understood with regard to the time-delay in photoionization. The present studies are amongst the first ones which employ relativistic many-body formalism. The present report is only a preliminary one; further studies are in progress.

References

[1] Schultze M; Fieß M, Karpowicz N, Gagnon J, Korbman M, Hofstetter M, Neppl S, Cavalieri A. L, Komninos Y, Mercouris Th, Nicolaides C. A, Pazourek R, Nagele S, Feist J, Burgdörfer J, Azzeer A. M, Ernstorfer R, Kienberger R, Kleineberg U, Goulielmakis E, Krausz F and Yakovlev V. S; (2010); *Delay in Photoemission*; Science; **328**; 1658-1662.

[2] Klunder K; Dahlstrom J. M, Gisselbrecht M, Fordell T, Swoboda M, Guenot D, Johnsson P, Caillat J, Mauritsson J, Maquet A, Taıeb R and L'Huillier A; (2011); *Probing Single-Photon Ionization on the Attosecond Time Scale*; PRL; **106**; 143002(1-4).

[3] Kheifets A. S. and Ivanov I. A; (2010); *Delay in atomic photoionization*, PRL; **105** (23).

[4] Moore L. R; Lysaght M. A, Parker J. S, van der Hart H. W and Taylor K. T; (2011); *Time delay between photoemission from the 2p and 2s subshells of neon*, Physical Review A; **84**.

[5] Dahlström J. M; Carette T and Lindroth E; (2012); *Diagrammatic approach to attosecond delays in photoionization*; Physical Review A; **86**;

[6] Eisenbud L. E; (1948); Ph. D. thesis; Princeton Univ.; (Unpublished).

[7] Wigner E. P; (1955); *Lower Limit for the energy Derivative of the Scattering Phase Shift*; Physical Review **98**; 145-147.

[8] Johnson W. R; Lin C. D; (1979);*Multichannel relativistic random-phase approximation for the photoionization of atoms*; Physical Review A; **20**, 964-977.

[9] Grant I. P; (2007); *Relativistic Quantum Theory of Atoms and Molecules*; Springer Science+ Business Media, LLC; 233 Springer Street, New York, NY 10013, USA.

[10] Johnson, W. R., Lin C. D, Cheng K. T., and Lee C. M; (1980) *Relativistic random phase approximation*; Physica Scripta; **21**, 409-422.

[11] Hemmers, O., R. Guillemin, D. Rolles, A.Wolska, D.W. Lindle, K. T. Cheng,W. R.Johnson, H. L. Zhou, and S. T. Manson (2004) *Nondipole Effects in the Photoionization of Xe 4d52 and 4d32: Evidence for Quadrupole Satellites*. Physical Review Letters; **93**; 1-4.

[12] Cooper J. W.; (1962); *Photoionization from Outer Atomic Subshells. A Model Study*; Physical Review; **128**; 681-693.

QUADRUPOLE EFFECTS IN THE LOW ENERGY PHOTOIONIZATION OF THE 3S SUBSHELL OF MG@C_{60}

Ashish Kumar[1], Sindhu Kalyadan[1], H. R. Varma[1], and P. C. Deshmukh[1,2]
[1]School of Basic Sciences, Indian Institute of Technology Mandi, Mandi, India
[2]Department of Physics, Indian Institute of Technology Madras, Chennai, India

1. INTRODUCTION

It is now known that non-dipole interactions play an important role in understanding the photoionization processes even at low energy [1]. In particular, non-dipole interactions must be taken into account to correctly interpret the photoelectron angular distribution. Recent studies predicted the existence of narrow region in the low energy region (~11eV) where quadrupole (E2) cross-section dominates the dipole (E1) cross section [2]. This is due the presence of Cooper minimum in E1 channels [3]. Interchannel coupling involving the quadrupole channels then result in significant measurable modifications of the angular distribution of photoelectrons from the 3s subshell.

Atoms caged inside an external quantum system like the fullerene have attracted considerable interest in the past decade due to applications in several branches of physics and chemistry [4-6]. The present work explores the effect of an external confining potential, due to the presence of fullerene cage, on the photoionization of Mg in this low energy region. The cage potential causes significant changes in atomic photoionization parameters like the cross-section and angular distribution. The external confining potential induces additional oscillations in photoionization cross-section and the existence of these oscillations, known as confinement resonances, has been verified in a recent experiment [7].

2. THEORETICAL MODEL AND METHODOLOGY

Relativistic random phase approximation (RRPA) is used in the present work to calculate the photoionization parameters of Mg@C_{60}. RRPA is a highly successful many-body theory which includes both correlation and relativistic effects [8]. In this work, confinement environment such as the presence of fullerene potential is simulated by using a spherical attractive potential, V(r) as shown below.

$$V(r) = \begin{cases} -U_0 < 0, if & r_c \le r \le \; r_c + \Delta \\ 0, & otherwise. \end{cases}$$

Here r_c =5.8 a.u. is the inner radius of the shell having thickness Δ =1.9 a.u. and U_0= -0.3 a.u. is the depth of potential well [9, 10].

3. RESULTS AND DISCUSSIONS

As for the free case, the presence of Cooper minimum (C.M.) in 3s results in the domination E2 cross-section over E1 cross section of Mg@C_{60} and is shown in Fig. 1. The region of interest, however, occur at a higher photon energy (~18 eV) compared to free Mg (~ 11 eV). This is due to the fact that the initial and final states are modified by the presence of fullerene cage. The large value of E2 cross-section results modification in the E1 angular distribution parameters as shown in Fig. 2. Similar to the case of free Mg atom, the second-order non-dipole photoelectron angular distribution parameters also apart from zero near to cooper minimum and is shown in Fig. 3. As a result the total angular distributions significantly deviate from the usual dipole angular distribution ($\cos^2\theta$) at low photon energies. This deviation is shown in Fig. 4.

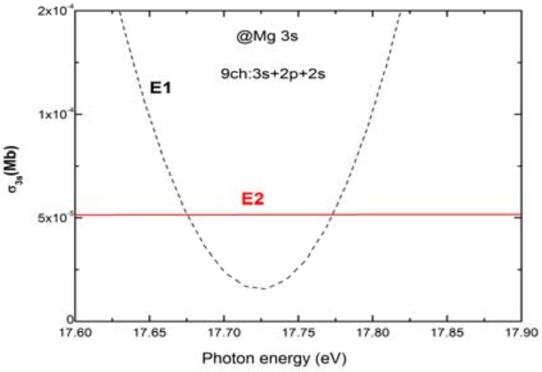

Figure 1. Dipole (E1) and quadrupole (E2) photoionization cross section for Mg@C_{60} 3s.

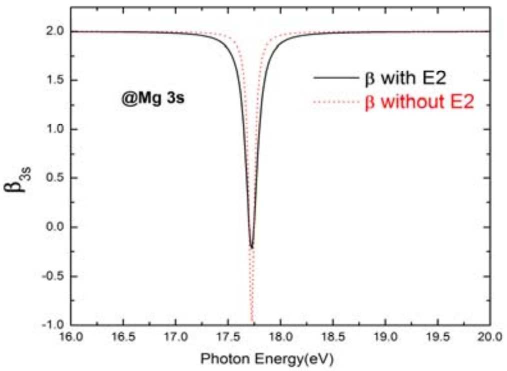

Figure 2. Dipole asymmetry parameter (β), calculated by considering the effect of E2 and without considering E2 for Mg@C_{60} 3s.

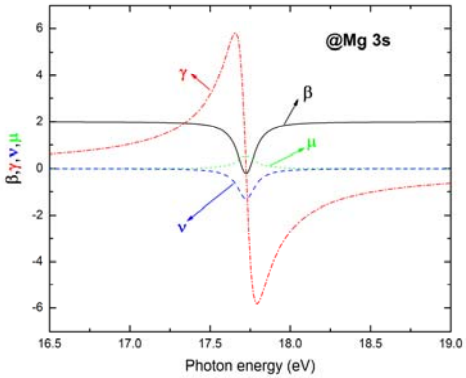

Figure 3. First order nondipole asymmetry parameter γ (dash dot line),and second-order nondipole angular distribution parameters, β (solid line), μ (dot line) and ν (dash line) for Mg@C_{60} 3s in the neighborhood of the dipole cooper minimum.

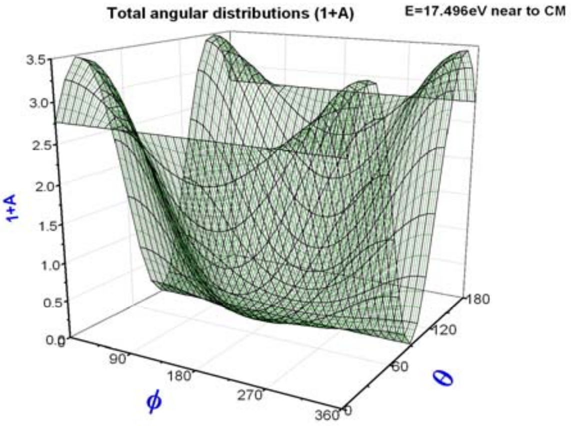

Figure 4. Shape of the photoelectron angular distribution, 1+A(θ,φ), for Mg@C_{60} 3s in the dipole cooper minimum region.

4. CONCLUSIONS

Similar to the case of free Mg, the presence of COOPER MINIMUM. in the dipole channels from 3s subshell results in a narrow region at low energies where non-dipole interactions are important. This region, however, occur at a higher photon energies compare to that of free Mg. The domination of non-dipole interactions results in significant modification in the total angular distribution parameter akin to the case of free Mg**.**

Acknowledgements: The authors are grateful to a grant (SR/S2/LOP-0038/2010-I) from the Department of Science and Technology, Government of India.

References

[1] Jung M et al (1996), Experimental determination of nondipolar angular distribution parameters for photoionization in the Ar K and Kr L shells , *Phys. Review A* **54**, 2127.

[2] Pradhan G B et al (2011), Cooper minima: a window on nondipole photoionization at low energy, *J. Phys. B: At. Mol. Opt. Phys.* **44,** 201001 and references therein.

[3] Cooper J W (1962), Photoionization from Outer Atomic Subshells. A Model Study, *Phys. Rev*. **128,** 681.

[4] Harneit W, Boehme C, Schaefer S, Huebener K, Fostiropoulos and Lips K (2007), Room Temperature Electrical Detection of Spin Coherence in C_{60}, *Phys. Rev. Lett*. **98,** 216601.

[5] Takeda A et al (2006), Superconductivity of doped Ar@C_{60}, *Chem. Commun*. **8,** 912.

[6] Ross R B et al (2009), Endohedral fullerenes for organic photovoltaic devices, *Nat. Mater.* **8**, 208.

[7] Kilcoyne A L D et al (2010), Confinement Resonances in Photoionization of Xe@C_{60}, *Phys. Rev. Lett***. 105,** 21300.

[8] Johnson W R and Lin C D (1979), Multichannel relativistic random-phase approximation for the photoionization of atoms , *Phys. Rev. A* **20,** 977.

[9] Xu Y B, Tan M Q and Becker U (1996), Oscillations in the photoionization cross-section of C_{60}, *Phys. Rev. Lett.* **76,** 3538.

[10] Wang L S, J M Alford, Chai Y, Diener M Smalley R E (1993), Photoelectron Spectroscopy and Electronic Structure of Ca@C_{60}, *Z. Phys. D.* **26,** 297-299.

CALCULATIONS OF MAGNETIC DIPOLE AND ELECTRIC QUADRUPOLE HYPERFINE CONSTANTS OF RB USING THE RELATIVISTIC COUPLED-CLUSTER METHOD

Alak Banik[1], B. K. Mani[2], S. Chattopadhyay[3], D. Angom[3]
and P. C. Deshmukh[4]
[1]Space Applications Center, Ahmedabad, India
[2]Department of Physics, University of South Florida, Tampa, Florida 33620, USA
[3]Physical Research Laboratory, Ahmedabad, India
[4]Indian Institute of Technology, Madras, Chennai, India
Email: alak@sac.isro.gov.in

Abstract

Hyperfine structure constants of Rubidium (Rb) are of importance for understanding of resonance absorption phenomena in vapor cell frequency standards. In the present work, magnetic dipole (A) and electric quadruple hyperfine constants (B) of $5^2S_{1/2}$ ground state for ^{85}Rb, ^{87}Rb are calculated using the relativistic coupled-cluster theory. We use even-tempered kinetically balanced Gaussian basis set. The basis set parameters are optimized to match with the spin-orbital energy and self-consistent field energy of GRASP92 [1] which solves Dirac-Hartree-Fock equation numerically. The hyperfine structure constant values of Rb are in good agreement with the experimental values.

1. INTRODUCTION

Time and frequency are two of the physical parameters which are being measured with high precision. Generation of high precision sources has evolved through high precision atomic experiments and subsequently utilizing the atomic resonances in numerous kinds of primary and secondary frequency standards. Rubidium is naturally available and the abundance in isotopic ratio of 72.2: 27.8 in ^{85}Rb, ^{87}Rb. The ground-state hyperfine transition $5^2S_{1/2}$, F = 2, $m_F = 0$ to $5^2S_{1/2}$, F = 1, $m_F = 0$ of ^{87}Rb is used in vapor cell rubidium frequency standards. It gives us the window to provide stringent test of the high precision atomic theory calculations. In the case of many-electron system with high Z atoms, determining accurate wavefunction for atomic structure and property calculation like hyperfine structure constants is a daunting task specifically to incorporate relativistic effects and electron correlation. The coupled-cluster (CC) theory has proved to be one of the most reliable many body method for precision atomic structure calculation.

2. THEORY

In the paper we present theory of hyperfine structure (HFS) constants of ^{85}Rb and ^{87}Rb in Sec2.1. A brief description of relativistic coupled-cluster theory based on singles and doubles (CCSD) approximations is described in Sec.2.2. The HFS constants in terms of property calculations from coupled cluster wavefunction from RCC theory is described in Sec 2.3. The results are presented and discussed in Sec. 3.

2.1 Hyperfine Structure Constant

Hyperfine structure splitting in an atom is due to the magnetic dipole and electric quadrupole interaction arising from term expansion of $\hat{H}_{HFS}$ between the electrons and nucleus with the nuclear spins **I** (I=3/2, for ^{87}Rb,I=5/2 for ^{85}Rb) of Rb.

The general form of hyperfine interaction is [2]

$$\hat{H}_{HFS} = \sum_{i=1}^{N} \sum_{k,q} (-1)^q t_q^k (\vec{r}_i) T_{-q}^k \tag{1}$$

where,

$t_q^k(\vec{r})$ and T_q^k are irreducible tensor operators of rank k in the electron and nuclear spaces respectively. The total angular momentum **J** of electrons and nuclear angular momenta **I** are coupled together to a total angular momentum **F** which is conserved. For magnetic dipole hyperfine, the explicit form of electronic and nuclear parts of tensor operators in Eq.(1) are

$$t_q^1(\vec{r}) = \frac{-i\sqrt{2}\left[\alpha \bullet \mathrm{C}_1(\vec{r})\right]_q}{cr^2} \qquad T_q^1 = \mu_q \tag{2}$$

where, $\mathrm{C}_1(\vec{r})$ is tensor operator of rank 1 in electronic space and μ_q is component of nuclear magnetic moment operator.

Similarly, for electronic quadrupole hyperfine,

$$t_q^2(\vec{r}) = -\frac{\mathrm{C}_q^2(\vec{r})}{r^3} \qquad T_q^2 = Q_q \tag{3}$$

Here C_q^2 is the tensor operator of rank q.

For Rb which is a one-valence atom, the magnetic dipole hyperfine constant (A) is

$$\alpha = \frac{g_I \mu_N}{j_v} \begin{pmatrix} j_v & 1 & j_v \\ -j_v & 0 & j_v \end{pmatrix} \left\langle n_v \kappa_v \left\| t^1 \right\| n_v \kappa_v \right\rangle$$

Similarly, the electric quadrupole hyperfine constant (B) for one-valence atom is

$$\alpha = 2Q \begin{pmatrix} j_v & 1 & j_v \\ -j_v & 0 & j_v \end{pmatrix} \left\langle n_v \kappa_v \left\| t^2 \right\| n_v \kappa_v \right\rangle$$

Here Q is the c-number quadrupole moment of the nucleus.

2.2 Relativistic Coupled-Cluster Theory *[3]*

The coupled-cluster theory is a non-perturbative many-body theory. The elements ^{87}Rb , ^{85}Rb are single valence system and its correlated wave function is calculated in two steps. First, the cluster operator of the core electrons i.e closed-shell part $\hat{T}$ is evaluated from the reference state $\left|\Phi_0\right\rangle$. Second, the cluster operator of the valence shell $\hat{S}$ is evaluated and the valence reference state [4] is

$$\left|\Phi_v\right\rangle = a_v^\dagger \left|\Phi_0\right\rangle \tag{4}$$

For open shell atom, the exact ground state is

$$\left|\Psi_v\right\rangle = e^{\hat{T}+\hat{S}} \left|\Phi_v\right\rangle \tag{5}$$

In the case of single valence system the higher order terms in the exponential terms of valence cluster operator do not contribute. Then the coupled-cluster wave function of the open shell system is

$$\left|\Psi_v\right\rangle = e^{\hat{T}} (1+\hat{S}) \left|\Phi_v\right\rangle \tag{6}$$

For an N electron system, the cluster operators are

$$\hat{T} = \sum_{i=1}^{N-1} T_i \quad ; \quad \hat{S} = \sum_{i=1}^{N} S_i \tag{7}$$

The summation index of closed shell cluster operator $\hat{T}$ is upto the N-1 core electrons and for open shell cluster operator $\hat{S}$, the index is upto the N electrons including the valence electron. In coupled-cluster singles and doubles approximation (CCSD), the operators in second quantized form are represented by

$$\hat{T} = \hat{T}_1 + \hat{T}_2 = \sum_{a,p} t_a^p a_p^\dagger a_a + \frac{1}{2!} \sum_{a,b,p,q} t_{ab}^{pq} a_p^\dagger a_q^\dagger a_b a_a$$

$$\hat{S} = \hat{S}_1 + \hat{S}_2 = \sum_p s_p^v a_p^\dagger a_v + \sum_{v,a,p,q} s_{va}^{pq} a_p^\dagger a_q^\dagger a_a a_v \tag{8}$$

[for details, pl see ref. 4]

Where,

$t_{\cdots}^{\cdots}$ *and* $s_{\cdots}^{\cdots}$ are the unperturbed cluster amplitudes.

abc…..(pqr…)… represent core (virtual) states and vwx…. Represent valence states. This approximation yields very good many-body effects for the unperturbed wave function for atoms or ions and in order to incorporate relativistic effects, Dirac-Coulomb Hamiltonian for N electron [12] is selected.

$$\hat{H} = \hat{H}_{DC}^{atomic} = \sum_{i=1}^{N} \left[c\boldsymbol{\alpha}_i \bullet \mathbf{p}_i + (\beta_i - 1)mc^2 - V_{nuc}(r_i) + \frac{1}{2}\sum_j \frac{e^2}{r_{ij}} \right] \tag{9}$$

For the nuclear potential, the nucleus with finite size and charge with Fermi density distribution is considered.

$$\rho_{nuc}(r) = \frac{\rho_0}{1 + e^{r-c/a}} \tag{10}$$

Where, $a = t4ln3$ and t is skin thickness. The parameter c is the half-charge radius where $\rho_{nuc}(r) = \rho_0 / 2$

Defining the normal ordered Hamiltonian, the exact ground-state and correlation energy for one valence system as follow

$$\hat{H}_N = \hat{H} - \langle \Phi_v | \hat{H} | \Phi_v \rangle$$

$$\left| \Psi_v^{(0)} \right\rangle = e^{T(0)+S(0)} \left| \Phi_v^0 \right\rangle$$

$$\hat{H}_N \left| \Psi_v \right\rangle = \Delta E_v \left| \Psi_v \right\rangle$$

where, $\Delta E_v = E_v - E_v^{(0)}$

We get

$$\hat{H}_N e^T (1+S) |\Phi_v\rangle = \Delta E_v e^T (1+S) |\Phi_v\rangle$$

$$e^{-T} \hat{H}_N e^T (1+S) |\Phi_v\rangle = \Delta E_v (1+S) |\Phi_v\rangle$$

$$\bar{H}_N (1+S) |\Phi_v\rangle = \Delta E_v (1+S) |\Phi_v\rangle \tag{11}$$

Using Campbell-Baker-Hausdorff formula, $e^{-T} \hat{H}_N e^T$ leads to a linear combination of nested commutators of Hamiltonian and cluster operator as shown below.

$\bar{H}_N = e^{-T} \hat{H}_N e^T$ is the dressed Hamiltonian and expanded in

$$\bar{H}_N = \hat{H}_N + [\hat{H}_N, T] + \frac{1}{2!}\left[[\hat{H}_N, T], T\right] + \frac{1}{3!}\left[\left[[\hat{H}_N, T], T\right], T\right] + ... \tag{12}$$

The cluster amplitude equations of the singles and doubles are obtained from equation (12) after projecting it into singly and doubly states.

$$\begin{aligned} \left\langle \Phi_v^p \right| \bar{H}_N + \{\bar{H}_N S_1\} + \{\bar{H}_N S_2\} \left| \Phi_v \right\rangle &= \Delta E_v^{att} \left\langle \Phi_v^p \right| S_1 \left| \Phi_v \right\rangle \\ \left\langle \Phi_{va}^{pq} \right| \bar{H}_N + \{\bar{H}_N S_1\} + \{\bar{H}_N S_2\} \left| \Phi_v \right\rangle &= \Delta E_v^{att} \left\langle \Phi_{va}^{pq} \right| S_2 \left| \Phi_v \right\rangle \end{aligned} \tag{13}$$

In these equations ΔE_v^{att} is the valence correlation energy defined in [4].

These set of coupled linear algebraic equations are solved using standard linear algebraic techniques. The above equation is solved iteratively with direct inversion of iterated subspace (DIIS) method to accelerate the convergence [10].

2.3 HFS Constants from RCC Theory

Using the correlated CC wave function from equation (4) and hyperfine interaction Hamiltonian from equation (1), we express HFS constants for one valence atomic system as [4]

$$\left\langle E_{HFS} \right\rangle = \frac{\left\langle \Psi_v \right| \hat{H}_{HFS} \left| \Psi_v \right\rangle}{\left\langle \Psi_v | \Psi_v \right\rangle} \tag{14}$$

The HFS constant in equation (14) can be either magnetic dipole (A) or electric quadrupole (B) constants depending on the form of hyperfine interaction Hamiltonian.

Expanding the contributing terms in numerator and denominator,

$$\left\langle \Psi_v \right| \hat{H}_{HFS} \left| \Psi_v \right\rangle = \left\langle \Phi_v \right| \tilde{H}_{HFS} + 2S^{\dagger}\tilde{H}_{HFS} + S^{\dagger}\tilde{H}_{HFS} S \left| \Phi_v \right\rangle$$

$$\left\langle \Psi_v | \Psi_v \right\rangle = \left\langle \Phi_v \right| (1 + S^{\dagger}) e^{T^{\dagger}} e^{T} (1 + S) \left| \Phi_v \right\rangle$$

Where, $\tilde{H}_{HFS} = e^{T^{\dagger}} H_{HFS} e^{T}$ is the dressed HFS Hamiltonian.

3. RESULT AND DISCUSSION

For any atomic calculation we need to choose an appropriate basis set. In the present work the basis set is even-tempered gaussian type orbitals (GTOs) generated with the Dirac-Hartree-Fock Hamiltonian. We expand the large component of the Dirac spinor in linear combination of GTOs.

$$P_{n\kappa}(r) = \sum_p C_{\kappa p}^L g_{\kappa p}^L\,; \qquad Q_{n\kappa}(r) = \sum_p C_{\kappa p}^S g_{\kappa p}^S$$

$$g_{\kappa p}^L(r) = C_{\kappa i}^L r^{n_\kappa} e^{-\alpha_p r^2}\,; \qquad \alpha_p = \alpha_0 \beta^{p-1}$$

Where, p = 0,1,….m is the GTO index and m is the number of Gaussian type functions. The exponent $\alpha_p = \alpha_0 \beta^{p-1}$, where α_0 and β are two independent parameters. The small components of the spin-orbitals are linear combination of $g^S_{\kappa p}$ which are generated from $g^L_{\kappa p}$ through the kinetic balance condition [11]. The basis parameters are optimized such that the core orbital energies are in good agreement
with the results of GRASP92 [1].

Table 1: Comparison between GTO and GRASP92 (in atomic unit)

Atom	GTO	GRASP92
Rb	-2979.6630	-2979.6649

We calculate the magnetic-dipole hyperfine constants A for the $5s_{1/2}$ ground state and the $5p_{1/2}$, $5p_{3/2}$ excited states of ^{85}Rb and ^{87}Rb.

Table 2: Magnetic dipole hyperfine constants of ^{85}Rb (in MHz)

State	This Work	Other RCCSDT[5]	Expt. Results[6]	% Error
$5s_{1/2}$	1032.043	1020.086	1011.9	1.99
$5p_{1/2}$	120.323	119.192	120.7	0.31
$5p_{3/2}$	24.154	24.224	25.029	3.49

Table 3: Magnetic dipole hyperfine constants of ^{87}Rb (in MHz)

State	This Work	Other RCCSDT[7]	Expt. Results[8]	% Error
$5s_{1/2}$	3497.800	3417.25	3417.341	2.30
$5p_{1/2}$	407.799	408.53	406.2	0.44
$5p_{3/2}$	81.865	83.14	84.845	3.51

Similarly, we calculate the electric quadrupole hyperfine constants B for the $5p_{3/2}$ $5d_{3/2}$, $5d_{5/2}$ excited states of ^{85}Rb and ^{87}Rb.

Table 4: Electric quadrupole hyperfine constants of ^{85}Rb (in MHz)

		Basis Set=147, Symmetry=9		Basis Set=151,Symmetry=11	
State	Expt. Results[9]	This Work	% Error	This Work	% Error
$5p_{3/2}$	26.032	24.897	4.36	24.939	4.19
$5d_{3/2}$		4.319		4.439	
$5d_{5/2}$		6.284		6.457	

Table 5: Electric quadrupole hyperfine constants of ^{87}Rb (in MHz)

		Basis Set=147, Symmetry=9		Basis Set=151,Symmetry=11	
State	Expt. Results[9]	This Work	% Error	This Work	% Error
$5p_{3/2}$	12.520	12.044	3.80	12.064	3.64
$5d_{3/2}$		2.089		2.147	
$5d_{5/2}$		3.040		3.124	

4. CONCLUSIONS

We have presented here hyperfine constant calculation based on relativistic coupled-cluster approach. The various contributions from general tensor operator representation of hyperfine Hamiltonian resulting into Rb ground state hyperfine constant is calculated based on derived coupled-cluster wavefunction.

The calculation is carried out for optimized set of Gaussian basis parameters & numbers of GTO orbitals.

For our calculations, the magnetic dipole hyperfine constants of ground state $5S_{1/2}$, our results deviate from the experimental value by 1.99% and 2.3% for ^{85}Rb and ^{87}Rb respectively. Similarly, the electric quadrupole hyperfine constants of exited state $5p_{3/2}$, our results deviate from the experimental value by 4.19% and 3.64% for ^{85}Rb and ^{87}Rb respectively .These deviations may be attributed to the triple excitation in RCC theory. We have computed the hyperfine structure constants of Rubidium using RCC theory and our results preliminary are in good agreement with the experimental and previous theoretical results.

In conclusion, the CC based computation of hyperfine structure constants for ^{87}Rb, ^{85}Rb are more accurate and could be improved further with the trade-off between computation resources and accuracy.

References

[1] F. A. Parpia, C. Froese Fischer and I. P. Grant, Comp., Phys. Comm. **94**, 249 (1996).

[2] W. R. Johnson, *Atomic Structure Theory : Lectures on Atomic Physics* (Springer, 2007).

[3] R. J. Bartlett, M. Musial, Rev. Mod. Phys. **79**, 291 (2007).

[4] B. K. Mani and D. Angom, Phys. Rev. A **81**, 42514 (2010).

[5] R. Pal et. al, Phys. Rev. A **75**, 42515 (2007).

[6] W. A. Wijngaarden and J. Li, Z. Phys. D: At., Mol. Clusters **32**, 67 (1994)

[7] M. S. Safronova and U. I. Safronova, Phys. Rev. A **83**, 052508 (2011).

[8] E. Arimondo, M. Inguscio, and P. Violino, Rev. Mod. Phys. **49**, 31 (1977).

[9] Dipankar Das and Vasant Natarajan, J. Phys. B: At. Mol. Opt. Phys. **41** (2008) 035001 (12pp)

[10] P. Pulay, Cheml Phys Lett, 73,393 (1980)

[11] R. K. Chaudhuri, P. K. Panda and B.P. Das Phys. Rev A 59,1187 (1999)

[12] I. Lindgren and J. Morrison, *Atomic Many-body Theory*, (Springer-Verlag, 1985)

DETERMINATION OF ELEMENTAL COMPOSITION IN ALLOYS USING LASER INDUCED BREAKDOWN SPECTROSCOPY

P. Kumar[1], K. P. Subramanian[1], A. Kumar[2] and R. K. Singh[2]
[1]Physical Research Laboratory, Navrangpura, Ahmedabad-380009
[2]Institute for Plasma Research, Gandhinagar – 382424, India

1. INTRODUCTION

The laser induced breakdown spectroscopy (LIBS) has emerged as an attractive scheme for the elemental analysis of samples. It offers a rapid, localized elemental analysis of solid or liquid materials with high spatial resolution without the need for sample preparation. The lead in LIBS research has origin in its application in space missions [1], however various other fields such as forensic science, forensic nuclear science, medical science and industrial and security applications [2] also benefit from the advancement of LIBS technique.

The experimentation needed for LIBS spectra recording is fairly simple and straightforward. Laser sparks are produced by striking focused, pulsed laser lights on a solid target kept either in air or in an evacuated cell. The light emissions from the laser spark are collected using suitable light collection optics and its spectra are analyzed using a ICCD spectrograph. Modeling the emissions from the plasma can give the composition of the target without requiring any standard calibration inputs and such procedure is known as Calibration Free- LIBS (CF-LIBS). Starting from Ciucci et al. in 1999 [3], presently, there are various algorithms available which can be used for CF-LIBS. All of these algorithms are based on three basic assumptions viz., validity of LTE for the evolving plasma, optically thin plasma condition and homogeneity of the plume. The algorithm works by inferring the number density of species in the plasma using the intensity values obtained experimentally for different species.

2. EXPERIMENTAL DETAILS

The experiment was performed under vacuum conditions, where the ambient pressure around the plume evolution region was ~10^{-2} mbar. The scheme of the experimental set used in the present study is shown in Figure 1.

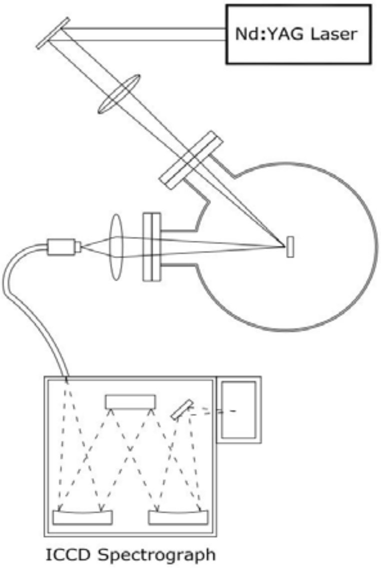

In order to offer fresh surface for ablation for each laser shot, it was necessary to mount the sample on a 2-stage translator (not shown in the figure). Laser light from a Nd:YAG laser (1064 nm, 30 mJ, 8 ns) was focused using a 30 cm focal length quartz lens and was made to incident on the target at an angle 45^O. The average fluence of laser in the experiment was about 2 J/cm^2. The space- and time-averaged emission from the plume was viewed normally by collection optics and was launched onto an optical fiber. The signal was analyzed by a 0.5 m focal length spectrograph (Acton Spectrograph) having a resolution ~ 0.3-nm and the spectrum was recorded by a ICCD (Andor). Trigger to ICCD was delayed by 200 ns with respect to the laser pulse and the gate width was set to 200 ns. The time reference was generated from a fast photodiode (not shown in the figure) viewing the partially reflected light from the optics and the delay and gate were controlled by an external electronic unit (SRS).

3. ANALYSIS OF THE SPECTRUM

The spectrum was recorded in a few frames of CCD covering overall spectral range 325 – 675 nm. Detailed procedures were adopted for the wavelength and intensity calibration of the recorded spectrum. By an in-house developed, automated software peaks in the spectra were identified and were compared with emission spectra of elements listed in Kurucz' database [4]. The calibrated spectrum in 325-675 nm spectral range is shown in Figure 2.

The identified line profiles were both Stark- and Doppler-broadened due to plasma fields and temperature respectively. For accurate determination of the line intensities, the integrated intensities were taken. For this, each of the identified line profiles were fitted with Viogt profiles according to the numerical scheme proposed by Abrarov et al. [5].

The Boltzmann plot was constructed by plotting $\ln(I_{ik}\lambda^3/gf_{ik})$ Vs upper state energy E_u, where I_{ik} is emission intensity, λ is the g is the degeneracy of state k and f_{ik} is the transition probability from state $k \rightarrow i$.

FIGURE 2. The calibrated LIBS spectrum for brass at 10^{-2} mbar pressure.

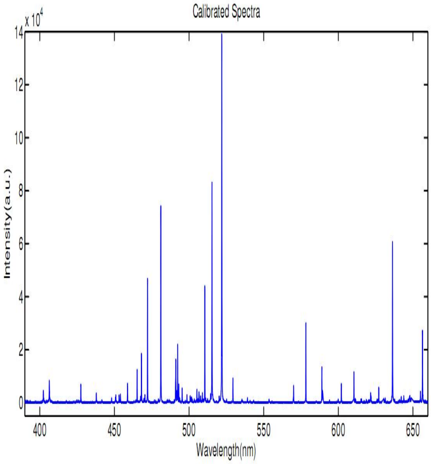

Figure 3. The Boltzmann plot constructed using CuI emission lines in brass LIBS spectrum.

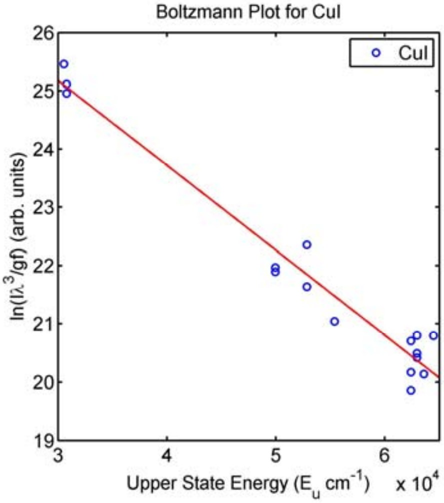

The temperature estimated from Boltzmann plot was 11,350 K.

From the ratio of intensity of CuI/CuII, and also using the estimated plasma temperature, the electron number density was determined. The ratios of all emission lines (as identified from the spectrum) were determined and stored. Assuming a trial value for the number density any of the species, the number densities of the rest of species were estimated from these ratios. Ionization of the species up to fourth ionized state was estimated using Saha equation, and the electron density was reestimated by imposing the quasi-neutrality condition of the plasma. The initial number density of the neutral was adjusted and the iteration was continued till the electron densities determined by Saha equation and by the quasi-neutrality conditions agreed to each other within the stipulated margin.

Figure 4. The algorithm developed to determine species concentration from calibrated LIBS spectra.

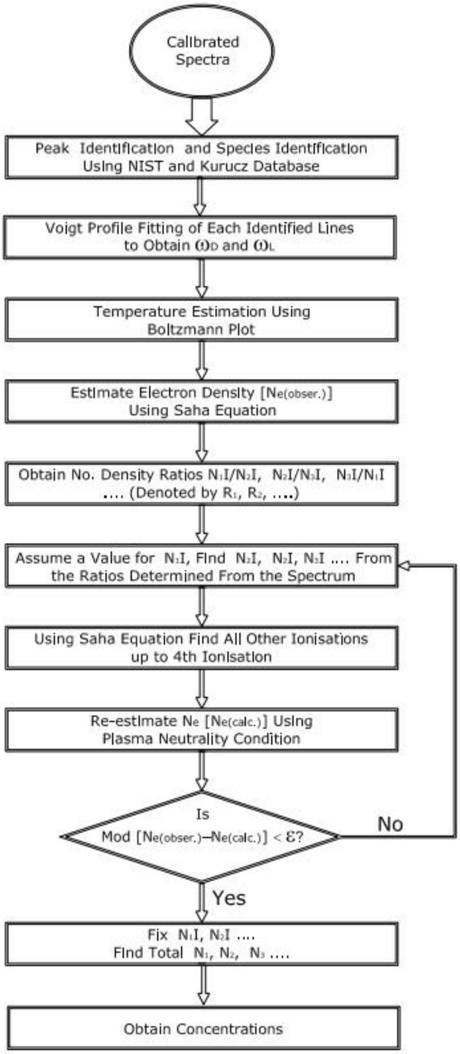

The algorithm used for the analysis of LIBS spectra is shown in Figure 4. Calibrated spectra were passed on to the CF-LIBS analysis programme (in MatLab). The programme was automated to identify the peaks in spectrum and report the species by comparing their wavelength with those available in Kurucz' database. Electron density was determined as explained in earlier section and species concentrations were determined by iterative procedures as explained before. From this, the total concentrations of all species were computed.

Table 1. Elemental concentration in brass.

Element	LIBS Measurement	EPMA Measurement
Copper	67.98	68.45
Zinc	32.02	31.55

The accuracy of results obtained from present work was checked by measuring the concentrations using an electron probe micro-analyzer (EPMA). The results are presented in Table 1. The agreement was about 0.7% for copper and 1.4% for zinc.

4. CONCLUSION

An algorithm, based on the method of ratios was developed for the LIBS data analysis for the determination of elemental composition in brass. The species concentrations in ionic form, often not revealed in the optical spectra, are estimated using Saha equation. The concentrations were determined by ratio of intensity method, which cancels out the unknown instrumental factor from the calculations. The convergence of the algorithm is fast and robust. This method can be applied to the estimation of elemental concentrations in other samples also.

References

[1] Knight A. K., Scherbarth N. L., and Cremers D. A., (2010), M. J., *Appl. Spectrosc.* **54(3)**, 331.

[2] David A., Cremers, and Leon J., (2006), *Radziemski, Handbook of Laser-Induced Breakdown Spectroscopy, John Wiley & Sons Ltd*, pp 31-42.

[3] Ciucci A., Corsi M., Palleschi V., Rastelli S., Salvetti A., and Tognoni E., (1999), Appl. Spectrosc. **53(8)**, 960.

[4] http://www.pmp.uni-hannover.de/cgi-bin/ssi/test/kurucz/sekur.html

[5] Abrarov S. M., Quine B. M., and Jagpal R. K., (2010), J. Quanti. Spectros. Radiati. Transf. **111**, 372.

KINEMATICS AND FRAGMENTATION DYNAMICS OF MULTIPLY CHARGED MOLECULES OF ATMOSPHERIC INTEREST UNDER IMPACT OF keV ELECTRONS

R. Shanker, P. Bhatt, N. Yadav and R. Singh
Atomic Physics Laboratory, Department of Physics, Banaras Hindu University, Varanasi-221005, India
Email: shankerorama@gmail.com

1. INTRODUCTION

The processes of dissociation of multiply ionized molecules have been studied extensively in the past [1,2 and references therein]. The understanding of such processes is important in wide areas of physical sciences ranging from planetary and interstellar space [2] to radiation damage of biological tissues [3]. In the complete Coulomb explosion (CE) of molecular ions, if all the fragment ions are detected in coincidence, they are able to provide kinematically complete information about the molecular breakup process [1,4]. In such processes, kinetic energy release (KER), given by the sum of kinetic energies (KEs) of the individual fragments, and angular correlations of different fragment ions are of central interest in determining the structural properties of the precursor molecular ion. The studies on polyatomic molecules have shown that the interaction with energetic radiations creates noticeable changes in the molecular geometry [5]. The energy deposited in the molecular system by these ionizing radiations is converted into the KEs of individual fragments plus the excitation energy of the molecular species which is emitted in the form of photons [6].

2. EXPERIMENTAL METHOD

The detailed description of the experimental setup can be found in our previous papers [7-8]. Briefly, a mono-energetic beam of keV electrons extracted from a commercial electron gun was made to collide with a dilute gaseous jet of free molecules (CO_2 or N_2O) effusing from a grounded hypodermic needle in a crossed beam geometry. A single stage linear TOF spectrometer is used in the present experiment; the positively charged fragment ions from the collision events are extracted by application of a homogeneous electric field towards a time- and position sensitive detector comprising of a dual micro channel plate (MCP) with $\phi = 40$ mm and a delay line anode [9]. The ejected electrons are extracted towards a channeltron placed opposite to the direction of ion extraction. The ejected neutral particles, if any, are not detected in the present setup. The electron signal serves as the timing reference for arrival of the ions at MCP and thus provides their TOFs while the signals from delay line anode provide the position information of the ions on the detector. Thus, for each ion detected in coincidence, we record the TOF (t) that the ion takes from its birth-place to reach the detector and the position (x, y) where the ion has hit the detector. The employed ion detector is capable of recording the (x, y, t) information of up to four concomitant ions hitting the detector. The (x, y, t) values of all ions are then converted into the corresponding momentum triplets (p_x, p_y, p_z) [7]. Once the momenta of ions are known, the dynamical properties of the ionized molecular system can be easily extracted and quantified. A typical ion-ion coincidence spectrum is presented in Fig.1.

Figure 1: Ion-ion coincidence spectrum (raw data) observed in 12 keV electron collisions with CO_2; ion-pairs resulting from dissociative ionization of (a) CO_2^{2+} and (b) CO_2^{3+}

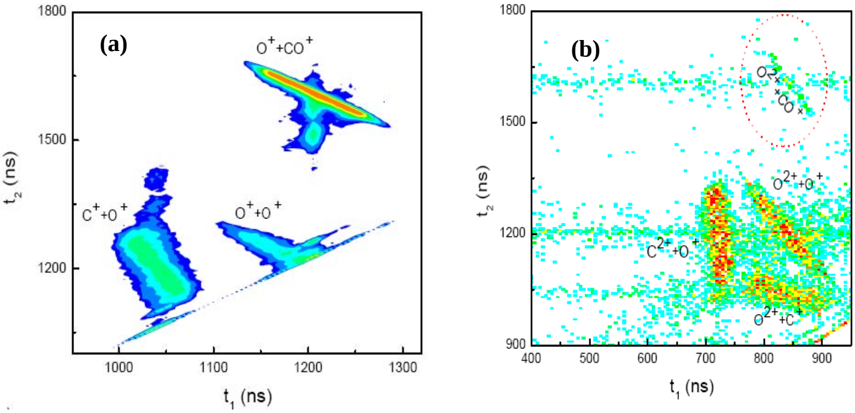

The KER for a given dissociation channel is obtained by summing the KEs of individual fragments produced in that channel; the angular correlation among departing fragments are obtained by calculating the free angle [10].

3. RESULT AND DISCUSSION

The KER distributions for dissociation channels of CO_2^{2+} and CO_2^{3+} are presented in Fig. 2(a) [10]; Fig. 2(b) and 2(c) represent KER distributions for dissociation channels of N_2O^{2+} and N_2O^{3+} [11], respectively. The vertical arrows represent the predictions of KER under CE model considering point charges on atoms at equilibrium distances; this model predicts higher values of KER as compared to our experimental data.

Figure 2: KER distributions for dissociation channels of CO_2^{q+} and N_2O^{q+} (q=2,3)

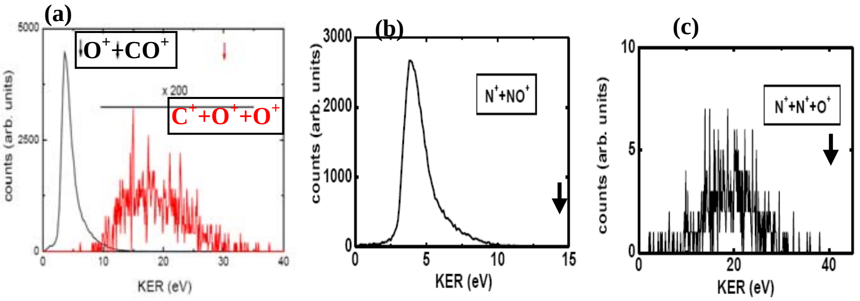

The bond angle and mechanism of dissociation for N_2O^{3+} ion into $N^++N^++O^+$ channel can be obtained by considering the parameters defined in Fig. 2 (a). The average bond angle of dissociating N_2O^{3+} is observed to be 140° (see, Fig. 2(b)); the distribution of χ around 90° shows the concerted nature of fragmentation (Fig. 2(c)) where both the bonds (N-N and N-O) break simultaneously and the terminal N and O ions fly back to back with large momentum leaving the central atom with almost negligible momentum [11]. By applying similar methodology for CO_2^{3+}, the bond angle is observed to be 120° and its dissociation also follows concerted mechanism [10].

Figure 2: The distribution of N-N-O bond angle θ (left) and the distribution of angle χ (right) as observed in $N^++N^++O^+$ fragmentation channel of N_2O^{3+} for 10 keV electron impact with N_2O.

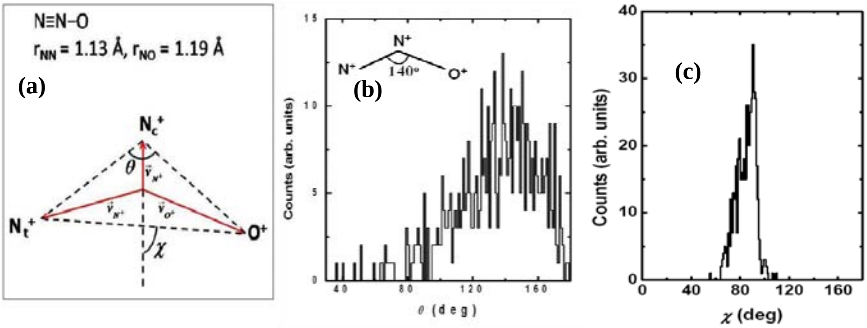

To illustrate further the dissociation dynamics, the Newton diagrams are obtained by taking the momentum vector of the ion arriving first at MCP as reference along x-axis and the momentum distribution of its concomitant fragments (second ion and third ion/neutral) are plotted with respect to it above and below the x-axis (see, Fig. 3). In case of the two-body dissociation process O^++CO^+, momentum vectors of most of the CO^+ ions are distributed around 170°±10° with respect to the momentum vectors of O^+ ions plotted along the x-axis [10]. The Newton diagram for $C^++O^++O^+$ channel is shown in Fig. 3(b) which shows that both the O^+ ions are ejected at about 102° with respect to the momentum vector of the C^+ ion plotted along x-axis. This diagram indicates the alteration of molecular geometry for the triply ionized state of a CO_2 molecule [10]. Similarly, Fig. 3(c) shows that most of the terminal N^+ and O^+ ions are emitted respectively at 90° and 106° relative to the central N^+ ion [11]

Figure 3: Newton diagrams for fragmentation channels (a) $\underline{O}^+$+CO^+, (b) $\underline{C}^+$+O^++O^+, and(c) $\underline{N}^+$+N^++O^+ originated from the dissociation of CO_2^{2+}, CO_2^{3+} and N_2O^{3+}, respectively in keV electron impact.

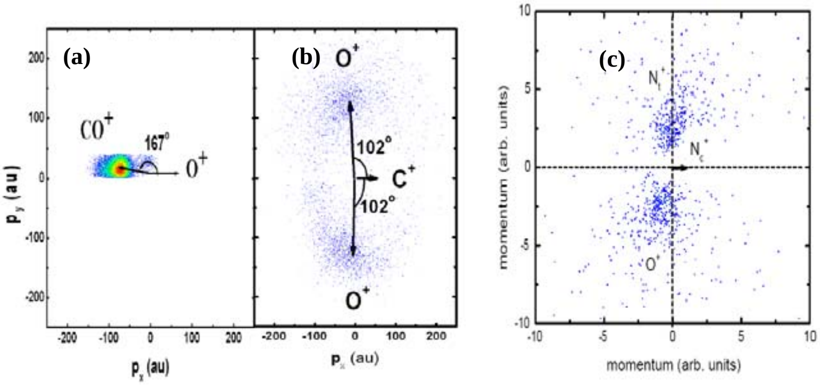

4. CONCLUSION

We have used a linear TOF spectrometer equipped with a multi-hit position sensitive detector to measure the momentum vectors of up to four concomitant fragment ions generated from keV electron collisions with molecules (CO_2 and N_2O). The KER distributions for different dissociation channels observed in these collision events are obtained. The CE model is found to overestimate our experimental KER values due to its oversimplified point charge assumption. The bent geometrical states are observed for triply ionized CO_2 and N_2O with an average bond angle of 120° and 140°, respectively; the dissociation of both of these ions follows a concerted pathway. The Newton diagrams plotted for the dissociation channels of CO_2^{3+} and N_2O^{3+} also verify the concerted mechanism of dissociation for these ions.

Acknowledgements

The work was supported by the Department of Science and Technology, New Delhi.

References

[1] Mathur D., (2004), Phys. Rep. **391**, 1.
[2] Price S. D., (2003), Phys. Chem. Chem. Phys. **5**, 1717.
[3] Boudaiffa B., Cloutier P., Hunting D., Huels M. A., and Sanche L., (2000) Science. **287**, 1658.
[4] Boudaiffa B., Cloutier P., Hunting D., Huels M. A., and Sanche L., (2000) Science. **287**, 1658.
[5] Siegmann B., Werner U., Lutz H. O., and Mann R., (2002), J. Phys. B **35**, 3755.
[6] Neumann *et al.*, (2010), Phys. Rev. Lett. **104**, 103201.
[7] Singh R., Bhatt P., Yadav N., and Shanker R., (2011), Meas. Sci. Technol. **22**, 055901.
[8] Bhatt P., Singh R., Yadav N., and Shanker R., (2011), Phys. Rev. A **84**, 042701 (2011).
[9] http://www.roentdek.com/
[10] Bhatt P., Singh R., Yadav N., and Shanker R., (2012), Phys. Rev. A **85**, 042707.
[11] Bhatt P., Singh R., Yadav N., and Shanker R., (2012), Phys. Rev. A **86**, 052708.

LOCHFRASS IN HYDROGEN MOLECULES

Chirag Jhala[1] and Manfred Lein[2]
[1]The Galaxy Education System, Rajkot, Gujarat
[2]Institute for Theoretical Physics, Leibniz Universitat, Hannover, Germany

1. INTRODUCTION

The pioneering work of Zewail [1, 2] opened a new frontier in the field of science where molecular reactions can be observed in the real-time domain using pump-probe spectroscopy. In a pump-probe experiment the target is first pumped in to some sample state by the application of a laser pulse. This sample state is left free to evolve in time. The evolution of the system is then probed by a second pulse. The ionization and fragmentation dynamics of H2 molecule and its isotopes in the presence of strong external fields have been studied extensively [3, 4]. Furthermore, a great amount of work has been already done on the time-resolved pump-probe studies of H2 molecules [5-9]. Earlier studies of vibrational wave packets in the electronic ground state can be found in [tbetal,hschwoereretal,tmmt]. A very interesting observation was made regarding the formation of electronic ground state vibrational wave packets in H2 (D2) molecules by strong-field ionization, first predicted in [10] and experimentally verified in [5]. When the neutral H2 molecule is subjected to a very short pulse, the molecule is preferentially ionized at large values of the internuclear distance R leading to a strong depletion at those R-values. If this R-dependent depletion process is fast enough, then a vibrational wave packet is created in the electronic ground state of the molecule that is mainly in a superposition of the ground and the first excited vibrational states. The R-dependent depletion process is known as lochfrass.

2. THEORY

We have considered a one-dimensional H2 molecule with two moving electrons and a nucleus to study the lochfrass effect. Multiconfiguration time-dependent Hartree (MCTDH) approach is used here to approximate the wave function of the H2 molecule. Within the MCTDH approach, we have found that 8 single-particle functions (SPFs) are enough to describe the correlated electron-nuclear and electron-electron dynamics [11,12]. We calculate the expectation value of the internuclear distance <R> in order to observe the R-dependent depletion process. The nuclear density is obtained by integrating the wave function over a limited range of the electronic coordinates to isolate the bound part and to observe the depletion. The R-expectation value **<R>**b of the bound part is given by,

$$\Gamma_{\text{lochfrass}} = \int_{-x_{box}}^{x_{box}} dx \int_{-y_{box}}^{y_{box}} |\psi(x,y,R)|^2 dy \tag{1}$$

$$\langle R \rangle_b = \int_0^{R_{\max}} \Gamma_{\text{lochfrass}}\, R\, dR, \tag{2}$$

where $|x_{box}| = |y_{box}| = 20$ a.u. In Figs. 1(a)-(d) we plot $<R>_b$ for the H_2 and D_2 molecules subjected to laser pulses with wavelengths 200 nm, 400 nm, 800 nm, and 1200 nm for the intensity 6×10^{14} W/cm^2 as a function of time. A $\sin^2$ n-cycle function with n/2 turn-on and turn-off times is used as the field envelope. The pulse length for all the wavelengths is 8 fs and the duration of the field-free propagation is 42 fs. As mentioned earlier in the case of H_2^+ and H_2 calculations, complex absorbing potentials are employed to avoid reflections from the boundary. The field strength attains the maximum around 3.5 fs. Looking at Fig. 1(c), we can see that up to this time $<R>_b$ increases from the equilibrium internuclear distance. From 3.5 fs onwards, due to the rapid ionization at large internuclear distances, the molecules deplete at large R. This causes $<R>_b$ to decrease. When the field becomes smaller, the intensity is not strong enough to cause any further ionization and as a result the wave packet starts to move towards large R leading to increasing $<R>_b$. The decrease and increase of $<R>_b$ continues repeatedly due to the oscillation of the electric field till the end of the pulse. The wave packet, created by this process, is formed from the vibrational states of the electronic ground state of the H_2 or D_2 molecule. The superposition of vibrational states remains in coherence for an extremely long time. In Fig. 1 we can see that, from 10 fs onwards the oscillation in $<R>_b$ are periodic over time for both H_2 and D_2 molecules. The period of oscillation for the H_2 and D_2 molecules is roughly 8 fs and 11 fs, respectively. It is interesting to see that in Figs. 1(a)-(d) the depletion of the wave packet is strongest for the 200 nm wavelength while weak for the 1200 nm wavelength. This gives a clear message that lochfrass effect is more pronounced for high-frequency fields and less pronounced for low frequency fields.

Figure 1: $<R>_b$ as function of time for H_2 and D_2 molecules in a laser pulse.

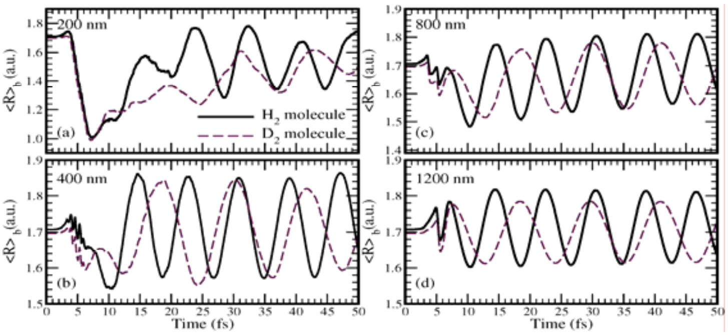

$<R>_b$ as function of time for H_2 and D_2 molecules in a laser pulse with intensity 6x10^{14} W/cm^2 and wavelengths (a) 200 nm, (b) 400 nm, (c) 800 nm, and (a) 1200 nm using eight-SPFs MCTDH calculation. The pulse length in all the plots is 8 fs.

3. RESULT AND DISCUSSION

The plot of spectral power is shown in Fig. 2. By calculating the autocorrelation spectra for the molecules, we can easily identify the occupied vibrational levels. To obtain these spectra, we have propagated an arbitrary initial state in real-time using the model Hamiltonian. The autocorrelation function from the propagated wave function is obtained at each time step and later Fourier transformed to obtain the spectrum. In Figs. 2(a) and 2(b), the dotted lines show the autocorrelation spectra for D_2 and H_2 molecule calculated using exact calculation. Here we have shown seven and five vibrational levels for D_2 and H_2 molecules, respectively. To see the levels occupied by the D_2 and H_2 molecules in the case of laser excitation, we take the Fourier transform of $<R>_b$. The energy axis has been shifted to compare the results with the autocorrelation spectrum. Figs. 2(a) and 2(b) show that the pump pulses of different wavelengths create vibrational wave packets in the ground and first excited vibrational states. The vibrational period $T_{vib} = 2\pi/\Delta E$ is obtained from the energy difference ΔE between the ground and the first excited vibrational level. For our 1D model calculation, the vibrational time periods obtained from the exact calculation for the D_2 and H_2 molecules are 10.93 fs and 8.33 fs respectively. The vibrational time periods obtained from the eight-SPFs MCTDH calculations for D_2 and H_2 in good agreement with these values. This vibrational period is in agreement with the values obtained from the Fig. 1.

Figure 2: Spectral power for H_2 and D_2 molecules in a laser pulse.

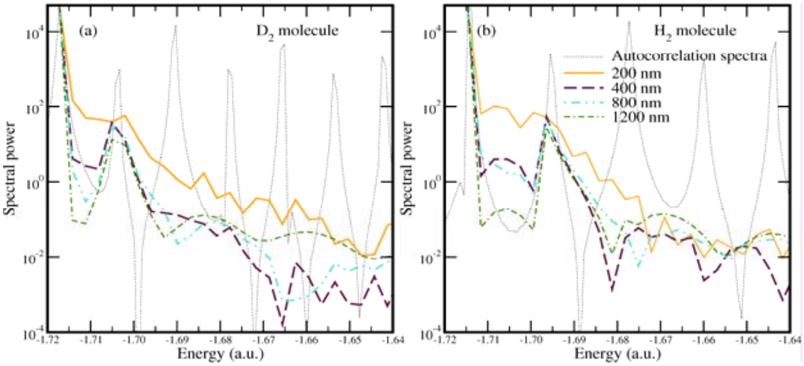

Spectral power for (a) D_2 molecule and (b) H_2 molecule obtained by taking a Fourier transform of $<R>_b$ in a laser pulse with pump wavelengths 200 nm, 400 nm, 800 nm, and 1200 nm and intensity 6 x10^{14} W/cm^2 using eight-SPFs MCTDH calculations. The pump pulse is 8 fs long. The dotted curves show spectra obtained by taking the Fourier transform of the autocorrelation function obtained using an arbitrary initial state.

We now probe the lochfrass process, created by the application of a pump pulse, by an additional pulse at various delay times. This probe pulse is of 800 nm wavelength and 8 fs long. The delay time between the pump and the probe pulse is varied from -5 fs to 50 fs in steps of 1 fs. The probe pulse has n_{probe} = 3 cycles. A $\sin^2$ function with n_{probe} /2 turn-on and turn-off times is used as the field envelope. The field intensity $6x10^{14}$ W/cm^2 is used. In Fig. 3, we have plotted the survival, photodissociation, and Coulomb explosion probabilities [11,13] as a function of time delay. The calculated vibrational time period (from Fig. 3) for the D_2 and H_2 molecules are 12 fs and 8 fs, respectively.

Figure 3: Survival, photodissociation, and Coulomb explosion probabilities for H_2 and D_2 molecules in a laser pulse.

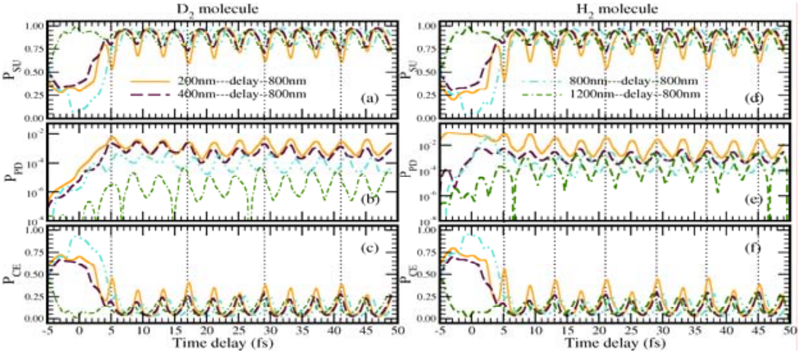

P_{SU}, P_{PD}, and P_{CO} for D_2 molecule (panels (a), (b), and (c)) and H_2 molecule (panels (d), (e), and (f)) obtained in a laser pulse with pump wavelengths 200 nm, 400 nm, 800 nm, and 1200 nm and intensity $x10^{14}$ W/cm^2 using eight-SPFs MCTDH calculation. The pump and probe pulses are 8 fs long.

4. CONCLUSION

We have discussed the lochfrass effect obtained for very short pulses using different pump wavelengths. The vibrational time periods of H_2 and D_2 molecule were calculated to be 11.57 fs and 8 fs, respectively. Depletion of the electronic ground state creates vibrational wave packets with these oscillation periods. A striking observation is that the application of the probe pulse showed the population of higher vibrational levels which lead to even faster oscillations of roughly 4 fs. It was shown that for high-frequency ultra-short laser pulses the lochfrass effect is more pronounced than for low-frequency pulses [13].

References

[1] Zewail A. H., (1988), *Laser Femtochemistry* - Science. **242**, 1645.

[2] Zewail A. H., (2000), *Femtochemistry: Atomic-Scale Dynamics of the Chemical Bond*. J. Phys. Chem. A. 104, 5660 (2000).

[3] Posthumus J. H., (2004), *The dynamics of small molecules in intense laser fields*. Rep. Prog. Phys. **67**, 623.

[4] Calvert C. R., Bryan W. A., Newell W. R., and Williams I. D., (2010), *Time-resolved studies of ultrafast wavepacket dynamics in hydrogen molecules*“, Phys. Rep. **491**, 1.

[5] Ergler Th., Rudenko A., Feuerstein B., Zrost K., Schroter C. D., Moshammer R., and Ullrich J., (2005), *Time-Resolved Imaging and Manipulation of* H_2 *Fragmentation in Intense Laser Fields*. Phys. Rev. Lett. **95**, 093001.

[6] Ergler Th., Rudenko A., Feuerstein B., Zrost K., Schroter C. D., Moshammer R., and Ullrich J., (2006), *Spatiotemporal Imaging of Ultrafast Molecular Motion: Collapse and Revival of the* D_2^+ *Nuclear Wave Packet*. Phys. Rev. Lett. **97,** 193001.

[7] Bryan W. A., English E. M. L., McKenna J., Wood J., Calvert C. R., Turcu I. C. E., Torres R., Collier J. L., Williams I. D., and Newell W. R., (2007), *Mapping the evolution of optically generated rotational wave packets in a room-temperature ensemble of* D_2. Phys. Rev. A **76**, 023414.

[8] Rudenko A., Feuerstein B., Zrost K., de Jesus V. L. B., Ergler T., Dimopoulou C., Schroter C. D., Moshammer R., and Ullrich J., (2005), *Fragmentation dynamics of molecular hydrogen in strong ultrashort laser pulses*. J. Phys. B **38**, 487.

[9] Rudenko A., Ergler Th., Feuerstein B., Zrost K., Schroter C. D., Moshammer R., and Ullrich J., (2006), *Real-time observation of vibrational revival in the fastest molecular system*. Chem. Phys. **329**, 193.

[10] Goll E., Wunner G., and Saenz A., (2006), *Formation of Ground-State Vibrational Wave Packets in Intense Ultrashort Laser Pulses*. Phys. Rev. Lett. **97**, 103003.

[11] Jhala C., and Lein M., (2010), *Multiconfiguration time-dependent Hartree approach for electron-nuclear correlation in strong laser fields*. Phys. Rev. A **81**, 063421.

[12] Jhala C., Dreissigacker I., and Lein M., (2010), *Absorbing boundaries in the mean-field approximation.* Phys. Rev. A **82**, 063415.

[13] Jhala C., *Ph.D. Thesis "Electron-Nuclear Correlation in Laser-Driven Diatomic Molecules", Kassel University, Kassel, Germany.* Phys. Lett. **443,** 17.

THEORY OF ELECTRON PHONON INTERACTION IN SEMICONDUCTOR CRYSTALS

S. C. Gairola*
Department of Physics (School of Sciences), H. N. B. Garhwal
University (A Central University) Campus Pauri-246001,
Uttarakhand, India
Email: *dgsureshc@yahoo.co.in; scgairola@rediffmail.com

1. INTRODUCTION

In real crystals, the harmonic theory does not explain the experimental observed physical properties. These can be well understood by taking impurity into consideration. This creates localized mode. An interaction of electron in harmonic and localized modes is taken into consideration . The work has been carried out on anharmonic crystals[1] but in present case electron phonon interaction is taken with isotopic impurity in low temperature limit.

2. FORMULATION OF THE PROBLEM

The phonon life time $\tau(\mathrm{kq},\varepsilon)$ is the reciprocal of phonon linewidth $\Gamma(\mathrm{kq},\varepsilon)$ as[2]

$$\tau(\mathrm{kq},\varepsilon) \quad = \quad \left(\Gamma(\mathrm{kq},\varepsilon)\right)^{-1} \tag{1}$$

3. EVALUATION OF PHONON LINEWIDTH

Let us take the Hamiltonian consists of harmonic part, electron part , defect part and electron phonon interaction part defined in reference[3] and references therein. The Fourier transformed phonon Green`s function can be evaluated using this Hamiltonian with the help of equation of motion technique of quantum dynamics[1,4-6] and Dyson equation approach as

$$G_{\mathrm{kk}'}(\varepsilon) = \varepsilon_{\mathrm{k}}\eta_{\mathrm{kk}'}\pi^{-1}\left[\varepsilon^2 - \bar{\varepsilon}_{\mathrm{k}}{}^2 + 2i\varepsilon_{\mathrm{k}}\Gamma(\mathrm{kq},\varepsilon)\right]^{-1} \tag{2}$$

where ,

$$\eta_{kk'} = \delta_{kk'} + 4C\left(-\vec{k},\vec{k}'\right)\varepsilon_k^{-1} \tag{3a}$$

$$\bar{\varepsilon}_k^{\,2} = \tilde{\varepsilon}_k^{\,2} + 2\varepsilon_k \Delta\left(kq,\varepsilon\right) \tag{3b}$$

$$\tilde{\varepsilon}_k^{\,2} = \varepsilon_k^{\,2} + 2^{-1}\pi^{-1}\varepsilon_k \left\{ \left\langle \left[M_{kq}(t), B_{k'}^{*}(t') \right] \right\rangle + \left\langle \left[M_{kq}(t), A_{k'}^{*}(t') \right]^0 \right\rangle \right.$$

$$+4\varepsilon_k^{-1}\sum_{k_1} C\left(\vec{k},-\vec{k}_1\right)\left\langle \left[M_{kq}(t), B_{k'}^{*}(t') \right]^0 \right\rangle + 8\left(\varepsilon^2 - \varepsilon_k^{\,2}\right)\varepsilon_k^{-1} C\left(-\vec{k},\vec{k}\right)$$

$$\left. -2g\varepsilon_k^{-1}\sum_{q} \left\langle \left[M_{kq}(t), b_Q^{*} b_q \right]^0 \right\rangle \right\}_{t=t'} \tag{3c}$$

where ,

$$M_{kq}(t) = 4\pi\sum_{k_1} R\left(-\vec{k},\vec{k}_1\right) A_{k_1} - 2\pi L_{kq}(t) \tag{4a}$$

$$R\left(\vec{k}_1,\vec{k}_2\right) = \varepsilon_{k_2}\varepsilon_{k_1}^{-1} C\left(\vec{k}_1,\vec{k}_2\right) + D\left(\vec{k}_1,\vec{k}_2\right) + 4\sum_{k_2'} C\left(-\vec{k}_1,\vec{k}_2'\right)$$

$$\times D\left(-\vec{k}_2',\vec{k}_2\right)\varepsilon_k^{-1} \tag{4b}$$

$$L_{kq}(t) = g\sum_{q}\left[\varepsilon_q \left(b_q^{*} b_q + b_Q^{*} b_q \right) + g\left(b_q^{*} b_q B_k + b_Q^{*} b_q B_k \right) \right] \tag{4c}$$

In eqs. 4b and 4c, $C\left(\vec{k}_1,\vec{k}_2\right)$, $D\left(\vec{k}_1,\vec{k}_2\right)$, g are mass change parameter, force constant change parameter and electron phonon coupling constant respectively. Phonon linewidth $\Gamma\left(kq,\varepsilon\right)$ is oblained as [1,4-7]

$$\Gamma\left(kq,\varepsilon\right) = \Gamma^{D}\left(kq,\varepsilon\right) + \Gamma^{ep'}\left(kq,\varepsilon\right) + \Gamma^{ep''}\left(kq,\varepsilon\right) \tag{5}$$

where ,

$$\Gamma^{D}\left(kq,\varepsilon\right) = 8\pi\varepsilon(\omega)\sum_{k_1} R\left(\vec{k}_1,-\vec{k}\right) R^{*}\left(\vec{k}_1,-\vec{k}\right)\varepsilon_{k_1}\delta\left(\varepsilon^2 - \tilde{\varepsilon}_{k_1}^{\,2}\right) \tag{6a}$$

$$\Gamma^{ep'}\left(kq,\varepsilon\right) = \left[g^2 T\left(1 + 4C\left(-\vec{k},\vec{k}'\right)\varepsilon_k^{-1}\right) + g^6 T^3 \left\{ 1 + 16\left(C\left(-\vec{k},\vec{k}'\right)\right)^2 \varepsilon_k^{-2} + \right.\right.$$

$$\left.\left. 8C\left(-\vec{k},\vec{k}'\right)\varepsilon_k^{-1} \right\} L\left(kqkQ\right) \right] A_{kq} B_{kq} J\left(kqk\right) E_{kqq}(-) E_{kqq}(+) \delta\left(\varepsilon - 2\varepsilon_q\right) \tag{6b}$$

$$\Gamma^{ep''}\left(kq,\varepsilon\right) = \left[g^2 T\left(1 + 4C\left(-\vec{k},\vec{k}'\right)\varepsilon_k^{-1}\right) + g^6 T^3 \left\{ 1 + 16\left(C\left(-\vec{k},\vec{k}'\right)\right)^2 \varepsilon_k^{-2} \right.\right.$$

$$\left.\left. +8C\left(-\vec{k},\vec{k}'\right)\varepsilon_k^{-1} \right\} L\left(kqkQ\right) \right] A_{kQ} B_{kQ} J\left(kqk\right) E_{kqQ}(-) E_{kqQ}(+)$$

$$\times\delta\left(\varepsilon-2\varepsilon_q\right) \tag{6c}$$

where D , ep denote defect and electron phonon interaction parts respectively .

$$A_{km}=\left(\tilde{\varepsilon}_k^{`2}+\tilde{\varepsilon}_m^{`2}\right)\;\;;\;\; B_{km}=\left(\tilde{\varepsilon}_k^{`2}-\tilde{\varepsilon}_m^{`2}\right)^{-4}\;;\;\; m=q,Q \tag{7a}$$

$$C_{kqk}\left(\mp\right)=\left\{\left(\tilde{\varepsilon}_k^{`}\mp 2\varepsilon_q\right)^2-\varepsilon_k^{2}\right\}^{-1}\;;D_{kqk}\left(\mp\right)=\left\{\left(\varepsilon_k\mp 2\varepsilon_q\right)^2-\tilde{\varepsilon}_k^{`2}\right\}^{-1} \tag{7b}$$

$$E_{kqm}\left(\mp\right)=\left\{\left(\varepsilon_k\mp 2\varepsilon_q\right)\pm\tilde{\varepsilon}_m^{`}\right\}^{-2}\quad;\;\; m=q,Q \tag{7c}$$

$$J\left(kqk\right)=8\pi^{-1}k_B\varepsilon_k\tilde{\varepsilon}_k^{`-2}\varepsilon_q^{2}C_{kqk}\left(-\right)C_{kqk}\left(+\right)D_{kqk}\left(-\right)D_{kqk}\left(+\right) \tag{7d}$$

$$L\left(kqkQ\right)=64\pi^{-1}k_B^{2}\tilde{\varepsilon}_k^{`-2}\sum_q\varepsilon_k A_{kQ}\left(\tilde{\varepsilon}_k^{`2}-\tilde{\varepsilon}_Q^{`2}\right)^{-2}\left(\varepsilon_k^{4}-8\varepsilon_k^{2}\varepsilon_q^{2}-2\right.$$

$$\left.\varepsilon_k^{2}\tilde{\varepsilon}_k^{`2}-8\tilde{\varepsilon}_k^{`2}\varepsilon_q^{2}+16\varepsilon_q^{4}+\tilde{\varepsilon}_k^{`4}\;\;\right)C_{kqk}\left(-\right)C_{kqk}\left(+\right)D_{kqk}\left(-\right)D_{kqk}\left(+\right) \tag{7e}$$

4. PHONON LIFE TIME

The total phonon life time eq.(1), in view of eq.(5) , can be taken as

$$\tau\left(kq,\varepsilon\right)\quad=\quad\left(\Gamma^{D}\left(kq,\varepsilon\right)\right)^{-1}+\left(\Gamma^{ep`}\left(kq,\varepsilon\right)\right)^{-1}+\left(\Gamma^{ep``}\left(kq,\varepsilon\right)\right)^{-1} \tag{8}$$

5. CONCLUSION

The delta function peaks at $\pm\tilde{\varepsilon}_{k_1}$ are depend on electron phonon coupling constant upto third order.The effect of electron phonon interaction provide the creation of two exciton bound state. The phonon linewidth due to this interaction depend linearly and non-linearly on mass change parameter. This shows that strong coupling between electron and phonon decrease the phonon life time through T^3 dependence on temperature. This concept may help in determining the physical properties.

References

1. Indu B. D. ; (1990) ; *Theory of Lattice Specific Heat of an Isotopically Disordered Anharmonic Crystal ; Int. J. Mod. Phys. B* ; **4** ; 1379-1393 .
2. Maradudin A. A. and Fein A. E. ; (1962) ; *Scattering of Neutrons by an Anharmonic Crystal* ; Phys. Rev. ; **128** ; 2589-2608 .
3. Gairola S. C. ; (2012) ; *Electronic Heat Capacity of an Isotopically Disordered Semiconductor Crystals* ; Ind. J. Phys. ; **86** ; 967-970 .
4. Zubarev D. N. ; (1960) ; *Double-Time Green Functions in Statistical Physics* ; Usp. Fiz. Nauk ; **71** , 71-116 [Eng. Transl. Soviet Physics Uspekhi ; **3 ;** 320-345(1960)] .

5. Sharma P.K and Bahadur R. ; (1975) ; *Thermal Conductivity for Phonon Scattering by Substitutional Defects in Crystals* ; Phys. Rev. B ; **12** ; 1522-1530 .
6. Sahu D. N. and Sharma P. K. ; (1983) ; *Thermal Conductivity of an Imperfect Anharmonic Crystal* ; Phys. Rev. B ; **28** ; 3200-3213 .
7. Pathak K. N. ; (1965) ; *Theory of Anharmonic Crystals* ; Phys. Rev. ; **139** ; A1569-A1580 .

HIGH RESOLUTION X-RAY SPECTRA FROM HIGHLY CHARGED IONS

S. Kasthurirangan[1], A. N. Agnihotri[2] and L. C. Tribedi[2]
[1]Institute of Chemical Technology, Matunga, Mumbai – 400019
[2]Tata Institute of Fundamental Research, Colaba, Mumbai – 400005

1. INTRODUCTION

X-ray spectroscopy is a highly important tool for the understanding of many fundamental atomic processes. High resolution x-ray spectra can provide direct information about the population of energy levels of various ionic states of a given species. The data so obtained can be used in a wide variety of fields, including astrophysics and the physics of plasmas [1]. We have obtained the high-resolution x-ray spectra from fast projectile ions in collisions with thin foil targets of C and Al usinga bent-crystal spectrometer.

2. EXPERIMENTAL DETAILS

A well-collimated beam of highly charged S ions of energy 56MeV was obtained from TIFR-BARC Pelletron facility inMumbai, and was made incident on a thin carbon foil. The ions were stripped to higher charge states in passing through the foil, including significant yield of higher charge states, and the x-rays emitted in the collision were recorded using a high resolution bent crystal spectrometer.

The thin foil targets are mounted on a target ladder arrangement, perpendicular to the beam, whereby the targets can be changed without disturbing the vacuum of the system. The entire spectrometer assembly is housed in a stainless steel vacuum chamber, which also has ports for the beam inlet and outlet, target mounting and a fine leak valve. A view port is available to facilitate the proper positioning of the target. The typical vacuum in the chamber is $2 - 3 \times 10^{-6}$Torr. The spectrometer used in this study is described in detail in [2]. Briefly, this spectrometer consists of a curved ADP (101) crystal mounted in a Johannson geometry, with a Rowland circle diameter of 25.4 cm. The detector is a gas-flow proportional counter, with a continuous circulation of P-10 gas.

The entire control of the spectrometer movement and the data acquisition is done using NI LabVIEW software, with suitable hardware interfacing. A program wasdeveloped and customised in-house to provide efficient data collection and instrumentcontrol. Both the program and the experimental setup were tested rigorously using keVenergy electron impact on Al target. The spectrometer has a resolution of 2.2 eV at an x-ray energy of 1486 keV (Al Kα), which has been observed both under electron impact and ion impact.

3. RESULT AND DISCUSSION

The x-ray spectrum from 56 MeV S projectile ions is shown in Fig. 1. The spectrumis sufficiently well-resolved to be easily subdivided into regions where x-ray lines from H-, He- or Li-like S ions dominate, although there is partial overlap between the He-like and Li-like regions of the spectrum. The energy axis is self-calibrated using the well- known H-like lines. The datashown in the figure have been corrected for Doppler shift, and represent the energiesemitted in the rest frame of the projectile. Similar trends are also observed in Si and Cl ions.

Figure 1: X-ray spectrum from highly charged S ions.

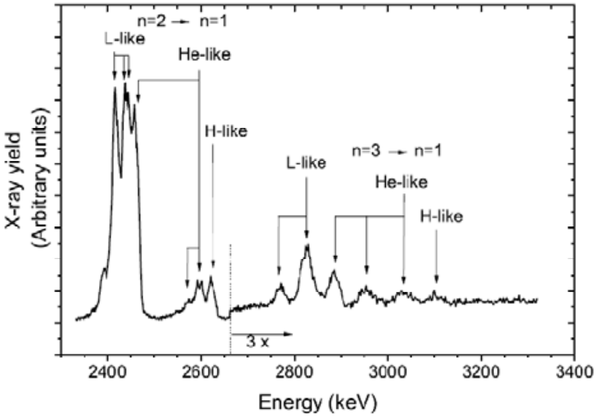

4. CONCLUSION AND OUTLOOK

A high resolution measurement of the x-rays can be used to study ion-solid collisions and the subsequent x-ray emission from highly charged ions formed therein. In a similar fashion, the x-ray spectroscopy of plasma [1,3] can lead to very valuable information which can then be utilised to manipulate the charge state balance prevalent in the plasma, leading to finer control over the charge states produced and their relative fractions.

References

[1] Gumberidze A, Trassinelli M, Adrouche N, Szabo C I, Indelicato P *et. al.* (2010) Rev. Sci. Instrum.**81** 033303

[2] Kumar A, Misra D, Thulasiram K V, Tribedi L C and Pradhan A K (2006) Nucl. Instrum.Meth. B **248** 247

[3] Kasthurirangan S, Agnihotri A N, Desai C A and Tribedi L C (2012) Rev. Sci. Instrum. **83** 073111

SCATTERING OF GAMMA AND X-RAY PHOTONS FOR MEDICAL APPLICATIONS AND DETECTION OF LANDMINES

B. S. Sandhu
Physics Department, Punjabi University, Patiala –14 7002, India
· Email: balvir@pbi.ac.in

Abstract: *The use of coherent and incoherent scatterings of gamma and X-ray photons for medical applications such as measurement of pulmonary edema, swelling and/or abnormal extravascular water storage in the lungs, mandibular bone density and stable iodine contents of thyroid are successfully explored. A scanner system is also presented for detection of explosives (landmines). The scattered intensity originating from interactions of photons with the phantom has the potential for above stated medical applications and detection of landmines.*

1. INTRODUCTION

The important processes resulting in scattering of low and medium energy γ-rays are classified as coherent (Rayleigh, Thomson and Delbrück) and incoherent (Compton) scatterings. The coherent scattering is scattering of gamma rays from bound electrons, and is predominant at low photon energies, small scattering angles and high Z-number materials; the scattered photon has the same energy as that of incident photon. In Compton scattering (incoherent), the incident photon upon interaction with a free electron is scattered with degraded energy.

Various X-ray or gamma-ray transmission non-destructive techniques are widely used in industrial and medical fields. Traditionally these techniques are realized by equipment ranging from simple radioisotope gamma-gauge to complex radioscopic imaging and computerized tomography systems. However, in the last decade, coherent (Rayleigh) and incoherent (Compton) scattering inspection techniques have emerged increasingly in various fields. Billy and Fred [1] developed a Compton densitometer for measuring pulmonary edema by using ^{57}Co radioactive source and an HPGe detector. The bone mineral density of the mandible had been investigated by Morgan et al [2] to study bone resorption following tooth loss and to determine the relationship between mandibular and skeletal bone mineral density. Our measurements [3] provide details of the use of Compton scattering to evaluate the density variation and part by part/sectional (tomographic) inspection of objects. The scattered intensity originating from interactions of 662 keV gamma photons with the object under investigation provides the desired information. The results have confirmed that experimental resolution for density variation in the inspected object is quite good. The method is quite sensitive, for showing inclusion of medium Z (atomic number) material (iron) in low Z material (aluminium) and detecting a void of ~2 mm in size for iron block, to investigate the inhomogeneities in the object. Moreover, the grey scale images using “MATLAB” also visualise the presence of defects/inclusion in metal samples.

In the present talk, the use of coherent and incoherent scatterings for medical applications such as measurement of pulmonary edema, swelling and/or abnormal extravascular water storage in the lungs, mandibular bone density and stable iodine contents of thyroid are explored. The present work provides low-dose inexpensive alternatives to the various other medical techniques. Moreover, the present scanner system helps in detection of explosives (landmines) such as TNT ($C_7H_5N_3O_6$) and RDX ($C_3H_6N_6O_6$), hence of great importance for defence personnel.

2. EXPERIMENTAL SET-UP AND MEASUREMENTS

Figure 1 shows the experimental set-up used in present work for measurement of Rayleigh and Compton scattered photons in narrow beam geometry. The principle of measurements is to observe the intensities of Rayleigh and Compton scattered gamma photons at a particular scattering angle using a high resolution semiconductor gamma ray detector.

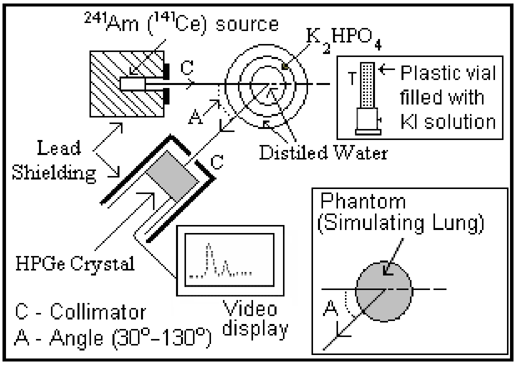

Fig. 1: Experimental set-up

An HPGe (high purity germanium detector) is housed in a lead castle similar to that used for the source and collimated in an identical manner. Lung and bone phantoms are prepared mixing appropriate amount of saw dust and K_2HPO_4, respectively, in distilled water. The aqueous solutions of K_2HPO_4 in the concentration range 0-30 g in steps of 6 g in 100 mL of water simulate the bone density ranging from 1000 to 1200 kg-m^{-3}.The solutions are placed in plastic containers positioned at the centre of rotation of the source and detector assemblies. The phantom simulating stable Iodine contents of thyroid is in the form of KI of different amounts ranging from 2 to 10 g in step of 2 g in 10 mL of distilled water filled in a plastic vial (10 mm diameter) kept in a stand with screw to adjust its height. A well collimated beam of 59.54 keV gamma-rays from of ^{241}Am source (strength 7.4 GBq), 145 keV from ^{141}Ce source for stable iodine contents of thyroid, irradiates the phantom. The distances of centre of phantom under study from the source collimator (radius 0.4 cm) and detector collimator (radius 0.4 cm) are kept 120 mm and 100 mm respectively. The scattered gamma rays are detected by a high resolution HPGe semiconductor detector (75 cc in volume) placed at desired scattering angle relative to the primary incident beam. The coherent to incoherent intensity ratios are measured for each phantom having different density values. The phantom-in scattered spectra are recorded for a period of 5 ks by placing different density phantoms. The details of the scanner system presented for detection of explosives (landmines) are given in our earlier measurements [3]. The data are accumulated on a PC based ORTEC Mastreo-32 Multi channel analyzer (MCA).

3. RESULTS AND CONCLUSION

The intensity ratio of Rayleigh to Compton scattered peaks, observed in the scattered spectrum originating from interactions of primary gamma-beam photons with the phantom under consideration, are corrected for photo-peak efficiency of the HPGe gamma detector, and absorption of photons in air column present between phantom and detector, and self absorption in the phantom. In fig. 2, Rayleigh to Compton intensity ratio, for phantoms simulating lung, is found to be decreasing linearly with increase in phantom density. This is because an increase in phantom density results in more scattering centres for gamma interactions through Compton scattering process while owing to low effective atomic number (7.18- 7.31 for various lung phantoms used in present work) of the phantom there is not much appreciable change in intensity of Rayleigh peak. This results in decrease in intensity ratio with increasing phantom density. The departure of some of the data points from linear nature is due to non uniformity of packing of mixture within thin plastic container. The best-fitted regression line of fig. 2 serves as calibration curve and provides the lung density of unknown sample of interest.

The intensity ratio originating from K_2HPO_4 solutions (simulating mandibular bone density) increases linearly (Fig. 3) with increase in concentration of K_2HPO_4 in distilled water within experimental errors as Rayleigh scattering contributes significantly in this case owing to enhanced Z_{eff} because of presence of Potassium (Z=19) and Phosphorus (Z=15). The best-fitted regression lines of fig. 3 serve as calibration curves in and provide the mandibular bone density of unknown sample.

The results for stable iodine contents of thyroid, presented in Fig. 4, show that as concentration of iodine in the solution increases, Rayleigh to Compton (R/C) intensity ratio increases linearly. The slope of linear curves also increases with scattering angle.

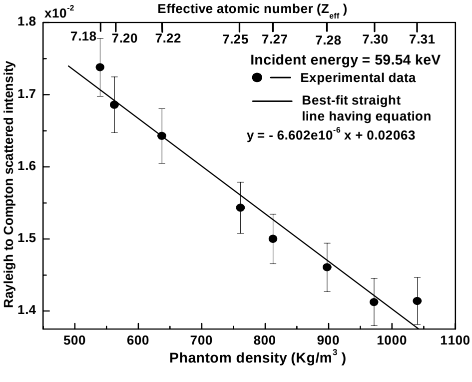

Fig. 2: Experimental variation of Rayleigh to Compton intensity ratio as function of lung phantom density.

The trend of our experimental results is in good agreement with the results of Puumalainen et al [4] measured for stable iodine content of tissue at for 59.54 keV incident gamma photons.

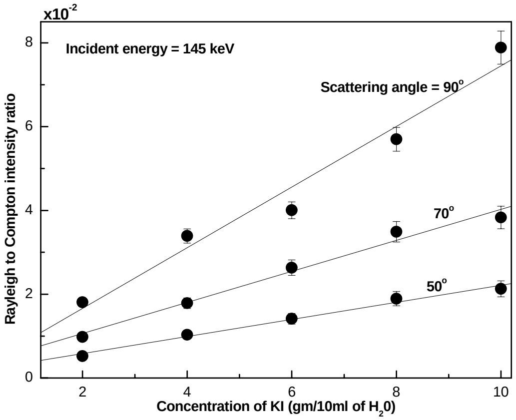

Fig. 3: Experimental variation of Rayleigh to Compton intensity ratio as function of mandibular bone density.

The scanner system, details given in measurements [3] is presented to detect the landmines comprising of explosives. The most widely used explosives; rich in nitrogen, for landmines are TNT ($C_7H_5N_3O_6$) and RDX ($C_3H_6N_6O_6$). These explosive materials have density less than that of metals and different from various types of soils [5].

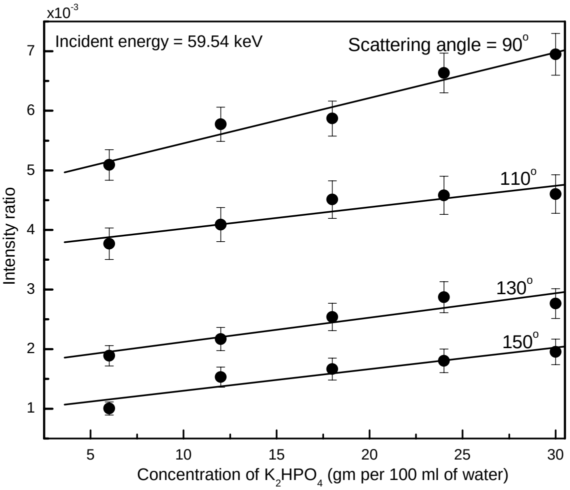

Fig. 4: Experimental variation of Rayleigh to Compton intensity ratio as KI concentration in 10 mL distilled water.

Therefore, a measurement of density helps to detect the presence of landmine. In the present work, experimental phantom for landmine detection is TNT stimulant [6] is prepared by mixing 17.3 g graphite, 23.9 g oxalic acid crystals and 58.8 g cyanuric acid. The explosive simulant mixture, as shown in Fig. 5, is filled in cylindrical plastic container (30 mm in diameter and 10 mm in length) and cylinder is placed in paper box (100 mm in length and breadth, and 45 mm in height) having soil of density 1.3706 g/cm^3. The explosive simulant phantom is buried at depth of ~ 2 cm in soil, so that gamma photons have to penetrate this much distance before interacting with buried material. The plot for scattered intensity values for different scan positions is shown in Fig. 6. As the density value for the soil (~1.371 g/cm^3) chosen for present experiment is more than that of explosive phantom (~1.127 gm/cm^3), so more scattering centres are offered by soil as compared to explosive simulant. This result in locating the range of explosive material buried in soil. The present results, for density value of soil are close to explosive simulant; show that technique is sensitive for detection of landmine under soil thickness of ~2 cm.

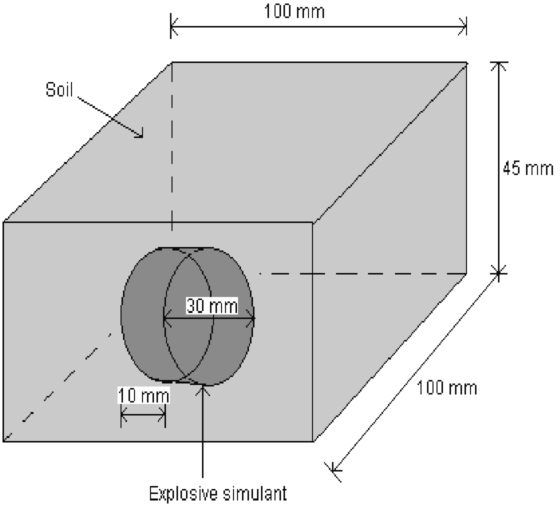

Fig. 5: Landmine phantom used in the present experiment.

The results of present experiments indicate that the technique has potential for a measure of pulmonary edema, mandibular bone density for either bone resorption studies or as a predictor of osteoporosis and stable iodine contents of thyroid. The present measurements provide a low dose inexpensive alternative to the use of dental radiographs in studies of mandibular bone density. Medical diagnostic techniques based on

Gamma rays scattering are relatively new and many are still under development. The use of a gamma emitting radioactive source to provide the radiation beam offers the advantages over an X-ray system of constant beam intensity, mono-energetic radiation, lower patient dose and apparatus that can be made small and portable. The scanner system can play an important role in landmine detection by providing material characterization to determine whether an anomaly contains an explosive material or not. Identifying and detecting explosive materials in airport baggage and buried land mines are highly beneficial for the human life safety.

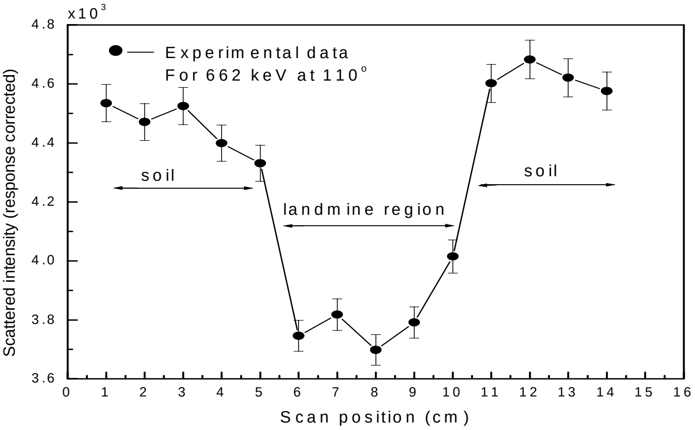

Fig. 6: Scattered intensity profile as a function of position showing range of explosive material.

References

1. Loo Billy W. and Goulding Fred S., *IEEE Trans. Nucl. Science,* **33** (1986) 531.
2. Morgan H.M., Shakeshaft J.T. and Lillicrap S.C., Br *J Radiol,* **72** (1999) 1069.
3. Sharma Amandeep, Singh Karamjit, Singh Bhajan & Sandhu B S, *Nucl. Instr. & Meth.,* B **269** (2011) 247.
4. Puumalainen P, Sikanen P, and Olkkonen H., *Nucl. Instr. & Meth,* **163** (1979**)** 261.
5. Tang S & Hussein E M A, *Appl Radiat Isot,* **61** (2004) 3.
6. Brooks F D, Drosg M, Buffler A & Allie M S, *Appl Radiat Isot,* **61** (2004) 27.

EFFECT OF THE BUFFER ON ELECTRON INDUCED DAMAGE TO ΦX174 DSDNA

Megha Murali, Preksha Kushwaha, B. J. Rao
and S. V. K. Kumar
Tata Institute of Fundamental Research, Homi Bhabha Road
Colaba, Mumbai 400 005

1. INTRODUCTION

After the first report on Low Energy Electron (LEE) induced damage to double strand supercoiled DNA (dsDNA) by Sanche's group in 2000 [1]many reports have appeared in the literature on various aspects of electron induced damage. In our earlier report[2]wehad stated that,as the resonance structures observed by the three groups [2] were to some degree different, the LEE induced damage is likely to be dependent on the protocols used in the preparation and irradiation of the DNA. In order to test if the protocols play a role in determining the extent of damage, we have studied strand breaks induced by electrons in the energy range 25 to 100eV for pure ΦX174 dsDNA suspended in 0.001 mMNaOHsolution and in Tris-HCl-EDTA buffer at pH 7.5.

2. THEORY/EXPERIMENT

The experimental procedure involved purifying the ΦX174 dsDNA (New England BiolabsN3021L) by dialysisusing cellulose membrane tubing(Sigma D9277) innano pure water to remove salts. The quality of the purified DNA was checked bymeasuring the absorption ratio at 260 and 280 nm and theconcentration determined. The DNA was accepted for experimentsif the A260:A280 ratio was above 1.95. The DNA wasstored at –20°C in small aliquots. Small quantities of DNAwere then mixed with either 0.001 mMNaOH solution or Tris-HCl-EDTA buffer at pH 7.5 such that 5 μl of themixture contained 200 ng of DNA. DNA solution so prepared was spotted on a biologically clean tantalum foil dried at room temperature in a clean atmosphere and irradiated by electrons in a UHV chamber at a pressure of 10^{-8}Torr. The newly developed electron irradiation setup is controlled by a computer such that a pre-specified dose irradiates the DNA at a given electron energy. DNA irradiated at a dose of 60nC at all energies is analysed on 1.0% agarose gel by standard electrophoresis procedure.

3. RESULT AND DISCUSSION

The Single Strand Breaks (SSBs) which result in the formation of relaxed form and the Double Strand Breaks (DSBs) occur due to strand breaks occurring within 10 base pairs apart on both the strands of the DNA are shown as linear form respectively in Fig 1, while the starting ΦX174 dsDNA is the supercoiled form. It can be seen that there is little variation in the relative yield of relaxed form whether the DNA is suspended in 0.001 mMNaOH or Tris-HCl-EDTA buffer at pH 7.5 buffer. There is general increase in the SSBs as a function of energy which can be expected as observed by Huels et al [3], however, our SSB yield seems to show a monotonic increase immaterial of the DNA environment compared to an initial increase and a saturation beyond 30 eV observed by them. This could be due the higher dose that was used by Huels et al which leads to saturation at lower energies.

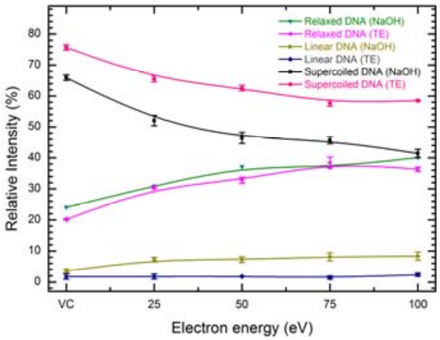

Figure 1: Single strand and double strand breaks induced by electrons to ΦX174 dsDNA

One possible mechanism for observing DSBsin the energy range 25 to 100 eV for 60nC irradiation dosecould be due to the incoming electron ionizing DNA components as it carries enough energy. The secondary electron that is produced during ionization of the DNA components of the first strand can then fragment the opposite strand either via dissociative ionization, dissociation or any resonant process provided the energy of the secondary electron matches the resonance energy. This is not the case in our previous experiments with pQE30 dsDNA[2]where the electron energy was either sub ionization or a little more than the ionization energyand could not have produced energetic secondary electrons duringits interaction with the DNA. The relative DSB yield, on the other hand, seems to be dependent on the DNA environment. It is clear that Tris-HCl-EDTA buffer seems to protect DNA from DSB. More theoretical investigations are needed to understand the mechanism of the protection, which probably will need inclusion of the molecular structureTris-HCl-EDTA and its binding to DNA and the vulnerability of the DNA to the electron impact dissociation process.

4. CONCLUSION

Our experiments have clearly shown that DNA is more vulnerable when suspended in 0.001 mMNaOH solution than in Tris-HCl-EDTA buffer at pH 7.5.The DSBs can be attributed to the electron ionizing one of the nucleotides on one strand which results in a strand break and energetic electron released from this ionization process attacking the opposite strand causing a second strand break.

References

1. Boudaıffa B.; Cloutier P.; Hunting D.; Huels M. A.; Sanche L.; *Resonant Formation of DNA Strand Breaks by Low-Energy (3 to 20 eV) Electrons*. (2000) Science. **287**, 1658-60.

2. Kumar S. V. K.; Pota T.; Peri D.; Dongre A. D.; Rao B. J.; *Low energy electron induced damage to plasmid DNA pQE30*. (2012) The Journal of Chemical Physics. **137**, 045101-7*and references cited therin*.
3. Huels M. A.; Boudaïffa B.; Cloutier P.; Hunting D.; Sanche L.; *Single, Double, and Multiple Double Strand Breaks Induced in DNA by 3−100 eV Electrons*. (2003) Journal of the American Chemical Society. **125**, 4467-77.

ELECTRON INTERACTIONS WITH DRY ICE: RELEVANCE IN MARTIAN POLAR CAPS AND CLOUDS

S. H. Pandya[1], K. N. Joshipura[1] and B. G. Vaishnav[2]
[1]Department of Physics, Sardar Patel University, Vallabh Vidyanagar-388 120, Gujarat, India
[2]Physical Research Laboratory Navrangpura, Ahmedabad-380 009 Gujarat, India
Email: [1]siddharth033@gmail.com, [2]knjoshipura@yahoo.com

1. INTRODUCTION

Planet Mars with its atmosphere containing mainly CO_2 has captured the attention of planetary and Space scientists, regardless of their working area, viz. ionospheric modeling, climatology, hydrology etc. Now, 2013 is going to be a year of Mars missions as planned by India and also by USA.

Our present interest is in dry ice i. e. solid CO_2. Recently Mars is found to have high altitude clouds containing dry ice [1]. The polar cap terrains of Mars also contain dry ice condensed above the water ice bed. Besides, the presence of formaldehyde in Martian atmosphere can be explained by the electron and photon driven reactions with CO_2, probably produced by complex reactions involving CO_2 and H_2O [2].

The present paper is perhaps a maiden attempt to study electron induced inelastic interactions in general and ionization in particular, with CO_2 in ice phase. In the Ionization process the target molecule is virtually removed from the crystalline structure, while the ejected electron(s) as also neutral and ionic species in turn give rise to different chemistries in the medium.

Among the various solids, ices in particular offer suitable targets from a theoretical point of view. In icy solids like water-ice, dry-ice, etc the embedded molecules more or less retain their identity. However, even in that case one needs to incorporate the effects of the condensed-matter medium, as discussed in [3].

2. THEORY

We have adopted presently the complex potential approach to address the basic e^- - CO_2 scattering problem, first in the case of isolated (gas) molecular target, to derive total inelastic cross sections Q_{inel}, which include total ionization cross sections Q_{ion}.

We omit here the equations and other details given in our recent publications [4, 5]. In the solid (ice) phase, the effective ionization threshold I_{th} is higher than the first ionization energy I_E. Therefore, in the absorption potential, the relevant energy parameter Δ, which indicates the onset of inelastic (ionization) processes, is set to be equal to I_{th}. The Q_{ion} are computed as already outlined in our papers [3-5]. The microscopic cross section Q_{ion} is employed to compute macroscopic (bulk) quantities like ionization mean free path (MFP) and ion production rates in CO_2 ice.

3. RESULT AND DISCUSSION

Fig.1. shows the present Q_{ion} for carbon dioxide (gas) molecules in the complex potential ionization contribution method [4], which find a good general accord with experimental and other data (not shown).

Figure 1: Ionization cross sections, Solid line – Dry ice (Δ fixed), dashed line - Dry ice (Δ varying), dotted line - CO_2 (gas) .

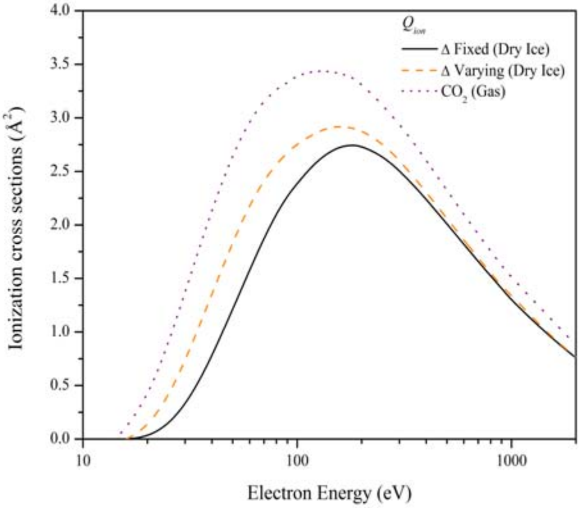

The gas-phase cross sections provide a background to examine the present Q_{ion} of CO_2 (ice), about which almost nothing is known. The latter Q_{ion} are computed by considering two variants [3–5], viz., (1) the Δ fixed at I_{th}, and (2) the Δ varying smoothly from I_E to I_{th}.

Table 1: Peak position and peak value for Q_{ion} in the present targets

Target	Peak Q_{ion} (Å^2)	Peak Position (eV)
CO_2 (Gas)	3.44	125
CO_2 (Ice)	2.74 (Δ Fixed)	180
	2.92 (Δ Varying)	160

Table 1 depicts the typical Q_{ion} values in the peak region. After the ionizing interaction both the scattered and the ejected electrons must have sufficient energy, in order to avoid recombination in the medium. Therefore $\Delta > I_E$, and thus the effect of the solid-state medium is to reduce the cross sections (Fig.1.) as compared to that in CO_2 (gas), especially at low and intermediate energies of electron impact.

4. CONCLUSION

Electron ionization in a solid (ice) is a difficult problem both theoretically and experimentally. An approximate calculation is possible as demonstrated presently. Electron ionization cross sections for the dry ice are smaller than those of CO_2 (gas), and the peak position shifts to a higher energy, as exhibited in Fig.1. and Tab 1.

References

[1] Montmessin F., Gondet B., Bibring J.-P., Langevin Y., Drossart P., Forget F., Fouchet T., (2007), *Hyperspectral imaging of convective CO_2 ice clouds in the equatorial mesosphere of Mars,* J. Geophys. Res., **112**, E11S90.

[2] Šiller L., Sieger M. T., Orlando T. M., (2003), *Electron-stimulated desorption of D_2O co-adsorbed with CO_2 ice at VUV and EUV energies*, J. Chem. Phys. **118**, 8898.

[3] Pandya S. H., Vaishnav B. G., Joshipura K. N., (2012) *Electron inelastic mean free paths in solids: A theoretical approach,* Chin. Phys. B **21**, 093402.

[4] Pandya S. H., Shelat F. A., Joshipura K. N., Vaishnav B. G. (2012) *Electron ionization of exotic molecular targets CN, C_2N_2, HCN, HNC and BF− Theoretical cross sections*, Int. J. Mass Spectrom. **323– 324**, 28.

[5] Pandya S. H., Kothari H. N., Joshipura K. N., (2010) *Calculations on electron impact ionization cross-sections for atomic-molecular targets: ionospheric applications, ADGEO (Planetary Science),* **25**, 243, World Scientific Publishing, Singapore.

PLASMA MODELING WITH ELECTRON EXCITATION OF INERT GASES AND TUNGSTEN IONS

D. T. Das, R. K. Gangwar, L. Sharma and R. Srivastava
Department of Physics, IIT Roorkee, Roorkee, 247667

1. INTRODUCTION

Optical emission spectroscopy (OES) combined with appropriate plasma model is widely used method of plasma diagnostics. Such a study yields plasma parameters *viz.* electron temperature, electron density and species population. OES is inexpensive and applicable in various plasma conditions where no other technique can be employed. There is a need to develop collisional radiative (CR) models for both inert gases and tungsten plasmas. Inert gases are added in trace amounts to various plasma for diagnostic purposes, known as trace rare gas (TRG) OES. Tungsten is of great interest in fusion engineering as a potential plasma-facing material in magnetic confinement devices. Dominant processes in plasma are due to electron impact collisions. The growing demand of electron-atom collision data can't be met solely through experimental measurements. Therefore, reliable fine-structure cross sections are required to be calculated using fully relativistic theory and incorporated in CR model for low and high temperature plasma modelling [3].

The inert gases and heavier atoms show several fine structure levels due to strong relativistic effect/spin-orbit coupling. Studying electron excitation of fine-structure transitions is a challenging problem and of fundamental importance. Several fine-structure transitions between the ground state to excited states and among the excited states are involved in plasmas. Experimental electron impact data are scarce and often the reported measurements are fine structure unresolved. Due to the complexity involved with fine-structure transitions the theoretical data used for plasma modelling are obtained from empirical or simple classical methods which are not reliable. Therefore, a fully relativistic theory which can describe fine structure excitations should be used. In this connection, we have performed fully relativistic distorted wave (RDW) for several fine structure transitions from ground as well as exited states to higher lying states of argon and other inert gases [4,7].

The study on spectra of emissions from electron excited highly charged tungsten ions is required as diagnostics for plasma parameters, e.g., ion temperature of the International Thermonuclear Experimental Reactor (ITER) core plasma. Despite the large body of literature on various W ions [5], there is a serious lack of excitation cross section data for various transitions of all the different ionic stages of tungsten ions [6]. The International Atomic Energy Agency (IAEA) has set up a committee of international scientists to promote the production and exchange of variety of tungsten data needed for ITER. For this purpose we have carried out RDW calculations for electron impact excitations of 3d–4p and 3d–nf (n = 4–8) transitions from the M-shell of the Zn-like W^{44}+, Cu-like $W^{45+,}$ Ni-like W^{46+} and Co-like W^{47+} ions [2].

Further, we have developed a CR model and we are incorporating our calculated electron impact cross sections of inert gases and tungsten ions for plasma diagnostics [3].

2. THEORY

The theoretical approaches for electron– atom collisions are mainly perturbative and non-perturbative methods. The current promising non-perturbative approaches are convergent close-coupling (CCC) [1] and *R*-matrix [8] methods. However, relativistic versions of these two methods have been reported only recently as applied to the fine structure transitions. Also their applicability is limited to low impact energies. Further, as we need to consider several fine structure transitions from ground and between excited states of atoms/ions in wide range of impact energy, using a non-pertubative approach only is not a good option. On the other hand under perturbative approaches, we have developed a fully relativistic distorted wave method which proved to be very successful. In our RDW method wavefunctions for both the bound_and continuum electrons are obtained by solving the Dirac equations. Therefore, the relativistic effects or the fine structure of the target states and spin of the incoming electron are included in a natural way.

The relativistic distorted-wave *T*-matrix for the electron impact excitation of an atom/ion having *N* electrons and nuclear charge *Z* from an initial state *a* to final state *b* can be written as (in atomic units)

$$T_{a\to b}^{RDW}=\left\langle \Phi_b^{rel}(\mathbf{1},\,\mathbf{2},\,...,\,\mathbf{N})\mathrm{F}_{\mathrm{b},\,\mu_\mathrm{b}}^{DW-}(\mathbf{k_b},\mathbf{N+1})\middle| V-U_b(N+1)\middle| \mathrm{A}\{\Phi_a^{rel}(\mathbf{1},\,\mathbf{2},\,...,\,\mathbf{N})\mathrm{F}_{\mathrm{a},\,\mu_\mathrm{a}}^{DW+}(\mathbf{k_a},\mathbf{N+1})\}\right\rangle$$

where Φ_{ch} represent *N*-electron target wavefunctions, $F_{ch,\mu_{ch}}^{DW(\pm)}$ are the projectile electron distorted wave function and ‘ch’ refers to the two channels, *i.e.*, initial ‘*a*’ and final ‘*b*. Here ‘+’ denotes an outgoing wave while ‘-’ refers to an incoming wave. $\mathbf{k}_{\mathrm{ch}}$ is the linear momentum of the projectile electron in the initial(final) channel. μ_{ch} is the spin projection of the projectile electron.

V is the usual interaction between the projectile electron and target atom/ion. Here (1, 2, .., *N*) represent the position coordinates of the target electrons and (N+1) is the position coordinate of the projectile electron with respect to the nucleus of the ion. U_b is the distortion potential which is taken to be a function of the radial coordinates of the projectile electron only. *A* is the antisymmetrizing operator to take account of the exchange of projectile electron with bound electrons. Further details of our RDW method can be found from our earlier work [4,7].

3. RESULT AND DISCUSSION

We have developed a CR model for argon plasma which incorporates detailed fine structure RDW excitation cross sections calculated by us [4,7]. In addition to the ground state and lowest ion level, we have included forty excited fine-structure levels having configurations $3p^5 4s$, $3p^5 4p$, $3p^5 3d$, $3p^5 5s$, $3p^5 5p$ [3]. In our CR model various excitation and de-excitation processes are incorporated to determine population densities of fine-structure levels of Ar. Thereafter, we solved particle-balance equations considering all states for various Ar plasmas and obtained excited atomic level populations as a function of electron temperature and density. We have also calculated intensities of 750.38 & 696.54 nm lines as a function of power compared with the experimental available measurements. Our CR model results for Ar are overall in good agreement with the recent OES measurements [3].

Further, we have applied our RDW method to study electron impact excitations of 3d–4p and 3d–nf (n = 4–8) transitions from the M-shell of the Zn-like W^{44}+, Cu-like $W^{45+,}$ Ni-like W^{46+} and Co-like W^{47+} ions [2]. These transitions have been identified in EBIT experiment at Lawrence Livermore National Laboratory to be the most intense lines in the M-shell x-ray spectra of Zn-like through Co-like W ions. We obtained results for excitation cross sections for these dipole allowed transitions considered in all the four ions and the linear polarization of the photon emissions due to the decay of the excited anisotropic states to the ground state [2]. We also calculated fitting parameters to our cross sections in order to make them available in the wide range of incident electron energies for plasma application purposes. For illustration, we have shown comparison of our RDW cross sections for transitions $4s \rightarrow n\overline{p}$ and *np* with *n* = 4 and 5 of Cu-like W^{45+} ions with the only available theoretical calculations of Zhang *et al* [9] for these transitions. We find that their results for *n* = 4 excitations are in complete agreement with our results while these slightly differ for *n* = 5 excitations. Thus the overall agreement can be said to be quite reasonable.

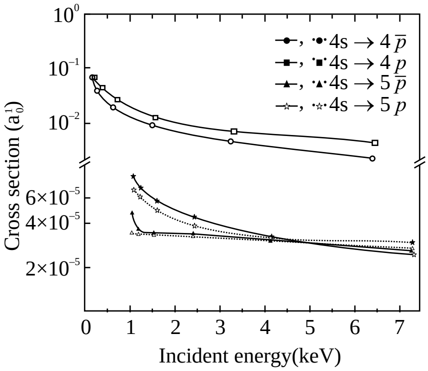

Cross sections in units of a_0^2 for excitation of Cu-like W^{45+} ions from its ground state $3s^2 3p^6 3d^{10} 4s$ (J = 1/2) to excited state $3s^2 3p^6 3d^{10} np$ where n = 4 and 5. ●, ■, ▲ and ★ with solid line denote our RDW calculation and □, ○, Δ and ☆ with dashed line refer the results from Zhang et al [9].

4. CONCLUSION

We have given here the details of our calculated and used fine structure RDW cross sections for Ar to develop a CR model for low temperature argon plasma. We have also described about our calculated RDW cross section and polarization results of different transitions in Zn-like through Co-like tungsten ions in the wide range of incident electron energies for their applications in plasma modelling studies.

References

[1]. Bostock C. J., Fursa D. V., Bray I., (2009), *Relativistic convergent close-coupling method: Calculation of electron scattering from hydrogenlike ions*, Phys Rev A **80,** 052708.

[2]. Das T., Sharma L. and Srivastava R., (2012), *Electron impact excitation of the M-shell electrons from Zn-like through Co-like tungsten ions*, Phys. Scr. **86,** 035301.

[3]. Gangwar R. K., Sharma L., Srivastava R. and Stauffer A. D., (2012), *Plasma modeling using detailed fine-structure cross sections for Ar*, J. Appl. Phys., **111,** 053307.

[4]. Gangwar R. K., Sharma L., Srivastava R. and Stauffer A. D., (2012), *Electron impact excitation of argon: cross sections of interest in plasma modeling*, Phys Rev A **81,** 052707.

[5]. Kramida A. E. and Shirai T. (2009), Energy levels and spectral lines of tungsten, W III through W. L. XXIV, At. Data Nucl. Data Tables, **95,** 305.

[6]. Sampson D. H., Zhang H. L., and Fontes C. J., (2009), *A fully relativistic approach for calculating atomic data for highly charged ions*, Phys. Rep. **477**, 111.

[7]. Srivastava R., Stauffer A. D., and Sharma L., (2006), *Excitation of the metastable states of the noble gases*, Phys. Rev. A **74**, 012715.

[8]. Zatsarinny O. and Bartschat K., (2009), *Fully relativistic B-spline R-matrix calculations for electron collisions with mercury*, Phys. Rev. A **79,** 042713.

[9]. Zhang H. L., Sampson D. H. and Fontes C. J., (1990), *Relativistic distorted wave collision strengths and oscillator strengths for the 33 Cu-like ions with 60* $\leq Z \leq$ *92*, At. Data Nucl. Data Tables **44**, 273.